SSI-rapport 95-15

Statens strålskyddsinstitut
Swedish Radiation Protection Institute

Postadress
171 16 STOCKHOLM

Gatuadress
Karolinska sjukhuset
Solna

Telefon
08-729 71 00

edited by H. Klein and L. Lindborg

Determination of the Neutron and Photon Dose Equivalent at Work Places in Nuclear Facilities of Sweden

An SSI - EURADOS comparison exercise. Part 1: Measurements and Data Analysis

ISSN 0282-4434

Pris: 100 kronor

Avdelning/Division:

Statens strålskyddsinstitut
Swedish Radiation Protection Institute

Nummer / Number: 95-15

Datum / Date of Issue: 1995-08-14

Antal sidor / Number of pages: 128

ISSN: 0282-4434

Titelblad/Title page

Författare / Author:
H. Klein, Physikalisch-Technische Bundesanstalt, Braunschweig und Berlin and
L. Lindborg, SSI

Dokumentets titel / Title of the document:
Determination of the Neutron and Photon Dose Equivalent at Work Places in Nuclear Facilities of Sweden. An SSI - EURADOS comparison exercise.
Part 1: Measurements and Data Analysis
Bestämning av neutron- och fotondosekvivalentraterna vid några arbetsplatser inom den svenska kärnkraftindustrin
En jämförelse av resultat erhållna med olika tekniker i arrangemang av SSI -EURADOS
Del 1: Mätningar och analys av data

Sammanfattning/Abstract:

See below:
Se nästa sida:

Nyckelord (valda av författaren) / Key words (chosen by the author):
Dosimetry, Radiation Protection, Neutron dosimetry, Nuclear Power Plant, Fuel Elements
Dosimetri, strålskydd, neutrondosimetri, kärnkraftverk, kärnbränsle

Abstract:

A large-scaled measurement programme of neutron and photon dose equivalent rates was organised in 1992 and 1993 at the nuclear power plant at Ringhals and at the Swedish Central Interim Storage Facility for spent Fuel Element at Oskarshamn. The aim was to evaluate the uncertainty in these kinds of measurements in realistic radiation fields. For that purpose, groups experienced with different techniques and - in some cases - several groups with a particular technique, were invited to take part.

Besides traditional remcounters the following categories of instruments were involved: Bonner Spheres systems, proton recoil detectors, tissue equivalent proportional counters (TEPC), super heated drop detectors (SDD), GM counters and different types of personal dosemeters.

Part I reports all initial results as presented by the individual participants as well as a first compilation of the results. A later report, *Part II*, will give detailed analysis of the results. The *final conclusions* have been accepted for publication in the journal Radiation Protection Dosimetry and this report is expected to be published in 1995.

Sammanfattning:

Ett omfattande mätprogram av neutron- och fotondosekvivalentraterna vid kärnkraftverket i Ringhals och lagret för utbränt kärnbränsle vid Oskarshamn, CLAB, genomfördes under 1992 och 1993. Syftet var att utvärdera osäkerheten i denna sorts mätningar under verkliga mätbetingelser. Ett stort antal internationella expertgrupper inbjöds därför att mäta på vissa specifika punkter. Grupperna använde ibland olika tekniker.

Förutom traditionella neutrondosmätare, typ remcounters, användes Bonner- sfärer, protonrekyldetektorer, vävnadsekvivalenta proportionalräknare (TEPC), s k droppdetektorer och olika persondosmätare.

Del1 innehåller alla initialt rapporterade resultat, en beskrivning av bestrålningsgeometrierna liksom en första jämförelse av resultaten. En senare rapport, Del 2, kommer att ge en detaljerad analys av resultaten. En sammanfattning av erfarenheterna har accepterats för publicering i Radiation Protection Dosimetry och väntas under hösten 1995.

Table of Content Page

1. INTRODUCTION

L. Lindborg
Swedish Radiation Protection Institute, S-171 16 Stockholm, Sweden

The radiation fields in nuclear power plants consist of a mixture of photons and neutrons of various energies. A detector is usually constructed to respond to one type of radiation only and is usually useful in a limited energy range. This is especially so for neutrons. Accurate descriptions of the radiation environment are therefore very complicated to obtain. During the last decade great effort has gone into improving of instruments suitable for this kind of measurement. However, their usefulness in practical field measurements is still not fully explored. In some areas such as inside the containment building of a reactor, the temperature is well above normal room temperatue (up to 45 C) and the acoustic and electromagnetic noise level may be very high. Such environmental conditions could influence a dosemeter reading.

Over the last decade the ICRU has introduced the operational dose equivalent quantities for radiation monitoring. The idea is that their numerical values should never be below those of the effective dose equivalent as defined by the ICRP. As this committee in 1990 suggested increased risk factors for neutrons and changed the definition of the risk quantity, the safety margin is unclear.

The objectives of this investigation were to determine the total ambient dose equivalent as well as the directional or personal dose equivalent at a few locations using different, independent techniques, and from the results to estimate the dosimetric uncertainty in a practical situation at workplaces of a nuclear reactor. The *neutron fluence* distribution as a function of the energy has been determined with several Bonner sphere systems. Proton recoil measurements were also carried out. The dose distribution of the *lineal energy* was determined with TEPCs of various design. Personal dosemeters were used to observe the *angular distribution of the radiation* along with *the personal dose equivalent.* Direct reading instruments such as REM counters, bubble detectors and GM counters showed the values of the integral *ambient dose equivalent.* The way in which the various quantities are related to the overall uncertainty in a dose equivalent measurement will be demonstrated by a comparison of the results.

In areas with high dose rates such as inside a reactor containment there is a need for accuracy not only from the traditional radiation protection point of view, but also from one of economy. If the power of a reactor can be maintained during inspection or maintenance without causing an unacceptably high effective dose equivalent to the personnel, this is important.

The impetus for this project came from discussions between the Swedish Radiation Protection Institute (SSI), the nuclear power plant, Ringhalsverket, and the Swedish Central Interim Storage Facility for Spent Fuel Elements, CLAB. Great improvements in dosimetry have been made during the last decade and the contribution made by EURADOS in coordinating these efforts is very important. Cooperation with its working groups on dosimetry in working environment was therefore very desirable and a final measurement programme was agreed upon between these bodies. The Research Secretariat of the Swedish Radiation Protection Institute (SSI) finally agreed to fund the project in such a way that all travellings costs of the participants were covered by the Secretariat. The budget was 225 000 SEK (25 000 ECU), which also covered the costs of a meeting of a small group to discuss the evaluation of the results.

2 DESCRIPTION OF THE IRRADIATION FIELDS

P. Drake
Vattenfall AB, Ringhals, S-430 22 Väröbacka, Sweden

2.1 Reactor fields

Ringhals 2 (875 MW_e), Ringhals 3 (915 MW_e) and Ringhals 4 (915 MW_e) are pressurized water reactors of Westinghouse design. The reactors were commissioned in 1975, 1981 and 1983 respectively. The measurements at Ringhals for this project were performed at reactors 2 and 4 [1].

Inside the reactor containment there is a steel tank with the fuel in fuel elements in the lower part surrounded with water for moderation of neutrons and for cooling the core. Fission neutrons from the fuel will be moderated by the surrounding water and the internal parts including control rods. The neutrons will undergo additional energy degradation as it passes through the walls of the steel tank, the construction material around the tank such as concrete, the air inside the containment and the concrete walls of the containment. The neutrons will also be scattered by the construction material, in the containment wall and in the air. Persons, who are inside the containment during operation, will be irradiated with neutrons from all directions with a wide energy spectrum. The neutrons will also react with the material in the containment and produce secondaries such as photons from (n;γ)-reactions. (n;γ)-reactions with hydrogen and iron will dominate the photon spectrum. Activation products circulating in the cooling water or fixed to the inner walls of the primary cooling system will also contribute to the photon spectrum.

Four different locations were chosen for the mixed neutron photon measurements at Ringhals. The locations were chosen to give several neutron spectra and dose equivalent rates in order to give a wide variation in the test conditions. The positions where the neutron spectra are thought to have the highest mean neutron energy, were not possible to choose due to high dose rates and to reactor safety regulations.

Inside the containments the noise levels are high. A disturbance from varying electro-magnetic fields was anticipated from the electric installations inside the containments.

There are several constraints on measurements inside reactor containments during operation.

1. Any equipment which is to be brought into the containment should be tested for possible unwanted influence on reactor safety instrumentation.
2. The amount of aluminum in detectors and electronics should be kept at a minimum as aluminum will react with sodium hydroxide in the spray which will be used in the case of an accident.
3. Fire hazards should be kept at a minimum.
4. All equipment must be fastened to a secure part in the containment structure to prevent the equipment from becoming a missile in the case of a main steam line break.
5. The time in the containment must be kept at a minimum due to the high radiation levels and the high temperatures.
6. The number of passages through the lock must be kept at a minimum to minimize the risk for decreasing the leak tightness of the doors in the lock.

7. Material should not be brought into the containment if it could clog the containment sump in cases where the containment spray is used.

The measurement program was accepted by the managers of operation at Ringhals 2 and 4 after we had written an instruction which showed how the safety constraints were handled. The work at Ringhals for each measurement period was also regulated by a work permit and a health physics permit.

The measurements were performed at three different occasions. The first occasion was a 2 weeks period in November 1992 when most of the systems were employed. The second occasion was a 2 weeks period in March 1993 when two time consuming tests were performed together with a few complementary dosemeter irradiations. The third occasion was a 3 weeks period in October 1993 when additional information was collected, at two positions at Ringhals 4, concerning the angular distribution of the neutron fields. Between the second and third occasion the reactor was refuelled with a new fuel pattern which decreased the intensity of both the photon and the neutron fields.

The stability of the radiation fields at the measuring positions was checked during the measuring periods with ex-core detectors (detectors which measure the neutron leakage from the reactor vessel and the reactor power). A change in the radiation field between the two main measuring periods was checked with a TEPC counter from the Swedish Radiation Protection Institute (SSI). In addition extra measurements were made at varying time intervals at all positions (most frequent inside the lock) with a Studsvik rem counter 2202D (serial number 8035) and a GM-counter detector (AD3, Automess, Ladenburg, Germany). Close to the two positions with the highest dose rates and next to the wall inside the containments a Gammameter 2414 and a Studsvik 2202D rem counter were used during the measurements in the first period and at Ringhals 2 an additional GM-detector was placed. These extra detectors were all connected to printers or plotters.

The first measurement position is inside the lock leading into the containment around the reactor at Ringhals 4. This position is behind a thick steel door. Here the equipment was tested for proper functioning before it was allowed inside the containment. This gave the Ringhals safety organisation a chance to see the equipment in operation and to make final arrangements for the measurements inside containment. At this position the neutron and the gamma parts of the dose equivalent rate were about 200 μSv/h and 70 μSv/h respectively. The temperature was about 20 °C.
This position is called **L**.

The second position is on the entrance level inside the containment in Ringhals 4. This position is shielded from direct irradiation from the core by the surrounding water in the reactor vessel and by the iron wall of the vessel in addition to this shielding the core is partly shadowed of concrete structures around the vessel and by a steel refuelling machine. Here the neutron and the gamma parts of the dose equivalent rate were about 1500 μSv/h and 400 μSv/h respectively. The temperature was about 45 °C.
This position is called **A**.

The third position is inside the containment of Ringhals 2 and it is similar to position A. Here the neutron and the gamma parts of the dose equivalent rate were about 1000 μSv/h and 400 μSv/h respectively. The temperature was about 45 °C.
This position is called **F**.

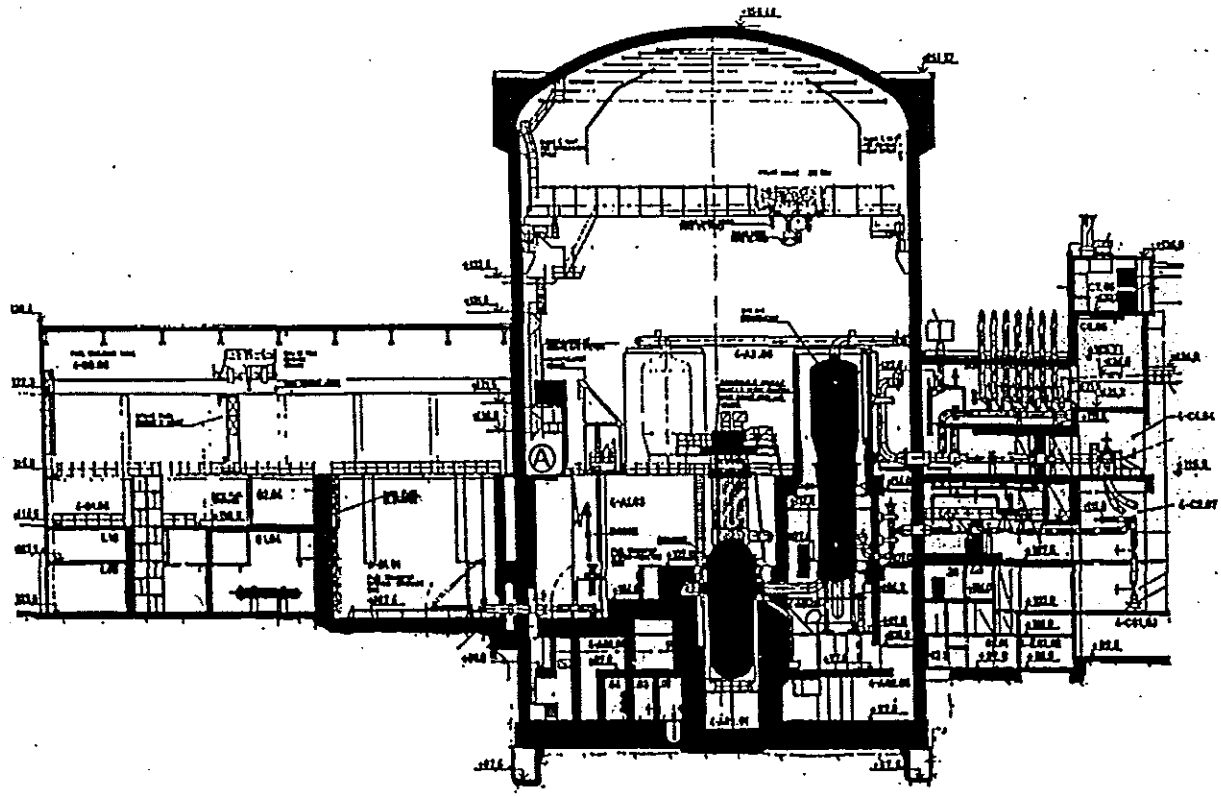

Figure 2.1.1 - Cross-section of Ringhals unit 4 showing position A and the reactor tank inside the containment.

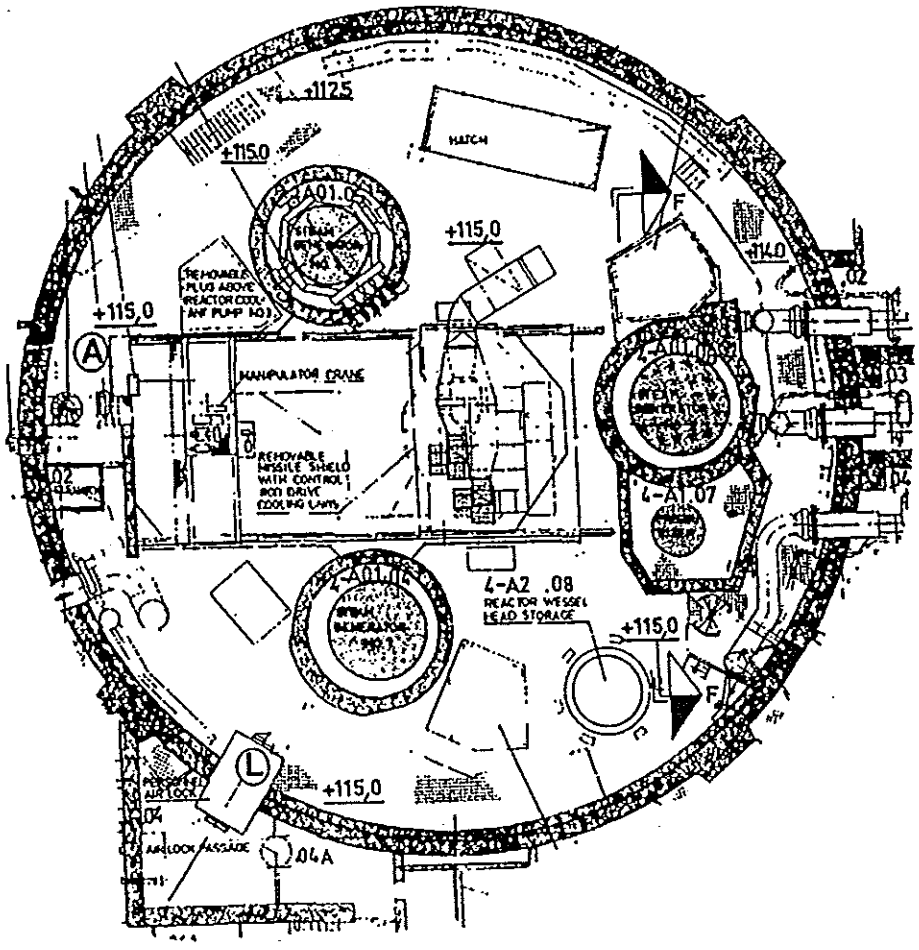

Figure 2.1.2 - Layout of Ringhals unit 4 containment showing positions A and L at the + 115 meter level inside the containment.

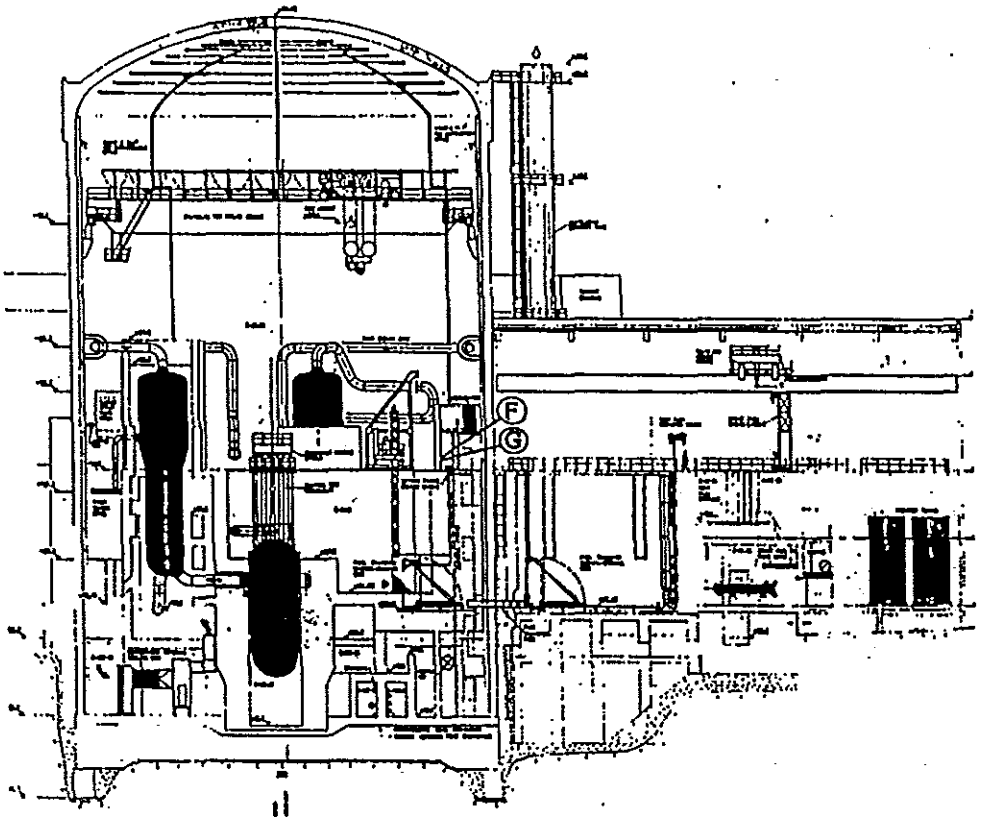

Figure 2.1.3 - Cross-section of Ringhals unit 2 showing positions F and G as well as the reactor tank inside the containment.

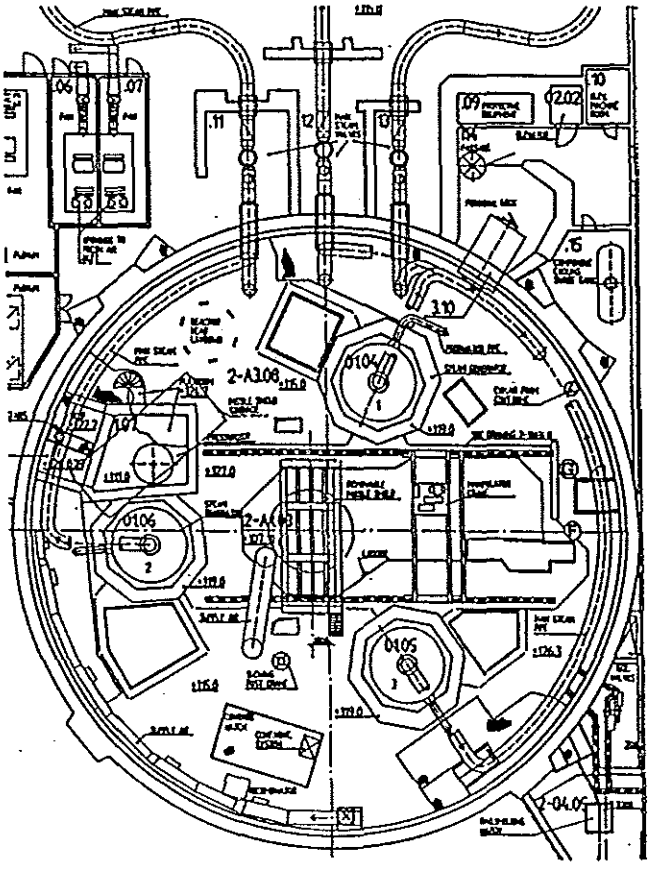

Figure 2.1.4 - Layout of Ringhals unit 2 containment ing positions F and G at the + 115 met inside the containment.

The fourth position is inside the containment of Ringhals 2. This position is close to position F and it is shielded by about 50 cm of extra concrete as compared to position F. Here the neutron and the gamma parts of the dose equivalent rate were about 100 μSv/h and 70 μSv/h respectively. The temperature was about 45 °C.
This position is called **G**.

The measurement positions at Ringhals are shown on the station layouts in Figures 2.1.1 - 2.1.4.

2.2 Fields around a Transport Cask for Spent Fuel

Spent fuel is transferred to transport casks under water in special fuel handling pools at the Swedish reactor units. The casks are then lifted up from the pools, the water is evacuated and the outsides of the casks are cleaned. The casks are transported to the Swedish Central Interim Storage Facility for Spent Nuclear Fuel (CLAB) at the Oskarshamn reactor site by a special transport system which includes dedicated trailers and a dedicated ship. During handling at the reactor sites and during transport the collective effective dose is only a small proportion of the collective effective dose from the operation and maintenance of the reactors.

The CLAB includes different handling positions for casks with spent fuel. At the positions were the casks are handled in air the dose equivalent rates can be substantial and malfunctions here are lead to high personnel doses [2].

The measurements at CLAB were performed during a two week period in November 1992 when are spent fuel cask from Ringhals 2 was received.

There are a few constraints also on measurements inside CLAB:

1. Fire hazards should be kept at a minimum.
2. The time in high radiation areas must be kept at a minimum.

The measurement program was accepted by the manager of CLAB. The work at CLAB was also regulated by a work permit and a health physics permit.

The stability of the radiation fields at the measuring positions were checked during the measuring periods with a Studsvik rem counter 2202D and a GM-counter detector (AD3, Automess, Ladenburg, Germany).

All measurements were performed inside a 25 metre long and 8 metre wide storage hall. The cask was always horizontal and centred in the room. The temperature was about 20°C

Three different locations were chosen for the mixed neutron gamma measurements at CLAB. The locations were chosen to give several neutron spectra and dose equivalent rates.

The first measurement position is at a 1 meter distance from the surface of the cask and at the same elevation as the centre of the cask. Here the neutron and the gamma parts of the dose equivalent rate were about 60 μSv/h and 90 μSv/h respectively.
This position is called **D**.

The second measurement position is at the opposite side of the cask and 0.83 metres from the front edge of the neutron shielding. This measurement position is at 1 metre distance from the

surface of the cask and at the same elevation as the centre of the cask. Here the neutron and photon parts of the dose equivalent rate were expected to be lower than at position D due to the closer proximity to the end of the cask and thereby a longer average distance to the spent fuel inside the cask.
This position is called **E**.

The third measurement position is at the same side of the cask as position E and above the neutron shielding. This measurement position is also at a 1 metre distance from the surface of the cask and at the same elevation as the centre of the cask. Here the neutron and the gamma parts of the dose equivalent rate were expected to be higher than at position D due to the decreased shielding.
This position is called **P**.

Figures 2.2.1 - 2.2.4 show the transport cask and the measurement positions at CLAB.

The measurements at CLAB were complemented in February 1994 by measurements on another transport cask-spent fuel combination at Ringhals with dosemeters on phantom and with a remcounter. The measurement positions were similar to positions E and D, but the distances to surrounding walls were smaller. These measurements were performed in order to get information concerning the angular distribution of the neutron and photon fields at position E as dosemeter measurements were not performed at this position at CALB in 1992.

References

[1] *Technical Description of Ringhals Nuclear Power Plant.* Vattenfall AB Ringhals, Väröbacka, Sweden. 1987.

[2] *Central Interim Storage Facility for Spent Nuclear Fuel - CLAB.* The Swedish Nuclear Fuel and Waste Management Company, Stockholm, Sweden. 1991. Information brochure.

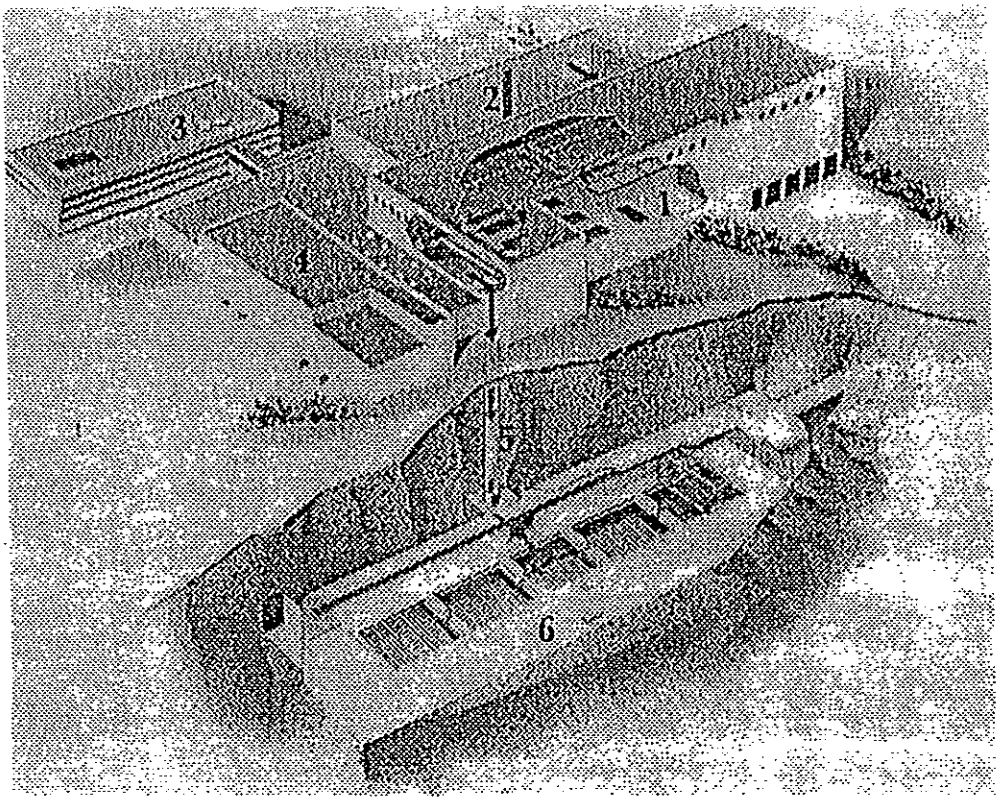

1. Reception building
2. Building for auxiliary systems
3. Office building
4. Electrical building
5. Fuel elevator
6. Storage building

Figure 2.2.1 - Overview of the Swedish Central Interim Storage Facility for Spent Nuclear Fuel (CLAB).

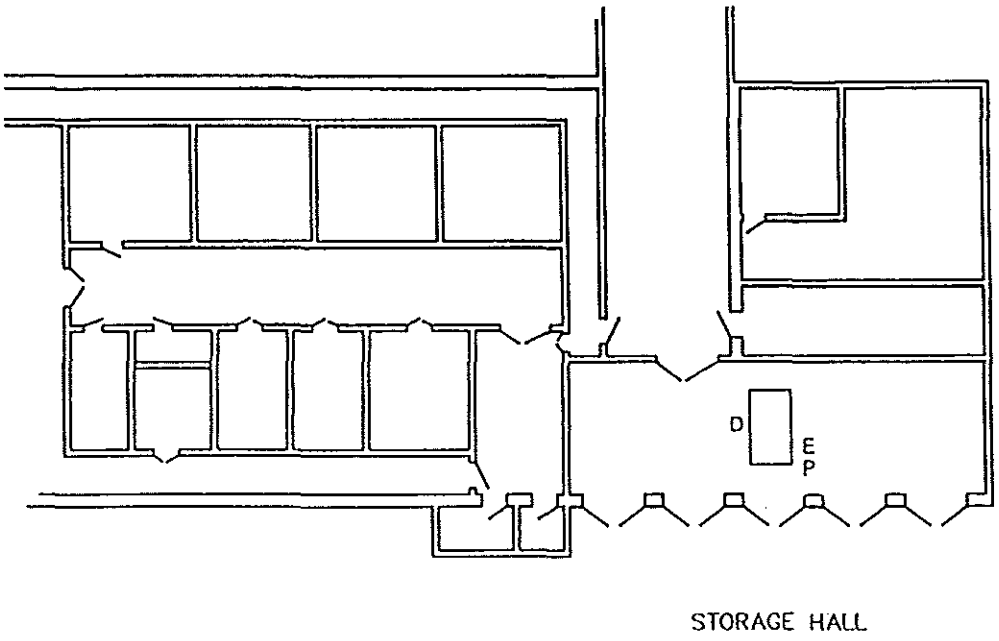

Figure 2.2.2 - Layout of CLAB showing positions D, E and P in the storage hall.

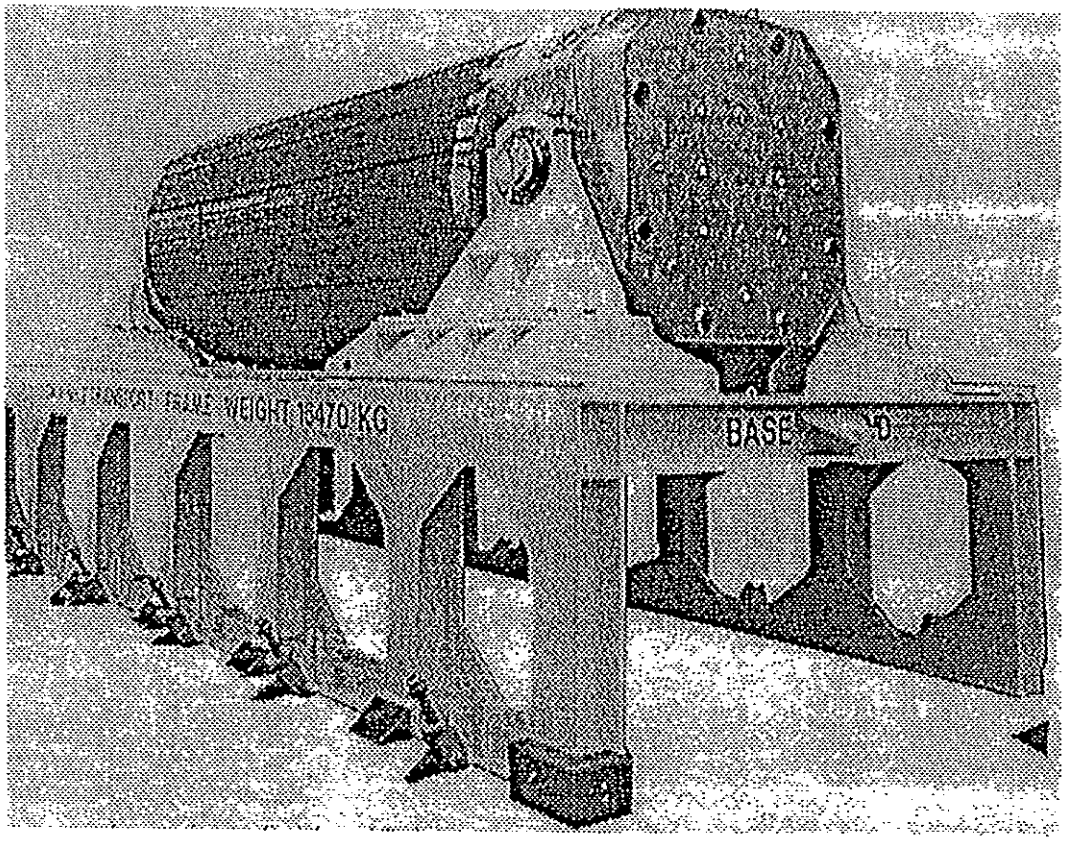

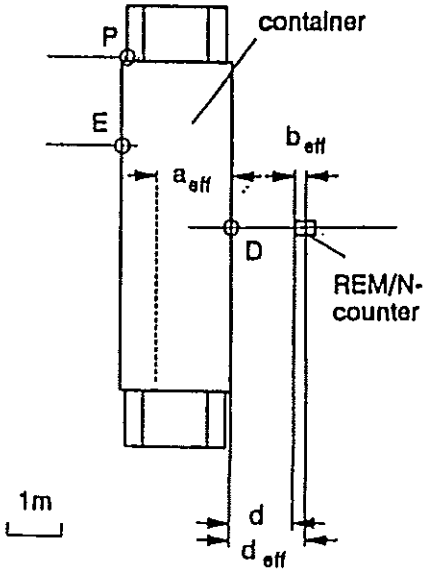

Figure 2.2.3 - The transport cask for spent nuclear fuel.

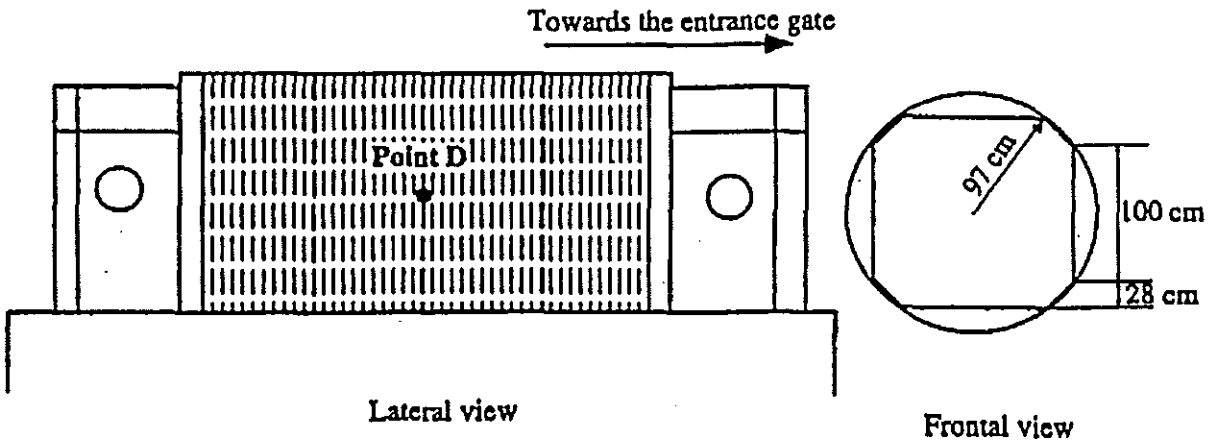

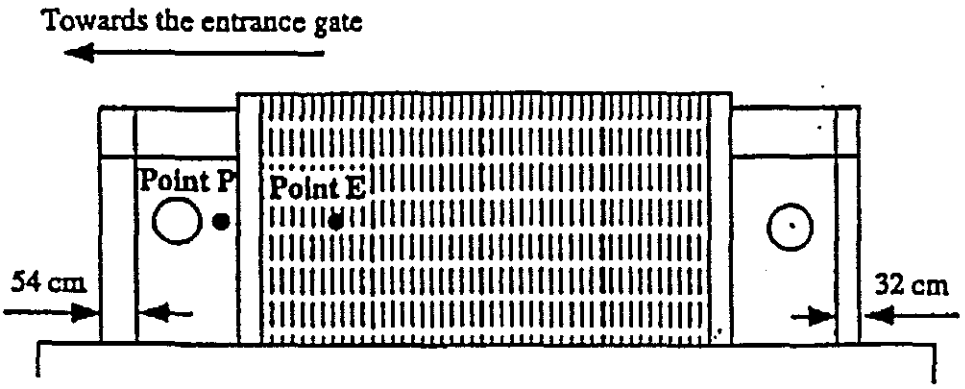

Lateral view

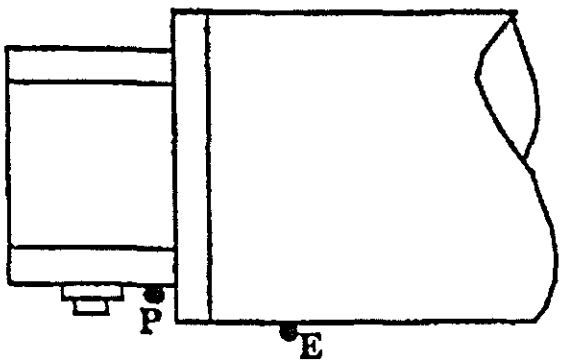

Top view

At the 3 measurement locations the centre of the spheres was at 1m from the surface of the container

Figure 2.2.4 - Measuringpositions D, E and P around the transport cask.

3. NEUTRON SPECTROMETRY

3.1 Measurements with the GSF Bonner Sphere Spectrometer and an Anderson & Braun-Type Rem Counter

H Schraube, J.Jakes, G.Schraube, and E.Weitzenegger
GSF - Forschungszentrum Neuherberg, D85758 Oberschleissheim Germany

3.1.1 Introduction

The GSF group participated in the joint intercomparison study at the sites of the Ringhals reactors R2 and R4, and the Central Storage of Used Fuel (CLAB) at Oskarsham in November 1992. The aim of study was to derive spectral data under well defined and reproducible conditions, and to obtain integral dose quantities as required in radiological protection. For this purpose a Bonner sphere spectrometer and a conventional REM-meter were used.

3.1.2 REM-Counter

A conventional Anderson & Braun Rem-counter (20th Century REM/N#7627-615) with pulse height registration in a multichannel-analyzer was employed to measure ambient dose equivalent rates as it is conventionally done in radiation protection survey routine. The Rem-counter had been calibrated face-on with an AmBe-source using the ambient dose equivalent conversion factor $h^*(10) = 386$ pSv·cm^2.

A total of 13 measurements were taken: 8 at CLAB, 2 at R4, and 3 at R2. The orientation of the counter was "face-on" with respect to the fuel container, and also "face-on" in direction to the estimated position of the reactor core. At CLAB, however, it was necessary to take measurements at several distances from the fuel containers, because of its extended radiating size. In this way an "effective" position of the source was derived.

In table 1, the data are listed with d_{eff} = distance between effective centre of counter to surface of container, N = integrated number of pulses counted, t_M = the measuring time, and the sdev = the standard deviation. At the experimental positions D and E, readings were taken at 3 different distances d = 80, 90, and 100 cm (i.e. d_{eff} = 95, 105, and 115 cm), in order to determine approximately the "effective centre" of the source and to permit an interpolation with respect to the Bonner-sphere position described later on.

In figure 1 the measurements are normalized to 100 cm from the container surface with the following conditions:
effective centre of the counter: b_{eff} = 15 cm behind the surface of the counter,
effective centre of the source : a_{eff} = 165 cm behind the surface of the container (see figure 2).

These data were obtained by a simultaneous semiempirical fit. The average dose rate data are: $H^*(10) = 43.9(1\pm0.02)$ (µSv/h) at position "E" and $H^*(10) = 53.0(1\pm0.003)$ (µSv/h) at position "D". At position "P" the value $H^*(10) = 50.6$ µSv/h is derived using the same data for the effective centres.

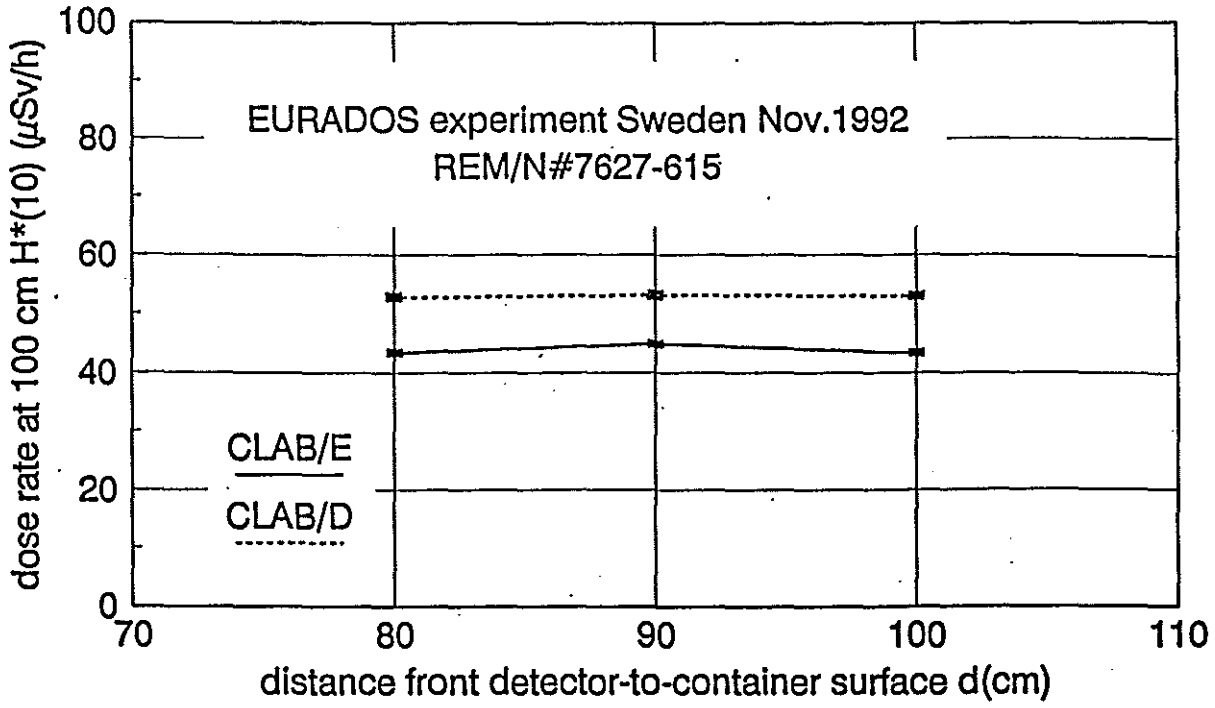

Figure 1: Dose equivalent rates obtained by means of the REM/N detector at CLAB/D and E, normalized to a 100 cm effective distance from the surface of the container (d refers to the detector front!).

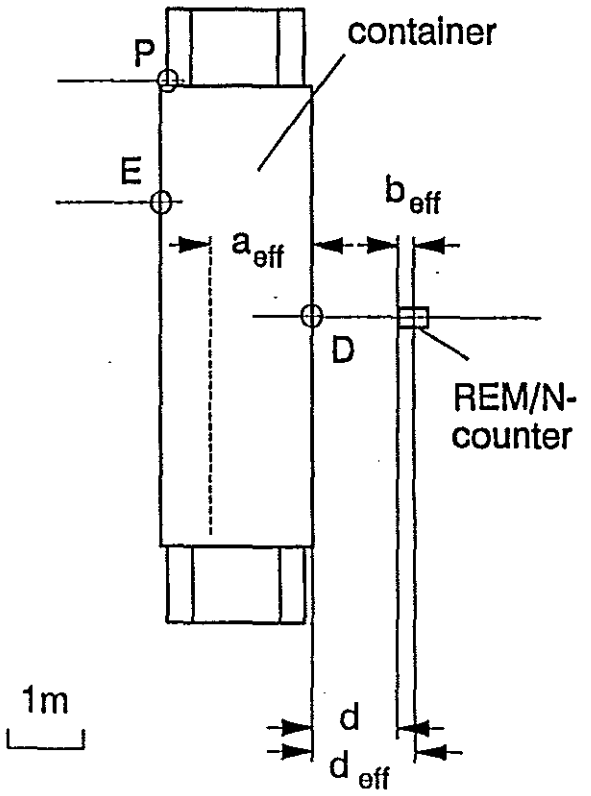

Figure 2: Experimental arrangement at the CLAB. The BSS was placed with its geometrical centre at d_{eff} = 100 cm.

The observed depth $a_{eff} = 165$ cm inside the container, as derived by the REM-counter measurements from outside of the container, is considerably larger than the half thickness of the container. This is due to the effect that the neutron source, i.e. the spent fuel element, is a line source rather than a point source.

Figure 1 proves the value of $a_{eff} = 165$ cm as the dose rate normalized to $d_{eff} = 1$ m via $1/r^2$ - law is independent from the experimental distances d_{eff}.

3.1.3. Bonner Sphere Spectrometer

The Bonner-sphere spectrometer (BSS) was equipped with a 4 x 4 mm cylindrical ^{6}LiI(Eu) scintillator, photomultiplier and multichannel analyzer. The responses of the BSS had been determined in an interlaboratory experiment with fast neutrons [1] and with thermal neutrons [2]. Recent Monte Carlo calculations [3] agreed well with the experimental findings when a calibration factor of 0.72 (±1% s.e.m) was applied to the calculated data.

3.1.3.1 Data Acquisition and Preparation

The BSS employed consisted of spheres with 2,3,4,7,8,10, and 12"diameter and the bare ^{6}LiI detector. From the pulse height distributions, the photon background was subtracted by nonlinear fitting procedure, to derive the number of neutron induced events. The Bonner spheres were placed with their geometrical centre to the reference points, as given by the organizers.

3.1.3.2 Unfolding of the Count Rate Vector

The iterative unfolding code SAND II [4] was employed to derive the spectral neutron fluence. For all conditions a unique start-spectrum was used as the first estimate with the following spectral components:

- a thermal Maxwellian (T=293K),
- a fast fission in the Cranberg representation and
- an 1/E slowing down part with intersections at 0.1 eV with the thermal and at 0.5 MeV with the fast neutron peak, respectively (see **figure 5** in the Appendix).

Estimated uncertainties of the count rate of each sphere were derived from the counting statistics of the total counts for each sphere, multiplied by a factor 1.5 to allow for the uncertainty of the background subtracting method. The squares of the inverse uncertainties were used as weights in the unfolding procedure. The response matrix in the interpolated form of Mares and Schraube [3] was used. The iterative calculation was finished when the relative improvement, expressed in changes of χ^2 from one iteration to the next one, became less than a factor 10^{-10}. This required between 1000 and 2500 iterations.

3.1.4 Results

The data of the total fluence rates and the dose-equivalent rates H^*/t_M applying the conversion function of Wagner et al.[5] are listed in **table 1** (see Appendix).

In **table 2** the full data set obtained from the unfolding procedure for all experimental sites is listed. Three different functions are applied to convert neutron fluence to dose equivalent:

i) maximum dose equivalent H_{made} in accordance with ICRP 21 [6],
ii) ambient dose equivalent after Wagner et al. [5], applying the Q(L) - relationship after ICRP 21 [6],
iii) ambient dose equivalent $H^*(10)$ applying the Q(L)-relationship after ICRU 60 [7] in the analytic form after Leuthold et al. [8].

The dose equivalent rates and the fluence rates are listed for five energy ranges >0.01 eV to 0.4 eV, >0.4 eV to 10 keV, >10 keV to 100 keV, >100 keV to 1 MeV and above 1 MeV. The integration over the 5 energy ranges for fluence and dose equivalent rates was done in a separate computer program using the spectral fluence data of the unfolding procedure. For comparison reasons, the integral data obtained directly from the unfolding code and reported in the first evaluation document are given as well. in the table. The differences due to calculation uncertainties of the two computer codes applied do not exceed 1%. One exception was CLAB-E were because of an error in the experimental data transmission of one Bonner sphere, the fluence rate was changed by ca.1%, the dose equivalent rate, however, by ca.16%.

In **figure 3** the dose rates measured at the 8 experimental positions are depicted. They refer to ambient dose equivalent H*(10) with Q(L) after ICRP 21. Generally, the REM/N counter reads more than the values calculated from the BSS-spectra. This overresponse is between 8 and 20% for the CLAB site, approximately 30% at the Ringhals R4 site, and between 20% and 64% at the Ringhals R2 site.

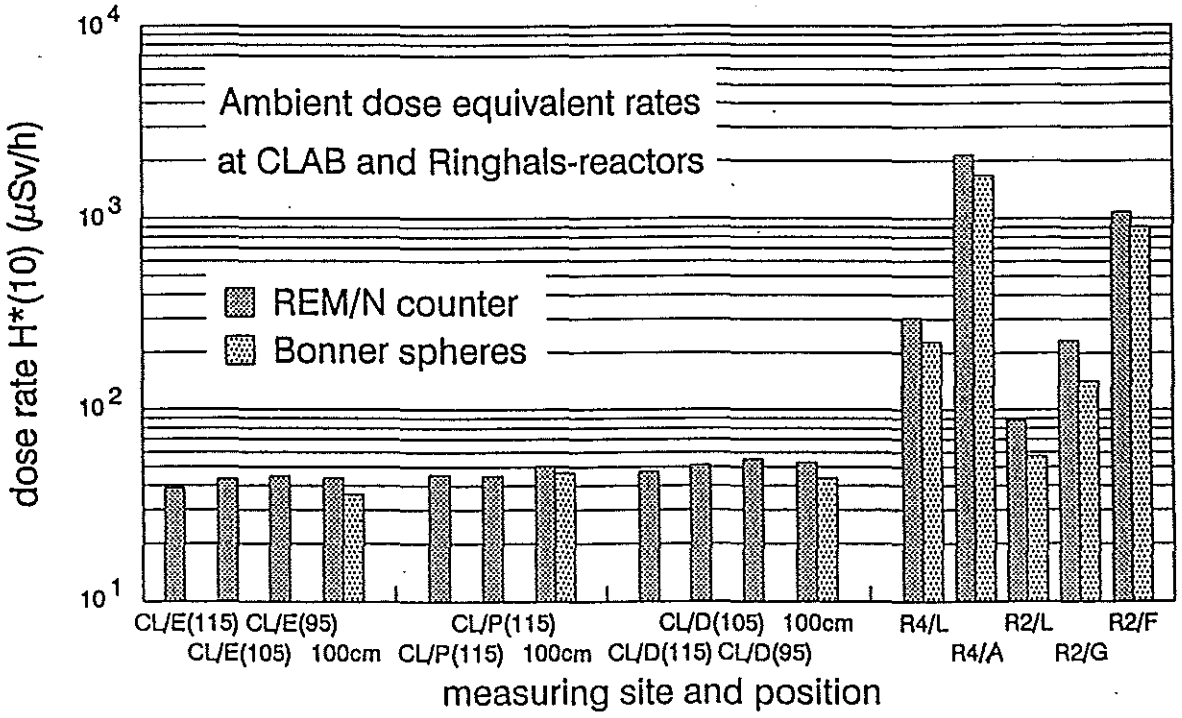

Figure 3: Dose equivalent rates obtained at the 3 CLAB and the 5 reactor positions using the REM/N detector and the Bonner sphere spectrometer. The REM/N data are reduced to 100 cm effective distance from the container (labeled with "100 cm") to permit a comparison with the Bonner sphere data at CLAB.

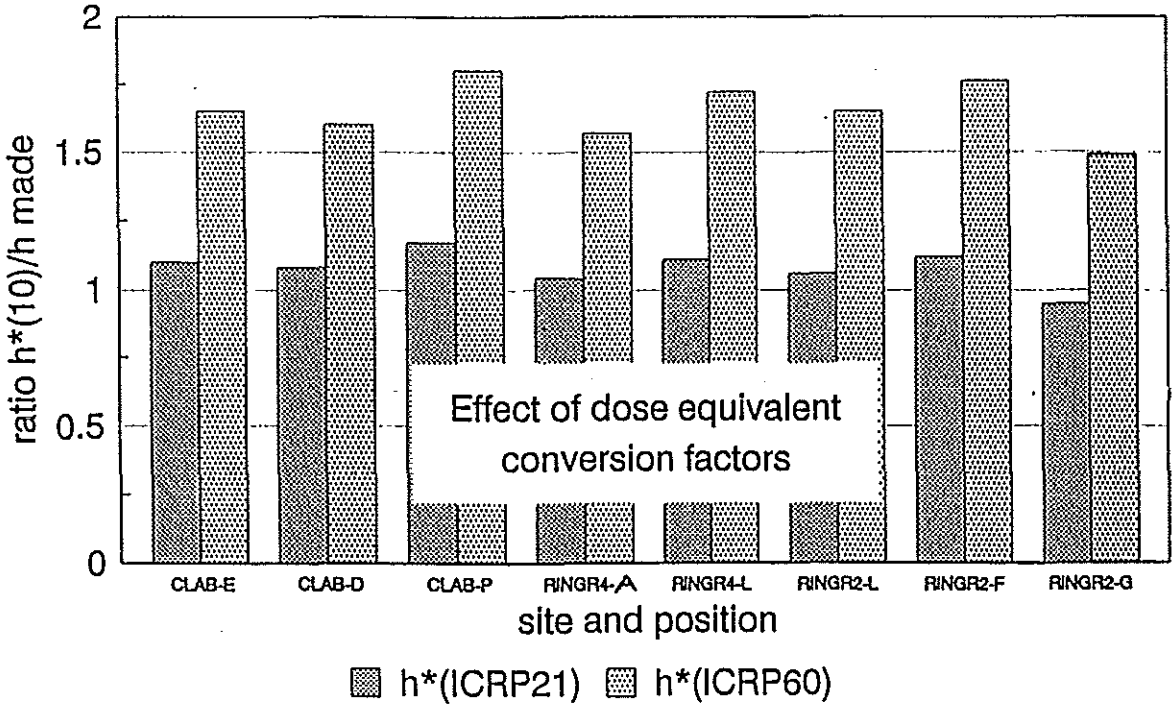

Figure 4: Effect of using ambient dose equivalent H*(10) H_{made} with Q (L) after ICRP 21 and ICRP 60, respectively, instead of maximum dose equivalent at the 8 experimental positions.

The effect of using different fluence-dose conversion can be derived from **table 2** (see Appendix) and is given in **figure 4** in graphical presentation. The change from H_{made} to H* (10) (with Q(L) after ICRP 21) increases the dose equivalent between 6 and 17%, but also decreases slightly in one case. The change to the H*(10)-function with the modified quality factor after ICRP 60, increases the dose equivalent by a factor between 1.5 and 1.8.

The unfolded spectral distributions are plotted in **figures 6** through **13** (see Appendix). For control reasons these spectra were again folded with the response matrix in order to receive an evaluated count rate. The ratios of the measured and the evaluated count rates gave some indication to the quality of the unfolding. The standard deviation of these ratios were in between 0.8 and 1.7%. At two positions, i.e. at Ringhals 4 positions L and A, however, the standard deviation was as high as 5% indicating some experimental imperfections with the 10" sphere.

3.1.5 References:

[1] Alevra, A.V., Cosack, M., Hunt, J.B., Thomas, D.J., Schraube, H., *Experimental determination of the response of four Bonner sphere sets to monoenergetic neutrons (II).* Radiat. Prot. Dosim. 40 (1992) 91-102.

[2] Thomas, D.J., Alevra, A.V., Hunt, J.B., Schraube, H., *Experimental determination of the response of four Bonner sphere sets to thermal neutrons.* Radiat. Prot. Dosim. 54, 1 (1994) 25-31.

[3] Mares, V., Schraube, H., *Evaluation of the response matrix of a Bonner sphere spectrometer with LiI detector from thermal energy to 100 MeV.* Nucl. Instr. Meth. in Physics Research **A 337** (1994) 461-473.

[4] Alevra, A.V., Siebert, B.R.L., Aroua, A., Buxerolle, M., Grecescu, M., Matzke, M., Mourgues, M., Perks, C.A., Schraube, H., *Unfolding Bonner-sphere data: A European intercomparison of computer codes.* PTB-laboratory report 7.22-90-1 January (1990).

[5] Wagner, S.R., Grosswendt, B., Harvey, J.R., Mill, A.J., Selbach, H.-J., Siebert, B.R.L., *Unified conversion functions for the new ICRU operational radiation protection quantities.* Radiat. Prot. Dosim. **12** (1985) 231.

[6] ICRP 15, ICRP 21: *Protection against ionizing radiation from external sources.* (Report of ICRP Committee 3, ICRP 15). *Data for protection against ionizing radiation from external sources* (ICRP 21). International Commission on Radiological Protection (1971).

[7] ICRP Publication 60: 1990. *Recommendations of the International Commission on Radiological Protection.* Annals of the ICRP, Pergamon Press 17, 2/3 (1991).

[8] Leuthold, G., Mares, V., Schraube, H., *Calculation of the neutron ambient dose equivalent on the basis of the ICRP revised quality factors.* Radiat. Prot. Dosim. **40** (1992) 77 - 84.

3.1.6 Appendix

The Appendix contains the Figures 5 - 13 and the Tables 1 and 2.

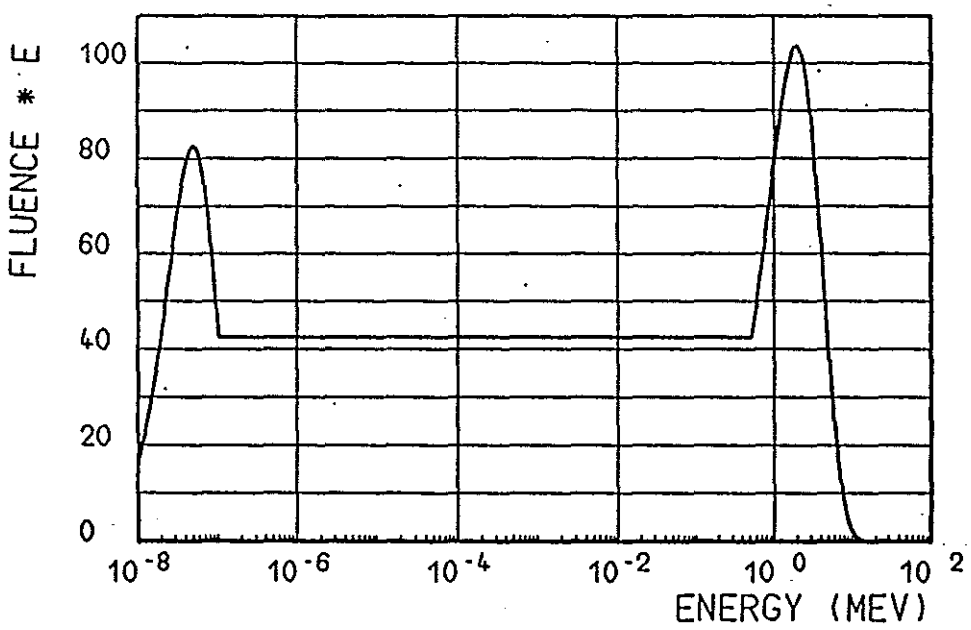

Figure 5: Start spectrum applied for unfolding of the Bonner sphere data.

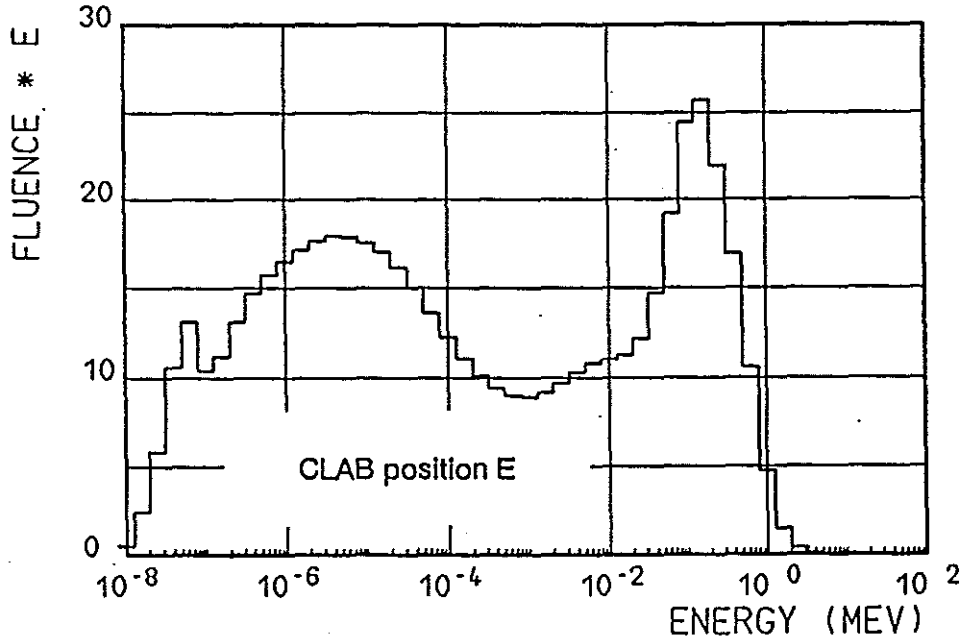

Figure 6: Unfolded spectral distribution (fluence rate per log. energy interval) $\Phi_E \cdot E\,(cm^{-2} \cdot s^{-1})$ obtained at the CLAB measuring position E.

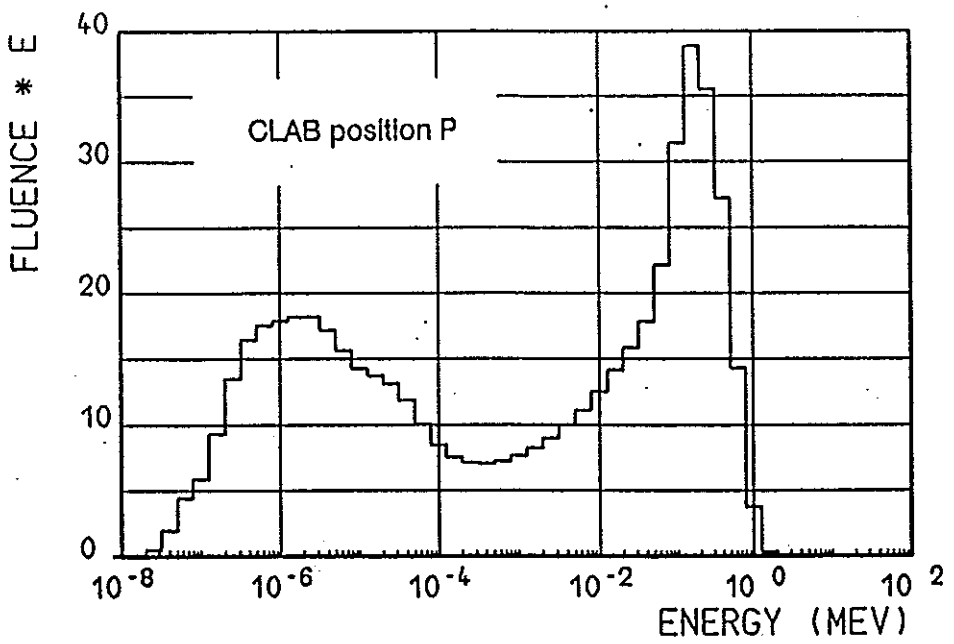

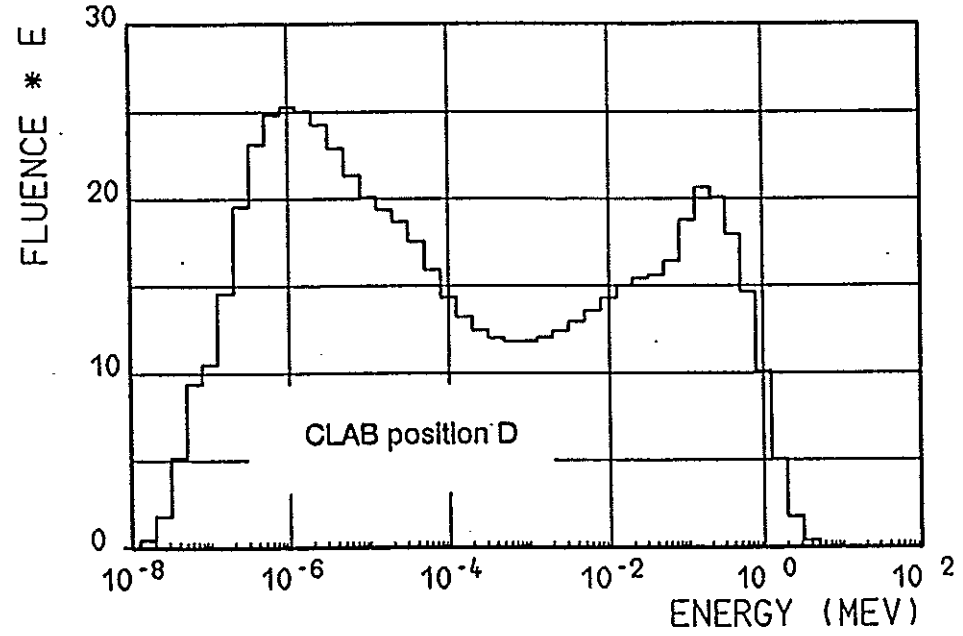

Figure7 and 8: Unfolded spectral distribution (fluence rate per log. energy interval) $\Phi_E \cdot E$ ($cm^{-2} \cdot s^{-1}$) obtained at the CLAB measuring positions P and D.

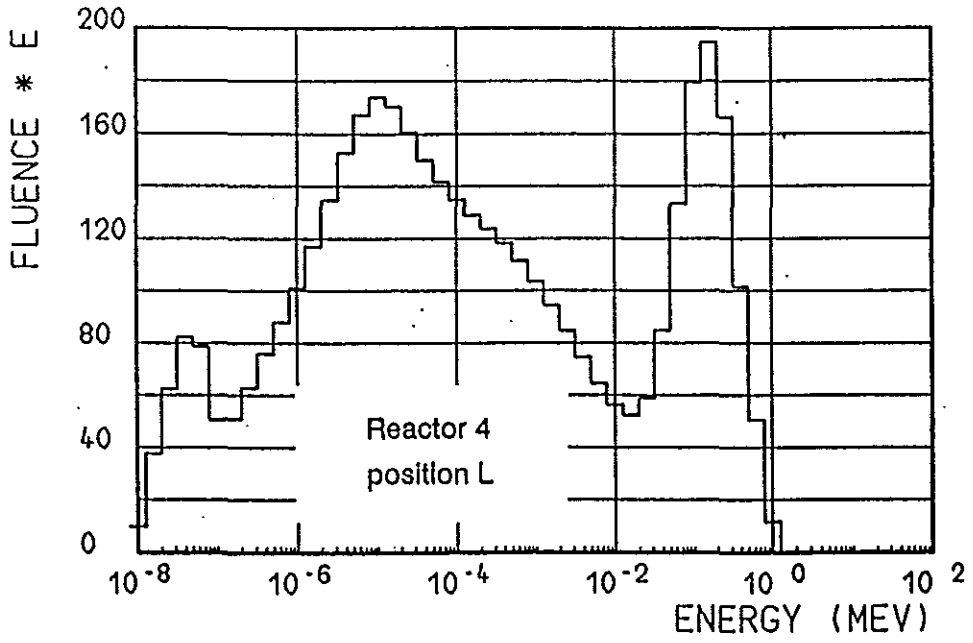

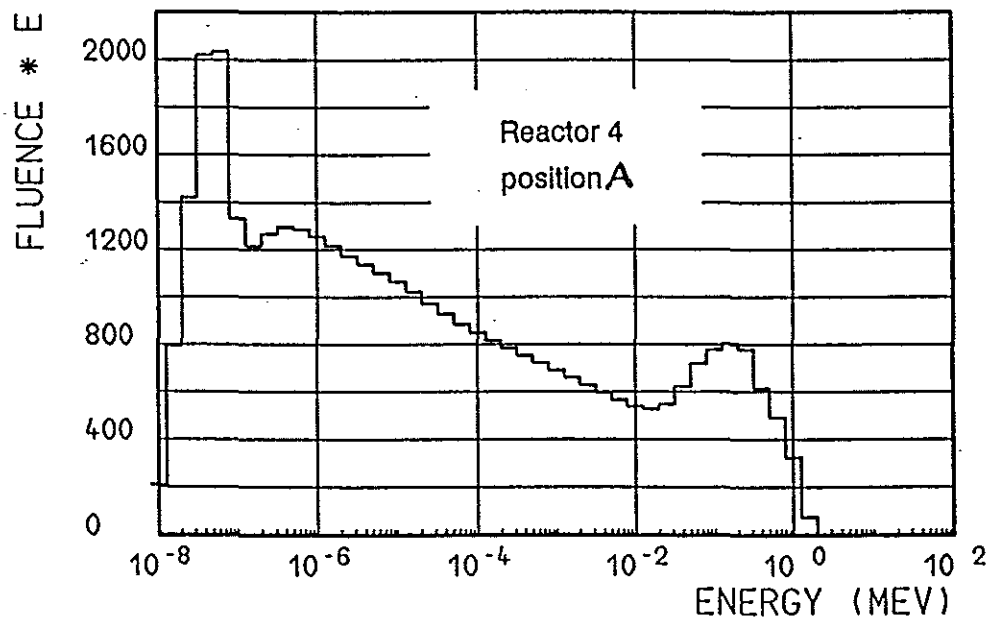

Figure 9 and 10: Unfolded spectral distributions (fluence rate per log. energy interval) $\Phi_E \cdot E$ ($cm^{-2} \cdot s^{-1}$) obtained at the reactor measuring positions L and A of the Ringhals reactor 4.

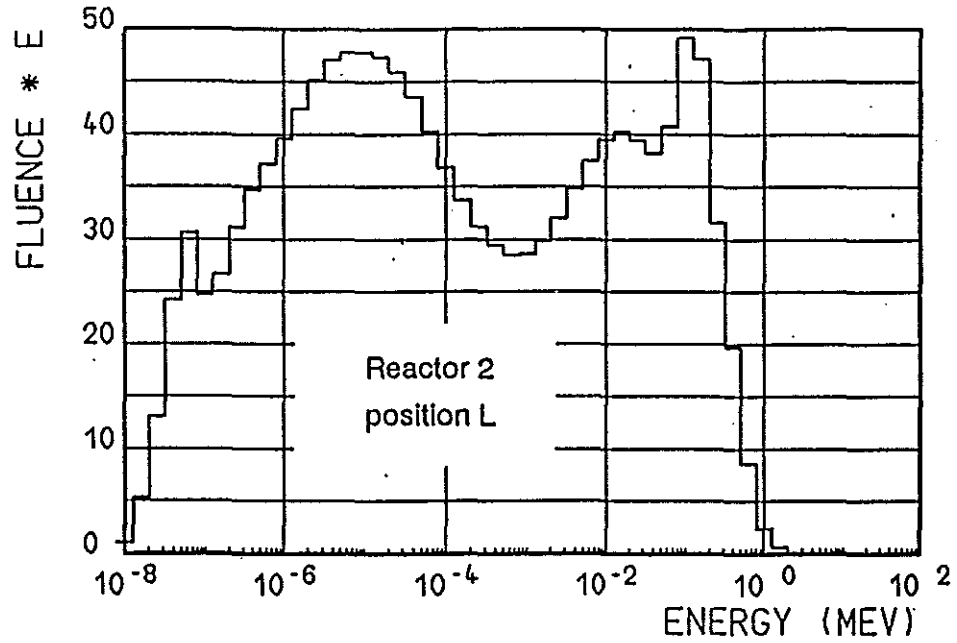

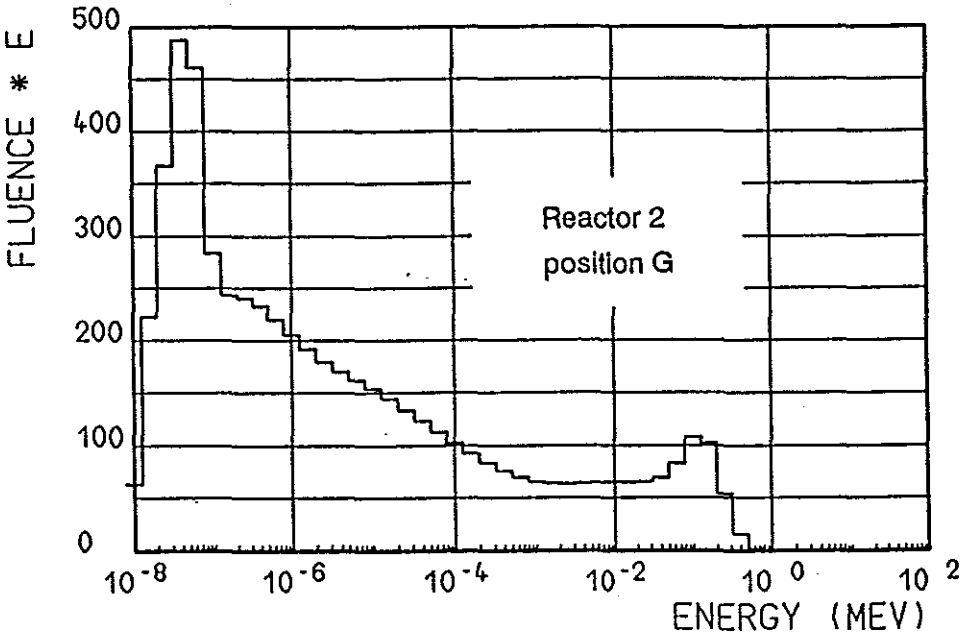

Figure 11 and 12: Unfolded spectral distributions (fluence rate per log. energy interval) $\Phi_E \cdot E$ ($cm^{-2} \cdot s^{-1}$) obtained at the reactor measuring positions L and G of the Ringhals reactor 2.

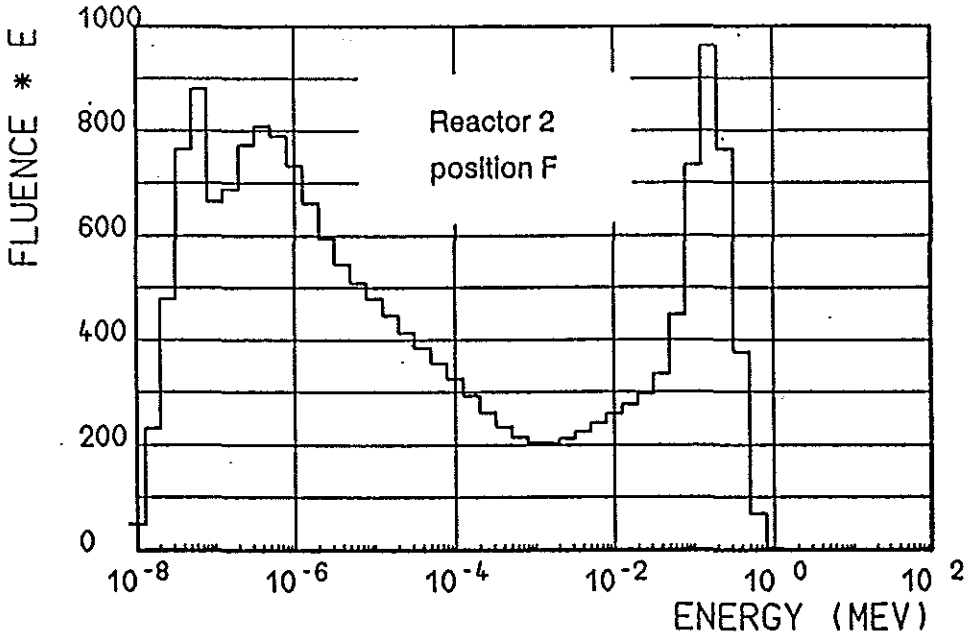

Figure 13: Unfolded spectral distributions (fluence rate per log. energy interval) $\Phi_E \cdot E$ ($cm^{-2} \cdot s^{-1}$) obtained at the reactor measuring position F of the Ringhals reactor 4.

Table1: Ambient dose equivalent data determined at CLAB-Okarsham and the Ringhals reactors employing theREM/N-counter and the Bonner sphere spectrometer (BSS). The distance deff refers to the estimated effective centre of the REM/N meter, and to the position of the thermal detector of the BSS, respectively.

CLAB-position	CL/E(115)	CL/E(105)	CL/E(95)	norm. to 100 cm		CL/P(115)	norm. to 100 cm	CL/D(115)	CL/D(105)	CL/D(95)	norm. to 100 cm
REM/N-counter:											
deff (cm)	115	105	95	100	115	115	100	115	105	95	100
H* (µSv)/h	38.8	43.2	45.1	43.9	45.7	45.0	50.6	47.5	51.2	54.9	53.0
N	18133	15165	15829		21542	21036		22199	11961	12835	
rel.sdev	0.007	0.008	0.008		0.007	0.007		0.007	0.009	0.009	
tM (s)	2000	1500	1500		2018	2000		2000	1000	1000	
Bonner Spheres:											
H*/tM (µSv)/h				36.3			46.7				43.9
PHI tot (1/cm^{2}s)				2.48E+02			2.47E+02				2.91E+02

reactor-position	R4/L	R4/A	R2/L	R2/G	R2/F
REM/N-counter:					
H* (µSv)/h	304.8	2157.6	87.9	232.6	1088.0
N	21380	50447	10271	11530	25439
rel. sdev	0.007	0.004	0.010	0.009	0.006
tM(s)	300	100	500	212	100
Bonner-Spheres:					
H*/tM (µSv)/h	228.0	1676.0	57.2	142.2	906.5
PHI tot (1/cm^{2}s)	1.93E03	1.72E04	6.24E02	2.64E03	8.36E03

file: tabschr1

Table 2: Summarized integral neutron fluence and dose equivalent data as obtained fromfrom measurements at CLAB and Ringhals-reactors by the GSF group. The data are calculated by folding of the spectral fluence rates by the three conversion functions: h*(10) after Leuthold et al.(1992), h*(10) after Wagner et al.(1985) and h(MADE)after ICRP21(1973). The originally reported integral data from the unfolding procedure are given as well.

place and position	energy range	PHI ($1/cm^2 \cdot s$)	H*10 Leuthold (ICRP60) (μSv/h)	H*10 Wagner (ICRP21) (μSv/h)	H_{made} (ICRP21) (μSv/h)
CLAB-E	P1	3.430E+01	1.809E+00	1.166E+00	1.430E+00
	P2	1.427E+02	6.520E+00	4.226E+00	5.560E+00
	P3	2.487E+01	6.350E+00	4.021E+00	3.610E+00
	P4	4.343E+01	3.751E+01	2.437E+01	1.940E+01
	P5	3.496E+00	3.243E+00	2.531E+00	2.580E+00
	TOT	2.488E+02	5.544E+01	3.632E+01	3.258E+01
	TOT(SAND)	2.510E+02			37.98
CLAB-D	P1	3.363E+01	1.830E+00	1.182E+00	1.439E+00
	P2	1.752E+02	8.467E+00	5.490E+00	7.177E+00
	P3	3.642E+01	5.911E+00	3.773E+00	3.427E+00
	P4	4.041E+01	3.960E+01	2.614E+01	2.126E+01
	P5	5.659E+00	9.292E+00	7.312E+00	7.464E+00
	TOT	2.913E+02	6.509E+01	4.388E+01	4.077E+01
	TOT(SAND)	2.940E+02			40.82
CLAB-P	P1	2.023E+01	1.112E+00	7.182E-01	8.723E-01
	P2	1.222E+02	5.947E+00	3.859E+00	5.006E+00
	P3	4.231E+01	7.780E+00	4.918E+00	4.402E+00
	P4	6.150E+01	5.558E+01	3.596E+01	2.838E+01
	P5	1.028E+00	1.652E+00	1.262E+00	1.283E+00
	TOT	2.473E+02	7.207E+01	4.673E+01	3.993E+01
	TOT(SAND)	2.500E+02			39.85
RINGR4-A	P1	4.987E+03	2.566E+02	1.653E+02	2.041E+02
	P2	9.221E+03	4.421E+02	2.862E+02	3.779E+02
	P3	1.417E+03	2.406E+02	1.530E+02	1.384E+02
	P4	1.492E+03	1.423E+03	9.346E+02	7.560E+02
	P5	1.095E+02	1.772E+02	1.364E+02	1.393E+02
	TOT	1.722E+04	2.539E+03	1.676E+03	1.616E+03
	TOT(SAND)	1.740E+04			1616.40

P1 :	>0.01 eV	- 0.4 eV
P2 :	>0.4 eV	- 10 keV
P3 :	>10 keV	- 100 keV
P4 :	>100 keV	- 1 MeV
P5 :	>1 MeV	

Table 2, cont'd: Sumarized integral neutron fluence and dose equivalent data

place and position	energy range	PHI (1/cm^2 · s)	H*10 Leuthold (ICRP60) (μSv/h)	H*10 Wagner (ICRP21) (μSv/h)	H_{made} (ICRP21) (μSv/h)
RINGR4-L	P1	2.155E+02	1.112E+01	7.164E+00	8.836E+00
	P2	1.226E+03	5.728E+01	3.701E+01	4.995E+01
	P3	2.058E+02	4.165E+01	2.616E+01	2.318E+01
	P4	2.803E+02	2.405E+02	1.543E+02	1.208E+02
	P5	2.790E+00	4.464E+00	3.392E+00	3.442E+00
	TOT	1.930E+03	3.550E+02	2.280E+02	2.062E+02
	TOT(SAND)	1.950E+03			200.52
RINGR2-L	P1	8.004E+01	4.234E+00	2.730E+00	3.347E+00
	P2	3.885E+02	1.826E+01	1.185E+01	1.572E+01
	P3	9.341E+01	1.502E+01	9.590E+00	8.713E+00
	P4	6.118E+01	5.000E+01	3.190E+01	2.490E+01
	P5	9.226E-01	1.501E+00	1.166E+00	1.189E+00
	TOT	6.240E+02	8.903E+01	5.724E+01	5.387E+01
	TOT(SAND)	6.300E+02			53.93
RINGR2-F	P1	2.260E+03	1.183E+02	7.628E+01	9.377E+01
	P2	4.080E+03	2.032E+02	1.314E+02	1.696E+02
	P3	8.531E+02	1.628E+02	1.026E+02	9.131E+01
	P4	1.170E+03	9.428E+02	5.954E+02	4.566E+02
	P5	7.889E-01	1.261E+00	9.580E-01	9.717E-01
	TOT	8.364E+03	1.428E+03	9.065E+02	8.121E+02
	TOT(SAND)	8.450E+03			815.40
RINGR2-G	P1	1.129E+03	5.753E+01	3.704E+01	4.586E+01
	P2	1.239E+03	6.145E+01	3.971E+01	5.148E+01
	P3	1.703E+02	2.938E+01	1.866E+01	1.681E+01
	P4	1.051E+02	7.510E+01	4.673E+01	3.564E+01
	P5	2.146E-02	3.434E-02	2.608E-02	2.647E-02
	TOT	2.643E+03	2.235E+02	1.422E+02	1.498E+02
	TOT(SAND)	2.680E+03			150.84

P1 :	>0.01 eV	- 0.4 eV
P2 :	>0.4 eV	- 10 keV
P3 :	>10 keV	- 100 keV
P4 :	>100 keV	- 1 MeV
P5 :	>1 MeV	

3.2 Measurements Performed by the Institute of Applied Radiophysics (IAR) Lausanne

A. Aroua, M. Grecescu
Institut de radiophysique appliquée, CH-1015, Lausanne, Switzerland

3.2.1 Introduction

A campaign of measurements involving different European laboratories has been organised in Sweden in November 1992. These measurements aimed to compare the performance of routine instrumentation used for radiation protection dosimetry in neutron fields (neutron spectrometers, TEPCs, monitors and passive detectors, etc.). The measurements took place at the Ringhals nuclear power station inside two PWR reactors and at the CLAB fuel storage facility in Oskarshamn near a spent fuel transport flask (see sections 2.1 and 2.2).

The Institute for Applied Radiophysics (IAR) participated to this campaign with a Bonner spheres spectrometer, an Andersson-Braun rem-counter and an energy compensated Geiger-Müller counter. Measurements have been performed at six locations as shown in Appendix 1.

This report presents the equipment and the experimental procedure, and discusses the spectrometric and dosimetric results.

3.2.2 Measuring equipment

3.2.2.1 Neutron fields

A. Multisphere spectrometer

The determination of the neutron ambient dose equivalent is based on the knowledge of the neutron spectrum. This one is measured by a neutron spectrometer based on a Bonner spheres system [1]. The system consists in a set of polyethylene spheres with the following diameters: 2, 2.5, 3, 4.2, 5, 6, 8, 9, 10, 12, 15 inches. The polyethylene density is 0.916 ± 0.003 g cm^{-3}.

The thermal neutron detector located in the centre of the spheres is a ^{3}He cylindrical proportional counter type 0,5NH10 (LCC, Détecteurs nucléaires Thomson-CSF).

Besides the spheres set, the following additional detectors are routinely used: the bare ^{3}He counter and the same counter surrounded by a 1.4 mm cadmium cover.

The 15 inch sphere has not been used in the measurements described in the present report.

The pulses of the proportional counter are amplified by a charge-sensitive preamplifier located close to the counter. The output signal is processed by a conventional electronic system. The pulse amplitude spectrum of the proportional counter and the position of the discriminator threshold rejecting the pulses due to gamma rays and to noise are monitored by a multichannel analyser.

B. Rem-counter

An Andersson-Braun rem-counter (Studsvik) has also been used to measure the neutron ambient dose equivalent [2].

3.2.2.2 Photon fields

The determination of the photon ambient dose equivalent is performed with a compensated Geiger-Müller counter type ZP 1320/PTFE (Alrad Instruments), which has a very low neutron sensitivity.

3.2.3 Response functions

3.2.3.1 Bonner spheres system

The response matrix of the Bonner spheres system has been determined in a broad range of neutron energies (from thermal up to 20 MeV) using a combined approach.

An experimental calibration has been performed with thermal neutrons and with monoenergetic neutrons with the following energies: 0.0082, 0.144, 0.25, 0.57, 1.2, 2.5, 5, 14.8 MeV.

The response functions up to 20 MeV have been calculated using the unidimensional neutron transport code ANISN and the recent condensed cross-section library BUGLE-80. The calculations have been subsequently extended up to 400 MeV using the HILO library.

The calculated response functions have been adjusted to the experimental calibration points. The values of the individual adjustment factors are represented in figure 1.

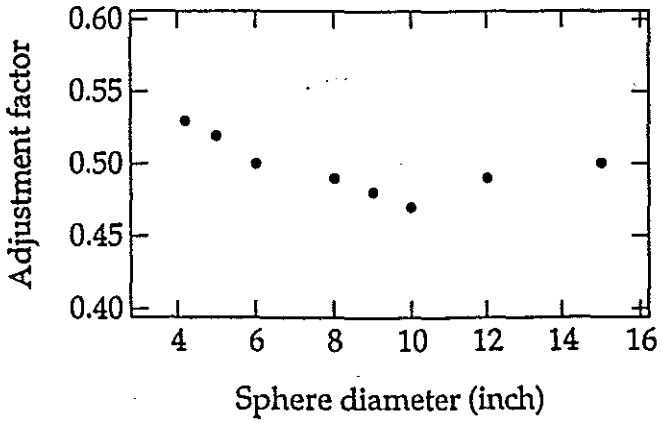

Figure 1: Individual adjustment factors for the Bonner spheres response functions

As the spread of the individual fit factors was fairly small, it has been decided to use the mean value as a unique adjustment factor for all spheres. The response matrix obtained in this way is represented in figure 2. The uncertainty of the matrix is estimated at about ±8% for the regions of maximum sensitivity of the response functions.

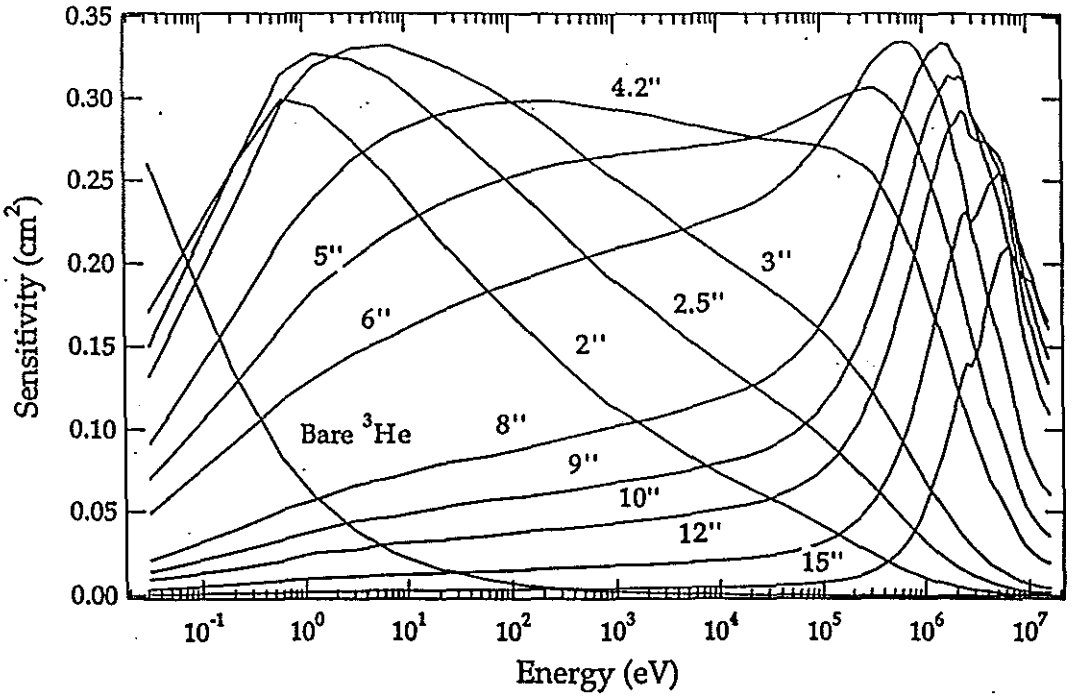

Figure 2: Response matrix of the IAR multisphere spectrometer

An experimental verification of the global performance of the Bonner spheres system (measuring procedure, response matrix, unfolding procedure) has been conducted by measuring calibrated neutron sources providing ISO reference spectra: Am-Be, bare ^{252}Cf and D_2O-moderated ^{252}Cf. The calibration of these sources in dose equivalent rate is traceable to PTB.

A detailed presentation of the determination of the Bonner spheres response matrix, including all approaches mentioned before, has been already published [1].

3.2.3.2 Rem-counter

The Andersson-Braun rem-counter used has been calibrated with the neutron sources providing ISO reference spectra: Am-Be, bare ^{252}Cf and D_2O-moderated ^{252}Cf, and characterised in a variety of operational neutron fields [2].

3.2.3.3 Geiger-Müller counter

The response function of the G.M counter has been determined for photon energies between 26 keV and 1.25 MeV using ISO narrow series of X-ray spectra and gamma rays. The response is fairly constant above 60 keV.

3.2.4. Unfolding procedure

The neutron spectrum is determined from the experimental data obtained with the Bonner spheres system and from the response matrix by using an unfolding procedure. The unfolding code used in the present work is based on the SANDPET version [3] of the SAND [4] code. Additional modifications have been introduced, yielding a new version called SANDIRA. The basic algorithm is unchanged, but the computation is now performed in 47 energy intervals instead of the 640 intervals initially used. All subroutines concerning foil activation have been removed. Subroutines for the calculation of various dosimetric quantities (ambient dose equivalent, absorbed dose, mean quality factor) have been added. The code has been adapted for running on a portable PC which allows for a quick preliminary evaluation of the results immediately after the measurements.

The treatment of uncertainties by the SAND code is very elementary. The statistical uncertainty of the Bonner spheres readings is introduced as input information. The code provides the deviations of the computed counting rates with respect to the measured ones and their variance. No covariance matrix or other estimate of uncertainty is produced.

A detailed study performed on predetermined spectra allowed to establish a correlation between the statistical uncertainty of the Bonner spheres readings and an average accuracy of the unfolded spectra [5].

An important ingredient of the unfolding is the *a priori* (guess) spectrum chosen for starting the procedure. Although the final result should not depend critically on the shape of the *a priori* spectrum, an adequate guess may speed up the convergence of the unfolding procedure and improve the quality of the final result. In the present work, the following *a priori* information was available : the original neutron source was based on uranium fission (either in the nuclear power plants or in the spent fuel) and a thermal neutron component should be present in the spectrum due to the effect of the protection barriers. Consequently, the following *a priori* spectrum has been used as input to the SAND code :

- low-energy region : thermal peak (standard option in SAND);
- high-energy region : fission peak (standard option in SAND);
- intermediate region : constant lethargy $E \cdot \phi_E(E)$ spectrum.

3.2.5. Evaluation of dosimetric quantities

3.2.5.1 Neutron field

A. Bonner spheres

The unfolding procedure yields the energy distribution of the neutron fluence density $\phi_E(E)$. The ambient dose equivalent is calculated by the relation :

$$H_n^*(10) = \int_{E_{min}}^{E_{max}} h_\phi(E) \cdot \phi_E(E)\, dE$$

where the conversion factor $h_\phi(E)$ is given by an interpolation analytical expression. Two sets of values have been computed, using the values of the conversion factor calculated according to ICRU 39 [6] and ICRP 60 [7] respectively.

B. Rem-counter

The reading of the Andersson-Braun rem-counter is converted into ambient dose equivalent using the conversion factor associated with californium-252 moderated in a 30 cm diameter sphere filled with heavy water (D_2O). The value of the conversion factor is 0.668 nSv/imp.

3.2.5.2 Photon field

The counting rate of the Geiger-Müller counter is converted to air kerma (K_a) by using the average value of the response which is fairly constant between 60 keV and 1.25 MeV. The ambient dose equivalent is calculated by the relation :

$$H^*_\gamma(10) = h\, K_a$$

where the conversion factor h is taken from ICRU 47 [8]. In the absence of any information on the photon spectrum, the value of the conversion factor at 1.25 MeV has been arbitrarily chosen.

3.2.6 Experimental results

Table 1 presents the results of the Bonner spheres measurements. The readings are converted to counting rates and corrected for the dead-time of the counting channel, including the proportional counter. The statistical uncertainty is evaluated from the readings, assuming a Poisson distribution. The monotonous variation of the counting rate versus sphere diameter (figure 3) provides an empirical check that no gross errors due to the malfunction of the equipment occurred during the measurements.

Table 2 presents the results of the rem-counter measurements and the corresponding ambient dose equivalent values. Table 3 presents the results of the G.M. counter measurements and the corresponding ambient dose equivalent values. The G.M. counter readings are corrected for a dead-time of 67 μs.

3.2.7 Results of the unfolding procedure

These results are based on the response matrix represented in figure 2. The spectra obtained at the 6 measurement locations are represented in figure 4. From these spectra, the neutron fluence has been evaluated in 5 energy supergroups according to the evaluator's request, as well as the following integral quantities : total fluence and ambient dose equivalent calculated according to ICRU 39 and ICRP 60. The numerical values are presented in table 4. The results have been communicated to the evaluator in March 1993.

Table 1: Readings of BS for all measured spectra
(N is the count rate (1/s) and SIG is the statistical uncertainty (%))

	Ringhals F		Ringhals G		Ringhals L	
Detector	N(1/S)	SIG(%)	N(1/S)	SIG(%)	N(1/S)	SIG(%)
Bare ^{3}He counter	722.41	0.42	336.84	0.61	83.02	1.10
^{3}He counter+Cd	80.76	1.24	22.00	1.68	20.83	1.54
2"	1454.99	0.29	493.89	0.51	327.18	0.55
2.5"	1782.78	0.27	520.36	0.49	435.04	0.48
3"	1947.79	0.25	547.92	0.48	503.00	0.44
4.2"	1942.35	0.25	486.20	0.51	541.75	0.43
5"	1734.24	0.27	410.73	0.55	480.03	0.46
6"	1350.08	0.30	315.42	0.63	388.45	0.51
8"	652.60	0.44	140.93	0.94	190.69	0.73
9"	460.69	0.52	96.36	1.14	134.61	0.87
10"	291.24	0.65	60.12	0.91	82.06	1.11
12"	114.57	1.05	23.43	1.46	32.48	1.26

	CLAB D		CLAB E		CLAB P	
Detector	N(1/S)	SIG(%)	N(1/S)	SIG(%)	N(1/S)	SIG(%)
Bare ^{3}He counter	13.22	0.97	11.03	0.95	10.37	0.98
^{3}He counter+Cd	3.25	1.39	2.57	1.39	2.11	1.54
2"	45.90	0.74	39.21	0.80	36.09	0.83
2.5"	62.72	0.63	50.01	0.71	49.10	0.71
3"	72.07	0.59	58.90	0.65	58.06	0.66
4.2"	76.17	0.57	62.53	0.63	64.78	0.62
5"	68.60	0.60	56.99	0.66	61.90	0.64
6"	55.15	0.67	46.23	0.74	51.17	0.70
8"	28.13	0.94	24.09	1.02	26.73	0.97
9"	20.13	0.79	17.21	0.85	19.00	0.81
10"	13.05	0.88	11.04	0.95	12.18	1.01
12"	5.50	0.95	4.62	1.24	5.10	0.70

Remarks:
1) The count rates are corrected for the deadtime of the detector.
2) The count rates at Ringhals are normalized to 100% monitor reading.
The normalization factor is 1/0.9986 for points F, G and 1/0.997 for point L

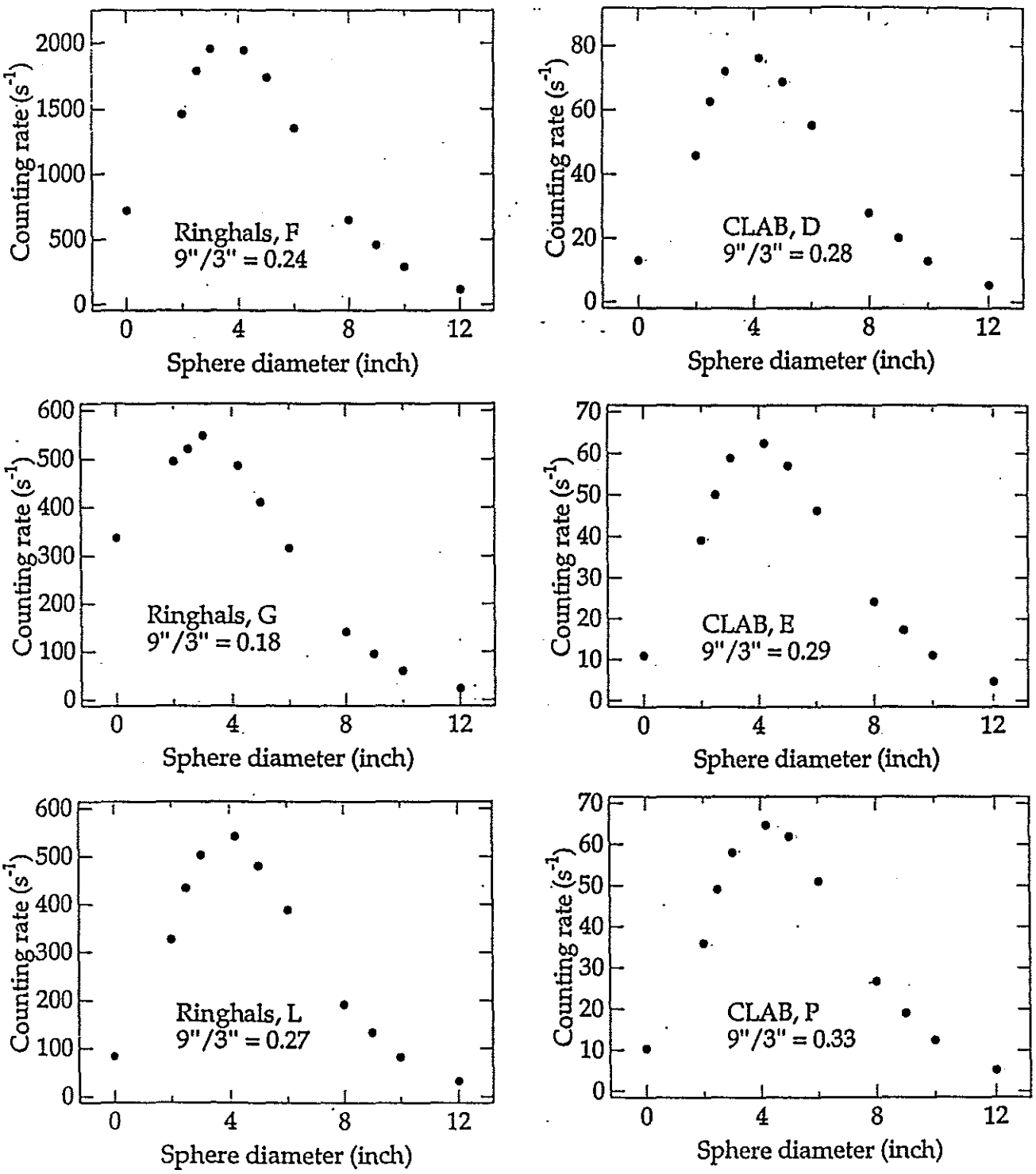

Figure 3: Variation of the counting rate versus sphere diameter

Table 2: Results of the Studsvik rem-counter measurements

Location	Display (μSv/h)	N(1/S)	SIG(%)	$H_n^*(10)$ (μSv/h)
Ringhals F	≈ 800	328	0.6	789
Ringhals G	≈ 100	51	1	122
Ringhals L	≈ 250	90	1	216
Clab D	≈ 50	17	0.8	41
Clab E	≈ 50	13.7	1.3	33
Clab P	≈ 50	16.9	1.2	41

Table 3: Results of the G.M. counter measurements

Location	N(1/S)	SIG(%)	$H_\gamma^*(10)$ (μSv/h)
Ringhals F	212	0.8	262
Ringhals G	81	1	97
Ringhals L	61	0.9	73
Clab D	28.6	1	34
Clab E	21.3	1	26
Clab P	21.7	1	26

Table 4: Integral results (Fluence in $n.cm^{-2}.s^{-1}$, Dose equivalent in $nSv.s^{-1}$)

	RING-F	RING-G	RING-L	CLAB-D	CLAB-E	CLAB-P
Fluence : < 0.414 eV	3.37E+03	1.67E+03	3.18E+02	5.05E+01	4.33E+01	4.25E+01
Fluence : 0.414 eV-10 keV	4.67E+03	1.09E+03	1.40E+03	1.89E+02	1.51E+02	1.43E+02
Fluence : 10 keV-100 keV	9.62E+02	1.10E+02	3.15E+02	4.51E+01	3.93E+01	5.18E+01
Fluence : 100 keV-1 MeV	3.19E+02	2.04E+01	9.01E+01	2.28E+01	2.21E+01	2.84E+01
Fluence : > 1 MeV	4.73E+00	1.07E-01	6.58E-01	1.67E+00	1.18E+00	9.68E-01
Total fluence	9.32E+03	2.89E+03	2.13E+03	3.09E+02	2.57E+02	2.67E+02
H*(10) ICRU39	1.40E+02	2.93E+01	3.46E+01	7.40E+00	6.60E+00	7.63E+00
H*(10) ICRP60	2.01E+02	4.03E+01	4.98E+01	1.09E+01	9.81E+00	1.15E+01

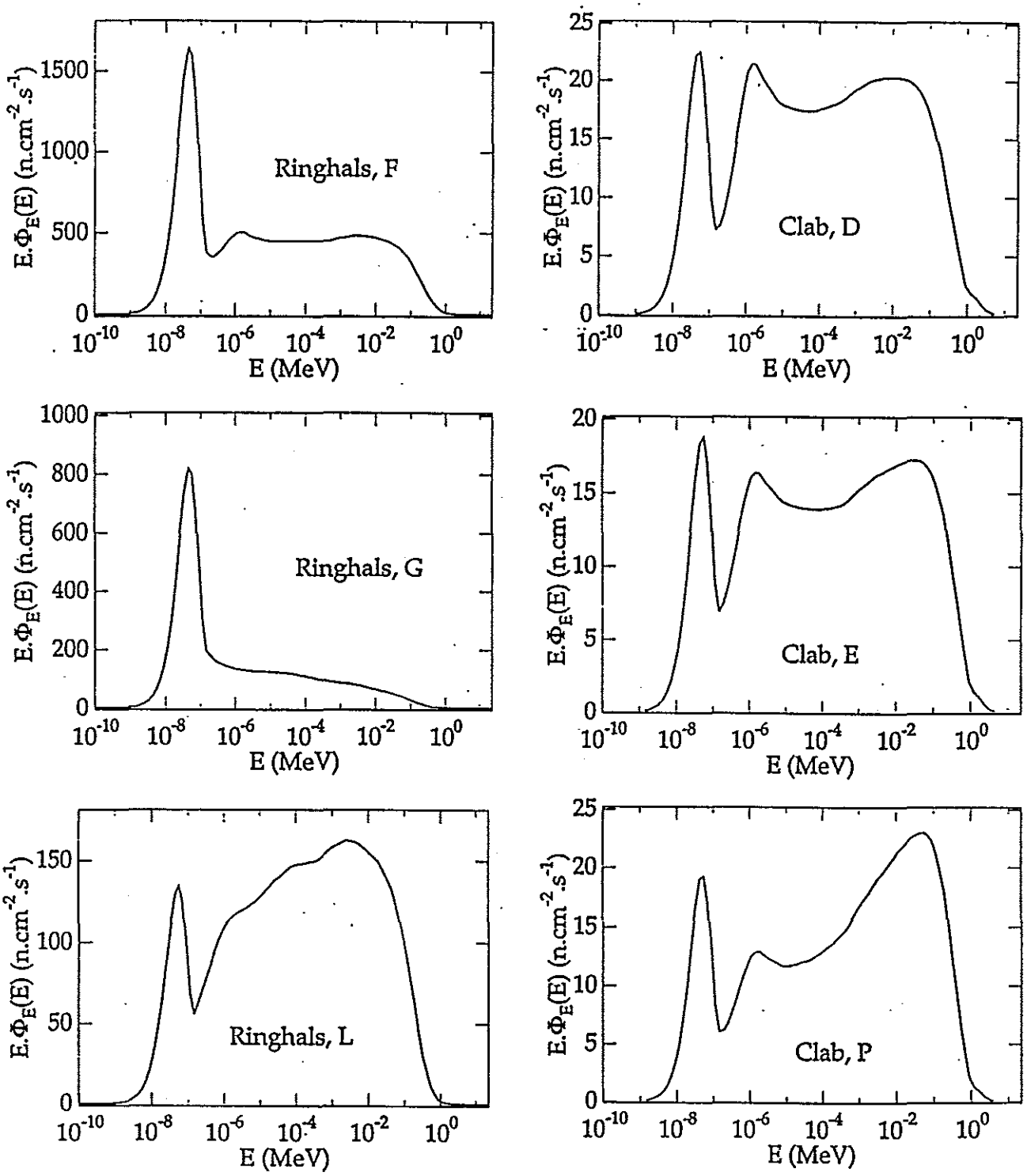

Figure 4: Neutron spectra measured at Ringhals and CLAB

3.2.8 Revised results

3.2.8.1 Revised response matrix

The evaluator's report presented at the EURADOS WG7. meeting in Prague [9] pointed to significant differences between the above reported results and those of other participants using Bonner spheres. A good agreement was obtained for the integral fluence values, but the distribution in the 5 energy supergroups is different, yielding lower values for the ambient dose equivalent. The spectra are generally softer than those of other participants. The evaluator's analysis of the results, based on several cross-checks, suggested that the problem was not due to the experimental counting rates or to the unfolding procedure.

A detailed investigation of the possible causes of this discrepancy has been subsequently performed.

The verification measurements previously performed with calibrated sources of Am-Be and Cf-252 (section 3.2.2.1) have been repeated [10]. A good reproducibility of the results has been obtained, both for the integral quantities and the spectra, which shows that no unexpected change of the system performance has occurred in between.

Comparative unfolding tests with several versions of the response matrix have been performed. All of them are based on the same set of experimental calibration points (section 3.2.2.1). The differences concern either the cross-section libraries used in the ANISN calculation, or the procedure for fitting the calculated response function to the calibration points. Eventually a new response matrix was established (figure 5). It is based on ANISN calculations performed with BUGLE-80 library (same as for the previously used response matrix) but each computed response function has been individually adjusted to the experimental calibration points. The difference between the old and the new response functions is illustrated in figure 6 for a few representative cases.

3.2.8.2 Revised results of the unfolding procedure

The revised results are based on the new response matrix (figure 5). The new spectra obtained at the 6 measurement locations are represented in figure 7, together with the previous spectra (version 1).

The representation of the old spectra (version 1) as continuous functions and of the revised ones as histograms is due to the reduction of the number of energy bins in the SANDIRA code from 640 to 47. It must be emphasised that in both cases the response matrix is defined in 47 energy intervals; performing the unfolding in the 640 bins format of the original SAND code involved an interpolation and extrapolation of the initial response functions; this has been considered undesirable. It has been verified that, when using the same response matrix, this modification has not introduced significant changes in the spectra (less than 1% difference for the ambient dose equivalent).

From the revised spectra, the neutron fluence in 5 energy supergroups and the integral quantities have been evaluated. The new values are presented in table 5. The relative change of the integral quantities with respect to version 1 is also presented in table 5.

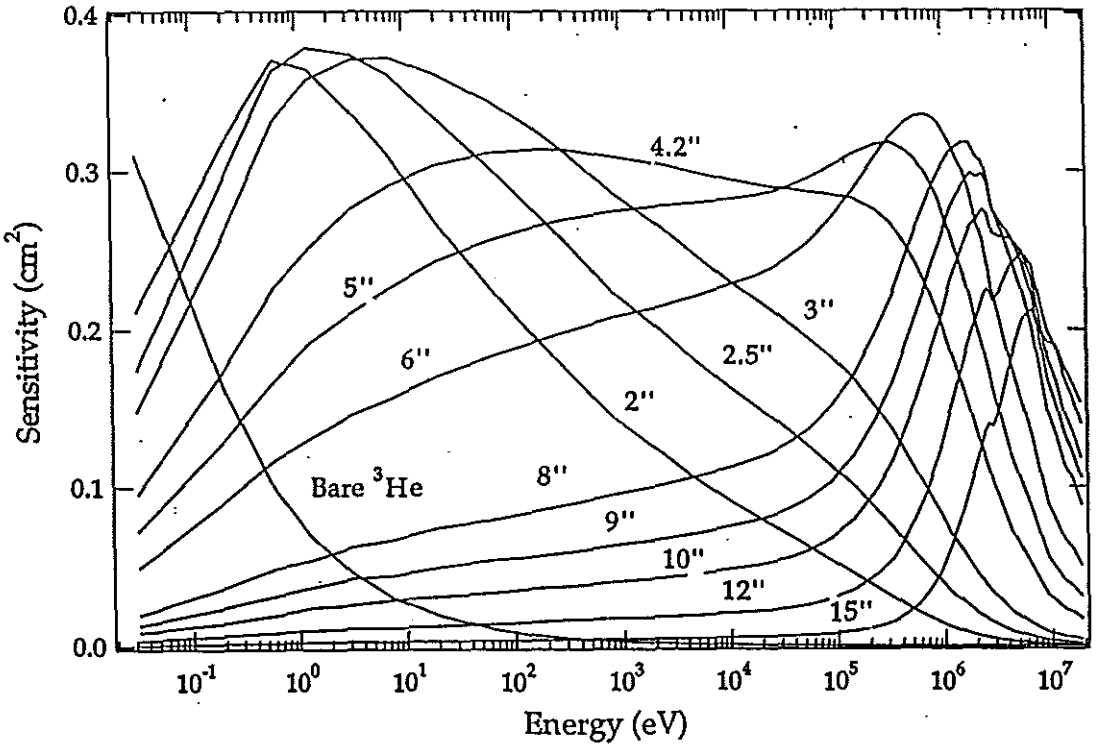

Figure 5: Revised matrix of the IAR multisphere spectrometer

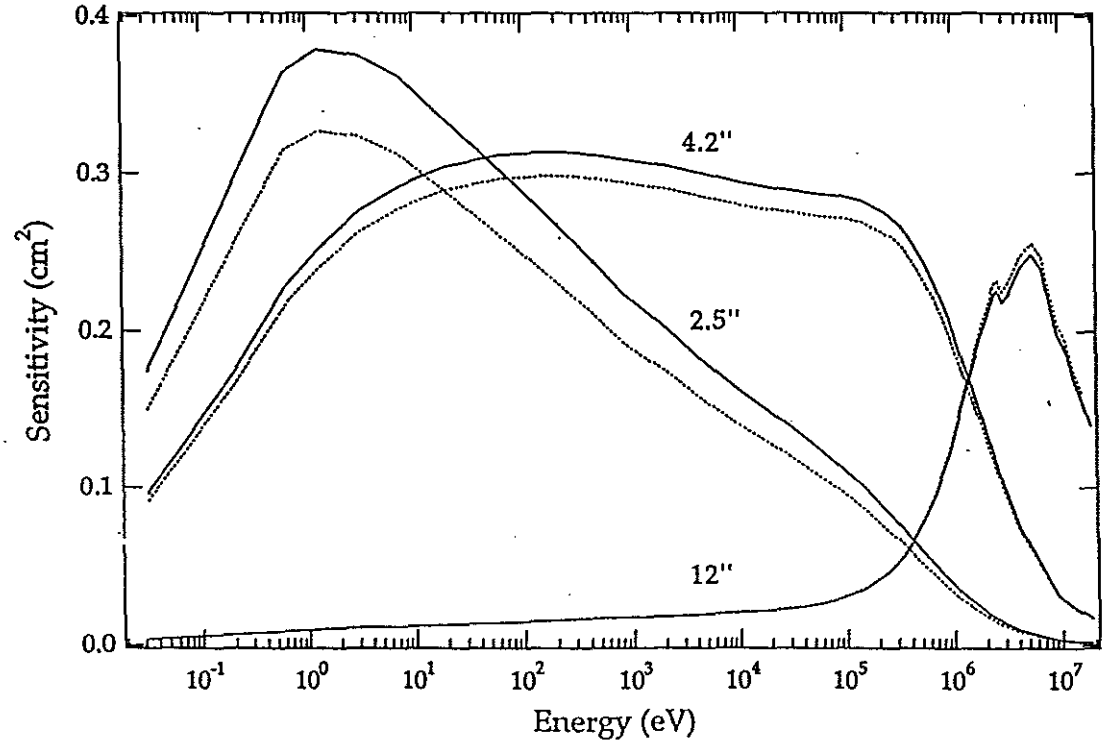

Figure 6: Comparison of old response functions (dashed line) and revised ones (solid line) for representative cases

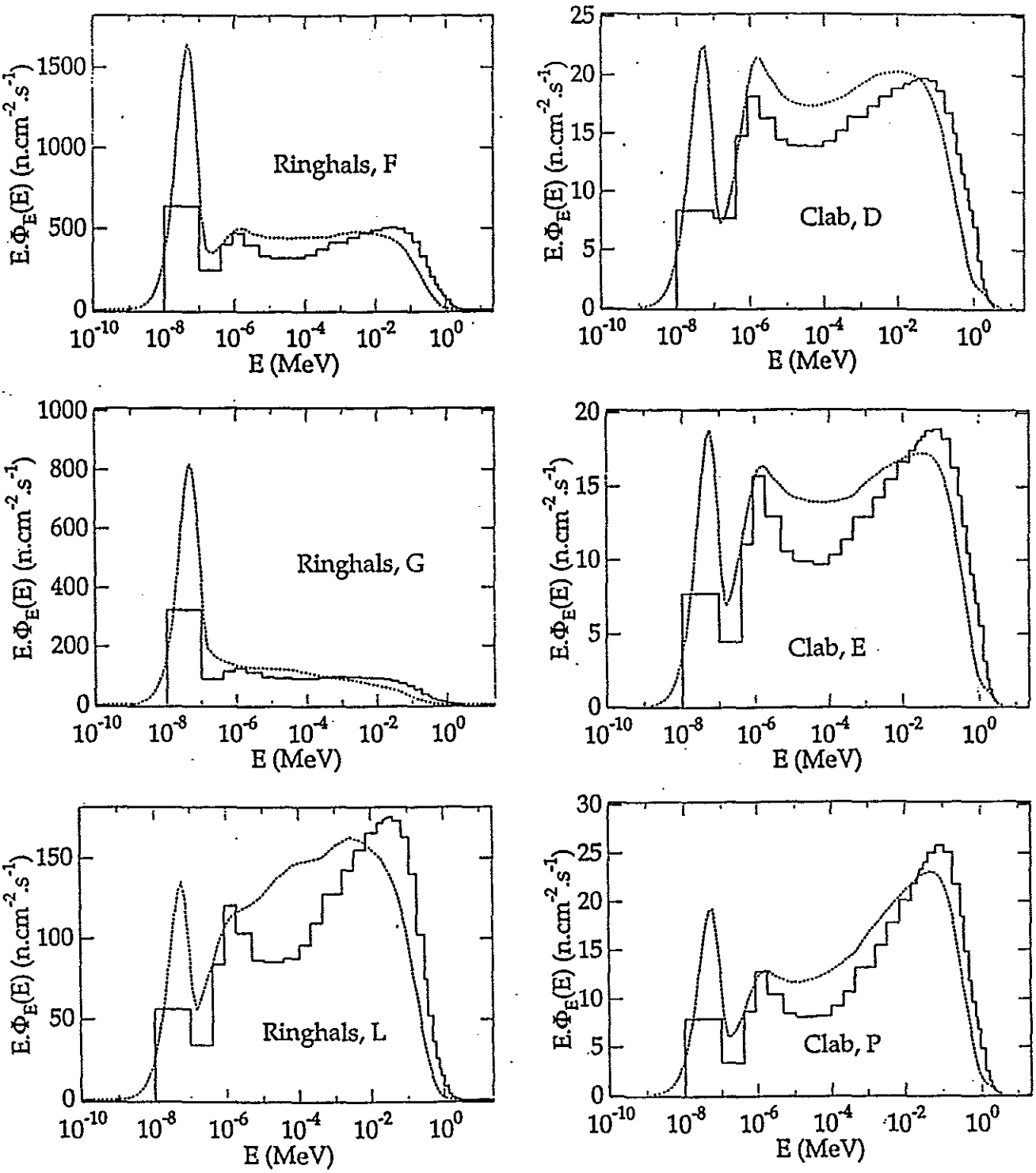

Figure 7: Revised neutron spectra (solid line) compared to the old ones (dashed line)

Table 5: Revised integral results (Fluence in $n.cm^{-2}.s^{-1}$, Dose equivalent in $nSv.s^{-1}$)

	RING-F	RING-G	RING-L	CLAB-D	CLAB-E	CLAB-P
Fluence : < 0.414 eV	2.18E+03	1.05E+03	2.11E+02	3.54E+01	2.87E+01	2.75E+01
Fluence : 0.414 eV-10 keV	4.02E+03	1.01E+03	1.14E+03	1.63E+02	1.26E+02	1.17E+02
Fluence : 10 keV-100 keV	1.17E+03	1.84E+02	4.03E+02	4.60E+01	4.26E+01	5.50E+01
Fluence : 100 keV-1 MeV	6.28E+02	6.86E+01	1.90E+02	3.42E+01	3.24E+01	4.14E+01
Fluence : > 1 MeV	4.62E+01	4.17E+00	6.67E+00	5.51E+00	4.33E+00	3.70E+00
Total fluence	8.04E+03	2.32E+03	1.95E+03	2.84E+02	2.34E+02	2.45E+02
New/Old	0.86	0.80	0.91	0.92	0.91	0.92
H*(10) ICRU 39	1.91E+02	3.33E+01	5.08E+01	1.01E+01	9.00E+00	1.03E+01
New/Old	1.36	1.14	1.47	1.36	1.36	1.35
H*(10) ICRP 60	2.94E+02	5.17E+01	7.89E+01	1.52E+01	1.35E+01	1.57E+01
New/Old	1.46	1.28	1.58	1.39	1.38	1.36

3.2.9 Discussion

The differences between the new and the old set of response functions are not dramatic. However, they introduce significant changes in the results.

The convergence of the unfolding procedure is faster with the new response matrix and the quality of the fit, estimated by the average standard deviation, has also improved.

The shape of the spectra has changed, the general trend being an enhancement of the high-energy region and its shift towards higher energies. In the thermal and epithermal regions the same structures observed in the old spectra are present. These are produced when the information of the cadmium-covered counter is considered.

The change in spectra has induced an increase of the ambient dose equivalent because of the increased weight of high-energy neutrons. The integral fluence has also been affected by the new response matrix.

In conclusion, the idea of using a unique normalization factor for fitting the response functions of all spheres to the calibration points must be abandoned, despite its aesthetic appeal. The response matrix obtained with individual adjustment factors for each sphere yields better results. This conclusion is supported by the experience of other groups performing neutron spectrometry with Bonner spheres [11].

References

[1] Aroua A., Grecescu M., Lerch P., Prêtre S. and Valley J.-F., *Evaluation and Test of the Reponse Matrix of a Multisphere Neutron Spectrometer in a Wide Energy Range, Part I, II, III.* Nucl. Instrum. Methods **A321** (1992) 8 - 316.

[2] Aroua A., Boschung M., Cartier F., Gmür K.,Grecescu M., Lerch P., Prêtre S., Valley J.-F. and Wernli C., *Study of the Response of Two Neutron Monitors in Different Neutron Fields.* Radiat. Prot. Dosim. **44** (1992) 183 - 187.

[3] Zijp W. L. and Nolthenius H. J., Private communication

[4] McElroy, W.N., Berg S., Crockett T. and Hawkins R. A, *Computer-Automated Iterative Method for Neutron Flux-Spectra Determined by Foil Activation. Rep.* AFWL-TR-67-41, Vols. I-IV (U.S. Air Force Weapons Lab., Kirtland, AFB, New Mexico, 1967).

[5] Aroua A., *Etude des champs neutroniques dans les centrales nucléaires et de l'influence de leur diversité sur la détermination des grandeurs de la protection radiologique.* Ph.D. Thesis No 942, Ecole Polytechnique Fédérale de Lausanne, Switzerland (1991).

[6] Wagner S. R., Grosswendt B., Harvey J. R, Mill A. J., Selbach H.-J. and Siebert B.R.L., *Unified Conversions Functions for the New ICRU Operational Radiation Protection Quantities.* Radiat. Prot. Dosim. **12** (1985) 231 - 235.

[7] Leuthold G., Mares V. and Schraube H., *Calculation of the Neutron Ambient Dose Equivalent on the Basis of the ICRP Revised Quality Factors.* Radiat. Prot. Dosim. **40** (1992) 77 - 84.

[8] ICRU Report 47, *Measurement of Dose Equivalents from External Photon and Electron Radiations.* (ICRU Publ., Bethesda, MD, 1992).

[9] Tichy M., *Evaluation of Spectral Neutron Fluence Measurements Performed at Ringhals and Oskarshamn, Sweden.* Presented at the EURADOS WG7 meeting in Prague (September 1993).

[10] Aroua A., Buchillier T. and Grecescu M., *Test de stabilité du spectromètre neutronique multisphère effectué au PSI du 31 août au 1 septembre 1993.* Rapport interne IRA (1993).

[11] Alevra A. V., Cosack M., Hunt J. B., Thomas D. J. and Schraube H., *Experimental Determination of the Response of Four Bonner Sphere Sets to Monoenergetic Neutrons (II).* Radiat. Prot. Dosim. **40** (1992) 91 - 102.

Appendix: Measurement locations

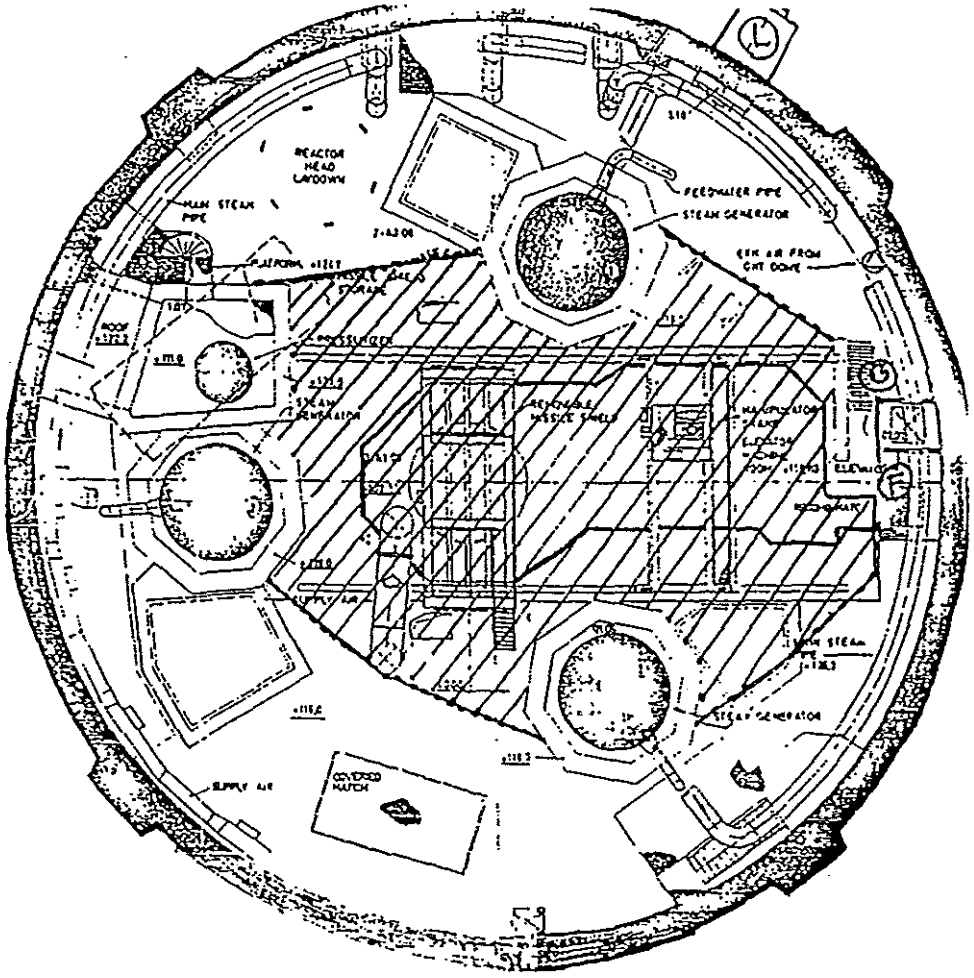

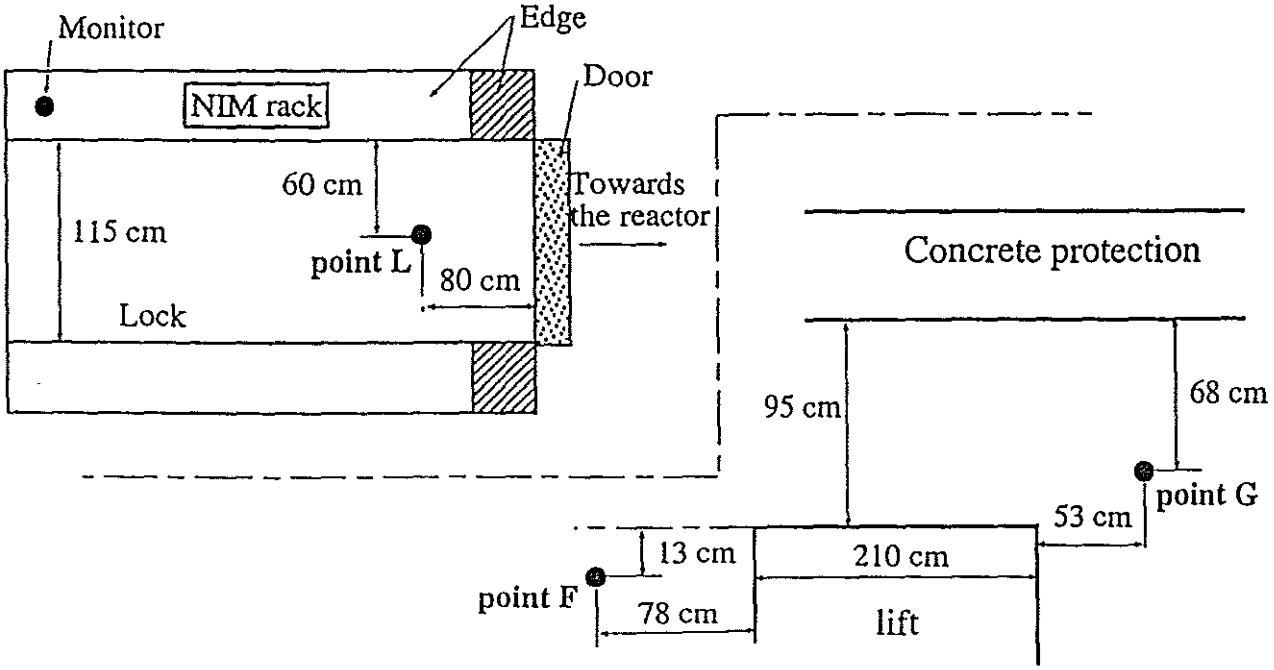

Appendix: Measurement locations

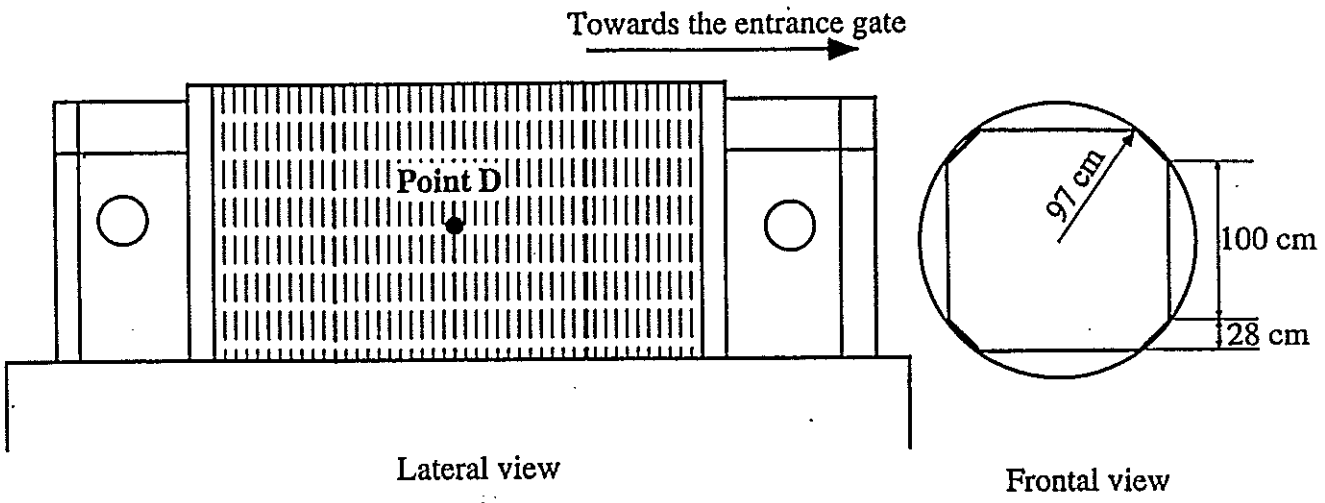

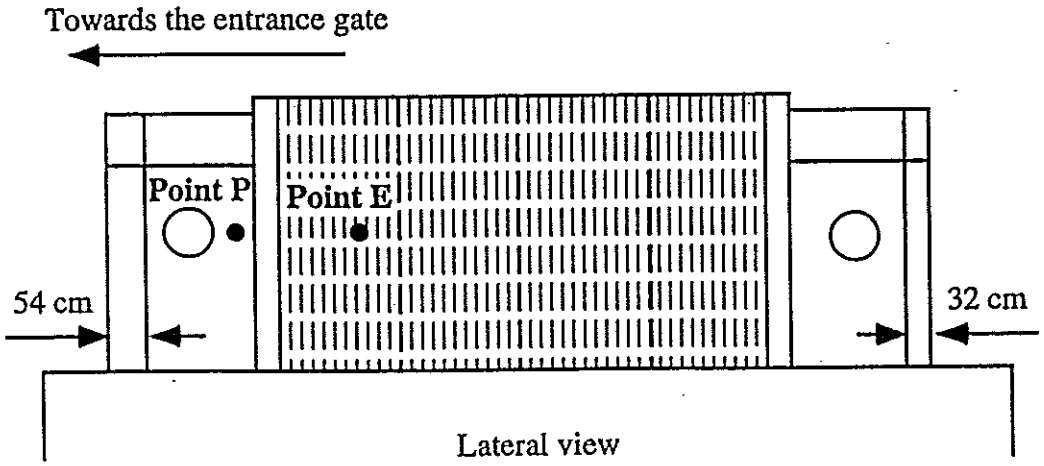

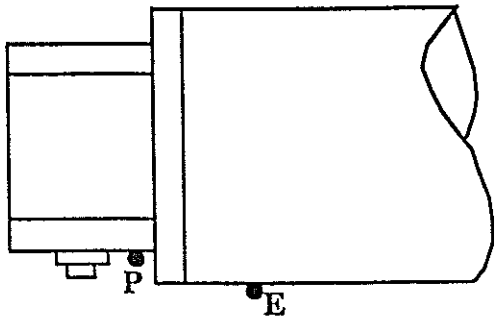

Top view

At the 3 measurement locations the centre of the spheres was at 1m from the surface of the container

3.3 Measurements with the PTB Bonner Sphere Spectrometer and a Leake-Type Rem Counter

A.V. Alevra.
Physikalisch-Technische Bundesansalt (PTB),
Bundesallee 100, D-38116 Braunschweig

3.3.1 Introduction

The PTB has taken part in a program of measurements organized in November 1992, both in Oskarshamn and Ringhalsverket. A short presentation of the measurements with Bonner spheres will be made, and the procedure used to unfold the spectral neutron fluence from the measured data will be briefly described. The input data and the results obtained are reported in graphical and numerical form as submitted to the evaluator for comparison with other results. Measurements were also performed with a Leake-type rem counter, the results of which are also reported and compared with the dosimetric data obtained with the Bonner spheres.

3.3.2 The PTB Bonner Spheres

There are two sets of Bonner spheres at PTB with two different types of central detector [1].

The PTB "C" set has as a central detector a spherical proportional counter (32 mm diameter) of type SP90, made by Centronic Ltd, UK, and filled with 200 kPa ($4.94 \cdot 10^{19}$ atom/cm^3) ^{3}He gas. This detector can be fitted in the centre of 12 polyethylene spheres with diameters from 3" to 18" (1 inch = 2.54 cm). The proportional counter itself is also used in measurements, bare or under a 1 mm-thick cadmium shielding.

The PTB "F" set has as a central detector a small cylindrical proportional counter (9 mm diameter, 10 mm length) of type 0.5NH1/1K, made by Thomson-CSF, France, and filled with 664 kPa ($1.64 \cdot 10^{20}$ atom/cm^3) ^{3}He gas. This detector can also be fitted in the centre of the same 12 polyethylene spheres of the "C" set, and additionally into two spheres with diameters of 2" and 2.5". This proportional counter is also used in measurements as a bare counter or under a 1 mm-thick cadmium shielding.

The polyethylene density is 0.946 g/cm^3.

The fluence response matrices for the two PTB Bonner sphere sets are essentially based on the experimental data reported in Refs. [1, 2]. They were obtained by fitting response functions reported in Ref. [3] to experimental points obtained with monoenergetic neutrons with energies between 1.17 keV and 14.8 MeV [1]. For energies below about 100 eV, the responses were then empirically modified and extrapolated in order to obtain agreement with the experimental data at thermal energies [2], which were overestimated by these calculations by a factor of about 2.

The response matrix of the PTB "C" Bonner sphere set is shown in Fig. 1 and given numerically in Appendix in Table 1. Similar data for the PTB "F" set are given in Fig. 2 and in Table 2 in the Appendix. In order to save space in Table 2 only, the numerical data for the 15" and 18" spheres are not given, but as will be seen later, these spheres were not used in the series of measurements reported here.

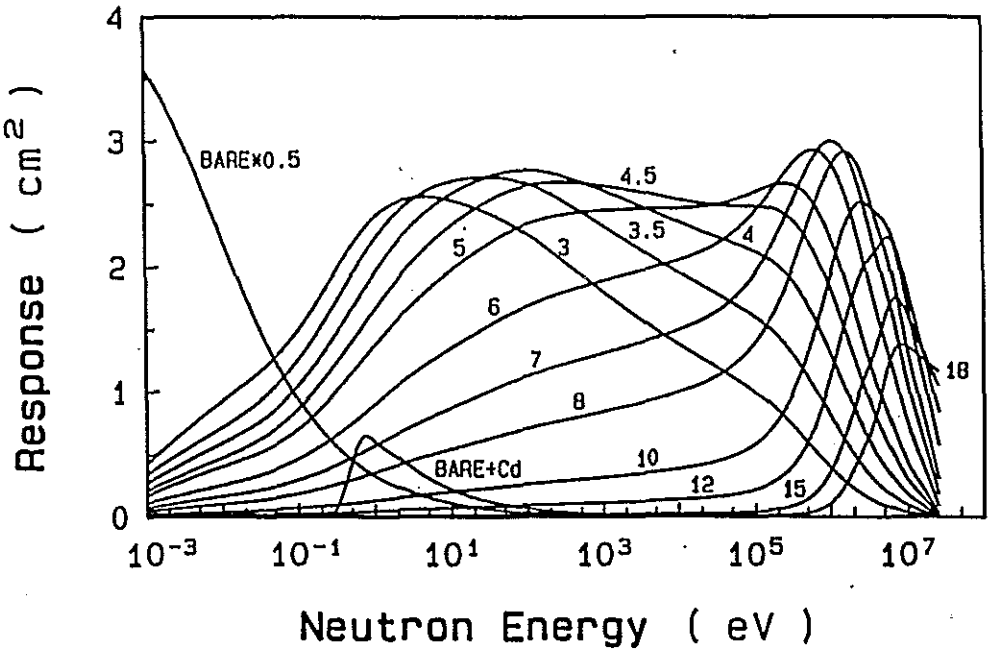

Fig. 1. The fluence response matrix of the PTB "C" Bonner sphere set.

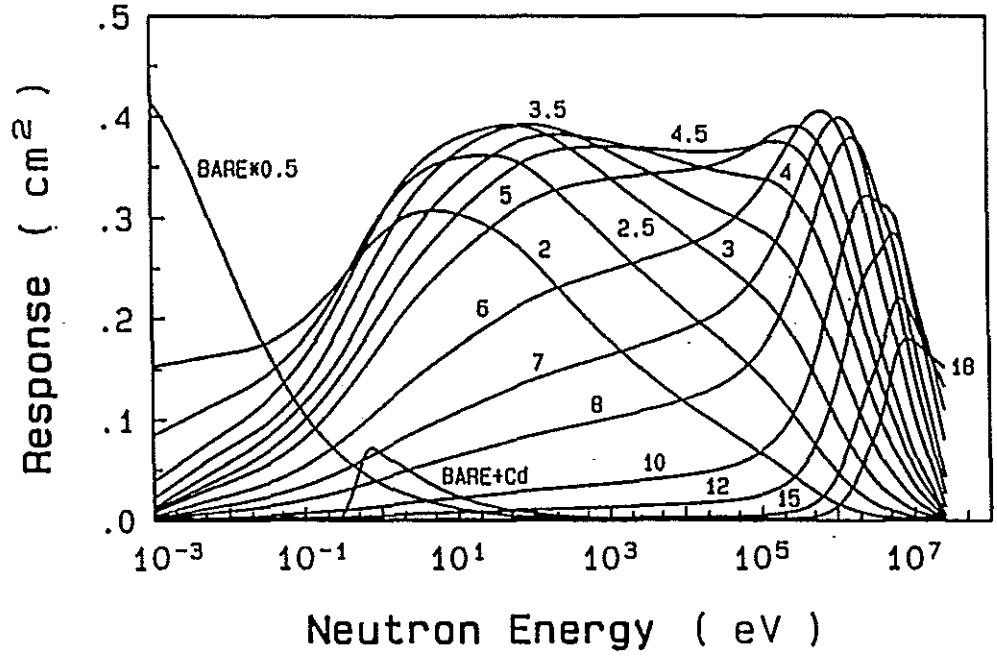

Fig. 2. The fluence response matrix of the PTB "F" Bonner sphere set.

In the lower part of Tables 1 and 2, the estimated uncertainties of the responses in terms of one standard deviation, as throughout this work, are given.

The figures and tables show that the responses of the set "F" are lower than the responses of the "C" set by a factor of about 7.5. For this reason the "F" set is intended to be used in high intensity neutron fields where the count rates of the "C" spheres are so high that pile-up and dead-time corrections can no longer be estimated. Unfortunately, the small size of the "F" counter has some functional shortcomings: low gas amplification and microphonic effects may hinder the use of this counter in noisy environments.

3.3.3 The Measurements

At the CLAB Laboratory in Oskarshamn, measurements using the PTB "C" Bonner sphere set were performed at three points, D, E and P (see section 2.2). The spheres used were: 0C0 (bare counter), c0C0 (bare counter under cadmium shielding), 3C0 (3"), 3C5 (3.5"), 4C0, 4C5, 5C0, 6C0, 7C0, 8C0, 10C (10") and 12C. The Leake rem-counter was also included in the measurements, with its own electronics replaced by the electronics and data aquisition system of the Bonner sphere spectrometer.

At Ringhalsverket, measurements were made at point G in the containment of a reactor and at point L in the "lock" (see sect. 2.1). For safety reasons, the time available for measurements at these places was strictly limited and only a reduced set of Bonner spheres could be used. This set consisted of a bare counter, a bare counter under cadmium and 3", 4", 5", 8" and 12" spheres. The high intensity of the neutron fields at Ringhalsverket made it advisable to use the PTB "F" set. This was only possible at point L, well screened from the various sources of noise. In the containment of the reactor, the noise level, both of acoustic and electro-magnetic origin, was so high that it was not possible to use the "F" set. With the "C" set we succeeded in measuring only at point G, where count rates as high as 5000 counts per second were recorded. With the Leake rem-counter, which uses the same type of central detector as the "C" set but has a fluence response near that of the "F" set, we were able to measure not only at points L and G, but also at point F.

The dead-time corrected count rates (readings) obtained from all the measurements reported in this work are given numerically in Table 3 in the Appendix, together with their statistical uncertainties. The uncertainties given for the response functions are those from Tables 1 and 2. All data given are normalized to 1 s measuring time. This is obviously reasonable for the measurements at CLAB, where the neutron source is constant in time. But even at Ringhalsverket, as the reactors were kept constant at their maximum power for the whole duration of the measurements, as also indicated by the existing radiation monitors, the normalization to 1 s measuring time is acceptable.

The stability of the measurement conditions is well illustrated by Fig. 3, which shows the readings at four of the measurement points as a function of the sphere diameter, at each point relative to the 5"-sphere reading. The data obtained with the bare counter under cadmium are not represented in these plots. "CLAB-D" is not shown here because the figure is practically identical with "CLAB-E". The smoothness of the curves testifies to the stability of the measurement conditions. The 6 points obtained at Ringhalsverket seem to be the most adequate minimum information necessary to draw the curves, indicating that the choice of the reduced set of spheres was appropriate. At all five points of measurement the relative reading of the 12" sphere is very low. This is an indication that the neutron spectra are rather soft, and that measurements with spheres of larger diameter were not necessary. The high count rate of

the bare counter at position "RING-G" indicates an important contribution of thermal neutrons, which is not the case at the other positions.

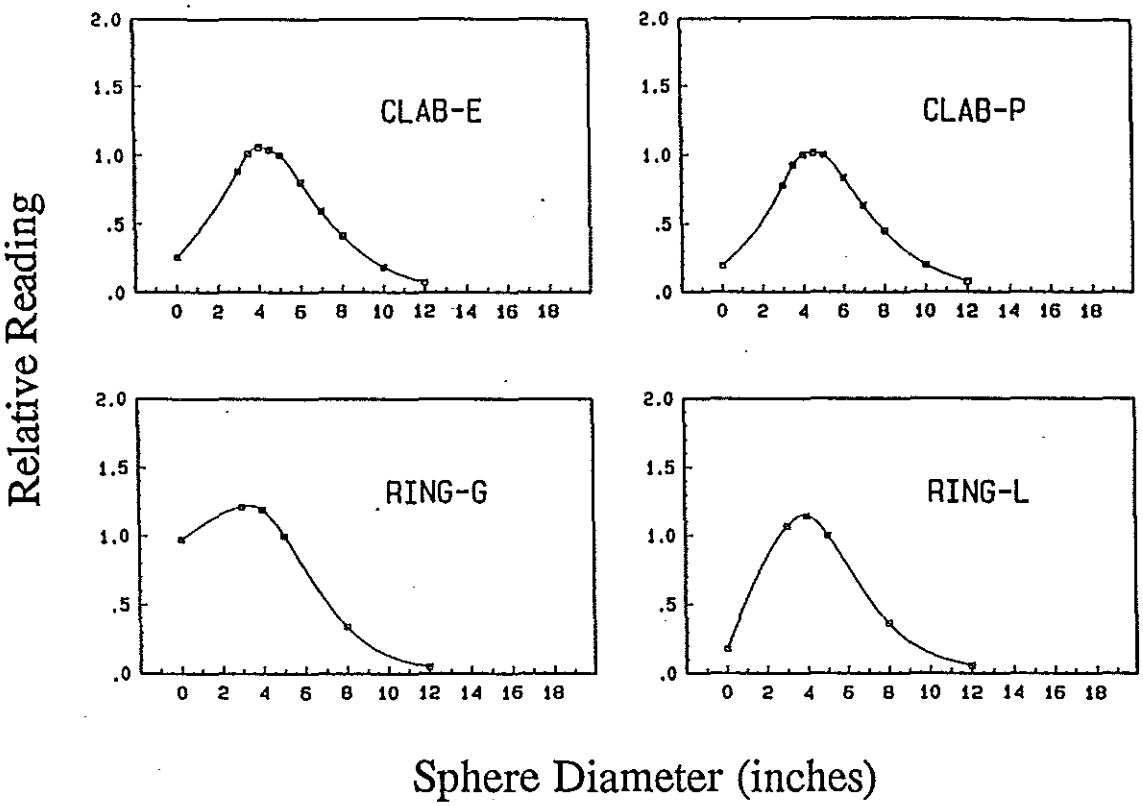

Figure 3: The dead-time corrected readings at the points of measurement indicated as a function of the sphere diameter at each point relative to the 5"-sphere reading.

3.3.4 Spectra Unfolding from the Measured Data

For the unfolding of the spectral neutron fluence from the Bonner sphere readings, a home-made code based on the SAND-II algorithm [4] is used. As is well known, a few-channel unfolding solution is not unique. The shape of the resulting spectral fluence is influenced by the guess spectrum given as input. For the whole series of measurements reported here there was no *a priori* information available to be used as guess spectrum (e.g. previous measurements or calculations). Instead, a large variety of input spectra had to be checked, and from the various solutions those found to be not only statistically compatible with the measured count rates but also physically acceptable were retained as final solutions. The criterion for the compatibility of a spectral solution with the measured count rates was the value of the reduced *chi-squared*:

$$\chi_r^2 = \frac{1}{n_D - 1} \sum_{d=1}^{n_D} \frac{\left[1 - \frac{M_d}{C_d}\right]^2}{\sigma^2(r_d)} \qquad (1)$$

where n_D is the total number of detectors used in measurements and included in the unfolding, M_d is the measured count rate of the d-th detector, C_d the calculated reading of the same detector, and $\sigma(r_d)$ is the absolute uncertainty of the ratio

$$r_d = \frac{M_d}{C_d} \tag{2}$$

If we denote by Φ^s the spectral solution described in n_E energy bins by a set of Φ_i^s ($i = 1,2,...,n_E$) values, Φ_i^s being the fluence in the i-th bin, then the calculated reading is obtained from:

$$C_d^s = \sum_{i=1}^{n_E} R_d(E_i) \cdot \Phi_i^s \tag{3}$$

where $R_d(E_i)$ is the response of the d-th sphere in bin i. The relative uncertainty of the ratio r_d is obtained from :

$$\sigma_{rel}^2(r_d) = \sigma_{rel}^2(M_d) + \sigma_{rel}^2(C_d^s) \tag{4}$$

where $\sigma_{rel}(M_d)$ is the relative statistical uncertainty of the reading as given in Table 3, and $\sigma_{rel}(C_d^s)$ is considered to consist only of the relative uncertainty of the response, also given in Table 3.

The strategy used in the unfolding procedure was as follows:

a) At the beginning, in order to avoid a *subjective* unfolding, guess spectra very different in shape were used.
b) A small number of iterations were allowed (usually 10) and the changes in shape resulting from the first few iterations were observed.
c) The value of the reduced *chi-squared* and also the deviations of the individual values of r_d from unity were observed.
d) The guess spectrum was then correspondingly modified, being constructed from physically appropriate components, taking into account the origin of the neutrons and the various moderating materials assumed to be present.
e) Steps b) to d) were repeated until the first 10 iterations no longer brought important changes in the shape of the input spectrum.
f) In the final step, which in many cases is not necessary, the last unfolding was repeated with a larger number of iterations (e.g 1000), which brought about only small changes in the spectrum shape and improved the value of the reduced *chi-squared.*

3.3.4.1 Solution spectra at the point CLAB-"D"

Four of the possible solutions obtained from the measured data at the point CLAB-D are shown in Fig. 4.

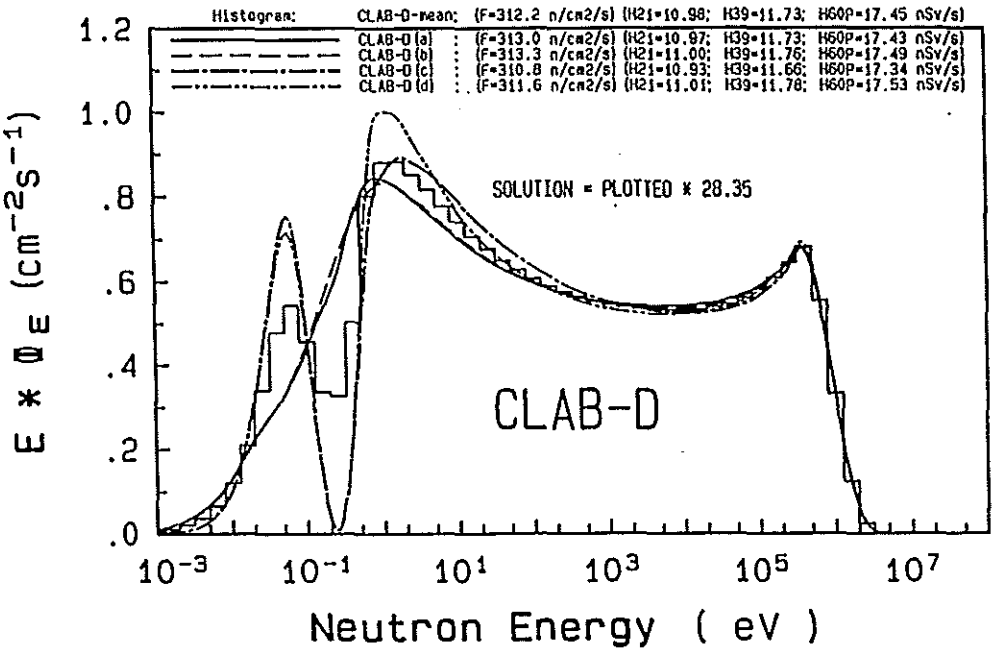

Figure 4: Four of the solution neutron spectra obtained from measurements at the point "CLAB-D" and their arithmetic mean (histogram)

Performing the steps a) to d) we were almost constrained to describe the higher energy part of the neutron spectrum as a superposition of two components: a contributon of a few percent of a rather low-energy *fission-like* spectrum, $\Phi_E^f \sim E^{1/2} \cdot e^{-E/500\ keV}$, followed by a *slowing-down* spectrum, $\Phi_E^{sd}(E) \sim E^{-1.03}$, which has an upper edge determined by the fission spectrum itself. The solution spectrum thus agreed well with the low count rates of the large spheres. In the lower energy part of the spectrum the *slowing-down* component was continued and, for physical reasons, a lower edge following the shape of a *thermal Maxwellian* spectrum, $\Phi_E^{th}(E) \sim E \cdot e^{-E/0.0253\ eV}$, was imposed without making any supplementary thermal contribution. Even when this was done, the input spectrum proved to contain too much low energy fluence, which contradicts the low reading of the bare counter. This contradiction was removed by the SAND-II iterations which reduced the neutron fluence in the lower energy part resulting in a smoothly decreasing fluence with decreasing energy. The unfolding was performed taking into account all the detectors used in the measurements, including the bare counter under cadmium shielding. The solution obtained, denoted CLAB-D(a), is shown in Fig. 4, the integral quantities derived from it, integral fluence, F, integral dose equivalent H21 (ICRP21), H39 (ICRU39) and H60P (ICRP60 in the PTB variant), being numerically given in the upper part of the figure. As the measurement with the bare counter under cadmium shielding produces very sensitive information in this energy region, we repeated the unfolding

without including the cadmium cover measurement. The resulting spectrum, denoted CLAB-D(b), is also shown in Fig. 4. The difference in shape between spectra a and b is insignificant and is less than 0.3% in integral quantities.

Another means (among others) of reducing the neutron fluence in the lower energy range was to introduce a cadmium cut (at about 0.4-0.5 eV), but in this case the calculated reading C_{bare} was too low and we had to add about 12% thermal fluence. The spectra obtained in this variant, with and without the cadmium cover measurement, are shown in Fig. 4 as CLAD-D(c) and CLAB-D(d) respectively. These spectra differ only slightly in shape, and the differences in integral quantities are of the order of only 1%.

In fact, all four solutions are fully compatible with the measured count rates and the response matrix used, within the estimated uncertainties for these quantities. The mean of these four spectra, the CLAB-D-mean shown in Fig. 4 as a histogram, or any linear combination of them, is also compatible. Even the integral fluence below the cadmium cut is practically the same in all these spectra. The Bonner sphere spectrometer alone cannot decide which variant better describes the reality. We could not, however, find a physical model to explain the spectra with a dip below the cadmium cut. A smooth reduction of the fluence with decreasing energy, or the intermediate situation represented by the mean spectrum, seem to be more plausible. We therefore selected the CLAB-D(a) spectrum as the final solution.

3.3.5 Results

The data obtained at the other four points of measurement reported here were treated in the same manner as the the CLAB-D data. For the position RING-G, due to the high count rate of the bare counter, we had to introduce an important *thermal Maxwellian* component which nevertheless continues smoothly into the *slowing-down* component.

The final neutron spectra obtained for the five points where measurements were performed are shown in Fig. 5 and in Figs. 6 to 9 in the Appendix, and given numerically in Table 4 in the Appendix. In the lower part of each figure the corresponding ratios, r_d, are shown. The left-hand uncertainty bars (in most cases smaller than the point size) indicate the statistical uncertainty of the measured count rate, the right-hand ones also include the uncertainty of the response as given in Table 3. In all cases the mean ratio values are very close to unity (deviations of maximum 0.02%) with an estimated uncertainty of less than 2%. These estimates have been obtained considering the uncertainties of the ratios, $\sigma(r_d)$, as fully uncorrelated. On the other hand, the very low values obtained for the reduced chi squared (no higher than 0.06) indicate that the attributed uncertainties $\sigma(r_d)$ contain an important correlated part, common to all spheres. A more detailed discussion of these aspects can be found in Ref. [11], where it is concluded that the PTB Bonner sphere spectrometer is capable of achieving an accuracy of $\pm$ 4% in the integral fluence determination. As a result of the spread in shape of the valid solutions, the uncertainty of the total dose eqivalent may reach $\pm$ 15%. In fact, the accuracy in dose equivalent also depends on the quality of the *a priori* information available, and if such information is missing (as in the present work) it also depends on the relative contribution of the high energy neutrons to the spectrum. The higher the fraction of neutrons corresponding to the rapidly increasing conversion factor in the energy range from 10 keV to 1 MeV, the larger the uncertainty of the integral dose equivalent.

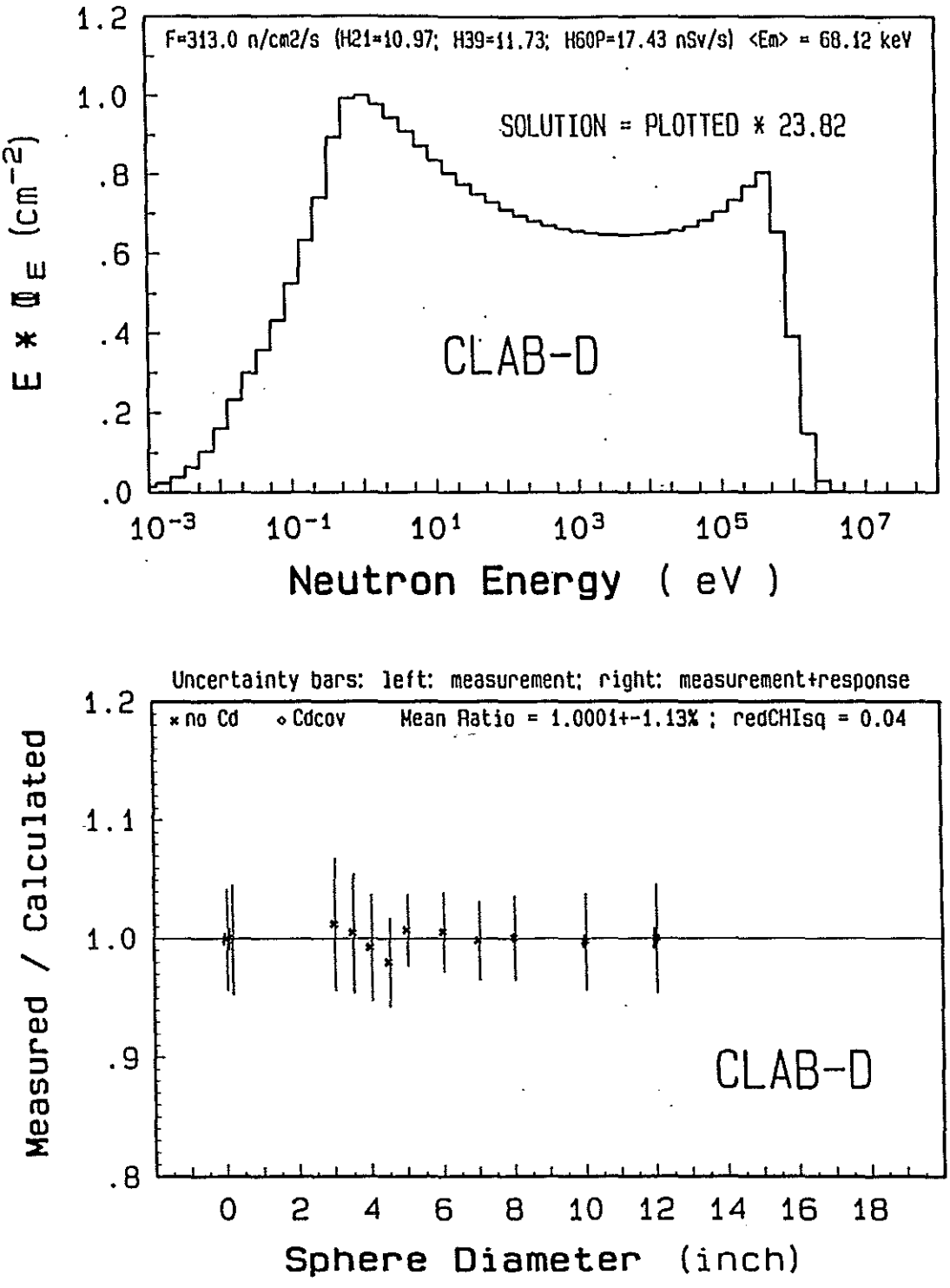

Figure 5: The neutron spectrum obtained at the CLAB-D point and the ratios $r_d = M_d/C_d$ (see text) calculated for this spectrum.

The dose equivalent values reported in this work are H21, H39, H60G and H60P using the *fluence-to-dose conversion function* according to ICRP21 [5], ICRU39 [6,7], ICRP60 in the GSF variant [8,9] or in the PTB variant [8,10].

In Table 5 (Appendix) we give the integral results derived from our solution spectra. The neutron fluence rate (in cm^{-2} s^{-1}) is given for five energy groups and in total, the dose eqivalent is given only in total (in μSv/h). The uncertainty of the integral fluence was estimated to be ± 5%, but was estimated to be larger in the energy groups, depending on the fraction of neutrons in a group. For the integral dose equivalent values the estimated uncertainties vary between ± 8% and ± 12%, depending on the hardness of the spectrum.

In the last two columns of the table we give the dose equivalent values obtained with the Leake-type rem-counter. For the calibration with a bare ^{252}Cf source the reading overestimates the spectrometric results by about a factor of two, but the calibration with a D_2O-moderated ^{252}Cf source also results in an overestimate, because the calibration field is still harder than the realistic fields investigated. The uncertainties attributed to the measurements with the Leake counter are correspondingly high.

3.3.6 Acknowledgements

The assistance of PTB colleagues in the technical development and maintenance of the Bonner sphere spectrometer is gratefully acknowledged, and also the cooperation of Swedish colleagues who made measurements possible in very difficult environmental conditions.

This work was partially supported by the Commission of the European Communities within the framework of the project FI3P-CT92-0002.

3.3.7 References

[1] Alevra, A.V., Cosack, M., Hunt, J.B., Thomas, D.J. and Schraube, H.,. *Experimental Determination of the Response of Four Bonner Sphere Sets to Monoenergetic Neutrons (II).* Radiat. Prot. Dosim. 40 (1992) 91 - 102.

[2] Thomas, D.J., Alevra, A.V., Hunt, J.B. and Schraube, H., *Experimental Determination of the Response of Four Bonner Sphere Sets to Thermal Neutrons.* Radiat. Prot. Dosim. 54 (1994) 25 - 31.

[3] Thomas, D.J., *Use of the Program ANISN to Calculate Response Functions for a Bonner Sphere Set with a ^3He Detector.* NPL Report RSA(EXT) 31 (1992).

[4] McElroy, W.N., Berg, S., Crockett, T. and Hawkins, R.G., *Sand-II, a Computer-Automated Iterative Method for Neutron Flux Spectra Determination by Foil Activation.* Report AFWL-TR-67-41., Vol. I-IV, Air Force Weapons Laboratory, New Mexico (1967).

[5] International Commission on Radiological Protection Publication 21, *Data for Protection against Ionizing Radiation from External Sources.* Supplement to ICRP Publication 15, Pergamon Press, Oxford, 1973.

[6] ICRU Report 39, *Determination of Dose Equivalent Resulting from External Radiation Sources.* ICRU Publications, Bethesda, 1985.

[7] Wagner, S., Großwendt, B., Harvey, I.R., Mill, A.J., Selbach, H.J. and Siebert, B.R.L., *Unified Conversion Function for the New ICRU Operational Radiation Protection Quantities.* Radiat. Prot. Dosim. 12 (1985) 231 - 235.

[8] International Commission on Radiological Protection Publication 60. *Recommendations of the International Commission on Radiological Protection.* Annals of ICRP 21, Pergamon Press, Oxford, 1991.

[9] Leuthold, G., Mares, V. and Schraube, H., *Calculation of the Neutron Ambient Dose Equivalent on the Basis of the ICRP Revised Quality Factors.* Radiat. Prot. Dosim. **40** (1992) 77 - 84.

[10] Schuhmacher, H, and Siebert, B.R.L., *Quality Factors and Ambient Dose Equivalent for Neutrons Based on the New ICRP Recommendation.* Radiat. Prot. Dosim. **40** (1992) 85 - 89.

[11] Alevra, A.V., *Accurate Neutron Fluence Measurements Using Bonner Spheres.* Reactor Dosimetry ASTM STP 1228, Harry Farrar IV, E. Parvin Lippincott, John G. Williams, and David W. Vehar., American Society for Testing and Materials, Philadelphia, 1994, in press.

3.3.8 Appendix

The Appendix contains the Tables 1 to 5 and Figures 6 to 9

Table 1. The fluence response matrix of the PTB "C" Bonner sphere set in cm^2; the energies are given in eV.

i	En	0C0	c0C0	3C0	3C5	4C0	4C5	5C0	6C0	7C0	8C0	10C	12C	15C	18C
1	1.000E-03	7.156E+00	.000E+00	4.300E-01	3.476E-01	2.750E-01	2.200E-01	1.734E-01	1.160E-01	7.500E-02	4.750E-02	1.939E-02	7.447E-03	1.421E-03	2.707E-04
2	1.585E-03	6.761E+00	.000E+00	5.344E-01	4.228E-01	3.408E-01	2.712E-01	2.230E-01	1.444E-01	9.420E-02	5.904E-02	2.401E-02	9.081E-03	1.731E-03	3.297E-04
3	2.512E-03	6.271E+00	.000E+00	6.377E-01	4.980E-01	4.064E-01	3.225E-01	2.721E-01	1.729E-01	1.134E-01	7.060E-02	2.862E-02	1.071E-02	2.041E-03	3.887E-04
4	3.981E-03	5.705E+00	.000E+00	7.388E-01	5.734E-01	4.716E-01	3.743E-01	3.201E-01	2.016E-01	1.324E-01	8.224E-02	3.324E-02	1.235E-02	2.351E-03	4.478E-04
5	6.310E-03	5.092E+00	.000E+00	8.367E-01	6.491E-01	5.362E-01	4.267E-01	3.665E-01	2.306E-01	1.513E-01	9.398E-02	3.786E-02	1.398E-02	2.661E-03	5.068E-04
6	1.000E-02	4.464E+00	.000E+00	9.302E-01	7.250E-01	6.000E-01	4.800E-01	4.109E-01	2.600E-01	1.700E-01	1.058E-01	4.248E-02	1.561E-02	2.971E-03	5.658E-04
7	1.585E-02	3.850E+00	.000E+00	1.020E+00	8.024E-01	6.639E-01	5.351E-01	4.536E-01	2.903E-01	1.888E-01	1.180E-01	4.709E-02	1.725E-02	3.281E-03	6.248E-04
8	2.512E-02	3.273E+00	.000E+00	1.112E+00	8.870E-01	7.334E-01	5.962E-01	4.989E-01	3.237E-01	2.091E-01	1.314E-01	5.220E-02	1.906E-02	3.625E-03	6.908E-04
9	3.981E-02	2.749E+00	.000E+00	1.216E+00	9.854E-01	8.151E-01	6.683E-01	5.524E-01	3.626E-01	2.329E-01	1.470E-01	5.797E-02	2.111E-02	4.014E-03	7.648E-04
10	6.310E-02	2.284E+00	.000E+00	1.339E+00	1.104E+00	9.157E-01	7.562E-01	6.193E-01	4.097E-01	2.620E-01	1.657E-01	6.458E-02	2.348E-02	4.460E-03	8.498E-04
11	1.000E-01	1.882E+00	.000E+00	1.490E+00	1.250E+00	1.042E+00	8.649E-01	7.050E-01	4.675E-01	2.982E-01	1.887E-01	7.229E-02	2.621E-02	4.978E-03	9.478E-04
12	1.585E-01	1.540E+00	.000E+00	1.673E+00	1.427E+00	1.197E+00	9.975E-01	8.130E-01	5.377E-01	3.429E-01	2.166E-01	8.129E-02	2.940E-02	5.581E-03	1.063E-03
13	2.512E-01	1.252E+00	.000E+00	1.873E+00	1.625E+00	1.376E+00	1.150E+00	9.396E-01	6.190E-01	3.949E-01	2.488E-01	9.190E-02	3.318E-02	6.295E-03	1.198E-03
14	3.981E-01	1.014E+00	2.321E-01	2.073E+00	1.832E+00	1.567E+00	1.316E+00	1.079E+00	7.089E-01	4.528E-01	2.845E-01	1.046E-01	3.768E-02	7.147E-03	1.360E-03
15	6.310E-01	8.179E-01	6.174E-01	2.253E+00	2.034E+00	1.763E+00	1.489E+00	1.226E+00	8.053E-01	5.150E-01	3.229E-01	1.196E-01	4.304E-02	8.162E-03	1.551E-03
16	1.000E+00	6.573E-01	6.043E-01	2.396E+00	2.218E+00	1.953E+00	1.664E+00	1.375E+00	9.059E-01	5.799E-01	3.631E-01	1.357E-01	4.874E-02	9.230E-03	1.755E-03
17	1.585E+00	5.272E-01	5.137E-01	2.489E+00	2.373E+00	2.127E+00	1.832E+00	1.519E+00	1.007E+00	6.452E-01	4.036E-01	1.505E-01	5.400E-02	1.023E-02	1.944E-03
18	2.512E+00	4.349E-01	4.310E-01	2.541E+00	2.491E+00	2.274E+00	1.980E+00	1.650E+00	1.101E+00	7.072E-01	4.422E-01	1.645E-01	5.901E-02	1.118E-02	2.124E-03
19	3.981E+00	3.454E-01	3.439E-01	2.560E+00	2.579E+00	2.396E+00	2.110E+00	1.770E+00	1.190E+00	7.663E-01	4.793E-01	1.781E-01	6.383E-02	1.208E-02	2.296E-03
20	6.310E+00	2.743E-01	2.740E-01	2.555E+00	2.641E+00	2.497E+00	2.226E+00	1.878E+00	1.274E+00	8.230E-01	5.151E-01	1.913E-01	6.850E-02	1.297E-02	2.464E-03
21	1.000E+01	2.178E-01	2.178E-01	2.533E+00	2.681E+00	2.579E+00	2.327E+00	1.976E+00	1.353E+00	8.780E-01	5.499E-01	2.041E-01	7.308E-02	1.384E-02	2.629E-03
22	1.585E+01	1.730E-01	1.730E-01	2.498E+00	2.705E+00	2.646E+00	2.416E+00	2.067E+00	1.429E+00	9.315E-01	5.842E-01	2.168E-01	7.761E-02	1.469E-02	2.792E-03
23	2.512E+01	1.374E-01	1.374E-01	2.453E+00	2.715E+00	2.699E+00	2.493E+00	2.149E+00	1.502E+00	9.838E-01	6.180E-01	2.294E-01	8.210E-02	1.555E-02	2.953E-03
24	3.981E+01	1.092E-01	1.092E-01	2.401E+00	2.714E+00	2.739E+00	2.559E+00	2.224E+00	1.571E+00	1.035E+00	6.514E-01	2.419E-01	8.658E-02	1.639E-02	3.114E-03
25	6.310E+01	8.667E-02	8.667E-02	2.339E+00	2.697E+00	2.763E+00	2.610E+00	2.288E+00	1.634E+00	1.082E+00	6.833E-01	2.540E-01	9.092E-02	1.722E-02	3.270E-03
26	1.000E+02	6.884E-02	6.884E-02	2.266E+00	2.664E+00	2.770E+00	2.647E+00	2.340E+00	1.691E+00	1.127E+00	7.136E-01	2.657E-01	9.509E-02	1.801E-02	3.420E-03
27	1.585E+02	5.468E-02	5.468E-02	2.183E+00	2.615E+00	2.760E+00	2.668E+00	2.379E+00	1.742E+00	1.168E+00	7.422E-01	2.769E-01	9.914E-02	1.878E-02	3.566E-03
28	2.512E+02	4.330E-02	4.330E-02	2.091E+00	2.553E+00	2.735E+00	2.676E+00	2.408E+00	1.786E+00	1.207E+00	7.693E-01	2.878E-01	1.031E-01	1.952E-02	3.708E-03
29	3.981E+02	3.436E-02	3.436E-02	1.994E+00	2.481E+00	2.698E+00	2.672E+00	2.427E+00	1.824E+00	1.243E+00	7.952E-01	2.984E-01	1.070E-01	2.025E-02	3.848E-03
30	6.310E+02	2.730E-02	2.730E-02	1.898E+00	2.408E+00	2.657E+00	2.662E+00	2.441E+00	1.859E+00	1.277E+00	8.211E-01	3.092E-01	1.109E-01	2.101E-02	3.990E-03
31	1.000E+03	2.167E-02	2.167E-02	1.805E+00	2.332E+00	2.612E+00	2.647E+00	2.451E+00	1.893E+00	1.311E+00	8.473E-01	3.204E-01	1.150E-01	2.179E-02	4.139E-03
32	1.585E+03	1.724E-02	1.724E-02	1.715E+00	2.257E+00	2.564E+00	2.630E+00	2.458E+00	1.926E+00	1.346E+00	8.746E-01	3.322E-01	1.194E-01	2.262E-02	4.296E-03
33	2.512E+03	1.348E-02	1.348E-02	1.627E+00	2.182E+00	2.514E+00	2.609E+00	2.462E+00	1.957E+00	1.381E+00	9.024E-01	3.445E-01	1.240E-01	2.349E-02	4.463E-03
34	3.981E+03	1.035E-02	1.035E-02	1.543E+00	2.107E+00	2.462E+00	2.585E+00	2.463E+00	1.987E+00	1.416E+00	9.311E-01	3.575E-01	1.289E-01	2.442E-02	4.639E-03
35	6.310E+03	7.977E-03	7.977E-03	1.462E+00	2.033E+00	2.410E+00	2.560E+00	2.464E+00	2.018E+00	1.454E+00	9.624E-01	3.719E-01	1.343E-01	2.546E-02	4.837E-03
36	1.000E+04	6.144E-03	6.144E-03	1.384E+00	1.961E+00	2.360E+00	2.537E+00	2.467E+00	2.054E+00	1.496E+00	9.980E-01	3.885E-01	1.406E-01	2.668E-02	5.067E-03
37	1.585E+04	4.711E-03	4.711E-03	1.308E+00	1.891E+00	2.311E+00	2.517E+00	2.474E+00	2.096E+00	1.547E+00	1.040E+00	4.086E-01	1.483E-01	2.816E-02	5.347E-03
38	2.512E+04	3.619E-03	3.619E-03	1.234E+00	1.822E+00	2.264E+00	2.501E+00	2.488E+00	2.150E+00	1.609E+00	1.093E+00	4.343E-01	1.582E-01	3.008E-02	5.712E-03
39	3.981E+04	2.773E-03	2.773E-03	1.159E+00	1.754E+00	2.221E+00	2.492E+00	2.513E+00	2.221E+00	1.691E+00	1.164E+00	4.690E-01	1.718E-01	3.271E-02	6.212E-03
40	6.310E+04	2.129E-03	2.129E-03	1.081E+00	1.682E+00	2.177E+00	2.488E+00	2.550E+00	2.316E+00	1.804E+00	1.262E+00	5.196E-01	1.921E-01	3.671E-02	6.973E-03
41	1.000E+05	1.670E-03	1.670E-03	9.984E-01	1.604E+00	2.129E+00	2.486E+00	2.598E+00	2.439E+00	1.951E+00	1.396E+00	5.918E-01	2.220E-01	4.271E-02	8.121E-03
42	1.585E+05	1.246E-03	1.246E-03	9.032E-01	1.508E+00	2.063E+00	2.472E+00	2.644E+00	2.586E+00	2.144E+00	1.581E+00	7.013E-01	2.701E-01	5.284E-02	1.009E-02
43	2.512E+05	9.702E-04	9.702E-04	7.895E-01	1.379E+00	1.958E+00	2.421E+00	2.664E+00	2.743E+00	2.384E+00	1.834E+00	8.729E-01	3.535E-01	7.211E-02	1.400E-02
44	3.981E+05	8.042E-04	8.042E-04	6.608E-01	1.216E+00	1.800E+00	2.310E+00	2.628E+00	2.878E+00	2.650E+00	2.153E+00	1.134E+00	5.001E-01	1.121E-01	2.310E-02
45	6.310E+05	7.445E-04	7.445E-04	5.242E-01	1.019E+00	1.581E+00	2.113E+00	2.496E+00	2.929E+00	2.881E+00	2.498E+00	1.495E+00	7.458E-01	1.978E-01	4.712E-02
46	1.000E+06	7.160E-04	7.160E-04	3.922E-01	8.056E-01	1.311E+00	1.830E+00	2.248E+00	2.839E+00	2.997E+00	2.788E+00	1.929E+00	1.116E+00	3.718E-01	1.118E-01
47	1.585E+06	7.032E-04	7.032E-04	2.756E-01	5.964E-01	1.017E+00	1.481E+00	1.893E+00	2.575E+00	2.919E+00	2.917E+00	2.339E+00	1.583E+00	6.770E-01	2.662E-01
48	2.512E+06	6.089E-04	6.089E-04	1.815E-01	4.110E-01	7.309E-01	1.106E+00	1.466E+00	2.134E+00	2.582E+00	2.751E+00	2.518E+00	1.962E+00	1.051E+00	5.273E-01
49	3.981E+06	3.836E-04	3.836E-04	1.135E-01	2.666E-01	4.915E-01	7.696E-01	1.054E+00	1.631E+00	2.093E+00	2.362E+00	2.430E+00	2.135E+00	1.385E+00	8.486E-01
50	6.310E+06	2.322E-04	2.322E-04	6.860E-02	1.669E-01	3.185E-01	5.155E-01	7.284E-01	1.198E+00	1.628E+00	1.947E+00	2.247E+00	2.226E+00	1.742E+00	1.301E+00
51	1.000E+07	1.426E-04	1.426E-04	3.605E-02	9.019E-02	1.772E-01	2.952E-01	4.288E-01	7.429E-01	1.061E+00	1.329E+00	1.677E+00	1.811E+00	1.611E+00	1.365E+00
52	1.585E+07	8.561E-05	8.561E-05	1.739E-02	4.426E-02	8.916E-02	1.525E-01	2.275E-01	4.152E-01	6.229E-01	8.183E-01	1.129E+00	1.328E+00	1.332E+00	1.265E+00
53	2.512E+07	.000E+00	.000E+00	.000E+00	.000E+00	1.095E-03	9.760E-03	2.619E-02	8.759E-02	1.854E-01	3.081E-01	5.822E-01	8.442E-01	1.052E+00	1.166E+00
	σ:	4.2 %	4.5 %	5.5 %	5.0 %	4.5 %	3.8 %	3.0 %	3.3 %	3.3 %	3.5 %	4.0 %	4.5 %	5.0 %	6.0 %
i	En	0C0	c0C0	3C0	3C5	4C0	4C5	5C0	6C0	7C0	8C0	10C	12C	15C	18C

Table 2. The fluence response matrix of the PTB "F" Bonner sphere set in cm²; the energies are given in eV.

i	En	0F0	c0F0	2F0	2F5	3F0	3F5	4F0	4F5	5F0	6F0	7F0	8F0	10F	12F
1	1.000E-03	8.299E-01	.000E+00	1.532E-01	8.468E-02	3.885E-02	2.200E-02	1.312E-02	1.070E-02	8.000E-03	4.400E-03	2.550E-03	1.500E-03	5.000E-04	1.100E-04
2	1.585E-03	7.833E-01	.000E+00	1.559E-01	9.238E-02	4.923E-02	3.271E-02	2.220E-02	1.775E-02	1.443E-02	8.692E-03	5.222E-03	3.153E-03	1.008E-03	3.329E-04
3	2.512E-03	7.256E-01	.000E+00	1.586E-01	1.001E-01	5.962E-02	4.329E-02	3.127E-02	2.485E-02	2.082E-02	1.299E-02	7.908E-03	4.808E-03	1.527E-03	5.557E-04
4	3.981E-03	6.587E-01	.000E+00	1.613E-01	1.078E-01	7.000E-02	5.362E-02	4.035E-02	3.206E-02	2.716E-02	1.728E-02	1.062E-02	6.467E-03	2.068E-03	7.786E-04
5	6.310E-03	5.860E-01	.000E+00	1.640E-01	1.155E-01	8.039E-02	6.356E-02	4.942E-02	3.942E-02	3.342E-02	2.158E-02	1.338E-02	8.130E-03	2.642E-03	1.002E-03
6	1.000E-02	5.117E-01	.000E+00	1.667E-01	1.232E-01	9.078E-02	7.300E-02	5.850E-02	4.700E-02	3.955E-02	2.587E-02	1.620E-02	9.800E-03	3.260E-03	1.224E-03
7	1.585E-02	4.393E-01	.000E+00	1.694E-01	1.309E-01	1.012E-01	8.201E-02	6.757E-02	5.492E-02	4.566E-02	3.023E-02	1.912E-02	1.150E-02	3.934E-03	1.447E-03
8	2.512E-02	3.717E-01	.000E+00	1.736E-01	1.399E-01	1.130E-01	9.153E-02	7.765E-02	6.364E-02	5.229E-02	3.494E-02	2.228E-02	1.332E-02	4.679E-03	1.690E-03
9	3.981E-02	3.107E-01	.000E+00	1.795E-01	1.508E-01	1.268E-01	1.027E-01	8.902E-02	7.371E-02	6.012E-02	4.034E-02	2.585E-02	1.539E-02	5.511E-03	1.960E-03
10	6.310E-02	2.570E-01	.000E+00	1.879E-01	1.641E-01	1.429E-01	1.166E-01	1.020E-01	8.564E-02	6.979E-02	4.678E-02	3.002E-02	1.782E-02	6.446E-03	2.268E-03
11	1.000E-01	2.109E-01	.000E+00	1.993E-01	1.804E-01	1.620E-01	1.344E-01	1.172E-01	1.000E-01	8.200E-02	5.459E-02	3.494E-02	2.073E-02	7.500E-03	2.619E-03
12	1.585E-01	1.719E-01	.000E+00	2.142E-01	2.001E-01	1.845E-01	1.569E-01	1.347E-01	1.171E-01	9.717E-02	6.402E-02	4.073E-02	2.420E-02	8.687E-03	3.023E-03
13	2.512E-01	1.393E-01	.000E+00	2.303E-01	2.233E-01	2.105E-01	1.830E-01	1.552E-01	1.367E-01	1.148E-01	7.488E-02	4.732E-02	2.818E-02	1.001E-02	3.496E-03
14	3.981E-01	1.125E-01	2.576E-02	2.489E-01	2.493E-01	2.393E-01	2.113E-01	1.791E-01	1.581E-01	1.342E-01	8.686E-02	5.456E-02	3.256E-02	1.146E-02	4.054E-03
15	6.310E-01	9.057E-02	6.837E-02	2.676E-01	2.783E-01	2.708E-01	2.404E-01	2.070E-01	1.810E-01	1.546E-01	9.965E-02	6.231E-02	3.726E-02	1.305E-02	4.712E-03
16	1.000E+00	7.265E-02	6.680E-02	2.833E-01	3.018E-01	3.001E-01	2.689E-01	2.356E-01	2.047E-01	1.754E-01	1.130E-01	7.044E-02	4.217E-02	1.476E-02	5.409E-03
17	1.585E+00	5.818E-02	5.668E-02	2.954E-01	3.213E-01	3.242E-01	2.952E-01	2.605E-01	2.282E-01	1.956E-01	1.264E-01	7.869E-02	4.714E-02	1.656E-02	6.057E-03
18	2.512E+00	4.768E-02	4.725E-02	3.036E-01	3.366E-01	3.435E-01	3.174E-01	2.825E-01	2.496E-01	2.142E-01	1.391E-01	8.656E-02	5.188E-02	1.828E-02	6.675E-03
19	3.981E+00	3.787E-02	3.771E-02	3.075E-01	3.476E-01	3.584E-01	3.360E-01	3.020E-01	2.689E-01	2.313E-01	1.509E-01	9.415E-02	5.642E-02	1.993E-02	7.270E-03
20	6.310E+00	3.007E-02	3.004E-02	3.079E-01	3.548E-01	3.696E-01	3.513E-01	3.189E-01	2.864E-01	2.472E-01	1.622E-01	1.013E-01	6.081E-02	2.154E-02	7.848E-03
21	1.000E+01	2.388E-02	2.388E-02	3.053E-01	3.592E-01	3.780E-01	3.638E-01	3.337E-01	3.024E-01	2.619E-01	1.731E-01	1.084E-01	6.512E-02	2.311E-02	8.416E-03
22	1.585E+01	1.897E-02	1.897E-02	3.003E-01	3.615E-01	3.841E-01	3.740E-01	3.467E-01	3.168E-01	2.755E-01	1.835E-01	1.153E-01	6.935E-02	2.468E-02	8.975E-03
23	2.512E+01	1.507E-02	1.507E-02	2.937E-01	3.624E-01	3.887E-01	3.820E-01	3.579E-01	3.299E-01	2.880E-01	1.935E-01	1.221E-01	7.353E-02	2.622E-02	9.527E-03
24	3.981E+01	1.197E-02	1.197E-02	2.850E-01	3.613E-01	3.917E-01	3.880E-01	3.674E-01	3.417E-01	2.997E-01	2.032E-01	1.287E-01	7.766E-02	2.776E-02	1.009E-02
25	6.310E+01	9.503E-03	9.503E-03	2.732E-01	3.562E-01	3.915E-01	3.915E-01	3.747E-01	3.515E-01	3.098E-01	2.121E-01	1.350E-01	8.161E-02	2.924E-02	1.063E-02
26	1.000E+02	7.548E-03	7.548E-03	2.587E-01	3.473E-01	3.882E-01	3.923E-01	3.794E-01	3.590E-01	3.181E-01	2.200E-01	1.407E-01	8.534E-02	3.064E-02	1.114E-02
27	1.585E+02	5.995E-03	5.995E-03	2.427E-01	3.357E-01	3.821E-01	3.905E-01	3.818E-01	3.643E-01	3.247E-01	2.270E-01	1.460E-01	8.885E-02	3.198E-02	1.163E-02
28	2.512E+02	4.747E-03	4.747E-03	2.261E-01	3.224E-01	3.737E-01	3.865E-01	3.822E-01	3.677E-01	3.297E-01	2.330E-01	1.510E-01	9.216E-02	3.325E-02	1.209E-02
29	3.981E+02	3.767E-03	3.767E-03	2.098E-01	3.082E-01	3.637E-01	3.806E-01	3.808E-01	3.694E-01	3.334E-01	2.383E-01	1.557E-01	9.531E-02	3.448E-02	1.254E-02
30	6.310E+02	2.993E-03	2.993E-03	1.942E-01	2.936E-01	3.530E-01	3.739E-01	3.784E-01	3.702E-01	3.363E-01	2.434E-01	1.602E-01	9.850E-02	3.574E-02	1.300E-02
31	1.000E+03	2.376E-03	2.376E-03	1.795E-01	2.790E-01	3.419E-01	3.667E-01	3.754E-01	3.704E-01	3.387E-01	2.482E-01	1.647E-01	1.017E-01	3.704E-02	1.348E-02
32	1.585E+03	1.890E-03	1.890E-03	1.655E-01	2.644E-01	3.305E-01	3.592E-01	3.720E-01	3.700E-01	3.406E-01	2.529E-01	1.692E-01	1.051E-01	3.841E-02	1.400E-02
33	2.512E+03	1.478E-03	1.478E-03	1.524E-01	2.502E-01	3.191E-01	3.513E-01	3.680E-01	3.692E-01	3.422E-01	2.574E-01	1.738E-01	1.085E-01	3.985E-02	1.454E-02
34	3.981E+03	1.135E-03	1.135E-03	1.401E-01	2.366E-01	3.075E-01	3.432E-01	3.636E-01	3.678E-01	3.435E-01	2.618E-01	1.784E-01	1.120E-01	4.136E-02	1.510E-02
35	6.310E+03	8.747E-04	8.747E-04	1.284E-01	2.231E-01	2.960E-01	3.349E-01	3.590E-01	3.665E-01	3.447E-01	2.665E-01	1.834E-01	1.159E-01	4.305E-02	1.575E-02
36	1.000E+04	6.736E-04	6.736E-04	1.175E-01	2.099E-01	2.846E-01	3.269E-01	3.548E-01	3.653E-01	3.463E-01	2.717E-01	1.890E-01	1.203E-01	4.500E-02	1.649E-02
37	1.585E+04	5.165E-04	5.165E-04	1.068E-01	1.967E-01	2.731E-01	3.191E-01	3.507E-01	3.646E-01	3.484E-01	2.779E-01	1.956E-01	1.256E-01	4.734E-02	1.739E-02
38	2.512E+04	3.968E-04	3.968E-04	9.728E-02	1.849E-01	2.623E-01	3.115E-01	3.472E-01	3.648E-01	3.518E-01	2.856E-01	2.038E-01	1.323E-01	5.037E-02	1.856E-02
39	3.981E+04	3.040E-04	3.040E-04	8.662E-02	1.708E-01	2.504E-01	3.043E-01	3.443E-01	3.662E-01	3.569E-01	2.960E-01	2.146E-01	1.410E-01	5.446E-02	2.016E-02
40	6.310E+04	2.334E-04	2.334E-04	7.685E-02	1.575E-01	2.381E-01	2.966E-01	3.419E-01	3.687E-01	3.640E-01	3.098E-01	2.293E-01	1.533E-01	6.043E-02	2.254E-02
41	1.000E+05	1.831E-04	1.831E-04	6.651E-02	1.426E-01	2.243E-01	2.882E-01	3.395E-01	3.722E-01	3.731E-01	3.276E-01	2.488E-01	1.702E-01	6.901E-02	2.608E-02
42	1.585E+05	1.367E-04	1.367E-04	5.573E-02	1.257E-01	2.073E-01	2.768E-01	3.347E-01	3.746E-01	3.824E-01	3.491E-01	2.745E-01	1.937E-01	8.213E-02	3.178E-02
43	2.512E+05	1.064E-04	1.064E-04	4.492E-02	1.076E-01	1.863E-01	2.598E-01	3.244E-01	3.720E-01	3.888E-01	3.729E-01	3.068E-01	2.264E-01	1.030E-01	4.173E-02
44	3.981E+05	8.817E-05	8.817E-05	3.406E-02	8.714E-02	1.604E-01	2.357E-01	3.055E-01	3.608E-01	3.877E-01	3.945E-01	3.438E-01	2.685E-01	1.354E-01	5.941E-02
45	6.310E+05	8.163E-05	8.163E-05	2.443E-02	6.666E-02	1.307E-01	2.037E-01	2.753E-01	3.360E-01	3.726E-01	4.052E-01	3.775E-01	3.154E-01	1.813E-01	8.949E-02
46	1.000E+06	7.851E-05	7.851E-05	1.635E-02	4.764E-02	1.000E-01	1.660E-01	2.345E-01	2.962E-01	3.398E-01	3.965E-01	3.970E-01	3.568E-01	2.381E-01	1.357E-01
47	1.585E+06	7.710E-05	7.710E-05	1.073E-02	3.249E-02	7.207E-02	1.263E-01	1.865E-01	2.440E-01	2.898E-01	3.632E-01	3.914E-01	3.785E-01	2.941E-01	1.951E-01
48	2.512E+06	6.676E-05	6.676E-05	6.466E-03	2.071E-02	4.824E-02	8.913E-02	1.370E-01	1.851E-01	2.269E-01	3.036E-01	3.498E-01	3.613E-01	3.221E-01	2.447E-01
49	3.981E+06	4.206E-05	4.206E-05	3.752E-03	1.233E-02	3.039E-02	5.898E-02	9.389E-02	1.305E-01	1.648E-01	2.340E-01	2.863E-01	3.137E-01	3.152E-01	2.692E-01
50	6.310E+06	2.546E-05	2.546E-05	2.054E-03	7.301E-03	1.869E-02	3.763E-02	6.195E-02	8.854E-02	1.150E-01	1.731E-01	2.250E-01	2.614E-01	2.958E-01	2.835E-01
51	1.000E+07	1.563E-05	1.563E-05	9.597E-04	3.745E-03	9.730E-03	2.065E-02	3.500E-02	5.125E-02	6.825E-02	1.081E-01	1.477E-01	1.800E-01	2.231E-01	2.325E-01
52	1.585E+07	9.387E-06	9.387E-06	6.771E-04	2.629E-03	5.821E-03	1.028E-02	1.786E-02	2.676E-02	3.651E-02	6.081E-02	8.743E-02	1.118E-01	1.519E-01	1.716E-01
53	2.512E+07	.000E+00	.000E+00	3.945E-04	1.512E-03	2.057E-03	.000E+00	7.360E-04	2.262E-03	4.773E-03	1.355E-02	2.718E-02	4.373E-02	8.066E-02	1.108E-01
	σ:	4.5 %	4.7 %	7.5 %	6.8 %	6.2 %	5.7 %	5.2 %	4.8 %	4.5 %	4.8 %	5.0 %	5.0 %	5.5 %	6.0 %
i	En	0F0	c0F0	2F0	2F5	3F0	3F5	4F0	4F5	5F0	6F0	7F0	8F0	10F	12F

Table 3: PTB Bonners sphere and LEAKE rem counter readings in various neutron fields in Sweden, November 1992

Det	CLAB-D.DAT Reading (count/s)	CLAB-E.DAT Reading (count/s)	CLAB-P.DAT Reading (count/s)	RING-G.DAT Reading (count/s)	St.Dev.of Response
0C0	1.492E+02 ± 0.475 %	1.334E+02 ± 0.561 %	1.061E+02 ± 0.450 %	3.996E+03 ± 0.185 %	4.200 %
c0C0	4.068E+01 ± 0.906 %	3.249E+01 ± 1.133 %	2.582E+01 ± 1.271 %	2.981E+02 ± 0.616 %	4.500 %
3C0	5.609E+02 ± 0.248 %	4.651E+02 ± 0.303 %	4.308E+02 ± 0.315 %	4.999E+03 ± 0.169 %	5.500 %
3C5	6.354E+02 ± 0.233 %	5.323E+02 ± 0.284 %	5.127E+02 ± 0.289 %		5.000 %
4C0	6.625E+02 ± 0.229 %	5.567E+02 ± 0.278 %	5.546E+02 ± 0.278 %	4.905E+03 ± 0.170 %	4.500 %
4C5	6.496E+02 ± 0.231 %	5.468E+02 ± 0.280 %	5.620E+02 ± 0.277 %		3.800 %
5C0	6.215E+02 ± 0.167 %	5.259E+02 ± 0.202 %	5.522E+02 ± 0.200 %	4.111E+03 ± 0.130 %	3.000 %
6C0	5.013E+02 ± 0.261 %	4.238E+02 ± 0.318 %	4.610E+02 ± 0.305 %		3.300 %
7C0	3.699E+02 ± 0.303 %	3.133E+02 ± 0.368 %	3.503E+02 ± 0.349 %		3.300 %
8C0	2.593E+02 ± 0.361 %	2.183E+02 ± 0.440 %	2.470E+02 ± 0.414 %	1.408E+03 ± 0.292 %	3.500 %
10C	1.142E+02 ± 0.542 %	9.660E+01 ± 0.658 %	1.094E+02 ± 0.619 %		4.000 %
12C	4.751E+01 ± 0.839 %	3.794E+01 ± 1.049 %	4.336E+01 ± 0.986 %	2.081E+02 ± 0.735 %	4.500 %
LEAKE	1.848E+01 ± 0.670 %	1.560E+01 ± 0.732 %	1.843E+01 ± 0.680 %	8.768E+01 ± 0.530 %	50.000 %

Det	RING-L.DAT Reading (count/s)	RING-F.DAT Reading (count/s)	St.Dev.of Response
0F0	1.001E+02 ± 0.747 %		4.500 %
c0F0	2.686E+01 ± 1.439 %		4.700 %
3F0	5.955E+02 ± 0.311 %		6.200 %
4F0	6.397E+02 ± 0.300 %		5.200 %
5F0	5.581E+02 ± 0.228 %		4.500 %
8F0	2.028E+02 ± 0.526 %		5.000 %
12F	3.084E+01 ± 1.344 %		6.000 %
LEAKE	1.173E+02 ± 0.400 %	4.051E+02 ± 0.300 %	50.000 %

Table 4: The fluence obtained with the PTB Bonner sphere spectrometer in various neutron fields in Sweden, November 1992

```
CLAB-D(E)(P): 12 detectors used: 0C0,c0C0,3C0,3C5,4C0,4C5,5C0,6C0,7C0,8C0,10C,12C;
RING-G:        7 detectors used: 0C0,c0C0,3C0,4C0,5C0,8C0,12C;
RING-L:        7 detectors used: 0F0,c0F0,3F0,4F0,5F0,8F0,12F;

                    In all cases 1000 iterations were done !

ELi is the lower margin, EUi is the upper margin of the i-th energy bin;
Ei is the logarithmic mean of the i-th energy bin: Ei²=ELi·EUi

The energies (Ei, ELi, EUi) are given in eV;
The spectral fluences (ΦEi) are given in 1/(cm²·eV·s)
```

i	Ei	ELi	EUi	CLAB-D ΦEi	CLAB-E ΦEi	CLAB-P ΦEi	RING-G ΦEi	RING-L ΦEi
1	1.0000E-03	7.9433E-04	1.2589E-03	3.3030E+02	3.6550E+02	3.3930E+02	1.2970E+04	3.5590E+03
2	1.5849E-03	1.2589E-03	1.9953E-03	3.4810E+02	3.8270E+02	3.5010E+02	1.3360E+04	3.5220E+03
3	2.5119E-03	1.9953E-03	3.1623E-03	3.6560E+02	3.9810E+02	3.5830E+02	1.3780E+04	3.4510E+03
4	3.9811E-03	3.1623E-03	5.0119E-03	3.8050E+02	4.0890E+02	3.6160E+02	1.4210E+04	3.3270E+03
5	6.3096E-03	5.0119E-03	7.9433E-03	3.8860E+02	4.1010E+02	3.5570E+02	1.4600E+04	3.1240E+03
6	1.0000E-02	7.9433E-03	1.2589E-02	3.8170E+02	3.9380E+02	3.3440E+02	1.4760E+04	2.8080E+03
7	1.5849E-02	1.2589E-02	1.9953E-02	3.4950E+02	3.5090E+02	2.9140E+02	1.4390E+04	2.3470E+03
8	2.5119E-02	1.9953E-02	3.1623E-02	2.8420E+02	2.7650E+02	2.2400E+02	1.2990E+04	1.7460E+03
9	3.9811E-02	3.1623E-02	5.0119E-02	2.1410E+02	2.0100E+02	1.5850E+02	1.0710E+04	1.2060E+03
10	6.3096E-02	5.0119E-02	7.9433E-02	1.6330E+02	1.4770E+02	1.1330E+02	7.5700E+03	8.4800E+02
11	1.0000E-01	7.9433E-02	1.2589E-01	1.2510E+02	1.0910E+02	8.1460E+01	4.1610E+03	6.0410E+02
12	1.5849E-01	1.2589E-01	1.9953E-01	9.5140E+01	8.0350E+01	5.8500E+01	2.0040E+03	4.3080E+02
13	2.5119E-01	1.9953E-01	3.1623E-01	7.0290E+01	5.7910E+01	4.1280E+01	1.1380E+03	3.0770E+02
14	3.9811E-01	3.1623E-01	5.0119E-01	5.3520E+01	4.2960E+01	3.2040E+01	5.5260E+02	2.6220E+02
15	6.3096E-01	5.0119E-01	7.9433E-01	3.7500E+01	2.9450E+01	2.3490E+01	2.7740E+02	1.9550E+02
16	1.0000E+00	7.9433E-01	1.2589E+00	2.3820E+01	1.8880E+01	1.4900E+01	1.6930E+02	1.2930E+02
17	1.5849E+00	1.2589E+00	1.9953E+00	1.4700E+01	1.1740E+01	9.1280E+00	1.0500E+02	8.3580E+01
18	2.5119E+00	1.9953E+00	3.1623E+00	8.9520E+00	7.1830E+00	5.5440E+00	6.4390E+01	5.3530E+01
19	3.9811E+00	3.1623E+00	5.0119E+00	5.4410E+00	4.3750E+00	3.3620E+00	3.9500E+01	3.4280E+01
20	6.3096E+00	5.0119E+00	7.9433E+00	3.2900E+00	2.6460E+00	2.0390E+00	2.4010E+01	2.1740E+01
21	1.0000E+01	7.9433E+00	1.2589E+01	1.9900E+00	1.5990E+00	1.2430E+00	1.4510E+01	1.3700E+01
22	1.5849E+01	1.2589E+01	1.9953E+01	1.2060E+00	9.6810E-01	7.6390E-01	8.7260E+00	8.5910E+00
23	2.5119E+01	1.9953E+01	3.1623E+01	7.3360E-01	5.8830E-01	4.7300E-01	5.2370E+00	5.3630E+00
24	3.9811E+01	3.1623E+01	5.0119E+01	4.4800E-01	3.5940E-01	2.9550E-01	3.1410E+00	3.3180E+00
25	6.3096E+01	5.0119E+01	7.9433E+01	2.7470E-01	2.2080E-01	1.8590E-01	1.8840E+00	2.0500E+00
26	1.0000E+02	7.9433E+01	1.2589E+02	1.6890E-01	1.3610E-01	1.1780E-01	1.1310E+00	1.2640E+00
27	1.5849E+02	1.2589E+02	1.9953E+02	1.0420E-01	8.4230E-02	7.5090E-02	6.8000E-01	7.7900E-01
28	2.5119E+02	1.9953E+02	3.1623E+02	6.4500E-02	5.2320E-02	4.8160E-02	4.0940E-01	4.8120E-01
29	3.9811E+02	3.1623E+02	5.0119E+02	4.0040E-02	3.2630E-02	3.1060E-02	2.4700E-01	2.9700E-01
30	6.3096E+02	5.0119E+02	7.9433E+02	2.4930E-02	2.0460E-02	2.0120E-02	1.4930E-01	1.8400E-01
31	1.0000E+03	7.9433E+02	1.2589E+03	1.5580E-02	1.2880E-02	1.3110E-02	9.0520E-02	1.1410E-01
32	1.5849E+03	1.2589E+03	1.9953E+03	9.7600E-03	8.1350E-03	8.5660E-03	5.5040E-02	7.1340E-02
33	2.5119E+03	1.9953E+03	3.1623E+03	6.1270E-03	5.1570E-03	5.6200E-03	3.3530E-02	4.4500E-02
34	3.9811E+03	3.1623E+03	5.0119E+03	3.8580E-03	3.2830E-03	3.7000E-03	2.0480E-02	2.7830E-02
35	6.3096E+03	5.0119E+03	7.9433E+03	2.4350E-03	2.0980E-03	2.4470E-03	1.2540E-02	1.7510E-02
36	1.0000E+04	7.9433E+03	1.2589E+04	1.5400E-03	1.3440E-03	1.6230E-03	7.6970E-03	1.1090E-02
37	1.5849E+04	1.2589E+04	1.9953E+04	9.7680E-04	8.6440E-04	1.0830E-03	4.7350E-03	7.0840E-03
38	2.5119E+04	1.9953E+04	3.1623E+04	6.2270E-04	5.5930E-04	7.2730E-04	2.9260E-03	4.5560E-03
39	3.9811E+04	3.1623E+04	5.0119E+04	3.9880E-04	3.6370E-04	4.9250E-04	1.8150E-03	2.9510E-03
40	6.3096E+04	5.0119E+04	7.9433E+04	2.5740E-04	2.3900E-04	3.3760E-04	1.1310E-03	1.9560E-03
41	1.0000E+05	7.9433E+04	1.2589E+05	1.6770E-04	1.5880E-04	2.3340E-04	7.0710E-04	1.3220E-03
42	1.5849E+05	1.2589E+05	1.9953E+05	1.1020E-04	1.0680E-04	1.6110E-04	4.3910E-04	9.0910E-04
43	2.5119E+05	1.9953E+05	3.1623E+05	7.2920E-05	7.1970E-05	1.0720E-04	2.6410E-04	6.1750E-04
44	3.9811E+05	3.1623E+05	5.0119E+05	4.8090E-05	4.6770E-05	6.3450E-05	1.1310E-04	2.8870E-04
45	6.3096E+05	5.0119E+05	7.9433E+05	2.4600E-05	2.0380E-05	2.3670E-05	3.2100E-05	7.9500E-05
46	1.0000E+06	7.9433E+05	1.2589E+06	9.3020E-06	5.4630E-06	4.9840E-06	5.1150E-06	1.0230E-05
47	1.5849E+06	1.2589E+06	1.9953E+06	2.2220E-06	7.3530E-07	5.1620E-07	3.7280E-07	5.1870E-07
48	2.5119E+06	1.9953E+06	3.1623E+06	2.6390E-07	4.1440E-08	2.4610E-08	8.9900E-09	8.4610E-09
49	3.9811E+06	3.1623E+06	5.0119E+06	1.0560E-08	6.8730E-10	4.0890E-10	3.7910E-11	2.5150E-11
50	6.3096E+06	5.0119E+06	7.9433E+06	7.5620E-11	1.5660E-12	1.1580E-12	9.3730E-15	4.4450E-15
51	1.0000E+07	7.9433E+06	1.2589E+07	3.5870E-14	2.0180E-16	2.7420E-16	2.7040E-20	1.0250E-20
52	1.5849E+07	1.2589E+07	1.9953E+07	2.2730E-19	2.1180E-22	8.7250E-22	1.3580E-27	1.3580E-27
53	2.5119E+07	1.9953E+07	3.1623E+07	8.5690E-28	8.5690E-28	8.5690E-28	8.5690E-28	8.5690E-28
	Φtotal (n/cm²/s)		=	313.0	264.2	261.8	2922	2038

Table 5. Integral results derived from the Bonner sphere spectra. The fluence rate is given for five energy groups and in total, the dose equivalent (see text) is given in total. In the last two columns the total dose equivalent (ICRP21) values are given as obtained with the LEAKE-type rem counter calibrated with a bare 252Cf source and a D2O-moderated 252Cf source.

All data are normalized to 1/s ; The fluences are given in [1/(cm²s)] ; The dose equivalent is given in [µSv/h] !

CLAB -D-	energy range	< 0.4 eV	.4eV-10keV	10keV-100keV	100keV-1MeV	> 1 MeV	1 meV-25 MeV	H21=Hmade	H39=H*(10)	H60 (GSF)	H60 (PTB)	LEAKE	H21/bCf	H21/mCf
	fluence	44.59	188.26	36.82	38.99	4.37	313.0	39.49	42.23	63.09	62.75		71.6	50.9
	uncertainty	± 7 %	± 7 %	± 6 %	± 6 %	± 12 %	± 5 %	± 10 %	± 10 %	± 10 %	± 10 %		± 100 %	± 50 %
CLAB -E-	energy range	< 0.4 eV	.4eV-10keV	10keV-100keV	100keV-1MeV	> 1 MeV	1 meV-25 MeV	H21=Hmade	H39=H*(10)	H60 (GSF)	H60 (PTB)	LEAKE	H21/bCf	H21/mCf
	fluence	39.91	152.81	33.37	36.12	2.01	264.2	32.14	35.05	53.14	52.88		60.4	43.0
	uncertainty	± 7 %	± 7 %	± 6 %	± 6 %	± 15 %	± 5 %	± 10 %	± 10 %	± 10 %	± 10 %		± 100 %	± 50 %
CLAB -P-	energy range	< 0.4 eV	.4eV-10keV	10keV-100keV	100keV-1MeV	> 1 MeV	1 meV-25 MeV	H21=Hmade	H39=H*(10)	H60 (GSF)	H60 (PTB)	LEAKE	H21/bCf	H21/mCf
	fluence	30.71	134.85	44.47	50.12	1.70	261.8	37.69	42.77	65.38	65.81		71.4	50.8
	uncertainty	± 7 %	± 7 %	± 6 %	± 6 %	± 15 %	± 5 %	± 12 %	± 12 %	± 12 %	± 12 %		± 100 %	± 50 %
RING -L-	energy range	< 0.4 eV	.4eV-10keV	10keV-100keV	100keV-1MeV	> 1 MeV	1 meV-25 MeV	H21=Hmade	H39=H*(10)	H60 (GSF)	H60 (PTB)	LEAKE	H21/bCf	H21/mCf
	fluence	239.12	1270.2	273.16	252.04	3.04	2038.	204.7	222.7	345.2	339.5		454.4	323.0
	uncertainty	± 7 %	± 7 %	± 6 %	± 6 %	± 20 %	± 5 %	± 10 %	± 10 %	± 10 %	± 10 %		± 100 %	± 50 %
RING -G-	energy range	< 0.4 eV	.4eV-10keV	10keV-100keV	100keV-1MeV	> 1 MeV	1 meV-25 MeV	H21=Hmade	H39=H*(10)	H60 (GSF)	H60 (PTB)	LEAKE	H21/bCf	H21/mCf
	fluence	1367.1	1269.9	170.21	112.84	1.61	2922.	174.4	164.7	255.7	238.5		339.6	241.5
	uncertainty	± 7 %	± 7 %	± 6 %	± 6 %	± 30 %	± 5 %	± 8 %	± 8 %	± 8 %	± 8 %		± 100 %	± 50 %
RING -F-	energy range	< 0.4 eV	.4eV-10keV	10keV-100keV	100keV-1MeV	> 1 MeV	1 meV-25 MeV	H21=Hmade	H39=H*(10)	H60 (GSF)	H60 (PTB)	LEAKE	H21/bCf	H21/mCf
	fluence	———	———	———	———	———	———	———	———	———	———		1569.	1116.
	uncertainty	———	———	———	———	———	———	———	———	———	———		± 100 %	± 50 %

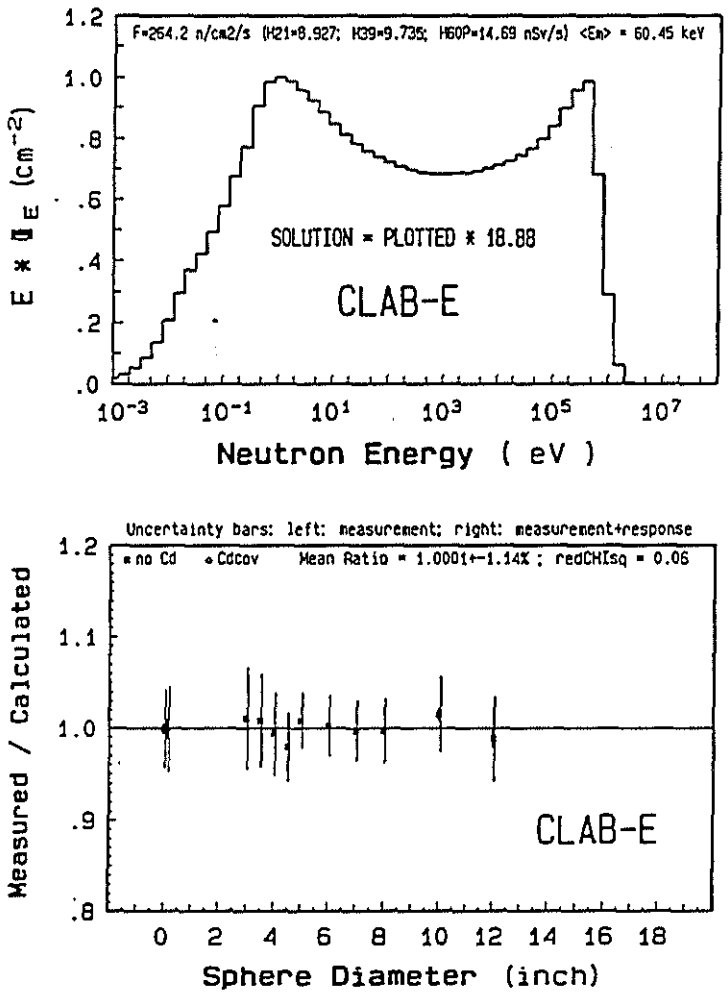

Figure 6. The neutron spectrum obtained at the CLAB-E point and the ratios $r_d = M_d/C_d$ (see text) calculated for this spectrum.

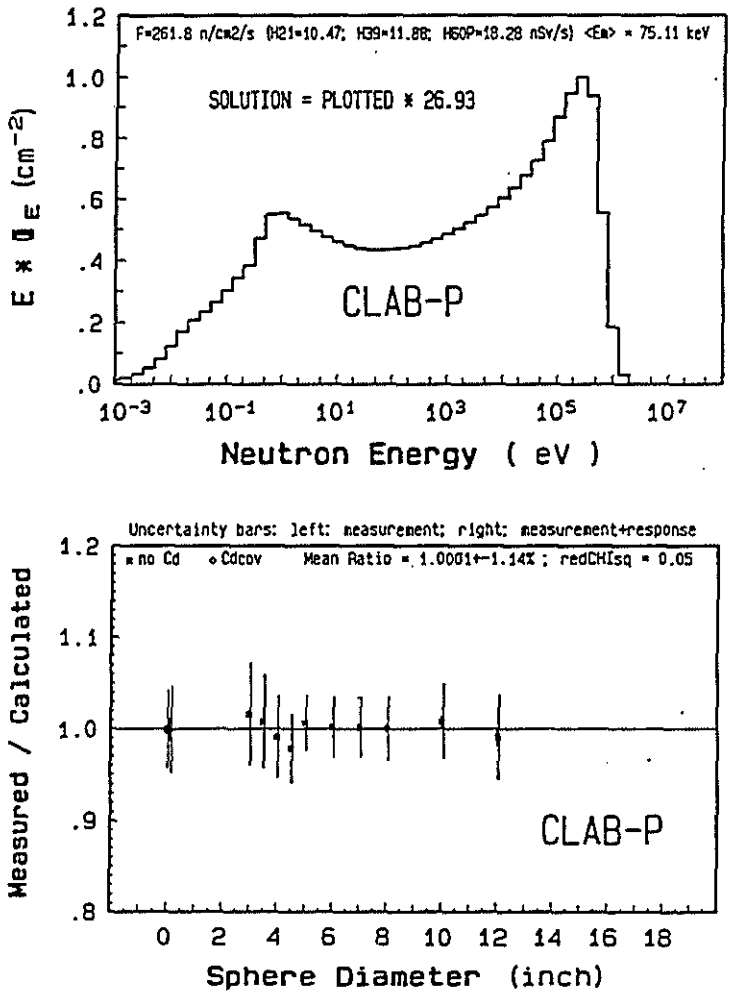

Figure 7. The neutron spectrum obtained at the CLAB-P point and the ratios $r_d = M_d/C_d$ (see text) calculated for this spectrum.

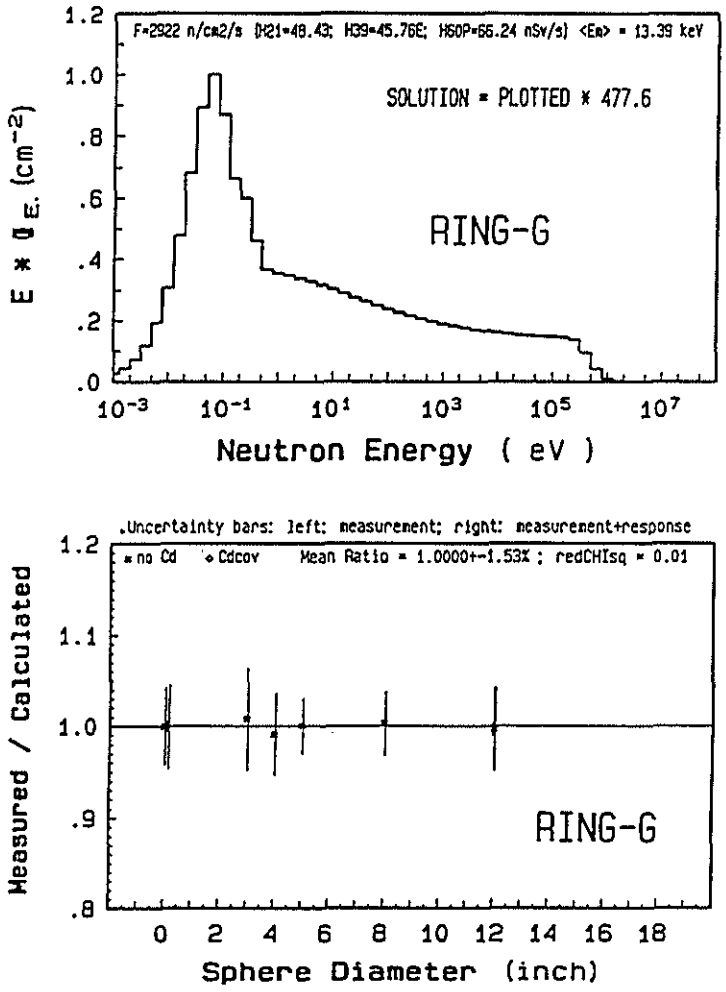

Figure 8. The neutron spectrum obtained at the RING-G point and the ratios $r_d = M_d/C_d$ (see text) calculated for this spectrum.

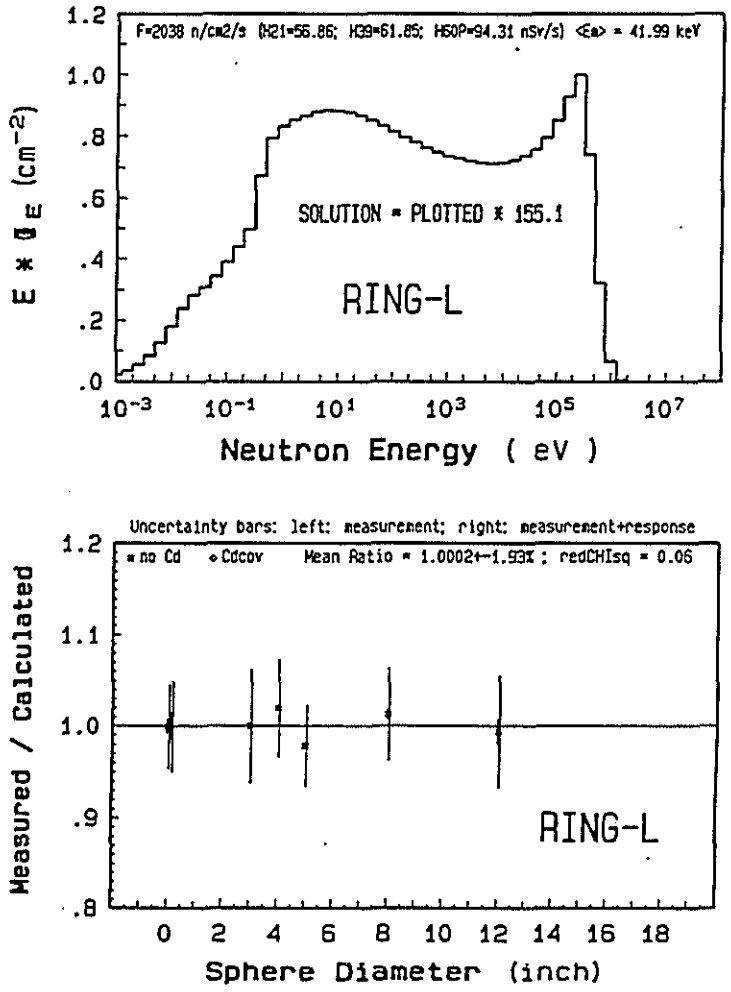

Figure 9. The neutron spectrum obtained at the RING-L point and the ratios $r_d = M_d/C_d$ (see text) calculated for this spectrum.

3.4 Spectrometry Measurements by NPL at Position A Ringhals Reactor

A.G. Bardell and D.J. Thomas
National Physical Laboratory (NPL), Teddington, Middlesex, U.K.

3.4.1. Introduction.

Spectrometry measurements were performed using a passive Bonner sphere (BS) spectrometer. Gold activation foils were used as the central thermal neutron detectors for the spheres with the foils being returned to NPL for determination of the induced activity. Measurements were also performed with a Harwell Neutron Dose-Equivalent Monitor model 0949 belonging to NPL, and a DINEUTRON belonging to the Health Physics section at Ringhals.

3.4.2 The Bonner Sphere Set

The Bonner sphere set used for this measurement consists of 2, 3, 4, 5, 6.5, 8, 10, and 12 inch diameter polyethylene spheres[1]. The spheres are made from material with a density of 0.922 g cm^{-3}, with removable polyethylene plugs which enable small gold foils to be located at the centre of each sphere [1]. The pure gold foils are 1 cm^2 in area with thicknesses in the range (96.0 - 97.0) mg cm^2. Each sphere is enclosed in an appropriately sized cylindrical cadmium metal shield to exclude neutrons below 0.5 eV.

The thermal neutron component of the field, below the cadmium cut off energy of 0.5 eV, was measured by irradiating bare and cadmium covered gold foils, of the same type used in the spheres. The thermal neutron fluence, according to the Westcott convention, was determined from the bare minus the cadmium covered foil activities [2].

3.4.3 The Measurements

The measurements were performed at Position A in Ringhals #4 reactor during the period 21-24 March 1993. The measurement position was defined by the location of a metal support plate attached to a horizontal securing wire which was tightly stretched across the measurement area. The height of the support plate was adjustable by means of a clamp on the two-part stand. All measurements were made with the centres of the spheres at 106 cm above the floor level.

Ideally the measurements should have been made by irradiating each sphere in turn at the measurement position. This would have resulted in either much reduced irradiation times or in an unacceptably long total measurement time. A compromise was made in which some of the spheres and the bare and cadmium covered gold foils were irradiated in combination, using a second support stand and centred on the measurement position, separated by approximately 30 cm along the direction of the securing wire (perpendicular to the normal to the reactor core). Irradiation start and finish times were recorded to the nearest minute, using a watch which was checked against standard time before and after the measurements.
Because extended measurement times were required to produce sufficient ^{198}Au activity for accurate counting an additional detector, a 30 cm long by 15 cm diameter polyethylene cylinder with a gold foil at the centre, was used to monitor possible changes in the fluence level

[1] The original set of spheres were made to exact inch diameters and are referred to by their diameters in inches, although the inch is not an SI unit of length.

over the total duration of the measurement. This monitor was positioned at floor level, approximately 2 m from the BS measurement position and secured to a handrail support near the edge of the floor overlooking the reactor core. For each BS or foil irradiation a similar gold foil was irradiated in the monitor cylinder.

Seven readings of the dose equivalent rate at the measurement position were taken, at the time of changing the spheres, with a Harwell 0949 remcounter belonging to NPL, used as supplied by the manufacturer. The remcounter was held at the measurement position and a mean display reading was noted. Similarly, four measurements were taken with a Dineutron detector belonging to Ringhals health physics section.

3.4.4 Foil Counting

All gold foils were returned to NPL for counting. Each foil was placed in turn in one of two anti-coincidence shielded $4\pi\beta$ proportional counters, and the β-counting rate at saturation was determined. The foil saturation β-disintegration rates were obtained using previously measured β-counting efficiencies.

To correct for variations in the radiation level over the measurement period the resulting foil activities for each irradiation combination were normalized by the ratio of the monitor foil activity for the irradiation to the mean of all the monitor foil activities over the total measurement period. The range of normalization factors was 0.9915 -1.0073 with a standard deviation on the mean of 0.57%. No normalisation has been applied for differences in the reactor power level between the period of this measurement and those made by other participants in November 1992.

The corrected foil disintegration rates were used as input data for the spectrum unfolding.

3.4.5 Spectrum Unfolding

Response functions for the BSs have been derived on the basis of in-house Monte Carlo calculations for the energy region up to 5 MeV. Data from the literature was used above this energy; and some limited experimental calibrations were performed at 23 keV, 511 keV, and 1.22 MeV [1]. The thermal component of the spectrum was determined separately from analysis of bare and cadmium-covered gold foils, and the BS analysis was restricted to the energy range above the effective cadmium cut-off energy of 0.5 eV.

The process of unfolding a neutron spectrum from BS data is mathematically under-determined. In the case of the present measurements count rates for eight spheres were used to determine a spectrum with 37 energy groups extending from the cadmium cut-off energy to 12.59 MeV.

A number of computer codes are available which, by varying the shape of some start spectrum, and comparing the predicted BS count rates for this spectrum with those actually measured, iterate towards an approximate solution. However, in order to determine a mathematically rigorous solution, some further information must be used. The further information used by STAY'SL [3], which was the code employed in the present analysis, is an initial *a priori* estimate of the spectrum with uncertainty data. Ideally, such an initial estimate should come from a neutron transport calculation of the spectrum based on knowledge of the source and surroundings. In the absence of a calculation for the specific situation, other appropriate

information, e.g. for a similar arrangement, can be used. Failing all else, an intelligent guess can be used, based on the known source of neutrons and the amount of shielding material present.

The quality of the information available for the *a priori* spectrum is reflected in the uncertainty in the final derived spectrum. The unfolding process essentially performs an adjustment of the *a priori* spectrum on the basis of the measured sphere count rates. Experience with the code has, however, shown [4] that a very reasonable estimate of the final spectrum can be obtained, even when little or no *a priori* information is available, provided a range of initial-estimate (guess) spectra are tried, in order to identify the most appropriate one. Also, reasonably large uncertainties must be assigned to the initial spectrum. Because the running time of STAY'SL is short, being only a matter of seconds, this trial and error process can be undertaken relatively quickly.

Previous measurements within reactor containment have indicated that the spectra are rather soft with little or no evidence of a fission neutron peak. For this reason the initial-estimate spectra consisted of a Maxwellian peak in the low MeV region coupled to a large 1/E component having an intensity which could be up to that of the maximum of the Maxwellian peak. Trials with spectra of this type quickly indicated that there were very few neutrons above 1 MeV and that there was no real indication of a peak at the upper energy end of the neutron distribution. The *a priori* spectrum chosen was therefore a 1/E distribution with an exponential fall-off at the upper energy end.

Large uncertainties were chosen for the *a priori* spectrum with a 50% relative standard deviation for the fluences in each bin, and with all bins fully correlated by a component having a 50% standard deviation. This does not provide a particularly realistic uncertainty matrix, but previous experience has shown that this combination provides sufficient freedom for STAY'SL to adjust the *a priori* spectrum, provided an appropriate one has been chosen, without introducing large unrealistic variations in the spectrum due to statistical variations in the measured sphere responses. For the response functions an uncertainty of 10% was chosen for the value for each of the 37 energy groups, and no covariance terms were included.

3.4.6 Results

The derived spectrum is tabulated in Table 1, and plotted in Figure 1 where it is shown as fluence rate per bin. Because the bins are of equal width on a lethargy scale the shape, although not the magnitude, is the same as for a plot of fluence rate per unit lethargy, or of $E \cdot \Phi(E)$, where $\Phi(E)$ is the differential fluence $d\phi/dE$. The thermal component is large and is not shown in the figure to simplify the presentation. In the absence of any reliable information about the temperature of the thermal neutron distribution, the bare and cadmium covered gold foil analysis only gives an estimate of the Westcott thermal fluence [1], and this is what has been quoted in Table 1. This can be related to the true thermal fluence only if the effective temperature is known, however, the consequences of using the Westcott fluence when calculating dose equivalent quantities should be small.

Table 1: Fluence rate values.

Bin No.	Energy* (eV)	Fluence rate (cm^{-2} s^{-1})
0	Thermal	5.251×10^{3}
1	5.012×10^{-1}	4.194×10^{2}
2	7.943×10^{-1}	4.042×10^{2}
3	1.259×10^{0}	4.088×10^{2}
4	1.995×10^{0}	4.041×10^{2}
5	3.162×10^{0}	4.067×10^{2}
6	5.012×10^{0}	4.372×10^{2}
7	7.943×10^{0}	4.237×10^{2}
8	1.259×10^{1}	3.883×10^{2}
9	1.995×10^{1}	3.885×10^{2}
11	3.162×10^{1}	3.771×10^{2}
11	5.012×10^{1}	3.742×10^{2}
12	7.943×10^{1}	3.649×10^{2}
13	1.259×10^{2}	3.521×10^{2}
14	1.995×10^{2}	3.485×10^{2}
15	3.162×10^{2}	3.409×10^{2}
16	5.012×10^{2}	3.497×10^{2}
17	7.943×10^{2}	3.556×10^{2}
18	1.259×10^{3}	3.422×10^{2}
19	1.995×10^{3}	3.260×10^{2}
20	3.162×10^{3}	3.189×10^{2}
21	5.012×10^{3}	3.242×10^{2}
22	7.943×10^{3}	3.279×10^{2}
23	1.259×10^{4}	3.367×10^{2}
24	1.995×10^{4}	3.426×10^{2}
25	3.162×10^{4}	3.349×10^{2}
26	5.012×10^{4}	3.366×10^{2}
27	7.943×10^{4}	3.673×10^{2}
28	1.259×10^{5}	3.945×10^{2}
29	1.995×10^{5}	3.336×10^{2}
30	3.162×10^{5}	2.786×10^{2}
31	5.012×10^{5}	1.430×10^{2}
32	7.943×10^{5}	5.095×10^{1}
33	1.259×10^{6}	1.067×10^{1}
34	1.995×10^{6}	7.411×10^{-1}
35	3.162×10^{6}	9.220×10^{-3}
36	5.012×10^{6}	7.784×10^{-6}
37	7.943×10^{6}	9.245×10^{-11}
	1.259×10^{7}	

* for bins 1 to 37 the energy value is that for the lower boundary of the bin

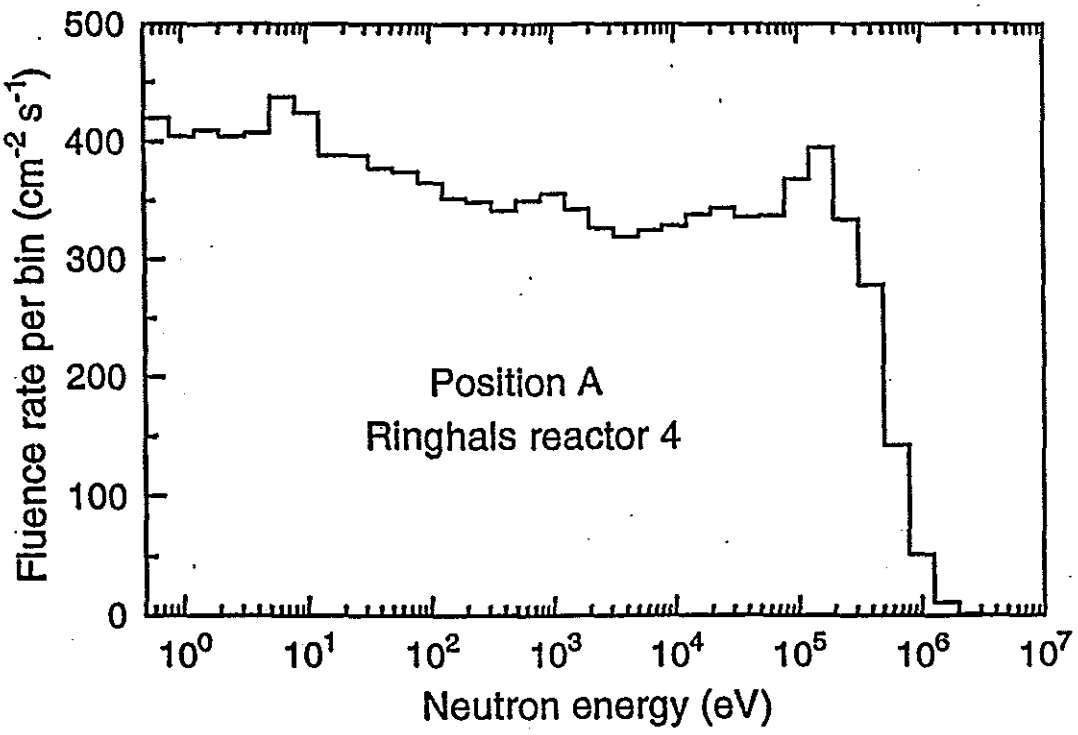

Figure 1: Measured spectrumat position A Ringhals reactor #4

Table 2: Total fluence and dose equivalent values.

Energy range	Fluence rate (cm^{-2} s^{-1})	Dose equivalent rates (mSv h^{-1})		
		ICRP 21 (MADE)	H*(10) Wagner et al	H*(10) Leuthold et al
Total	1.636×10^4	1.375	1.425	2.194
Thermal	5.251×10^3 (32.1%)	0.202 (14.7%)	0.159 (11.2%)	0.247 (11.2%)
0.5012 eV to 10 keV	8.000×10^3 (48.9%)	0.328 (23.8%)	0.240 (16.8%)	0.370 (16.9%)
10 keV to 100 keV	1.696×10^3 (10.4%)	0.165 (12.0%)	0.174 (12.2%)	0.272 (12.4%)
100 keV to 1 MeV	1.377×10^3 (8.4%)	0.631 (45.9%)	0.803 (56.4%)	1.241 (56.6%)
1 MeV to 20 MeV	3.982×10^1 (0.2%)	0.049 (3.6%)	0.049 (3.4%)	0.064 (2.9%)

The small scale structure in the spectrum of Figure 1 may well not be realistic. The response functions were based mainly on Monte Carlo calculations, and since they have not been smoothed, structure in these functions, arising from statistical variations in the calculations for each energy group, can feed through into structure in the spectrum.

In Table 2 the total fluence rate and total values for various dose equivalent quantities are given along with the values for these quantities in various broad energy regions. The dose equivalent quantities given are: MAximum Dose Equivalent (MADE) [5]; ambient dose equivalent, H*(10), with the Q(L) relationship of ICRP 21 [5] as presented by Wagner et al. [6]; and ambient dose equivalent calculated by Leuthold et al. [7] using the Q(L) relationship of ICRP 60 [8]. Also shown are the percentages of the total values in each of the broad energy regions.

Uncertainties in the fluence and dose equivalent values are extremely difficult to estimate. From previous experience [4] the uncertainty in the total fluence should be less than 10%, and in the dose equivalent quantities less than 20%.

The seven readings taken with the Harwell 0949 remcounter belonging to NPL gave a mean dose equivalent rate at the measurement site of 2.68 mSv h^{-1}, with a standard deviation of 4%. The scatter, or noise, on individual readings was approximately ± 0.05 mSv h^{-1}. The response is roughly a factor of two greater than the two dose equivalent values (MADE and H*(10) Wagner et al.) which are based on the Q(L) relationship of ICRP 21. The precise values for the over-response are given in column two of Table 3.

Table 3: Ratio of Harwell 0949 Neutron Dose-Equivalent Monitor response to the dose equivalent value derived from the measured spectrum. Data is presented both for the measured instrument response, and also for the predicted response if the instrument were calibrated with one of three radionuclide sources.

Dose equivalent quantity	Measured response/dose equivalent value from spectrum	Predicted response after calibration/dose equivalent value from spectrum		
		Calibration field		
		AmBe	^{252}Cf	D_2O mod. ^{252}Cf
ICRP 21 (MADE)	1.95	2.69	2.31	1.71
H*(10) Wagner et al.	1.88	2.55	2.17	1.62
H*(10) Leuthold et al.	1.22	1.94	1.78	1.37

The measurements taken with the Dineutron detector belonging to Ringhals health physics section gave a mean of 1.50 mSv h^{-1}, with a standard deviation of 2% for four readings. The good performance perhaps reflects the fact that this instrument was designed specifically for this type of environment. No normalization for changes in reactor power level over the measurement period were applied to either of these dosemeter measurements.

Since a reasonable evaluation of the response function of the Harwell 0949 instrument is available [9], the response can be predicted by integrating the measured spectrum with the response function. This gave a value of 2.59 mSv h^{-1} in good agreement with the measured response. This lends support to both the measured spectrum and the response function used.

For this instrument the calibration of the display is set by the manufacturer, although it can be checked using a standard jig and test source. This setting does not, however, correspond to a calibration in any of the usual radionuclide source fields. Using the available response function the reading in any field can be predicted, including that in any of the usual calibration fields. This technique has been used to predict the correction factors which would be derived if the instrument were calibrated to give the correct answer in the fields of either Am-Be, ^{252}Cf, or heavy water moderated ^{252}Cf source. These correction factors depend, of course, on the dose equivalent quantity considered. The last three columns of Table 3 give the predicted ratio, response/true-value, calculated assuming the instrument had been corrected to give the right dose equivalent value in one of the three standard calibration fields. This data is given for the three dose equivalent quantities considered in Table 2. It would appear that, for this spectrum, the readings with the manufacturers settings are preferable to those obtained after calibration in the standard fields, except perhaps for calibration with heavy water moderated ^{252}Cf, .

Overall, in this soft spectrum, the Harwell instrument over-responds, regardless of calibration field or dose equivalent quantity. It should be remembered that the instrument was originally designed before any of the dose equivalent quantities considered here were devised. The basic reason for the over-response is, however, that the response is too high at intermediate neutron energies where much of the fluence occurs in this spectrum. Over other parts of the energy range the instrument can under-respond.

Note.

No re-normalization of the results has been performed and they represent fluence and dose equivalent rates for the power level of the reactor at the time of the measurements (21-24 March 1993). To relate these values to those of other measurements the relevant reactor power levels need to be taken into consideration.

3.4.7 References

[1] E.J. Axton and A.G.Bardell, *Neutron Production from electron accelerators used for medical purposes*, page 109 in Proceedings of a conference on Neutrons from Medical Accelerators, NBS Special Publication 554, H.T. Heaton and R. Jacobs Eds (Government Printing Office, Washington) 1979.

[2] E.J. Axton, *Absolute Measurement of the Neutron Flux Density in the A.E.R.E. Reactor 'GLEEP'*, Reactor Science and Technology (Journal of Nuclear Energy Parts A/B) 17 (1963) 125 - 135.

[3] F.G. Perey, *Least-squares Dosimetry Unfolding; the Program STAY'SL*, Oak Ridge National Laboratory Report ORNL/TM-6062, October 1977.

[4] A.V. Alevra et al., *Unfolding Bonner Sphere Data: A European Intercomparison of Computer Codes*, PTB Report - PTB-7.22-90-1, January 1990.

[5] International Commission on Radiological Protection Publication 21, *Data for Protection against Ionizing Radiation from External Sources: Supplement to ICRP Publication 15*, (Pergamon Press, Oxford) 1973.

[6] S.R. Wagner et al., *Unified Conversion Functions for the New ICRU Operational Radiation Protection Quantities*, Radiat. Prot. Dosim. 12 (1985) 231 - 235.

[7] G. Leuthold, V. Mares, and H. Schraube, *Calculation of the Neutron Ambient Dose Equivalent on the Basis of the ICRP Revised Quality Factors*, Radiat. Prot. Dosim. **40** (1992) 77 - 84.

[8] International Commission on Radiological Protection Publication 60, *1999 Recommendations of the International Commission on Radiological Protection*, (Pergamon Press, Oxford) 1991.

[9] Private communication from D.T. Bartlett, NRPB. The response function is based mainly on data published by K.G. Harrison in Nucl. Instrum. & Meths **166** (1979) 197 - 201.

3.5. Measurements of the ZfK-KAI / Rossendorf

W. Hansen, D. Richter, W. Vogel
FZ Rossendorf, P.O. Box 510119, D-01314 Dresden

3.5.1 Introduction

In CLAB fast neutron spectra were measured at 2 (of 3) positions P and D of the spent fuel container in 1.0 m distance from the container surface. Additional measurements at the third reference point E could not be realised because of the limited total measuring time. At Ringhals neutron spectra measurements have been carried out at 2 positions A and L of reactor unit 4.

The physical principle of the neutron spectrometer applied is the proton recoil method using 2 kinds of detectors:

i) proton recoil proportional counters (filled with hydrogene or methane) and
ii) a solid organic scintillator (stilbene).

The gas filled proportional counters allow the neutron spectra to be measured in the range from about 10 keV to about 1.2 MeV, the stilbene scintillator from about 700 keV to 10 MeV and more, so that a sufficient energy region of overlapping exists. The neutron spectra are obtained in a good energy resolution.

A basic feature of gas filled proportional counters is the limited dynamic range for their application. Therefore, the measurement of a full range neutron spectrum requires the use of several proportional counters with different properties (dimensions and/or gas fillings). This is a time consuming procedure. The total spectrum is then a combination of the results measured in overlapping energy ranges. A second disadvantage of the gas filled counters is a quite low sensitivity due to the low nuclear density of the filling gas and the usual dimensions and, consequently, long measuring times at low neutron fluxes as in working environments in order to obtain acceptable statistics (at least several hours per energy range). A summary of the measurements performed is given in Tab. 1.

3.5.2 Description of the spectrometers (detectors and evalution procedure)

3.5.2.1 Measurements with the proportional counter spectrometer

For the spectrometer one set of spherical counters (well known type SP2 or similar and SP9) and one set of cylindrical counters is available. The counters are characterised in Tab. 2. For the measurements at CLAB and Ringhals we decided for the cylindrical counters. Compared to the spherical ones they have the disadvantage of showing an anisotropy effect, but - and this was the reason for their use - they have a larger sensitive volume and, consequently, higher sensitivity for neutrons. In order to minimize the effect of anisotropy, the counters were positioned

- at CLAB: horizontally parallel to the spent fuel container surface,
- at Ringhals position A: horizontally and perpendicularly to the containment centre,
- at Ringhals position L: vertical orientation.

Location	measuring point	detector	upper energy limit	date	time	integral number of events
CLAB	P	Sc30/25	2.5 MeV	20.11.92	11.54 - 15.01	50374
	D	"	"	"	15.54 - 18.18	54368
	P	CHM-48	670 keV	20/21.11.92	23.25 - 07.25	72734
	D	"	"	21.11.	08.08 - 17.40	72702
	P	CHM-49	1.2 MeV	21/22.11.92	19.29 - 04.17	27260
	D	"	"	22.11. 92	04.32 - 13.02	33689
	D	CHM-47	370 keV	"	15.07 - 21.57	31523
	P	"	"	22/23.11.92	22.38 - 06.48	45068
Ringhals	L	Sc30/25	2.5 MeV	16.03.93	15.35 - 20.30	261835
	A	"	"	18.03.93	15.37 - 17.25	310992
	L	CHM-49	1.2 MeV	17.03.93	09.49 - 13.53	45538
	A	"	"	18.03.93	18.08 - 20.01	132947
	L	CHM-48	670 keV	17. 03.93	14.58 - 20.41	276686
	A	"	"	19.03.93	09.15 - 11.31	651323
	L	CHM-47	370 keV	16/17.03.93	22.01 - 08.07	336405
	A	"	"	19. 03.93	12.10 - 4.05	384573

Table 1: Summary of the measurements performed

Detector	SP9	SP2-4	NOK1043	CHM-47	CHM-48	CHM-49
Type	spherical			cylindrical		
Gas filling	H_2	H_2 + 300 ppm ^3He		90% H_2 + 9.8% CH_4 + 0.2% ^3He		95% CH_4 + 5% N_2
Dimensions in mm	ϕ32	ϕ40		ϕ31 x 100		
Pressure in kPa	100	400	1000	100	300	400
Number of H-nuclei $x10^{-24}$ in the active volume	0.000910	0.00710	0.0178	0.00439	0.0132	0.0299
usable energy range in keV	5 ... 220	80...650	300...1100	5...270	10...580	300...1350
Resolution of the calibration peak	15 %	5 %	6 %	2.5 %	3.5 %	6 %

Table 2: Characterisation of the recoil proton proportional counters

The main neutron incidence is then preferably nearly 90° where response functions vary only slowly in dependence on angle.

For energy calibration at CLAB a ^{252}Cf neutron source covered with PE-bricks was used. At Ringhals, there was a sufficient amount of thermal neutrons in the surroundings of the reactor. In order to suppress the influence of the thermal neutron background during the measurements the counters were almost completely covered with a shield made from 1.0 mm Cd and about 5 mm B_4C (the latter for low energy epithermal neutrons).

Usually, the lower energy limit of the spectrometer can be decreased considerably if electronic pulse shape discrimination is applied in order to suppress the gamma influence on spectra. This requires biparametric measurements in 2048 channels and sufficient count rates for acceptable statistics (otherwise unreasonably long measuring times). Such count rates were not given in the experiments. Therefore, we have carried out the experiments without pulse shape discrimination and had to accept a higher energy limit of some tens of keV.

The unfolding procedure of the proton recoil spectra is a home-made iteration code [1]. It includes wall effect corrections and in case of CHM-49 the correction of carbon recoils. The response matrix was calculated with a Monte Carlo code [2] and checked experimentally with monoenergetic neutrons [3].

The idea of the unfolding procedure is to change the bad conditioned (because of the shape of response function) integral equation

$$P(E) = N \cdot \int_{E}^{E_{max}} \sigma(E') \cdot p(E,E') \cdot \Phi(E') \cdot dE'$$

by its differentiation to E'. The advantage is that the differentiated response function has now a peak instead of a step at neutron energy E'. In order to realize this evaluation procedure an iteration becomes necessary (starting with the simply differentiated proton recoil spectrum) which is converging in a few steps. The iteration is stopped if the changes in the resulting neutron spectrum are lower than a defined level.

By this iteration procedure only the wall effect from neutrons in the measuring range itself (up to E_{max}) is corrected. Previously, the influence of neutrons above E_{max} (so-called downscattering correction) is substracted from the measured proton recoil spectrum

$$P(E) = P_{meas.}(E) - P_{max}(E)$$

with

$$P_{max}(E) = N \cdot \int_{E_{max}}^{\infty} \sigma(E') \cdot p(E,E') \cdot \Phi_o(E') \cdot dE'$$

where $\Phi_o(E)$ is the neutron flux assumption above measuring range (taken from measurements in higher energy ranges or stilbene scintillation measurements or calculations). Experiences show only an unsignificant or even negligible influence of the precise shape of this flux assumption on the final result.

For the example of the measurement with the counter CHM-48 at Ringhals (lock position L) the different steps of the evaluation procedure are shown in Fig. 1. It can be seen that downscattering correction (from neutrons above measured energy range) and wall effect

correction (from neutrons in the measured energy range) have an opposite direction. The final effect depends on spectrum shape.

The evaluation procedure was verified in several experiments in well known standard neutron fields and (for spherical counters) also compared to the classical SPEC4 code by Benjamin et al. [4]. A description of the electronic features of the spectrometer is published in [5].

3.5.2.2 Measurements with the stilbene scintillation spectrometer

The stilbene scintillation spectrometer is used in the energy range above 700 keV. The diameter of the crystal applied is 30 mm, its height 25 mm. The crystal is mounted to a photomultiplier FEU-93. For the discrimination of the photons the charge comparison method is applied.

The calibration of the energy scale is realized by measuring the gamma spectra of different gamma sources (e.g. compton edge of ^{54}Mn (639 keV), ^{137}Cs (478 keV), ^{22}Na (340 keV) and the photo peak of ^{241}Am (60 keV)). The compton energy is defined at 0.6 of the maximum height of the compton edge. In order to verify the experimental resolution the 2 compton edges of ^{60}Co at 0.960 MeV and 1.116 MeV, respectively, must be well distinguished.

The evaluation procedure of the stilbene spectra is a simple differentiation of the proton recoil spectrum but including the following corrections:

a) nonlinear light output function
This function has been determined experimentally with monoenergetic neutrons for the given crystal-photomultiplier combination [6].

b) anisotropy effect of stilbene
Unfortunately, the light output of stilbene depends on the angle α between neutron incidence direction and optical axis of the crystal according to the equation

$$L(\alpha) = L(\alpha = 0°) \cdot (1 + 0.2 \sin\alpha)$$

Problems arise in case of non-unidirectional neutron flux. In order to minimise the anisotropy uncertainty in the CLAB measurements the stilbene detector was positioned vertically, so that

i) all neutrons over the length of the spent fuel container have the same neutron incidence angle of about 90° and
ii) the average angle from neutrons coming from upper and lower parts of the container is close to 90° where the sinus function has only small changes in dependence on angle.

For the evaluation an average angle of 80° was assumed. Investigations show that changes in this angle lead to only negligible changes in the neutron spectrum so that the influence of uncertainties in the angle is very small in that range. For demonstration, Fig. 2 shows evaluated neutron spectra for different angles. Between 90° and about 75° changes in the neutron spectrum are really negligible.

Corresponding considerations for the Ringhals experiments led to vertical detector position in the lock and to horizontal orientation in the containment.

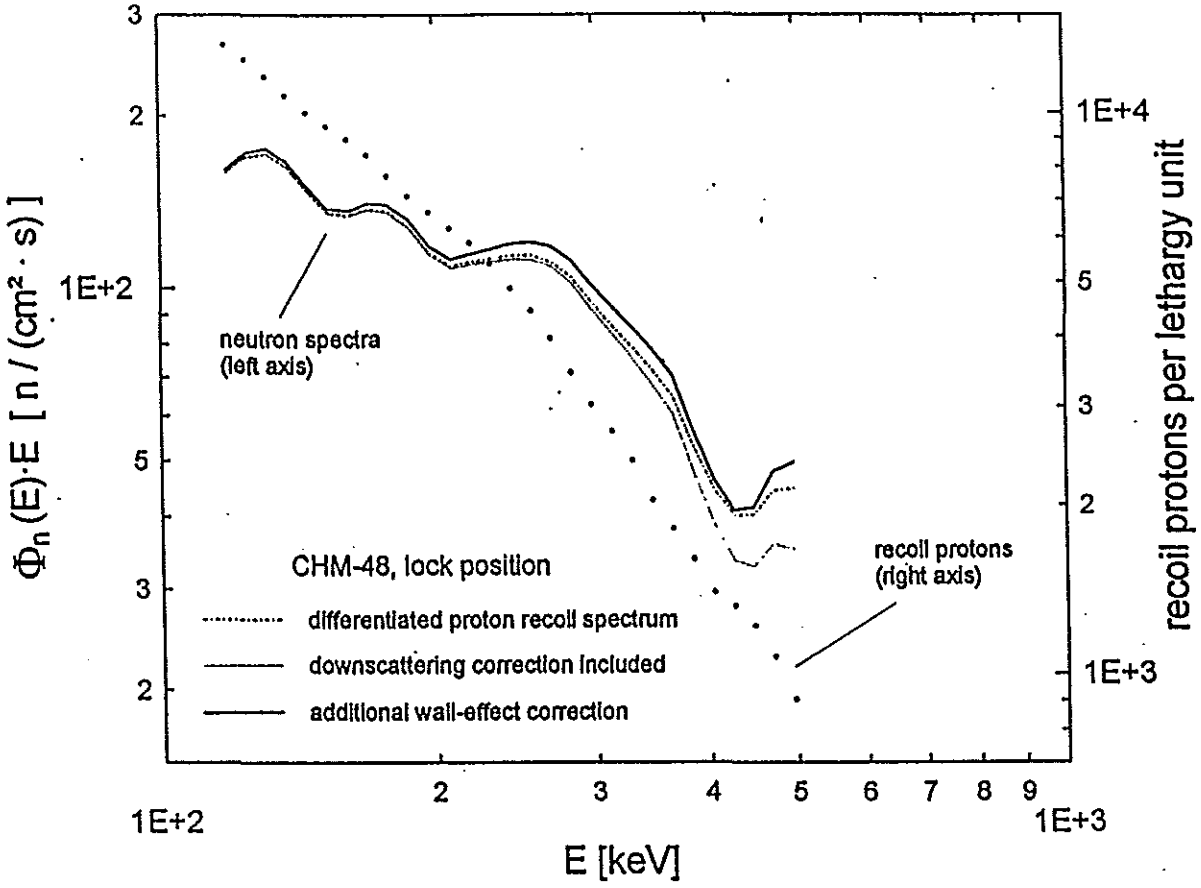

Fig. 1: Evaluation procedure for proton recoil spectra

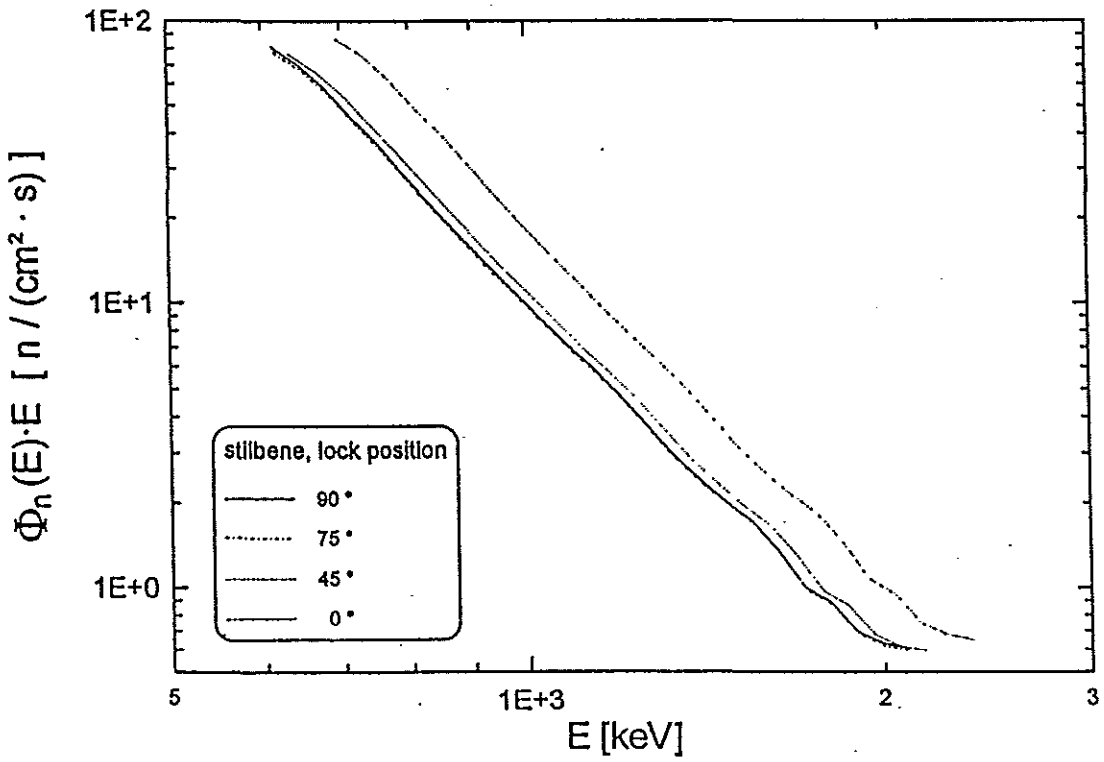

Fig. 2: Influence of different angles of neutron incidence for stilbene

c) energy dependent sensitivity of the crystal in the form

$$\varepsilon(E) = 1 - e^{\Sigma(E)\cdot l_{eff}}$$

d) correction of neutron reactions on carbon resulting in α-particles
These reactions come into occurence only for neutron energies above about 8 MeV. Therefore, this effect doesn't play any role in the measurements at CLAB and Ringhals due to the shape of spectrum.

The simple differentiation procedure for the proton recoil spectra is considered to be sufficiently accurate for the given crystal sizes, energy ranges between 1 and 10 MeV and continuous spectra. Under these conditions, errors in resulting neutron spectra due to evaluation should not exceed 3...5 % because of a compensation of wall effect and multiscattering processes to a large degree. This mentioned error should be acceptable with regard to the general experimental uncertainties.

3.5.3 Results

Final results of the spectrum measurements are given as numerical data in Tab. 3 (lower energy limit of each group and the group flux $\Phi(u)\cdot\delta u$). $\Phi(u)$ is the flux in 1/s/cm² per lethargy interval and δu the (uniform) width of the lethargy interval ($\delta u = -\ln 0.95 \approx 0.0513$).

The graphical representation can be seen in Fig. 3. The structure in the shape of the measured group fluxes is a result of resonances in the neutron cross-section of iron mainly. The resolution of the dips is limited because of a necessary smoothing of the measured proton recoil spectrum.

The highest energy in the measured spectrum amounts to about 2.3 MeV. Because of the low and strongly decreasing neutron flux and the restricted measuring time the energy range was not extended considerably above 2 MeV.

At low energies the spectra end at about 70 keV (CLAB) and 35...45 keV (Ringhals). Because of the sensitivity of the counters to photons and the bad neutron/photon ratio at energies below 100 keV the measured spectra were rejected below these energies. Electronic pulse shape discrimination was not applied due to very low absolute neutron flux. In the limited time acceptable counting statistics were not achievable.

For both, proportional counter and scintillation spectrometry, dead time corrections were not necessary. Highest count rates were in the order of 10 to 100 counts per second.

A difficult problem is the estimation of uncertainties. A systematic determination of errors and also a covariance matrix is not available. Classic error estimation would overestimate the uncertainties found in real application. Experience for experimental uncertainties was obtained in measurements of standard spectra (^{252}Cf, ΣΣ secondary standard, SCHERZO-556 reactor configuration and others) or due to intercomparison of different spectrometers. As an example, a measurement of the ^{252}Cf standard neutron spectrum is represented in Fig. 4.

Because of the limited measuring time, the low neutron flux and, consequently, quite poor statistics uncertainties of about 10-15% should be reasonable for the measured group fluxes.

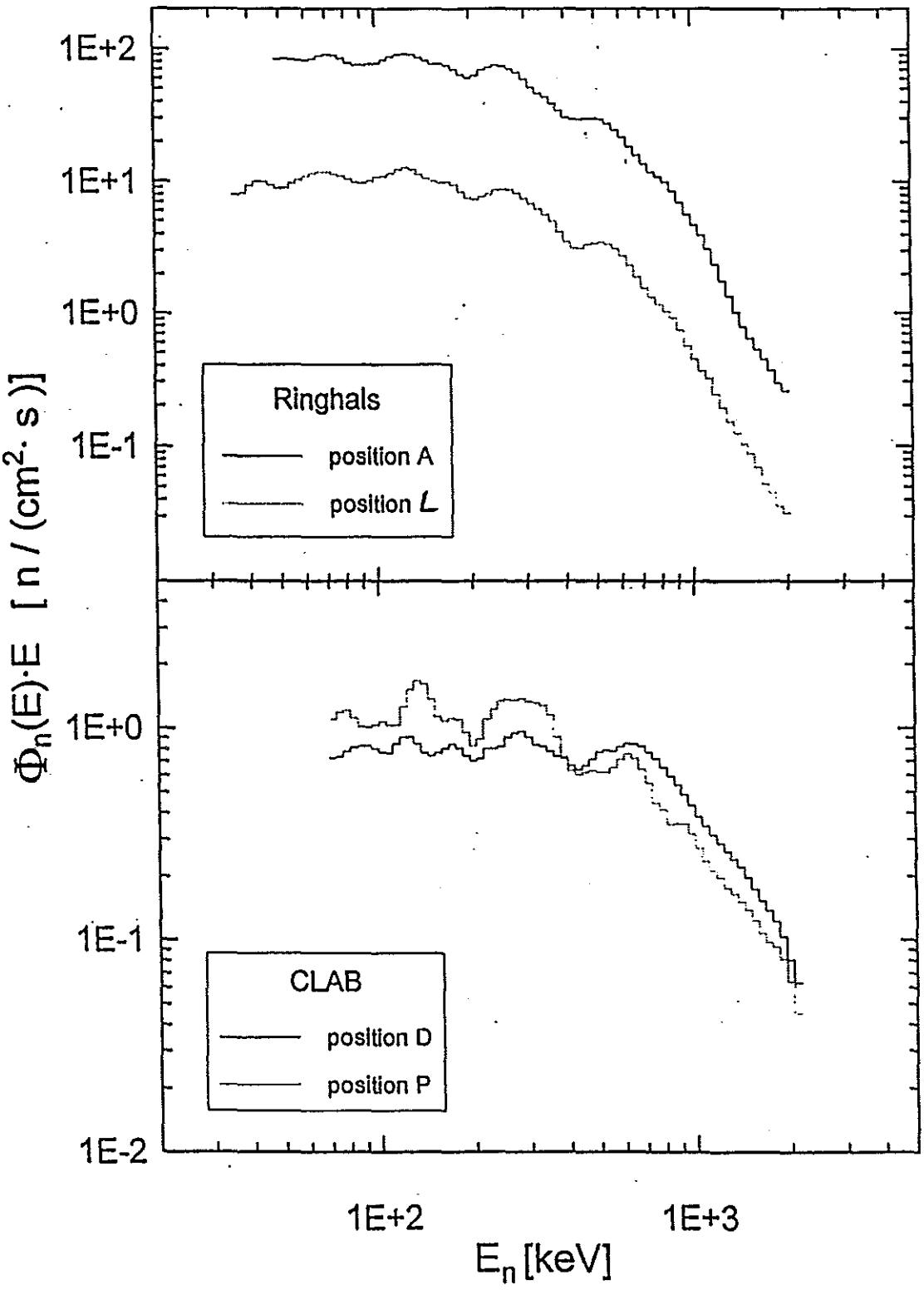

Fig. 3: Measured neutron spectra at Ringhals and CLAB

lower energy limit [MeV]	group flux Φ(u)-δu [1/s/cm²]				lower energy limit [MeV]	group flux Φ(u)-δu [1/s/cm²]			
	CLAB Position P	CLAB Position D	Ringhals Position A	Ringhals Position L		CLAB Position P	CLAB Position D	Ringhals Position A	Ringhals Position L
3.55E-02				8.02E+00	2.91E-01	1.33E+00	9.05E-01	5.98E+01	7.42E+00
3.73E-02				8.27E+00	3.06E-01	1.31E+00	8.34E-01	5.20E+01	6.79E+00
3.93E-02				9.38E+00	3.22E-01	1.27E+00	8.20E-01	4.67E+01	6.22E+00
4.14E-02				1.00E+01	3.39E-01	1.15E+00	7.79E-01	4.37E+01	5.61E+00
4.36E-02				9.97E+00	3.57E-01	9.04E-01	7.36E-01	3.90E+01	4.96E+00
4.58E-02				9.44E+00	3.75E-01	7.30E-01	7.19E-01	3.43E+01	4.12E+02
4.83E-02			8.42E+01	8.95E+00	3.95E-01	6.29E-01	6.63E-01	3.04E+01	3.46E+00
5.08E-02			8.55E+01	8.98E+00	4.16E-01	6.04E-01	6.39E-01	2.95E+01	3.16E+00
5.35E-02			8.46E+01	9.75E+00	4.38E-01	6.17E-01	6.66E-01	2.99E+01	3.11E+00
5.63E-02			8.30E+01	1.03E+01	4.61E-01	6.30E-01	7.12E-01	3.00E+01	3.32E+00
5.92E-02			8.29E+01	1.09E+01	4.85E-01	6.21E-01	7.68E-01	3.04E+01	3.41E+00
6.24E-02			8.51E+01	1.16E+01	5.11E-01	6.16E-01	7.87E-01	2.96E+01	3.43E+00
6.56E-02			8.94E+01	1.19E+01	5.38E-01	6.50E-01	7.79E-01	2.73E+01	3.33E+00
6.91E-02	1.10E+00	7.25E-01	9.20E+01	1.18E+01	5.66E-01	7.13E-01	8.18E-01	2.46E+01	3.09E+00
7.27E-02	1.19E+00	7.36E-01	9.06E+01	1.14E+01	5.96E-01	7.54E-01	8.47E-01	2.16E+01	2.73E+00
7.66E-02	1.21E+00	7.79E-01	8.56E+01	1.10E+01	6.27E-01	7.25E-01	8.42E-01	1.84E+01	2.31E+00
8.06E-02	1.12E+00	8.14E-01	7.97E+01	1.04E+01	6.60E-01	6.39E-01	8.20E-01	1.58E+01	1.89E+00
8.48E-02	1.03E+00	8.25E-01	7.69E+01	9.94E+00	6.95E-01	5.51E-01	7.69E-01	1.35E+01	1.54E+00
8.93E-02	1.02E+00	8.23E-01	7.67E+01	9.80E+00	7.31E-01	4.42E-01	7.18E-01	1.18E+01	1.33E+00
9.40E-02	1.04E+00	8.01E-01	7.83E+01	1.01E+01	7.70E-01	4.13E-01	6.56E-01	1.09E+01	1.16E+00
9.90E-02	1.07E+00	7.70E-01	7.88E+01	1.09E+01	8.11E-01	3.54E-01	5.94E-01	9.93E+00	1.03E+00
1.04E-01	1.04E+00	7.64E-01	8.39E+01	1.10E+01	8.53E-01	3.57E-01	5.42E-01	8.48E+00	9.20E-01
1.10E-01	1.04E+00	8.45E-01	8.82E+01	1.16E+01	8.98E-01	3.55E-01	4.88E-01	6.96E+00	7.43E-01
1.15E-01	1.26E+00	9.10E-01	9.19E+01	1.24E+01	9.45E-01	3.19E-01	4.34E-01	5.63E+00	5.68E-01
1.21E-01	1.52E+00	9.10E-01	9.35E+01	1.28E+01	9.95E-01	2.72E-01	3.83E-01	4.68E+00	4.49E-01
1.28E-01	1.67E+00	8.46E-01	9.18E+01	1.24E+01	1.05E+00	2.36E-01	3.47E-01	3.96E+00	3.64E-01
1.35E-01	1.61E+00	7.65E-01	8.73E+01	1.13E+01	1.10E+00	2.14E-01	3.16E-01	3.09E+00	3.18E-01
1.42E-01	1.37E+00	7.44E-01	8.21E+01	1.06E+01	1.16E+00	1.97E-01	2.87E-01	2.36E+00	2.45E-01
1.49E-01	1.14E+00	7.67E-01	7.79E+01	1.02E+01	1.22E+00	1.76E-01	2.62E-01	1.78E+00	1.94E-01
1.57E-01	1.08E+00	8.04E-01	7.77E+01	9.95E+00	1.29E+00	1.64E-01	2.41E-01	1.35E+00	1.53E-01
1.65E-01	1.11E+00	8.43E-01	7.63E+01	9.92E+00	1.35E+00	1.51E-01	2.21E-01	1.01E+00	1.24E-01
1.74E-01	1.10E+00	8.04E-01	7.08E+01	9.45E+00	1.42E+00	1.38E-01	1.98E-01	7.85E-01	1.03E-01
1.83E-01	9.56E-01	7.44E-01	6.47E+01	8.41E+00	1.50E+00	1.23E-01	1.73E-01	6.40E-01	8.81E-02
1.93E-01	8.24E-01	7.02E-01	6.14E+01	7.50E+00	1.58E+00	1.07E-01	1.53E-01	5.27E-01	6.97E-02
2.03E-01	8.87E-01	7.19E-01	6.40E+01	7.29E+00	1.66E+00	9.73E-02	1.37E-01	4.44E-01	5.22E-02
2.14E-01	1.10E+00	8.01E-01	7.02E+01	7.65E+00	1.75E+00	9.25E-02	1.22E-01	3.65E-01	4.50E-02
2.25E-01	1.23E+00	8.02E-01	7.29E+01	8.08E+00	1.84E+00	8.17E-02	1.04E-01	2.94E-01	3.59E-02
2.37E-01	1.34E+00	8.18E-01	7.61E+01	8.78E+00	1.94E+00	6.40E-02	8.08E-02	2.57E-01	3.20E-02
2.49E-01	1.36E+00	9.07E-01	7.41E+01	8.83E+00	2.04E+00	4.51E-02	6.32E-02		
2.62E-01	1.35E+00	9.50E-01	7.18E+01	8.67E+00	2.15E+00				
2.76E-01	1.37E+00	9.68E-01	6.75E+01	8.19E+00					

Table 3: Numerical results of the experiments

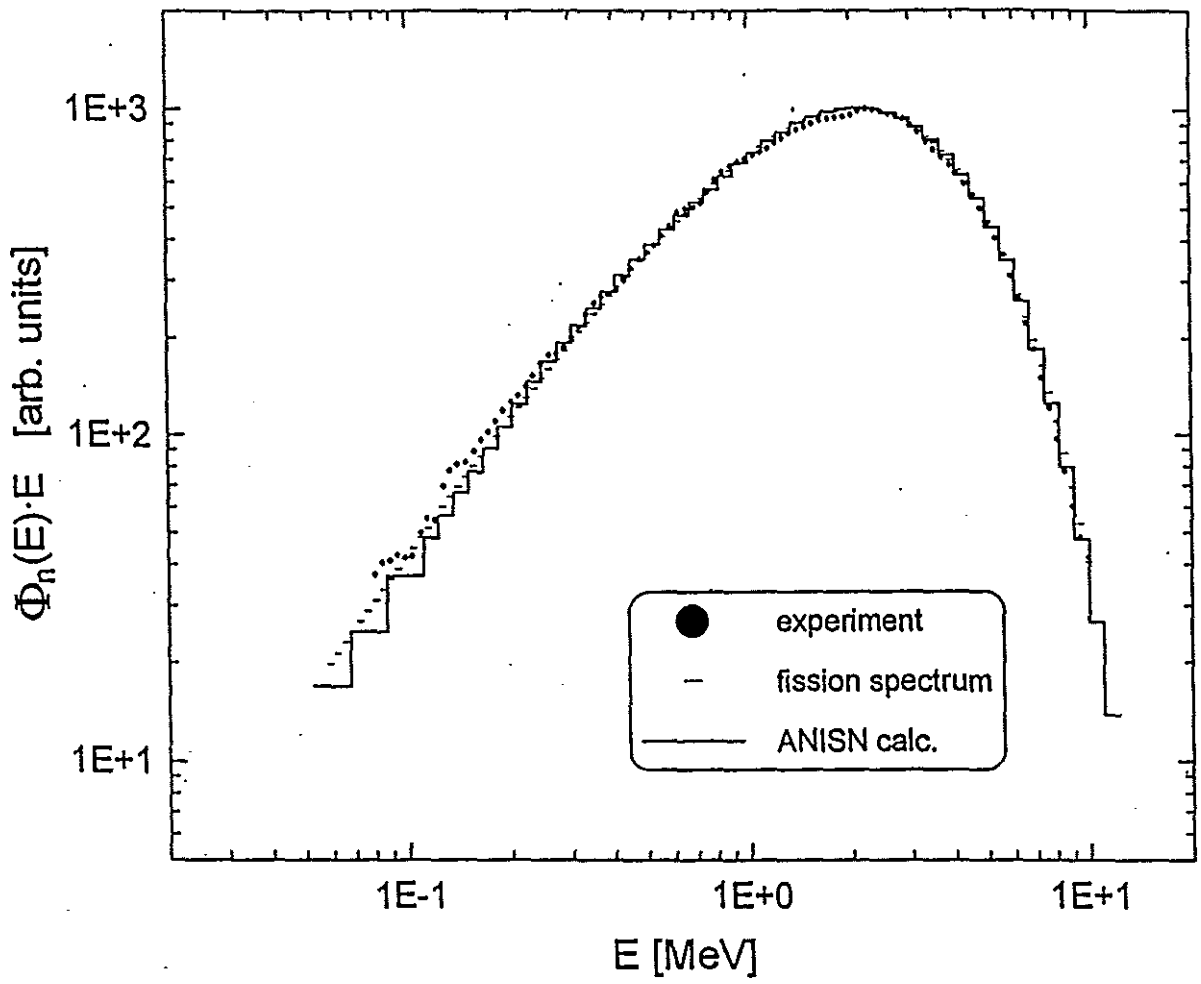

Figure 4: Measured ^{252}Cf neutron standard and comparison to calculations

3.5.4 References

[1] D. Albert, W. Hansen, *Auswerteverfahren zum Rossendorfer Rückstoßprotonen-Zählrohrspektrometer.* Kernenergie **20** (1977) 95

[2] H.U. Barz, *Monte-Carlo-Berechnungen der Ansprechfunktionen von Protonenrückstoßzählern.* ZfK-Arbeitsbericht RPT-6/72, Rossendorf 1972

[3] W. Hansen et al., *Experimente mit monoenergetischen Neutronen zur Bestimmung von Ansprechfunktionen wasserstoffgefüllter Proportionalzählrohre.* Kernenergie **21** (1978) 348

[4] P.W. Benjamin, C.D. Kemshall, A. Brickstock, *The Analysis of Recoil Proton Spectra.* AWRE-0-09/68, 1968

[5] D. Albert, W. Hansen, H. Köpernik, W. Vogel, *Die elektronische Apparatur des Rossendorfer Rückstoßprotonenzählrohr-Spektrometers.* Kernenergie **21** (1978) 82

[6] D. Albert et al., *Determination of Light Efficiency of Stilbene Scintillators and their Application to Incore Spectrometry of Fast Neutrons.* Nucl. Instr. Meth. **200** (1982) 397

Supplement (October 1994)

Re-normalization of Neutron Spectra for Ringhals A and L

The proton recoil method covers an important energy range of the investigated spectra where neutron fluxes and dose equivalent conversion factors change strongly with energy, so that the proton recoil results are valuable for the verification of the Bonner sphere spectra in that critical region.

Whereas the neutron spectra measured with proton recoil techniques (proportional counters and stilbene scintillator) did well confirm the Bonner sphere results in the CLAB positions P and D, problems of the absolute normalization arose in the Ringhals experiments. The intercomparison did reveal an overestimation of the absolute fluxes in Ringhals A and L positions by proton recoil measurements.

Due to this obvious discrepancy the primary measuring data were re-evaluated. It was found out:

- All neutron spectra of the proportional counters agree well with each other in the different, overlapping energy ranges with respect to their absolute scale.
- Usually the proportional counter spectra should overlap and agree absolutely with the stilbene scintillation results within the energy range 0,8 ... 1,1 MeV. But, in case of the Ringhals experiments a discrepancy in the absolute normalization could be observed between both spectrometers in such a way that the scintillation spectra were higher for about 30 % (Ringhals L) or even 50 % (Ringhals A) in comparison to the proportional counters. This discrepancy occurred only in Ringhals, not in CLAB.
- Obviously, it was a wrong decision in the previous evaluation to chose the scintillation spectra as a base for the absolute flux and to normalize the proportional counter results to that level. This leads to an overestimation of the complete neutron spectrum in the inter-comparison.
- From the actual point of view, the proportional counter results being consistent over a wide range of energy are more reliable and should be preferred for the definition of the absolute scale. The problem with the absolute normalization of the scintillation results exists only at Ringhals and could be probably connected with the very hard measuring and environmental conditions.

A precise re-evaluation of the data leads to the conclusion that the previous neutron spectra have to be multiplied by a factor of

x 0.7000 **for Ringhals L and**
x 0.4879 **for Ringhals A.**

The shape of the spectra remains unchanged.

In case of the CLAB measurements the mentioned problems did not occur. Here, the different parts of the experimental neutron spectra agree well with each other as it is usual in other applications of the spectrometers, too.

An illustration for the discussion is given in Fig. 1S of this supplement for position Ringhals L. The values of the modified neutron spectra are given in Tab. 1S. They replace those of Tab. 3 in the previous report and differ in the absolute normalization for Ringhals A and L spectra.

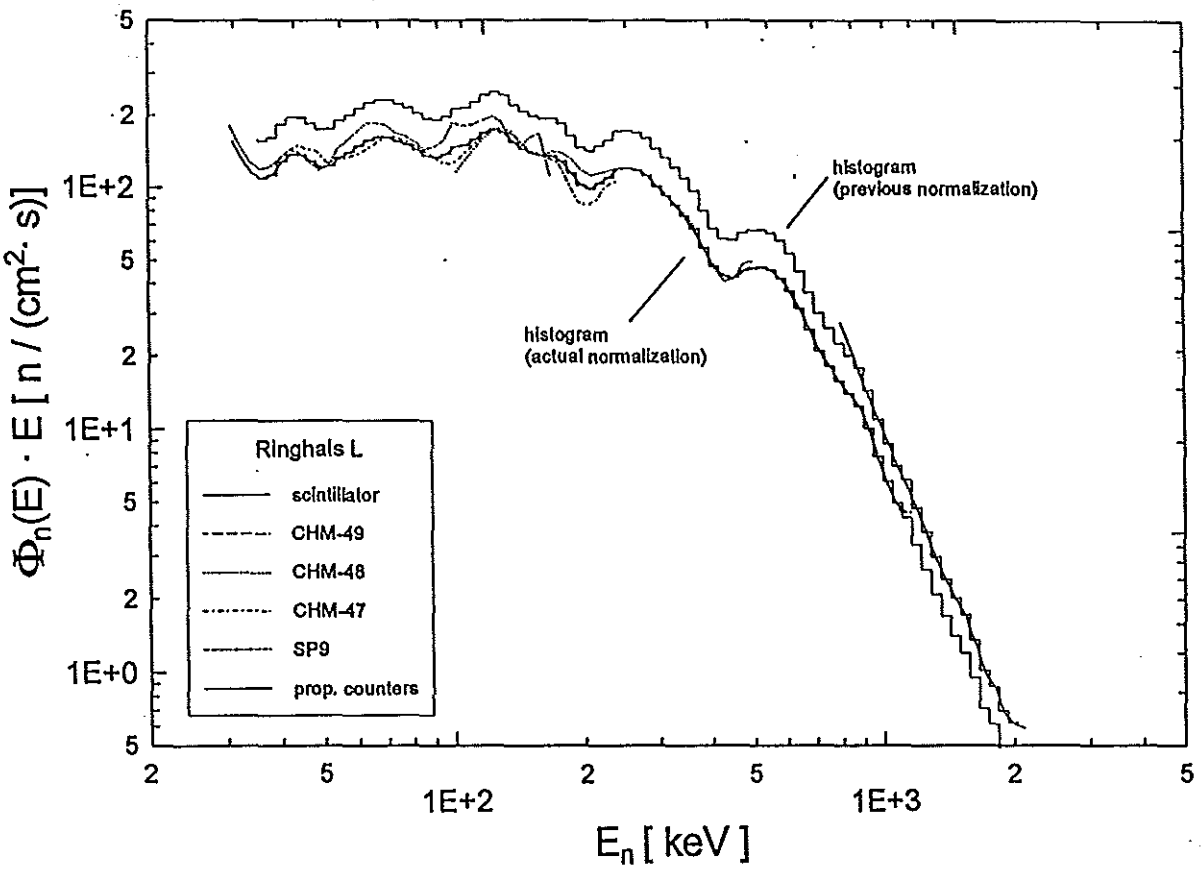

Figure 1: Re-normalization of the neutron spectrum for Ringhals L

lower energy limit [MeV]	group flux Φ(u)·Δu [1/s/cm²]				lower energy limit [MeV]	group flux Φ(u)·Δu [1/s/cm²]			
	CLAB Position P	CLAB Position D	Ringhals Position A	Ringhals Position L		CLAB Position P	CLAB Position D	Ringhals Position A	Ringhals Position L
3.55E-02				5.61E+00	2.91E-01	1.33E+00	9.05E-01	2.92E+01	5.19E+00
3.73E-02				5.79E+00	3.06E-01	1.31E+00	8.34E-01	2.54E+01	4.75E+00
3.93E-02				6.57E+00	3.22E-01	1.27E+00	8.20E-01	2.28E+01	4.35E+00
4.14E-02				7.02E+00	3.39E-01	1.15E+00	7.79E-01	2.13E+01	3.93E+00
4.36E-02				6.98E+00	3.57E-01	9.04E-01	7.36E-01	1.90E+01	3.47E+00
4.58E-02				6.61E+00	3.75E-01	7.30E-01	7.19E-01	1.67E+01	2.88E+00
4.83E-02			4.11E+01	6.27E+00	3.95E-01	6.29E-01	6.63E-01	1.48E+01	2.42E+00
5.08E-02			4.17E+01	6.29E+00	4.16E-01	6.04E-01	6.39E-01	1.44E+01	2.21E+00
5.35E-02			4.13E+01	6.83E+00	4.38E-01	6.17E-01	6.66E-01	1.46E+01	2.17E+00
5.63E-02			4.05E+01	7.22E+00	4.61E-01	6.30E-01	7.12E-01	1.46E+01	2.33E+00
5.92E-02			4.04E+01	7.64E+00	4.85E-01	6.21E-01	7.68E-01	1.48E+01	2.39E+00
6.24E-02			4.15E+01	8.09E+00	5.11E-01	6.16E-01	7.87E-01	1.44E+01	2.40E+00
6.56E-02			4.36E+01	8.31E+00	5.38E-01	6.50E-01	7.79E-01	1.33E+01	2.33E+00
6.91E-02	1.10E+00	7.25E-01	4.49E+01	8.28E+00	5.66E-01	7.13E-01	8.18E-01	1.20E+01	2.16E+00
7.27E-02	1.19E+00	7.36E-01	4.42E+01	7.99E+00	5.96E-01	7.54E-01	8.47E-01	1.05E+01	1.91E+00
7.66E-02	1.21E+00	7.79E-01	4.18E+01	7.72E+00	6.27E-01	7.25E-01	8.42E-01	8.97E+00	1.62E+00
8.06E-02	1.12E+00	8.14E-01	3.89E+01	7.31E+00	6.60E-01	6.39E-01	8.20E-01	7.70E+00	1.32E+00
8.48E-02	1.03E+00	8.25E-01	3.75E+01	6.96E+00	6.95E-01	5.51E-01	7.69E-01	6.59E+00	1.08E+00
8.93E-02	1.02E+00	8.23E-01	3.74E+01	6.86E+00	7.31E-01	4.42E-01	7.18E-01	5.78E+00	9.32E-01
9.40E-02	1.04E+00	8.01E-01	3.82E+01	7.07E+00	7.70E-01	4.13E-01	6.56E-01	5.31E+00	8.15E-01
9.90E-02	1.07E+00	7.70E-01	3.85E+01	7.60E+00	8.11E-01	3.54E-01	5.94E-01	4.85E+00	7.22E-01
1.04E-01	1.04E+00	7.64E-01	4.09E+01	7.69E+00	8.53E-01	3.57E-01	5.42E-01	4.14E+00	6.44E-01
1.10E-01	1.04E+00	8.45E-01	4.30E+01	8.13E+00	8.98E-01	3.55E-01	4.88E-01	3.40E+00	5.20E-01
1.15E-01	1.26E+00	9.10E-01	4.48E+01	8.67E+00	9.45E-01	3.19E-01	4.34E-01	2.75E+00	3.98E-01
1.21E-01	1.52E+00	9.10E-01	4.56E+01	8.97E+00	9.95E-01	2.72E-01	3.83E-01	2.28E+00	3.14E-01
1.28E-01	1.67E+00	8.46E-01	4.48E+01	8.67E+00	1.05E+00	2.36E-01	3.47E-01	1.93E+00	2.55E-01
1.35E-01	1.61E+00	7.65E-01	4.26E+01	7.90E+00	1.10E+00	2.14E-01	3.16E-01	1.51E+00	2.23E-01
1.42E-01	1.37E+00	7.44E-01	4.01E+01	7.41E+00	1.16E+00	1.97E-01	2.87E-01	1.15E+00	1.72E-01
1.49E-01	1.14E+00	7.67E-01	3.80E+01	7.14E+00	1.22E+00	1.76E-01	2.62E-01	8.66E-01	1.36E-01
1.57E-01	1.08E+00	8.04E-01	3.79E+01	6.96E+00	1.29E+00	1.64E-01	2.41E-01	6.60E-01	1.07E-01
1.65E-01	1.11E+00	8.43E-01	3.72E+01	6.94E+00	1.35E+00	1.51E-01	2.21E-01	4.95E-01	8.69E-02
1.74E-01	1.10E+00	8.04E-01	3.46E+01	6.61E+00	1.42E+00	1.38E-01	1.98E-01	3.83E-01	7.22E-02
1.83E-01	9.56E-01	7.44E-01	3.16E+01	5.89E+00	1.50E+00	1.23E-01	1.73E-01	3.13E-01	6.16E-02
1.93E-01	8.24E-01	7.02E-01	2.99E+01	5.25E+00	1.58E+00	1.07E-01	1.53E-01	2.57E-01	4.88E-02
2.03E-01	8.87E-01	7.19E-01	3.12E+01	5.10E+00	1.66E+00	9.73E-02	1.37E-01	2.16E-01	3.66E-02
2.14E-01	1.10E+00	8.01E-01	3.42E+01	5.36E+00	1.75E+00	9.25E-02	1.22E-01	1.78E-01	3.15E-02
2.25E-01	1.23E+00	8.02E-01	3.56E+01	5.66E+00	1.84E+00	8.17E-02	1.04E-01	1.43E-01	2.52E-02
2.37E-01	1.34E+00	8.18E-01	3.71E+01	6.14E+00	1.94E+00	6.40E-02	8.08E-02	1.26E-01	2.24E-02
2.49E-01	1.36E+00	9.07E-01	3.61E+01	6.18E+00	2.04E+00	4.51E-02	6.32E-02		
2.62E-01	1.35E+00	9.50E-01	3.50E+01	6.07E+00	2.15E+00				
2.76E-01	1.37E+00	9.68E-01	3.29E+01	5.74E+00					

Table 1S: Numerical results of the experiments

4. TEPC Measurements

Th. Schmitz[1], U. Nilsson[2], A Marchetto[3], V.D. Nguyen[4], H. Schuhmacher[5], A.J. Waker[6]

[1] *Forschungszentrum Jülich, Jülich, Germany*
[2] *Statens Strålskyddsinstitut, Stockholm, Sweden*
[3] *CEA de Grenoble, Grenoble, France*
[4] *CEA de Fontenay aux Roses, Fontenay auc Roses, France*
[5] *Physikalisch Technische Bundesanstalt Braunschweig, Braunschweig, Germany*
[6] *AECL Research, Chalk River, Canada*

4.1 Introduction

Low pressure tissue equivalent proportional counters (TEPC) are suitable for measuring absorbed dose, D, as well as the frequency distribution of lineal energy in a small volume by single particles [1, 2]. Due to the relation between lineal energy and LET, in principal, dose distributions in terms of LET can be determined and dose equivalent can be evaluated by applying the definition of the quality factor as a function of LET from ICRP [3, 4]. The reading can then be used as an estimate of ambient dose equivalent, H*(10) [5]. The combined properties of a cavity chamber and a pulse height spectrometer can also be used to assess the neutron and photon components of dose equivalent separately in mixed radiation fields.

There are two independent measurement methods for determining averages of distributions in lineal energy. With the pulse height analysis technique, single event spectra are measured and averages can be calculated from these distributions. The variance technique determines the dose average of the energy weighted lineal energy spectrum from a multiple event measurement. The latter method, however, does not allow to separate dose fractions due to photon and neutron radiation. The gamma dose has to be determined by another detector, e.g. a Geiger-Müller counter.

Several groups in Europe and North America have developed dose equivalent meters based on a TEPC for area monitoring. Different detector designs, electronic equipment for data processing and evaluation procedures are used in order to achieve good dose equivalent response and to provide diagnostic information in terms of photon and neutron dose fractions and mean and neutron quality factors. The groups met in 1986 and 1987 for intercomparison measurements in defined, monoenergetic neutron fields at the PTB Braunschweig. The dose equivalent response as a function of neutron energy was studied, taking into account the differences in system design and calibration procedures [6, 7, 8].

This chapter introduces the TEPC measurement systems, which participated in the intercomparison described in this report. A short description of the measurement principle and the data evaluation is given. Finally the results, as reported by the participants are presented and are briefly discussed. It will be the basis for a more detailed analysis of the data, which will be given in a further report.

4.2 Detector Systems

4.2.1 Description of Systems

Six groups have participated in the intercomparison:

Abbreviation	Laboratory Name	City, Country	Responsible
AECL	AECL-Research	Chalk River, Canada	A.J. Waker
KFA	Forschungszentrum Jülich	Jülich, Germany	Th. Schmitz
CEA-Gren.	Centre d'Etudes Nucleaires	Grenoble, France	A. Marchetto
CEA.-Font-	Centre d'Etudes Nucleaires	Fontenay aux Roses	V.D. Nguyen
PTB-Handi	Physikalisch Techn. Bundesanstalt	Braunschweig, Germany	H. Schuhmacher
SSI	Statens Strålskyddsinstitut	Stockholm, Sweden	U. Nilsson

Table 4.1: Groups participating with TEPC systems

AECL is a laboratory system [9], which uses two commercial linear amplifier channels, two analog to digital converters (ADC) for data acquisition and a portable computer for data analysis and evaluation. KFA is a compact system, which uses one nonlinear amplifier channel, a multichannel analyser and a portable computer for data analysis and evaluation [10]. CEA-Gren.is a portable system, which uses a double multichannel analyser for data acquisition. It was developed for practical radiation protection [11, 12].CEA-Font. is a portable, battery operated system, which was developed for measuring dose equivalent during space flights [13]. PTB-Handi is also a portable, battery operated system, which was developed by the University of the Saarland for practical radiation protection [14]. It applies a specially designed electronic system, which uses 16 channels of approximately exponentially increasing width to record the pulse height distributions. SSI is a compact, battery operated system based on the variance technique. The electronic equipment consists of an electrometer positioned on the detector and a microprozessor unit for data acquisition and data analysis [15].

All systems use tissue equivalent proportional counters (TEPC) as detectors. Table 4.2 lists the important properties of the detectors used. The sensitive volume of the counters, differ in shape and size. Four detectors (AECL, CEA-Gen., PTB-Handi, SSI) are spherical, while the others are cylindrical (KFA, CEA-Font.), the height being equal to the diameter. The volumes range from 98.17 cm^3 to 3300 cm^3. The walls are made from A-150 tissue equivalent (TE) plastic and the wall thicknesses range from 1 mm to 6.26 mm.

Except for KFA, all detectors are enclosed in thin metal covers, which serve as vacuum container and as electrostatic shield. The KFA detector uses a 14 mm polyethylene cap as vacuum container and a thin aluminum foil as electrostatic shield.

Three of the counters (AECL, CEA-Gren. and PTB-Handi) are commercially available detectors, whereas the others were designed and built by the groups who use them.

The counters were filled with tissue equivalent gas. The gas pressures were chosen in order to simulate tissue spheres with a density of 1 g/cm^3 and diameters between 1 µm and 4.5 µm.

	AECL	KFA	CEA-Gren.	CEA-Font.	PTB-Handi	SSI
Containment						
Shape	cylindrical	cylindrical	cylindrical	cylindrical	cylindrical	thimble
Diameter (mm)	150	127	150	76	88.8	220
Height (mm)	180	190	180	100	100	300
Wall material	aluminium	polyethylene	aluminium	nickel	stainl. steel	aluminium
Wall thickness (mm)	1.27	14	1.27	0.3	0.76	2
Sensitive Volume						
Shape	spherical	cylindrical	spherical	cylindrical	spherical	spherical
Diameter (mm)	125.7	70	125.7	50	59	184
Height		70		50		
Wall material	A-150	A-150	A-150	A-150	A-150	A-150
Wall thickness (mm)	2.29	1	2.29	4	2.5	6.26
Volume (cm^3)	1039.93	269.4	1039.93	98.17	107.54	3300
TE-Gas based on	propane	methane	propane	propane	propane	methane
Sim. Diameter (µm)	2	1	2	3	2	2/4.5[1]

[1] 2µm Counter B/ 4.5µm Counter A

Table 4.2: Physical characteristics of the TEPC used in the intercomparison

4.2.2 Data Evaluation

The determination of absorbed dose in the wall material, D, with a tissue equivalent proportional counter is generally based on cavity chamber principles, using the relation

$$D_{Wall} \approx D_{Gas} = \frac{q \cdot W}{m \cdot e} \qquad (1)$$

where q is the total charge produced in the cavity by ionising particles, W the mean energy required to produce an ion pair in the gas, e the electron charge and m the mass of the gas in the sensitive volume.

The detectors, with the exception of the SSI system, perform an analysis of the measured pulse height distribution in order to determine absorbed dose and dose equivalent. The distribution, often simply called microdosimetric spectrum, is scaled in terms of lineal energy[2], y, by using an appropriate calibration factor. The absorbed dose is then calculated according to

$$D = C_D \, N \, y_F \qquad (2)$$

where C_D is a calibration factor, N is the total number of events and y_F denotes the frequency mean lineal energy of the measured pulse height distribution in terms of lineal energy, f(y):

$$\bar{y}_F = \int_0^\infty y \cdot f(y) dy \qquad (3)$$

[2] Lineal energy is defined as the quotient of ε by l, where ε is the energy imparted to the matter in a volume of interest by single energy deposition events (by single uncorrelated charged particles) and l is the mean chord length in that volume: $y = \varepsilon/l$. The unit of y is J/m, but most commonly, the unit used for this quantity is keV/µm [16].

For the SSI system the absorbed dose is calculated as:

$$D = C_d' \cdot D_{gas} \tag{4}$$

C_d' is a calibration factor equal to the ratio of the true absorbed dose, D, and the observed absorbed dose in the gas, D_{gas}.

For all systems except SSI, the mean quality factor, Q, is determined according to

$$Q = \int_0^\infty q(y) \cdot d(y) dy \tag{5}$$

and for SSI according to the linear relation [15]

$$Q = a + b \cdot y_D \text{ with } \bar{y}_D = \int_0^\infty y \cdot d(y) dy \tag{6}$$

where $d(y)$[3] is the probability density of the tissue absorbed dose and the function q(y) approximates $q(L_\infty)$, the quality factor definition of ICRP, by setting $y = L_\infty$ or $y = 9/8\ L_\infty$. The parameters a and b are chosen empirically to fit the quality factor as closely as possible. The total dose equivalent is then determined according to

$$H = Q \cdot D \tag{7}$$

In the variance method $\overline{y_D}$ is derived from the variance V(q) of the measured charge

$$\overline{y_D} = V(q) \cdot \frac{W}{e \cdot l \cdot q \cdot M} \tag{8}$$

where l is the mean chord length of the sensitive volume and M the gas multiplication factor. No calibration is needed.

4.2.3 Neutron-Gamma Discrimination

The discrimination of events due to neutrons and gamma rays, is based on the differences in the stopping power of electrons released in photon interactions and the stopping power of protons and heavier charged particles released in neutron interactions with the detector material. This difference is reflected in the pulse height distribution by the fact, that electrons and the heavier ions contribute, principally, to different parts of the lineal energy spectrum, f(y). There is, however, an interval, where both, electron and proton events overlap.

For a tissue diameter of 2 µm, simulated by the TEPC, the spectra for gamma rays extend from the detection threshold to lineal energies of about 10 keV/µm. Protons produced in neutron interactions may be associated with lineal energies in the range from the detection threshold up to the 'proton edge' at around 140 keV/µm. In the radiation fields of the Ringhals reactors and

---

[3] The probability density d(y) can be derived from the event size distribution F(y) according to [16]

$$d(y) = \frac{1}{\bar{y}_F} \cdot y \cdot f(y)$$

around the transport cask with spent fuel elements at CLAB, the main contribution of the protons in the spectra are observed above the range of the gamma rays.

Thermal neutrons produce in the counter walls secondary gamma rays by the non-elastic H(n,γ) reaction with hydrogen. Likewise, epithermal neutrons, if they are moderated (thermalised) in a thick counter wall, as in the case of the KFA system, cause a significant gamma dose in the counter. Therefore, the gamma doses determined by a TEPC in the reactor fields and at CLAB are due to prompt gammas emitted from the source and also secondary gammas produced by thermal or thermalised neutrons in the counter.

There are two methods, practically employed for discriminating between photon and neutron dose fractions.

1. A pure, photon-induced microdosimetric spectrum is fitted to the mixed-radiation spectrum (AECL) and the difference of both spectra is then related to neutron induced events only.
2. Use of a fixed threshold in lineal energy (KFA, CEA-Gren., CEA-Font, PTB-Handi).

The evaluation of the intercomparison of TEPC instruments, which was performed in 1986 and 1987 at the PTB-Braunschweig, did not indicate a preference to be given to either of the two methods in the case of mixed fields, where the energy spectrum of neutrons is broad [1].

The thresholds used by the different systems, which use this method were: 10 keV/μm (KFA, CEA-Gren.), 6 keV/μm (PTB-Handi) and 7 keV/μm (CEA-Font.).

4.2.4 Calibration

All systems except the SSI system are calibrated in terms of lineal energy y by using an α-particle source, which is built into the counter. The detector of the KFA system does not have a built in α-source. A second version of the detector, however, does have an α-source. The α-calibration of this second detector is transferred to the KFA counter via corresponding measurements with a ^{60}Co test-source. Absorbed dose and dose equivalent can then be calculated from measured spectra according to equations 2, 5 and 7.

The calibration factor C_D in equation 2 can be determined by a second calibration measurement. However, for well known detectors it is given by

$$C_D = \frac{c}{d_p^2} \qquad (9)$$

where c is 0.204 Gy μm/keV for spherical and 0.136 Gy μm/keV for right cylindrical counters. d_p is the real diameter of the counters sensitive volume, given in μm. The latter possibility is used by all systems.

The dose equivalent response[4] of TEPCs is close to one for photon energies above 20 keV [17]. The response to neutrons varies quite considerably as a function of incident neutron energy and leads to an underreading in neutron fields, which contain a significant dose fraction of neutrons in the keV region. It has been suggested [1] to use the response in a neutron field,

[4]The dose equivalent reponse, R_H, is defined in this section to mean the ratio of the detector reading, H, and the 'true' ambient dose equivalent H*(10).

e.g. that in a D_2O-moderated ^{252}Cf field, to correct the neutron dose equivalent reading. This method was applied by all systems, except CEA.-Gren, for which the correction factor is determined from the mean dose equivalent response to monoenergetic neutrons between 73 keV and 2.5 MeV.

The correction factors determined depend on the counter geometry and the neutron source used. AECL uses a factor of 1.44, PTB-Handi a factor of 1.41, CEA-Gren. a factor of 1.75 and KFA a factor of 1.5.

Table 4.3 summarises the calibration procedures of the different systems.

Table 4.3: Summary of calibration procedures

	AECL	KFA	CEA-Gren.	CEA-Font.	SSI	PTB-Handi
a) lineal energy	internal α-source	based on α-source measurement	internal α-source	internal α-source	absolute measurements	internal α-source
b) dose equivalent	correction of neutron dose equivalents due to the response in a calibrated ^{252}Cf-field	correction of neutron dose equivalents due to the response in calibrated, moderated ^{252}Cf-fields	correction of neutron dose equivalent due to the mean response to monoenergetic neutrons	direct calibration in terms of external neutron and gamma sources	correction of dose equiva-lent reading due to the response in a calibrated ^{252}Cf-field	correction of neutron dose equivalents due to the response in calibrated, moderated ^{252}Cf-fields

4.3 Results and Discussion

Tables 4.5 to 4.11 report the absorbed dose rate, dose equivalent rate and quality factor data as reported by the participants. The dose data give the total dose rates as well as the neutron and gamma dose rates. The quality factors are reported as average total field and as neutron quality factors. Dose equivalent values are stated for an evaluation using the quality factor definition according to ICRP 15 [3] (all systems) and for the new quality factor definition according to ICRP 60 [18] (AECL, KFA, PTB-Handi). Due to the different measurement principle, SSI only reports total dose and dose equivalent rates. The gamma dose equivalent stated for SSI was derived from separate measurements with Geiger-Müller counters. The abbreviations used for the different systems are according to table 4.1. The abbreviations for the different quantities are given in table 4.4. The identification of the measurement point is according to the nomenclature used in chapter 2.

For the measurement of CEA-Font. at Ringhals 4, in the Lock, only the neutron dose and dose equivalent rates are reported, since the gamma component is distorted, probably due to a noise problem (see the yd(y) distribution; also, V.D. Nguyen reported that there was a problem during this particular measurement).

In Tables 4.12 to 4.14 the readings of the detectors with respect to absorbed dose rate (Table 4.12), total dose equivalent rate and mean quality factors (4.13) and neutron dose equivalent

rate and neutron quality factor (4.14) are compared. For each measurement location, the average reading of the system and the standard deviation of the mean are given (Tables 4.12b, 4.13b and 4.14b). Only the dose equivalent and quality factor readings according to the old ICRP 15 definition are given, since this definition is still used for legal quantities [3]. The total absorbed dose rate, total dose equivalent rates and total neutron dose equivalent rates are also compared in Figures 4.1 to 4.3.

The absorbed dose readings of all systems show the same general trend (Figure 4.1). The reading of the PTB-Handi system is always above the average reading of the systems by between 13% and 25% (on average 17%). On the contrary, the CEA-Font. system is always lower than the average by between 8% and 32% (on average 19%). The standard deviation of the results is between 7% and 16%.

The ICRP 15 total dose equivalent rate readings (Figure 4.2, Table 4.13) deviate between 9% and 24% (on average 18%) from the average readings. As for the absorbed dose rates, PTB-Handi is consistently above the average by between 7% and 36%. CEA-Font. is again always lower than the average by 25% to 39%. The same trend is observed with regard to the neutron dose equivalent rate readings (Figure 4.3 and Table 4.14). The standard deviations are about 10% larger than in case of the total dose equivalent.

There are two rather obvious reasons for the increased standard deviations in the average dose equivalent reading:

1. The weighting of the quality factor is most effective at lineal energies above 10 keV/μm. In this region, the number of counts in the measured pulse height distribution is comparably low and therefore, the statistical uncertainty in this part of the distribution is higher than in the parts below lineal energies of 10 keV/μm.
2. As described in chapter 4.2.4 the neutron dose equivalent is additionally weighted by a correction factor. The neutron dose equivalent reading depends on the neutron-gamma discrimination method used and in case of the threshold method, on the value of the threshold. The differences in method and in the values used contribute to the standard deviation of the average dose equivalent readings.

A major part of the standard deviation of the average values, however, is due to the consistently higher readings of PTB-Handi and the consistently lower readings of CEA-Font. The reasons for this have to be further investigated.

4.3.1 Comparison of Spectra

The conventional format for presenting spectra measured with a TEPC entails the use of a logarithmic scale in lineal energy, y, and plotting d(y) (see chapter 4.2) multiplied by y at a linear scale. This is equivalent to presenting d(y) per logarithmic increment d(log y/y_0) and maintains the proportionality between the absorbed dose fraction associated with an interval of y and the area under the plotted curve. Spectra plotted in this format are normalized to give equal areas under the curve.

In Figures 4.4-4.10 the spectra of the different systems are compared. In parts a) of the Figures, the spectra of AECL, KFA and PTB-Handi are compared, in parts b) the spectra of CEA-Gren. and CEA-Font. are shown. The SSI system does not measure pulse height spectra, as described in chapter 4.2.

The spectra of AECL, HANDI and KFA are consistent. The spectra of both CEA systems show a marked difference in the gamma parts of the distributions below about 1 keV/µm. The reason for this is unclear, but might be due to either the pulse height analysis or the influence of electronic noise.

In case of the AECL system, a ^{60}Co spectrum was fitted to the lower part of the spectrum, whereas in case of HANDI and KFA no fitting was performed. Therefore, the shape of the gamma distribution in case of AECL does not change significantly between the measurement positions, whereas differences are observed by HANDI and KFA. Generally, the photon spectra at the reactors seem to be harder, resulting in more pronounced shoulders and peaks in the respective distributions. The neutron parts of the KFA system are generally more narrow, reflecting the influence of the thicker counter wall, which moderates the initial neutron spectrum. This indicates that an important fraction of the incident neutrons must have energies below 100 keV/µm.

There is no significant contribution to the spectra above the proton edge at about 140 keV/µm. This indicates that the incident neutron spectra do not have a significant contribution at energies above about 1 MeV to 2 MeV.

4.4 References

[1] Menzel, H.G., Lindborg, L., Schmitz, Th. Schuhmacher, H. and Waker, A.J., *Intercomparison of Dose Equivalent Meters Based on Microdosimetric Techniques: Detailed Analysis and Conclusions. Radiat.* Prot. Dosim. **29** (1989) 55 - 68.

[2] Schuhmacher, H., *Tissue-Equivalent Proportional Counters in Radiation Protection Dosimetry: Expectations and Present State.* Radiat. Prot. Dosim. **44** (1992) 199 - 206.

[3] ICRP Publication 15, *Protection Against Ionising Radiation from External Sources.* International Commision on Radiological Protection. (Oxford: Pergamon), 1970.

[4] ICRP Publication 21, *Data for Protection Against Ionising Radiation from External Sources: Supplement to ICRP Publication 15.* International Commision on Radiological Protection. (Oxford: Pergamon), 1971.

[5] ICRU Report 39, *Determination of Dose Equivalent for External Radiation Sources.* International Commision on Radiation Units and Measurements. (Bethesda, MD: ICRU Publications), 1985.

[6] Dietze, G., Guldbakke, S., Kluge, H., Schmitz, Th., *Intercomparison of Radiation Protection Instruments Based on Microdosimetric Principles.* PTB Report, PTB-ND-29 (1986).

[7] Dietze, G., Booz, J., Edwards, A.A., Guldbakke, S., Kluge, H., Leroux, J.B., Lindborg, L., Menzel, H.G., Nguyen, V.D., Schmitz, Th., Schumacher, H., *Intercomparison of Dose Equivalent Meters Based on Microdosimetric Techniques.* Radiat. Prot. Dosim. **23**, No. 1-4 (1988) 227 - 234.

[8] Alberts, W.G., Dietze, E., Guldbakke, S., Kluge, H. and Schuhmacher, H., *International Intercomparison of TEPC Systems used for Radiation Protection.* Radiat. Prot. Dosim. **29** (1989) 47 - 53.

[9] Waker, A.J., *Microdosimetric Radiation Field Characterisation and Dosimetry in a Heavy Water Moderated Reactor Environment.* Radiat. Prot. Dosim. **52**, No. 1-4, (1994) 415 - 418.

[10] Schmitz, Th., Morstin, K., Olko, P., Booz, J., *The KFA Counter: A Dosimetry System for Use in Radiation Protection.* Radiat. Prot. Dosim. Vol. **31**, Nos. 1-4 (1990) 371 - 375.

[11] Marchetto, A., Leroux, J.B., Herbaut, Y., Latu, M., Tinelli, P., *CIRCEG, a Portable Device for Photon Neutron Dosimetry.* Radiat. Prot. Dosim. **23** (1988) 253 - 256

[12] Marchetto, A., Herbaut, Y., *Influence of Photon Radiation on Neutron Dose Equivalent Measurement in Radiation Protection with CIRCEG.* Radiat. Prot. Dosim. **44** (1992) 207 - 211.

[13] Nguyen, V.D., Lebaron-Jacobs, L., Bouisset, P., Kerlau, G., Itié, C., Montagne, C., Pelcot, D. and Lebuisson, M.C., *Real Time Determination of the Quality Factor and Dose Equivalent of Cosmic Radiation Aboard French Airliners.* Proc. 40th Int. Congr. of Aviation and Space Medicine, 5-9 Sep. 1992, Tokyo, in press

[14] Kunz, A., Pihet, P., Arend, E. and Menzel, H.G., *An Easy-to-Operate Portable Pulse-Height Analysis System for Area Monitoring with TEPC in Radiation Protection.* Nucl. Instrum. Meth. in Phys. Res. **A299** (1990) 696 - 701.

[15] Lindborg, L., Kliauga, P., Marino, S., Rossi, H.H., *Variance-Covariance Measurements of the Dose Mean Lineal Energy in a Neutron Beam.* Radiat. Prot. Dosim. **13**, No. 1-4, (1985) 347 - 351.

[16] ICRU Report 36, *Microdosimetry. International Commision on Radiation Units and Measurements.* (Bethesda, MD: ICRU Publications), 1983.

[17] Schmitz, Th., Kramer, H.M., Booz, J., *Assessment of the Photon Response of a TEPC; Implementation of Operational Quantities into Radiation Protection.* Radiat. Prot. Dosim. **29**, No. 1-2 (1989) 69 - 73.

[18] ICRP Publication 60, *Recommendations of the International Commision on Radiological Protection International Commission on Radiological Protection..* (Oxford: Pergamon), 1991.

[19] Lindblom, E. and Samuelson, G., *Determination of the Quality Factor by the Variance Technique.* Proc. of the 4th Symposium on Neutron Dosimetry, EUR 7448 (Luxembourg: CEC), (1981) 279 - 288.
(not cited !?)

Abbrev.	Lab.Name	City/Country	Responsible
AECL	AECL-Research	Chalk River, Canada	A.J. Waker
KFA	Forschungszentrum Jülich	Jülich, Deutschland	Th. Schmitz
CEA-Gren.	Centre d'Etudes Nucleaires	Grenoble, France	A. Marchetto
CEA-Font.	Centre d'Etudes Nucleaires	Fontenay aux Roses, France	V.D. Nguyen
PTB-Handi	Physikalisch Techn. Bundesanstalt,	Braunschweig, Deutschland	H. Schuhmacher Th. Schmitz (Op.)
SSI	Statens Stralskyddsinstitut	Stockholm, Sweden	L. Lindborg

Abbreviations	
D/t	Total Dose Rate
Dg/t	Gamma Dose Rate
Dn/t	Neutron Dose Rate
Q/Qn	Total-/Neutron Quality Factor
H/t	Total Dose-Equivalent Rate
Hg/t	Gamma Dose Equivalent Rate
Hn/t	Neutron Dose Equivalent Rate

Table 4.4

RINGHALS
Reactor 4, Lock

System	D/t µGy/h	Dg/t µGy/h	Dn/t µGy/h	ICRP 21 Q	H/t µSv/h	Hg/t µSv/h	Hn/t µSv/h	Qn	ICRP60 Q	H/t µSv/h	Hg/t µSv/h	Hn/t µSv/h	Qn
AECL	52.49	41.58	10.92	3.54	185.64	47.43	138.21	12.66	4.85	254.66	42.29	212.37	19.45
KFA	52.92	43.54	9.38	3.17	167.69	46.34	121.35	12.94	4.17	220.48	43.54	176.94	18.86
CEA-Gren.	54.90	37.70	17.20	3.81	209.00	44.00	165.00	9.59					
CEA-Font.			14.36				122.50	8.53					
PTB-Handi	63.20	48.50	14.70	3.62	229.00	50.00	179.00	12.18	4.60	291.00	48.50	242.00	16.46
SSI B-200	52.40			2.10	151.00	70.90	80.00						
A-1200	56.40			2.00	155.00	74.20	80.60						
B-400	55.30			2.10	159.00	74.60	84.20						

Table 4.5

Reactor 4, Pos. A

System	D/t µGy/h	Dg/t µGy/h	Dn/t µGy/h	ICRP 21 Q	H/t µSv/h	Hg/t µSv/h	Hn/t µSv/h	Qn	ICRP60 Q	H/t µSv/h	Hg/t µSv/h	Hn/t µSv/h	Qn
AECL	334.73	260.64	74.08	3.70	1239.27	297.30	941.97	12.72	5.07	1696.65	265.12	1431.53	19.32
KFA	327.09	258.28	68.82	3.80	1242.53	276.42	966.10	14.04	5.18	1692.90	258.28	1434.62	20.85
CEA-Gren.	295.00	210.20	84.80	3.55	1046.00	259.40	786.60	9.28					
CEA-Font.	293.47	225.66	67.81	2.56	752.37	231.34	521.04	7.68					
PTB-Handi	418.00	316.00	101.00	3.80	1590.00	327.00	1260.00	12.48	4.98	2080.00	317.00	1760.00	17.43
SSI B200	314.00			2.30	987.00	487.00	500.00						
A-1200	342.00			2.20	1042.00	517.00	525.00						
B-400	335.00			2.30	1095.00	526.00	569.00						

Table 4.6

Reactor 2, Pos. F

System	D/t µGy/h	Dg/t µGy/h	Dn/t µGy/h	ICRP 21 Q	H/t µSv/h	Hg/t µSv/h	Hn/t µSv/h	Qn	ICRP60 Q	H/t µSv/h	Hg/t µSv/h	Hn/t µSv/h	Qn
AECL	195.43	157.73	37.70	3.37	659.31	179.88	479.43	12.72	4.53	884.62	160.44	724.18	19.21
KFA	231.85	186.42	45.43	3.57	827.57	199.58	627.98	13.82	4.78	1108.93	186.42	922.51	20.31
CEA-Gren.	181.50	134.70	46.80	3.20	581.00	155.00	426.00	9.10					
CEA-Font.	188.71	160.73	27.99	2.13	402.87	163.23	239.65	8.56					
PTB-Handi	230.00	178.00	52.10	3.57	822.00	184.00	639.00	12.26	4.61	1060.00	178.00	886.00	17.01
SSI B-200	198.00			2.10	593.00	311.00	281.00						

Table 4.7

Reactor 2, Pos. G

System	D/t µGy/h	Dg/t µGy/h	Dn/t µGy/h	ICRP 21 Q	H/t µSv/h	Hg/t µSv/h	Hn/t µSv/h	Qn	ICRP60 Q	H/t µSv/h	Hg/t µSv/h	Hn/t µSv/h	Qn
AECL	65.37	59.60	5.77	2.17	141.82	67.97	73.85	12.79	2.61	170.56	60.63	109.93	19.04
KFA	67.76	59.10	8.66	2.50	169.33	63.04	106.29	12.27	3.09	209.40	59.10	150.30	17.36
PTB-Handi	79.40	69.30	10.10	2.04	162.00	71.50	90.80	8.99	2.30	183.00	69.40	113.00	11.19
SSI B-200	64.00			1.50	136.00	115.00	21.00						

Table 4.8

CLAB
Pos. D

System	D/t µGy/h	Dg/t µGy/h	Dn/t µGy/h	ICRP 21 Q	H/t µSv/h	Hg/t µSv/h	Hn/t µSv/h	Qn	ICRP60 Q	H/t µSv/h	Hg/t µSv/h	Hn/t µSv/h	Qn
AECL	26.91	24.13	2.78	2.36	63.50	27.52	35.97	12.96	2.94	79.09	24.54	54.54	19.65
KFA	26.19	23.63	2.56	2.12	55.57	25.31	30.26	11.81	2.57	67.20	23.63	43.57	17.00
CEA-Gren.	24.30	20.34	3.96	2.59	62.90	23.80	39.10	9.87					
CEA-Font.	19.10	16.33	2.77	1.98	37.89	16.50	21.38	7.71					
PTB-Handi	28.80	24.40	4.42	2.51	72.20	25.20	47.10	10.66	3.05	87.70	24.40	63.30	14.32
SSI A-900	23.70			1.60	52.40	33.00	19.40						
B-200	25.20			1.60	55.90	33.00	22.90						

Table 4.9

Pos. E

System	D/t µGy/h	Dg/t µGy/h	Dn/t µGy/h	ICRP 21 Q	H/t µSv/h	Hg/t µSv/h	Hn/t µSv/h	Qn	ICRP60 Q	H/t µSv/h	Hg/t µSv/h	Hn/t µSv/h	Qn
AECL	19.95	17.94	2.01	2.35	46.87	20.46	26.41	13.17	2.96	58.97	18.25	40.72	20.31
KFA	20.49	18.36	2.12	2.10	43.11	19.62	23.49	11.07	2.52	51.60	18.36	33.24	15.66
CEA-Gren.	19.10	15.93	3.17	2.59	49.50	18.60	30.90	9.75					
CEA-Font.	16.39	14.01	2.37	2.13	34.83	14.16	20.66	8.70					
PTB-Handi	23.30	19.40	3.83	2.64	61.50	20.10	41.50	10.84	3.22	75.10	19.40	55.70	14.54
SSI A-900	19.00			1.60	41.40	22.40	19.10						
B-200	19.70			1.60	44.60	22.20	22.40						

Table 4.10

Pos. P

System	D/t µGy/h	Dg/t µGy/h	Dn/t µGy/h	ICRP 21 Q	H/t µSv/h	Hg/t µSv/h	Hn/t µSv/h	Qn	ICRP60 Q	H/t µSv/h	Hg/t µSv/h	Hn/t µSv/h	Qn
AECL	23.23	20.83	2.40	2.37	55.00	23.76	31.24	13.02	2.98	69.17	21.19	47.98	20.00
KFA	22.22	19.84	2.38	2.09	46.34	21.08	25.26	10.61	2.50	55.48	19.84	35.64	14.98
CEA-Gren.	23.10	18.99	4.11	2.71	62.50	22.30	40.20	9.78					
CEA-Font.	14.83	12.31	2.52	2.18	32.31	12.46	19.85	7.88					
PTB-Handi	25.90	21.30	4.58	2.80	72.40	22.00	50.50	11.03	3.45	89.30	21.30	68.10	14.87
SSI B-200	22.40			1.60	51.40	23.10	28.40						

Table 4.11

Detector Intercomparison

Total Dose Rate

Position	AECL Abs. D/t [µGy/h]	KFA D/t [µGy/h]	CEA-Gren D/t [µGy/h]	CEA-Font D/t [µGy/h]	PTB-HANDI D/t [µGy/h]	SSI D/t [µGy/h]
Reac. 4, L	52.49	52.92	54.90		63.20	54.70
Reac. 4, A	334.73	327.09	295.00	293.47	418.00	330.33
Reac. 2, F	195.43	231.85	181.50	188.71	230.00	198.00
Reac. 2, G	65.37	67.76			79.40	64.00
CLAB , D	26.91	26.19	24.30	19.10	28.80	24.45
CALB, E	19.95	20.49	19.10	16.39	23.30	19.35
CALB, P	23.23	22.22	23.10	14.83	25.90	22.40

Table 4.12a

Position	Average D/t [µGy/h]	Std.Dev D/t [µGy/h]
Reac. 4, L	55.64	3.90
Reac. 4, A	333.10	41.39
Reac. 2, F	204.25	19.58
Reac. 2, G	69.13	6.08
CLAB , D	24.96	3.03
CALB, E	19.76	2.04
CALB, P	21.95	3.41

Table 4.12b

Total Quality Factors

Total Dose Equivalent Rates

Position	AECL		KFA		CEA-Gren.		CEA-Font.		PTB-Handi		SSI	
	Q	H/t [µSv/h]	Q	H/t [µSv/h]	Q	H/t [µSv/h]	Q	H/t [µSv/h]	Q	H/t [µSv/h]	Q	H/t [µSv/h]
Reac. 4, L	3.54	185.64	3.17	167.69	3.81	209.00			3.62	229.00	2.07	155.00
Reac. 4, A	3.70	1239.27	3.80	1242.53	3.55	1046.00	2.56	752.37	3.80	1590.00	2.25	1014.50
Reac. 2, F	3.37	659.31	3.57	827.57	3.20	581.00	2.13	402.87	3.57	822.00	2.10	593.00
Reac. 2, G	2.17	141.82	2.50	169.33					2.04	162.00	1.50	136.00
CLAB , D	2.36	63.50	2.12	55.57	2.59	62.90	1.98	37.89	2.51	72.20	1.60	54.15
CALB, E	2.35	46.87	2.10	43.11	2.59	49.50	2.13	34.83	2.64	61.50	1.60	43.00
CALB, P	2.37	55.00	2.09	46.34	2.71	62.50	2.18	32.31	2.80	72.40	1.60	51.40

Table 4.13a

Position	Average Q	Std. Dev.	Average H/t	Std. Dev. [µSv/h]
Reac. 4, L	3.24	0.62	189.27	26.91
Reac. 4, A	3.28	0.63	1147.44	257.35
Reac. 2, F	2.99	0.63	647.63	147.34
Reac. 2, G	2.05	0.36	152.29	13.78
CLAB , D	2.19	0.34	57.70	10.65
CALB, E	2.24	0.35	46.47	8.10
CALB, P	2.29	0.40	53.33	12.55

Table 4.13b

Position	AECL		KFA		CEA-Gren.		CEA-Font.		PTB-Handi		SSI
	Qn	Hn/t [µSv/h]	Qn	Hn/t [µSv/h]	Qn	Hn/t [µSv/h]	Qn	Hn/t [µSv/h]	Qn	Hn/t [µSv/h]	Hn/t [µSv/h]
Reac. 4, L	12.66	138.21	12.94	121.35	9.59	165.00			12.18	179.00	81.60
Reac. 4, A	12.72	941.97	14.04	966.10	9.28	786.60	7.68	521.04	12.48	1260.00	531.33
Reac. 2, F	12.72	479.43	13.82	627.98	9.10	426.00	8.56	239.65	12.26	639.00	281.00
Reac. 2, G	12.79	73.85	12.27	106.29					8.99	90.80	21.00
CLAB , D	12.96	35.97	11.81	30.26	9.87	39.10	7.71	21.38	10.66	47.10	21.15
CALB, E	13.17	26.41	11.07	23.49	9.75	30.90	8.70	20.66	10.84	41.50	20.75
CALB, P	13.02	31.24	10.61	25.26	9.78	40.20	7.88	19.85	11.03	50.50	28.40

Table 4.14a

Position	Average Qn	Std. Dev.	Average Hn/t [µSv/h]	Std. Dev.
Reac. 4, L	11.84	1.33	137.03	34.24
Reac. 4, A	11.24	2.37	834.51	258.97
Reac. 2, F	11.29	2.08	448.84	153.65
Reac. 2, G	11.35	1.68	72.99	32.13
CLAB , D	10.60	1.78	32.49	9.36
CALB, E	10.71	1.49	27.29	7.27
CALB, P	10.46	1.68	32.58	10.12

Table 4.14b

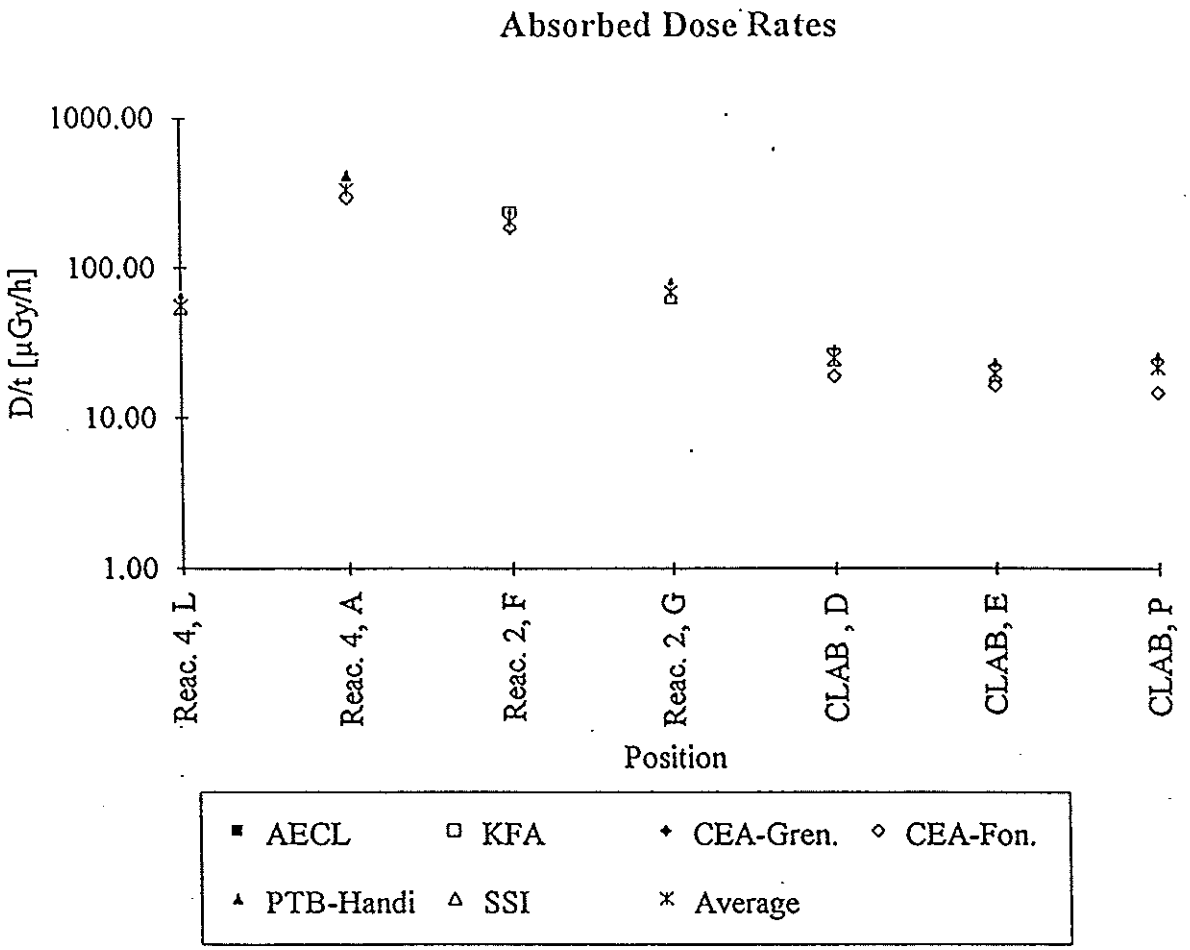
Absorbed Dose Rates
1000.00
100.00
10.00
1.00
D/t [µGy/h]
Reac. 4, L
Reac. 4, A
Reac. 2, F
Reac. 2, G
CLAB , D
CLAB, E
CLAB, P
Position
AECL
KFA
CEA-Gren.
CEA-Fon.
PTB-Handi
SSI
Average

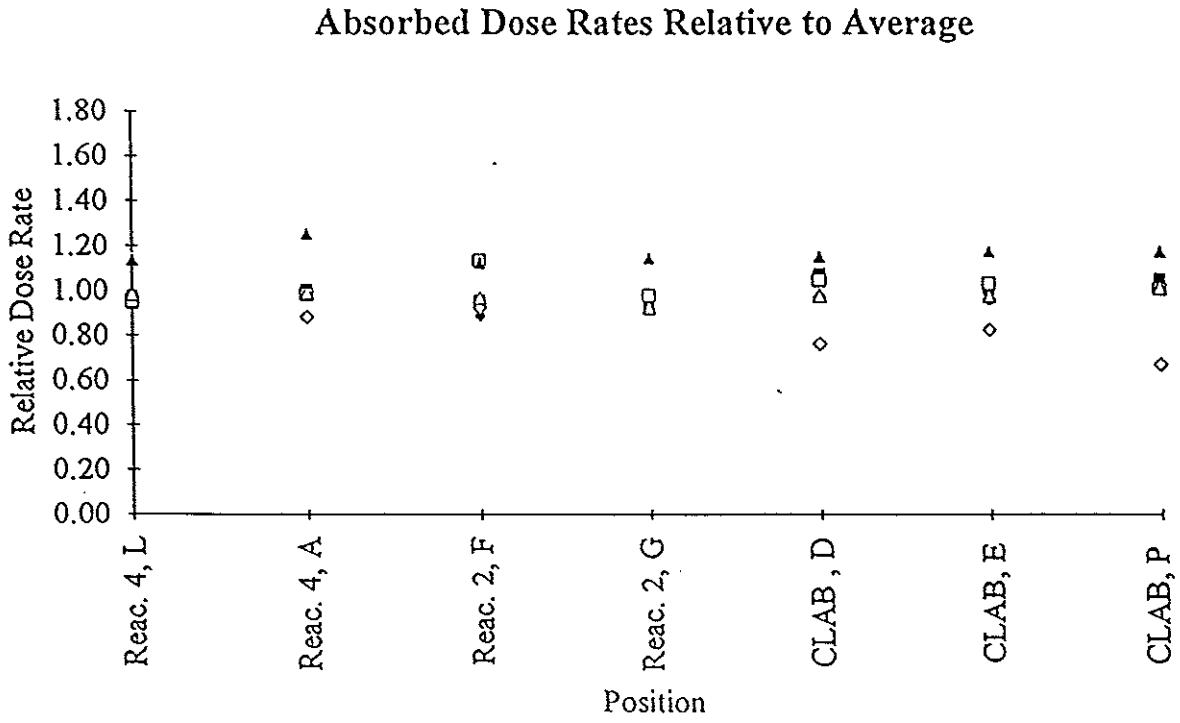
Absorbed Dose Rates Relative to Average
1.80
1.60
1.40
1.20
1.00
0.80
0.60
0.40
0.20
0.00
Relative Dose Rate
Reac. 4, L
Reac. 4, A
Reac. 2, F
Reac. 2, G
CLAB , D
CLAB, E
CLAB, P
Position

Figure 4.1

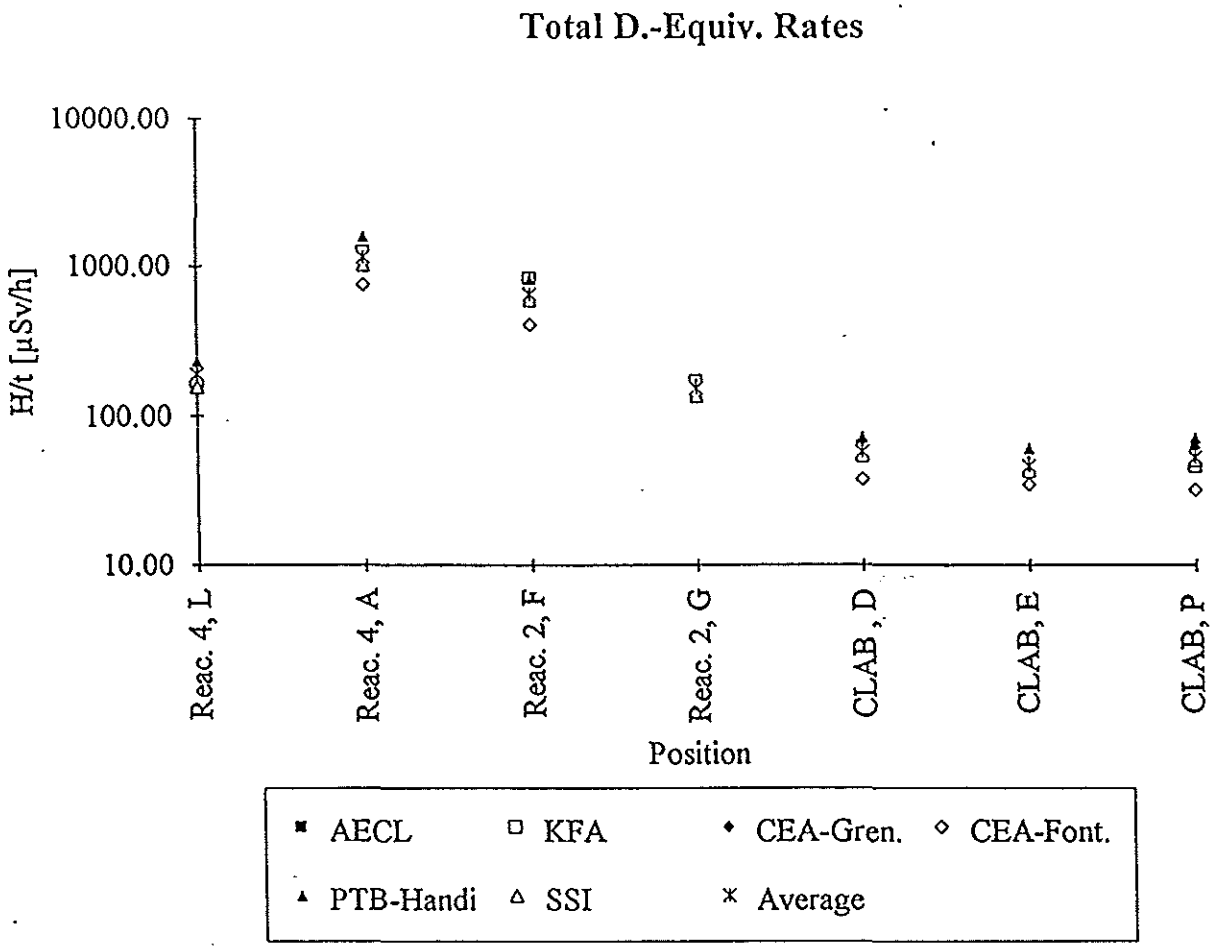
Total D.-Equiv. Rates
10000.00
1000.00
100.00
10.00
H/t [µSv/h]
Reac. 4, L
Reac. 4, A
Reac. 2, F
Reac. 2, G
CLAB , D
CLAB, E
CLAB, P
Position
AECL
KFA
CEA-Gren.
CEA-Font.
PTB-Handi
SSI
Average

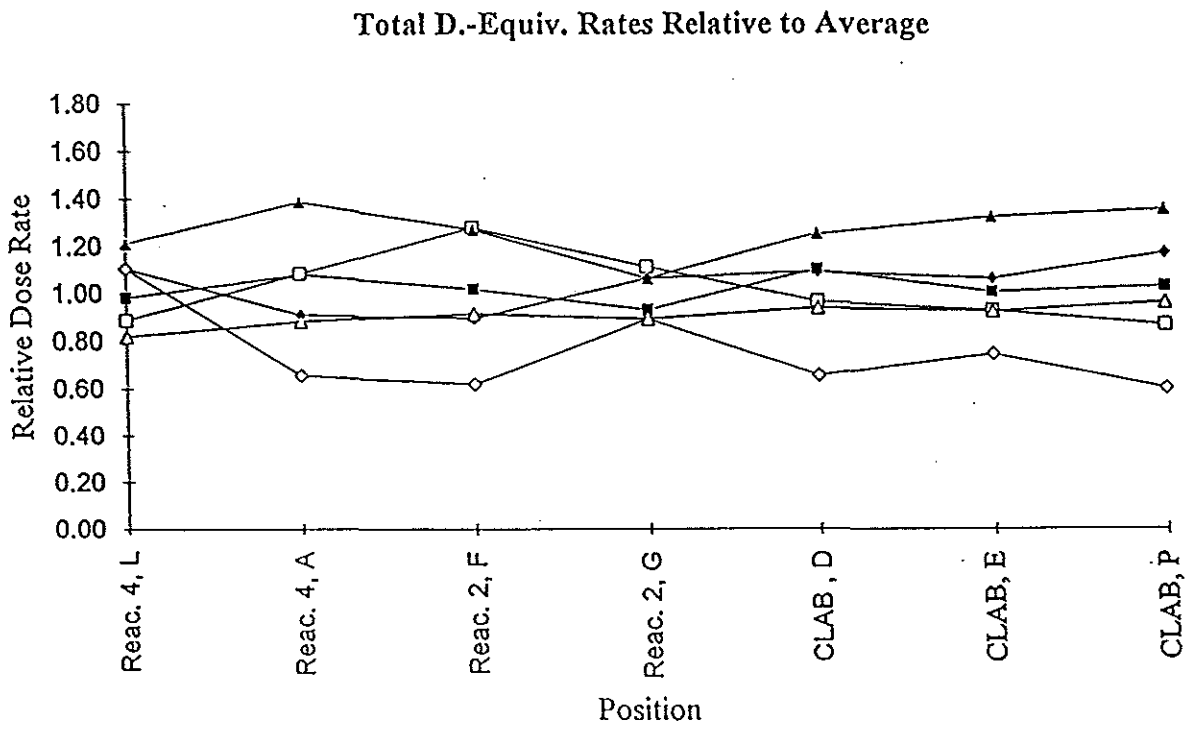
Total D.-Equiv. Rates Relative to Average
1.80
1.60
1.40
1.20
1.00
0.80
0.60
0.40
0.20
0.00
Relative Dose Rate
Reac. 4, L
Reac. 4, A
Reac. 2, F
Reac. 2, G
CLAB , D
CLAB, E
CLAB, P
Position

Figure 4.2

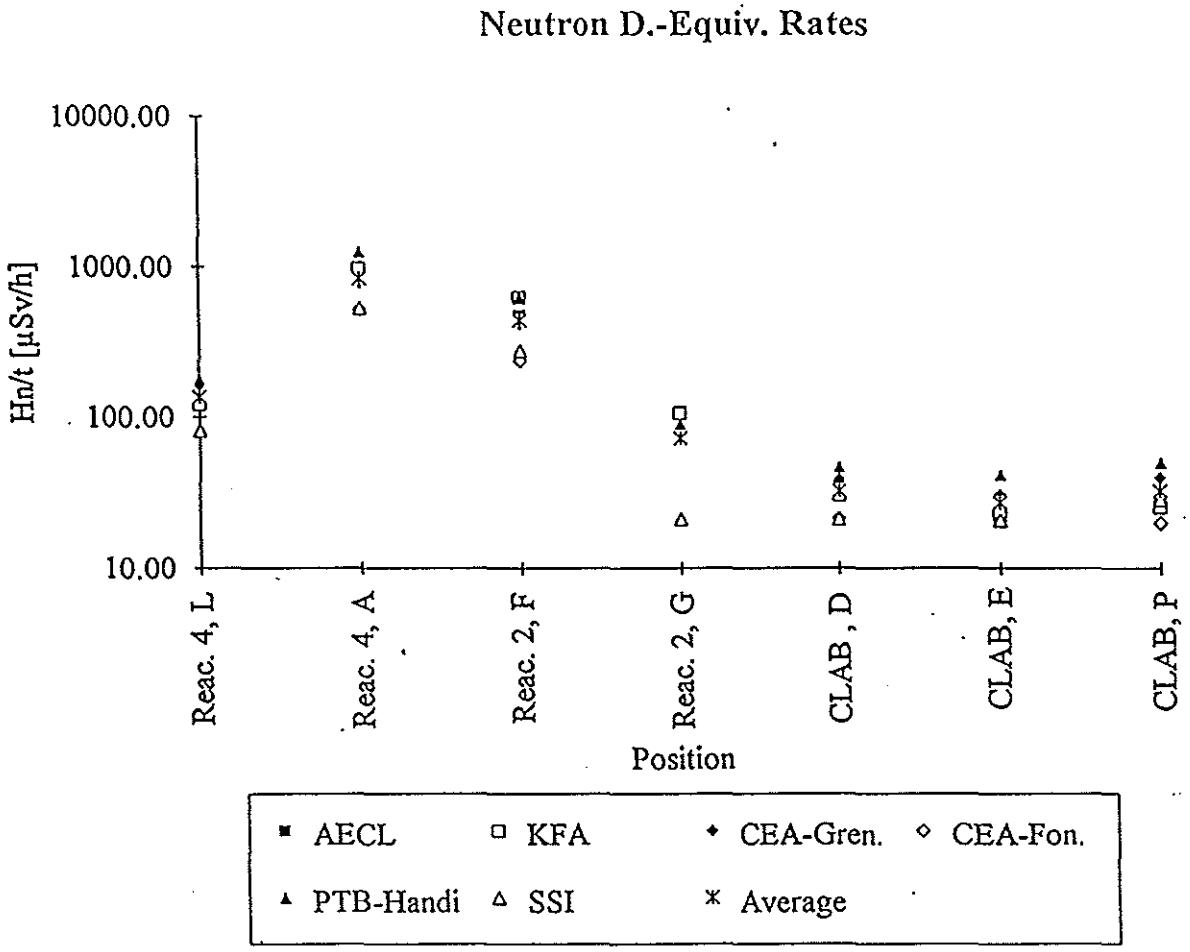
Neutron D.-Equiv. Rates
10000.00
1000.00
100.00
10.00
Hn/t [µSv/h]
Reac. 4, L
Reac. 4, A
Reac. 2, F
Reac. 2, G
CLAB , D
CLAB, E
CLAB, P
Position
AECL
KFA
CEA-Gren.
CEA-Fon.
PTB-Handi
SSI
Average

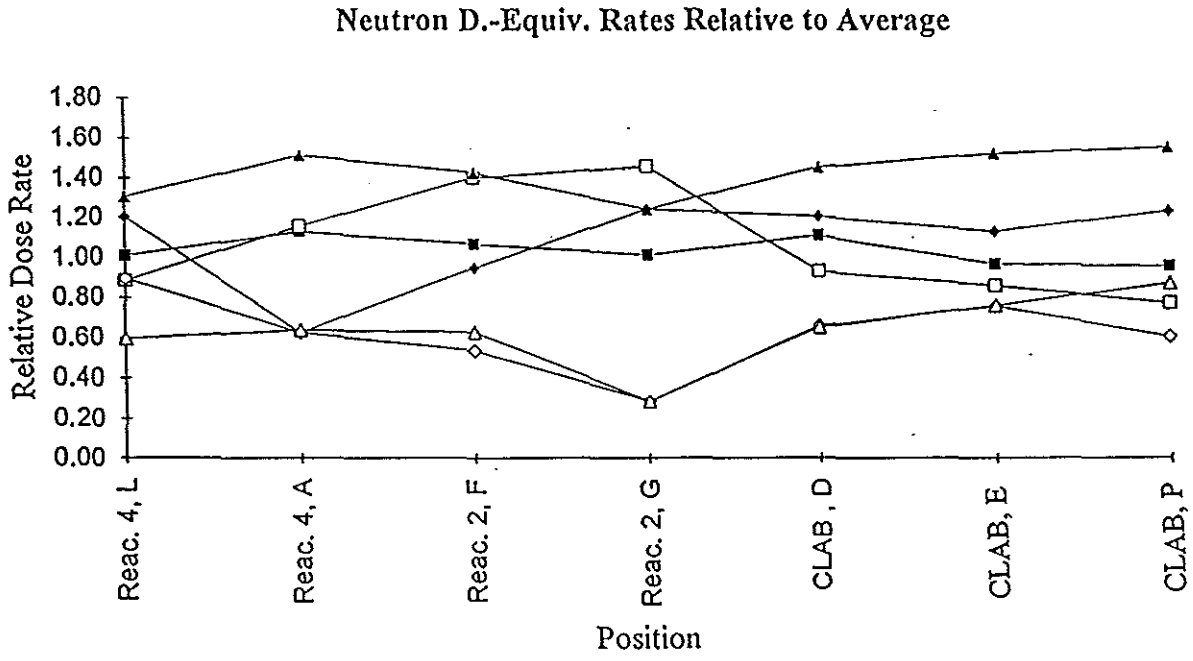
Neutron D.-Equiv. Rates Relative to Average
1.80
1.60
1.40
1.20
1.00
0.80
0.60
0.40
0.20
0.00
Relative Dose Rate
Reac. 4, L
Reac. 4, A
Reac. 2, F
Reac. 2, G
CLAB , D
CLAB, E
CLAB, P
Position

Figure 4.3

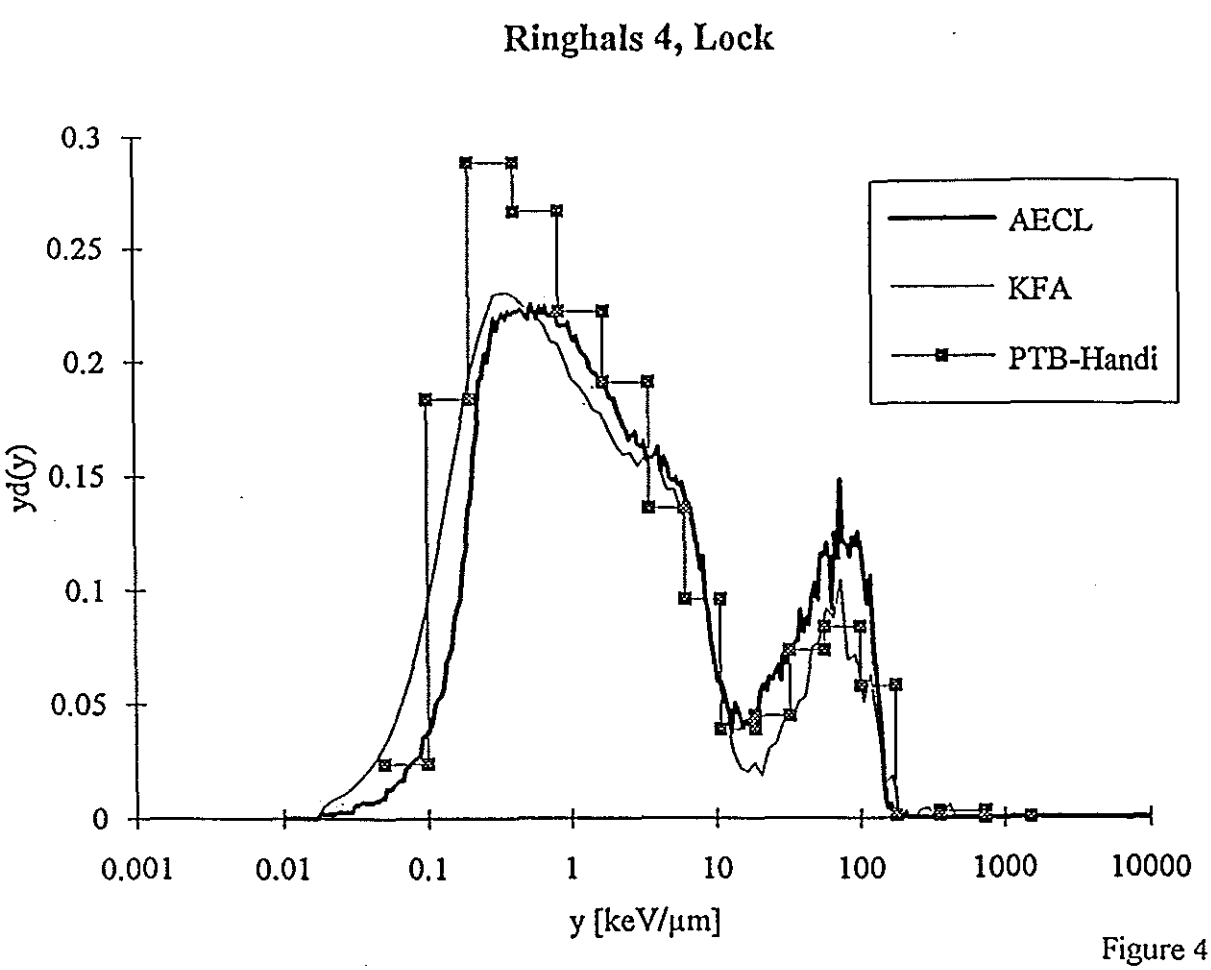

Figure 4.4a

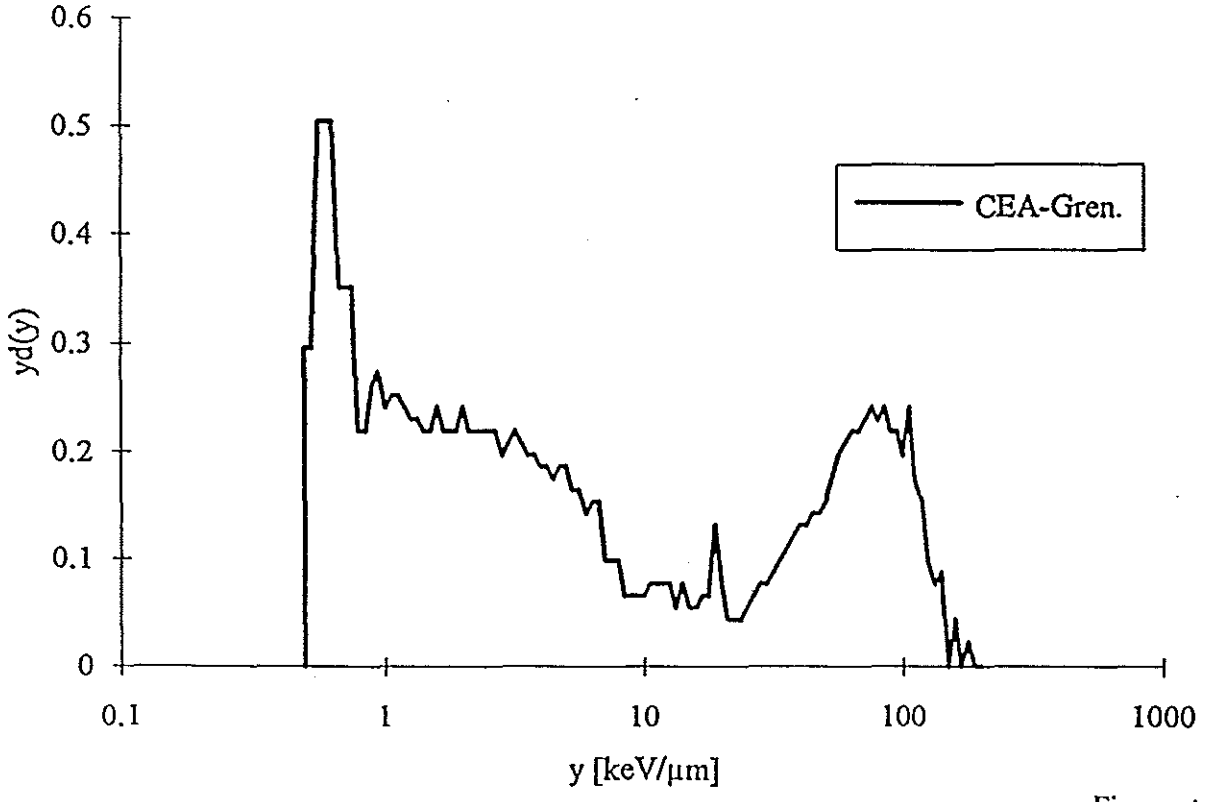

Figure 4.4b

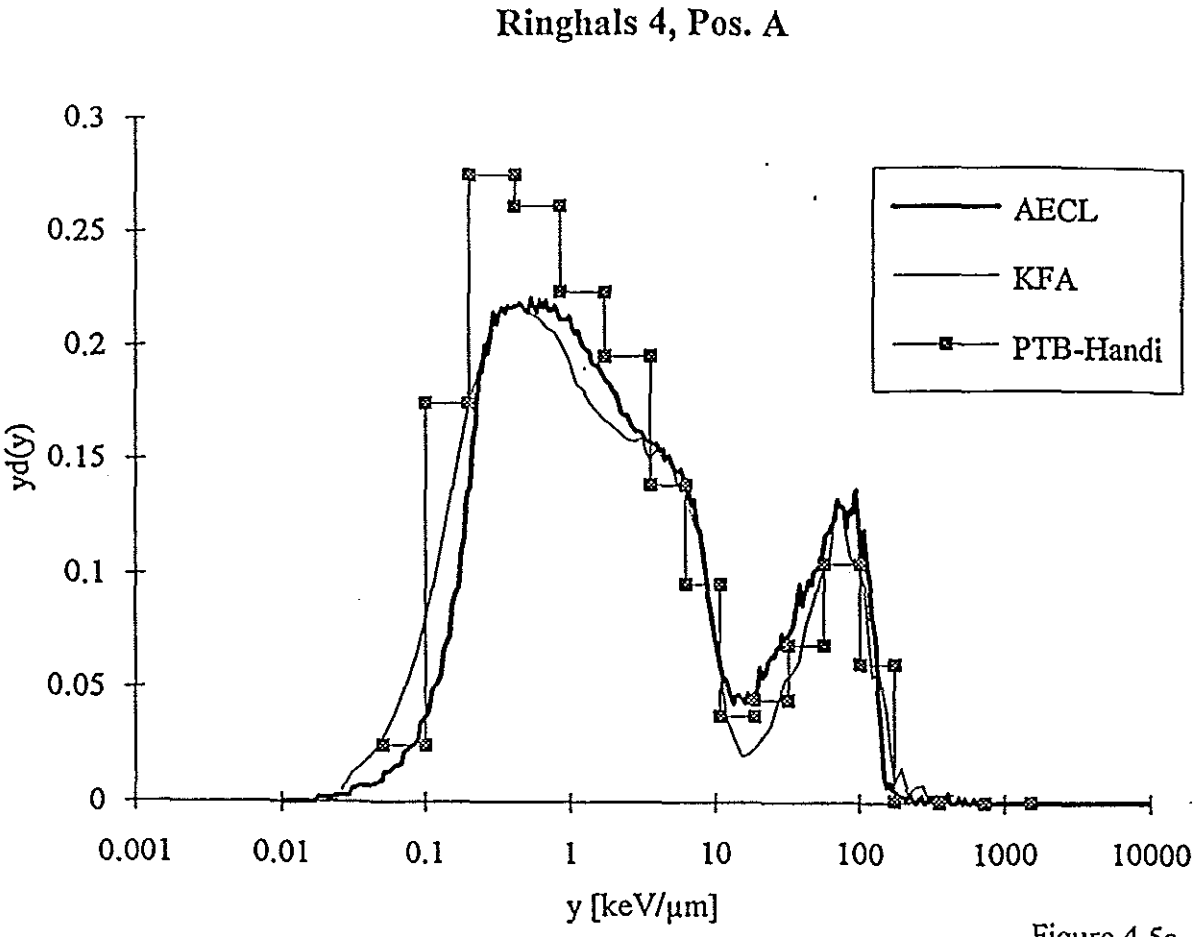

Figure 4.5a

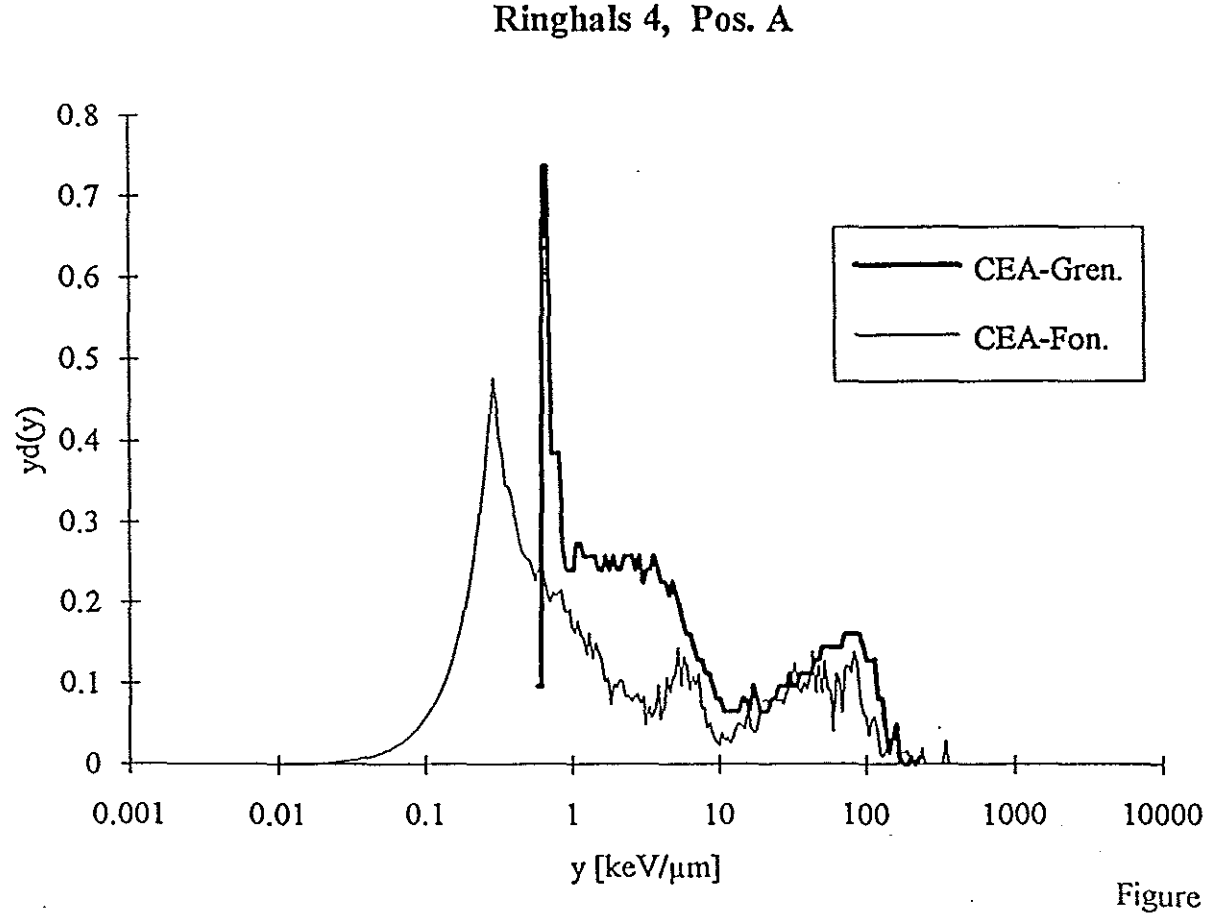

Figure 4.5b

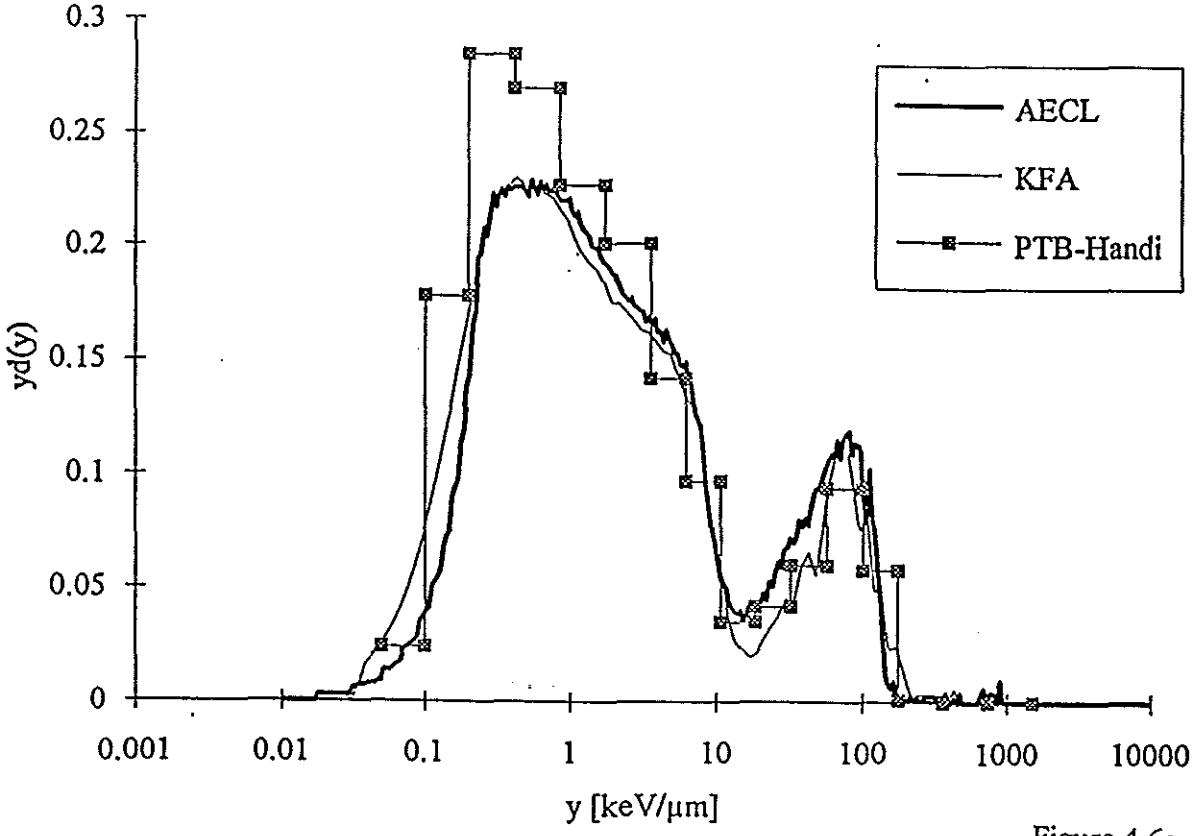

Figure 4.6a

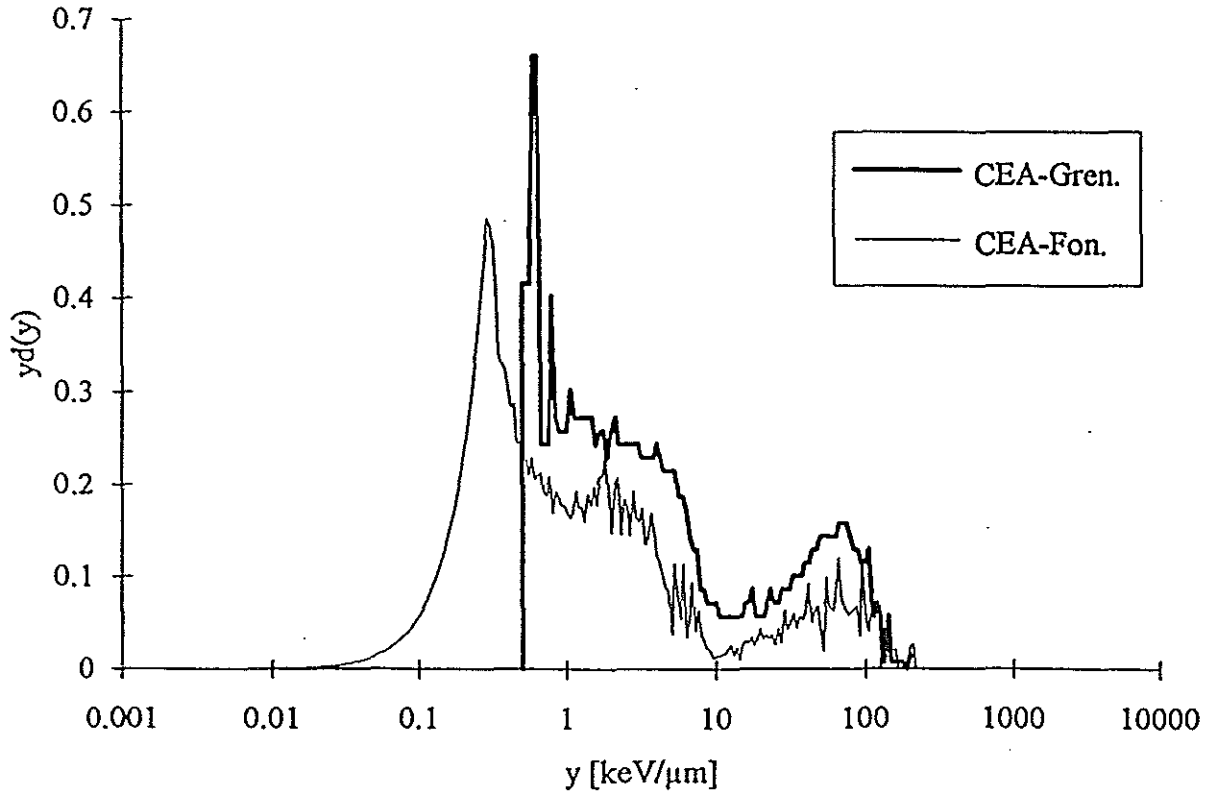

Figure 4.6b

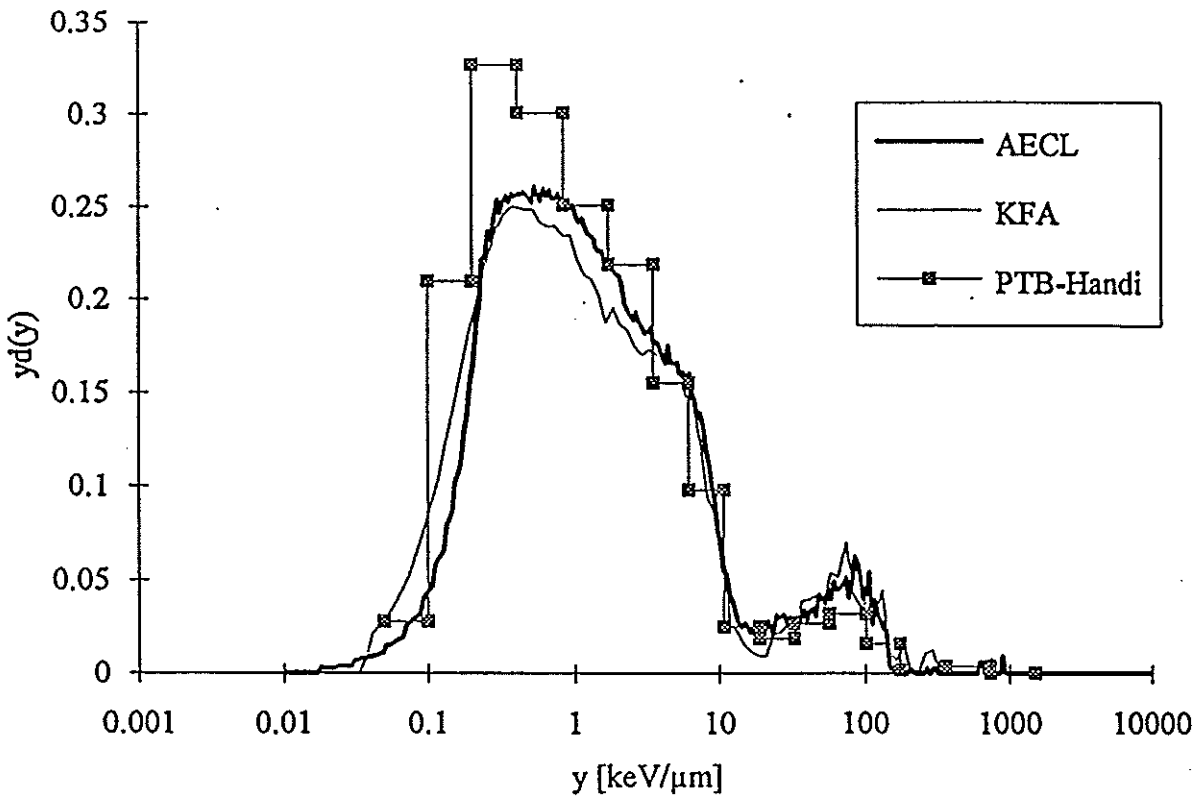
Ringhals 2, Pos. G
0.35
0.3
0.25
0.2
0.15
0.1
0.05
0
yd(y)
0.001
0.01
0.1
1
10
100
1000
10000
y [keV/µm]
AECL
KFA
PTB-Handi

Figure 4.7

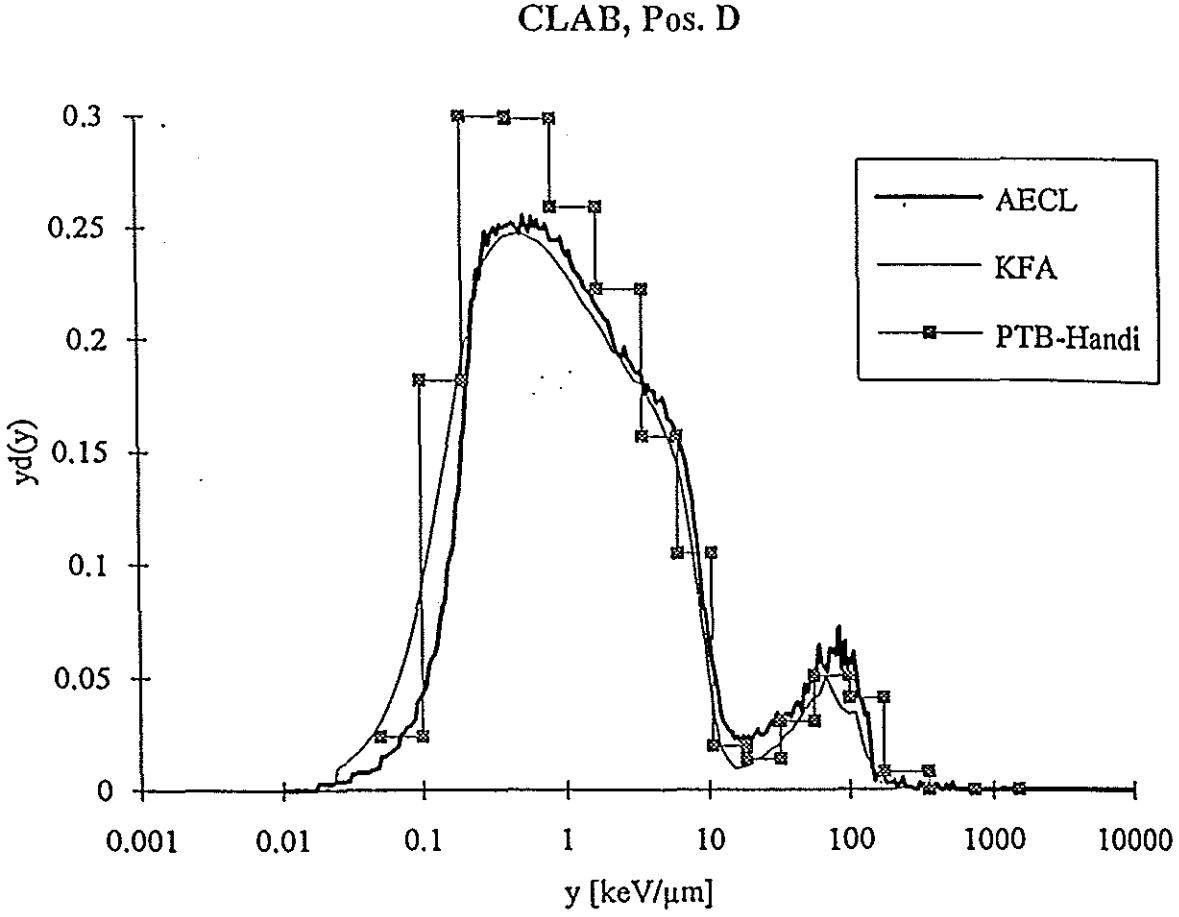

Figure 4.8a

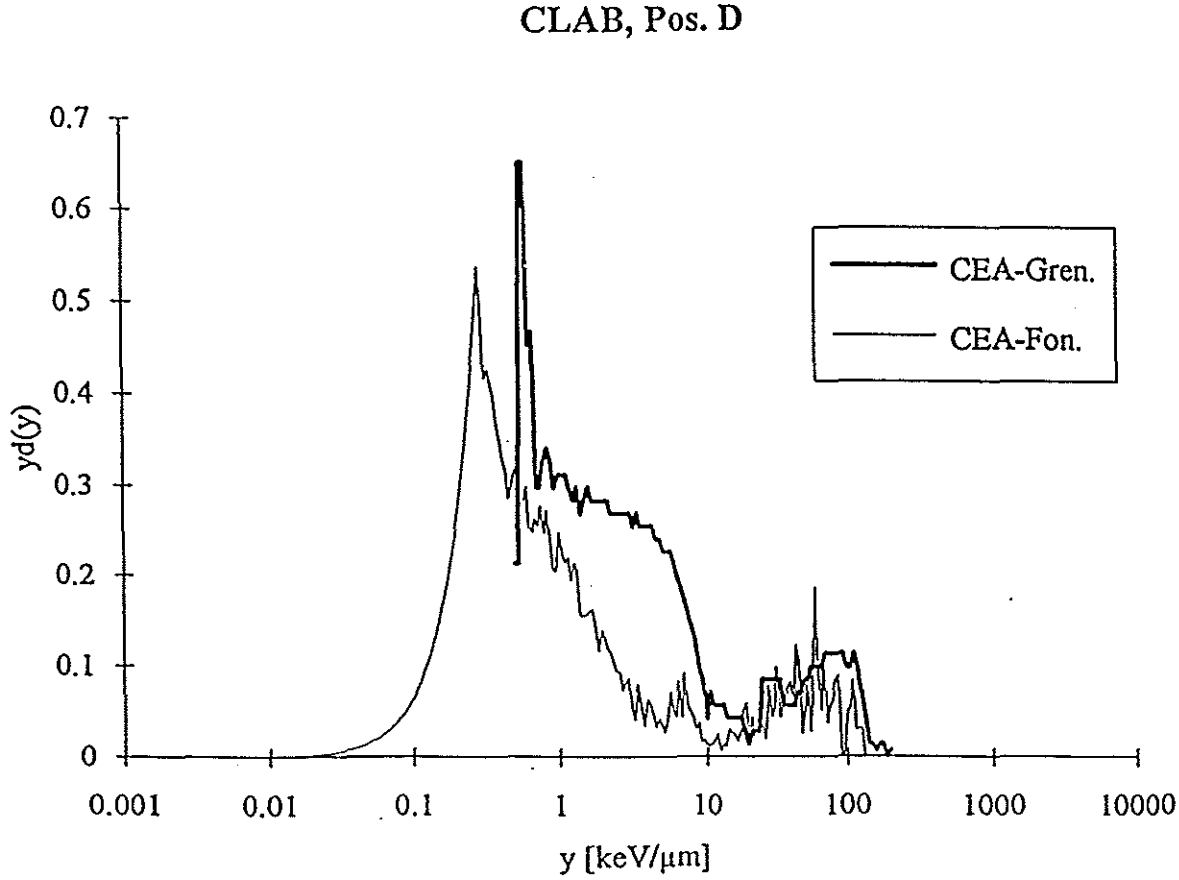

Figure 4.8b

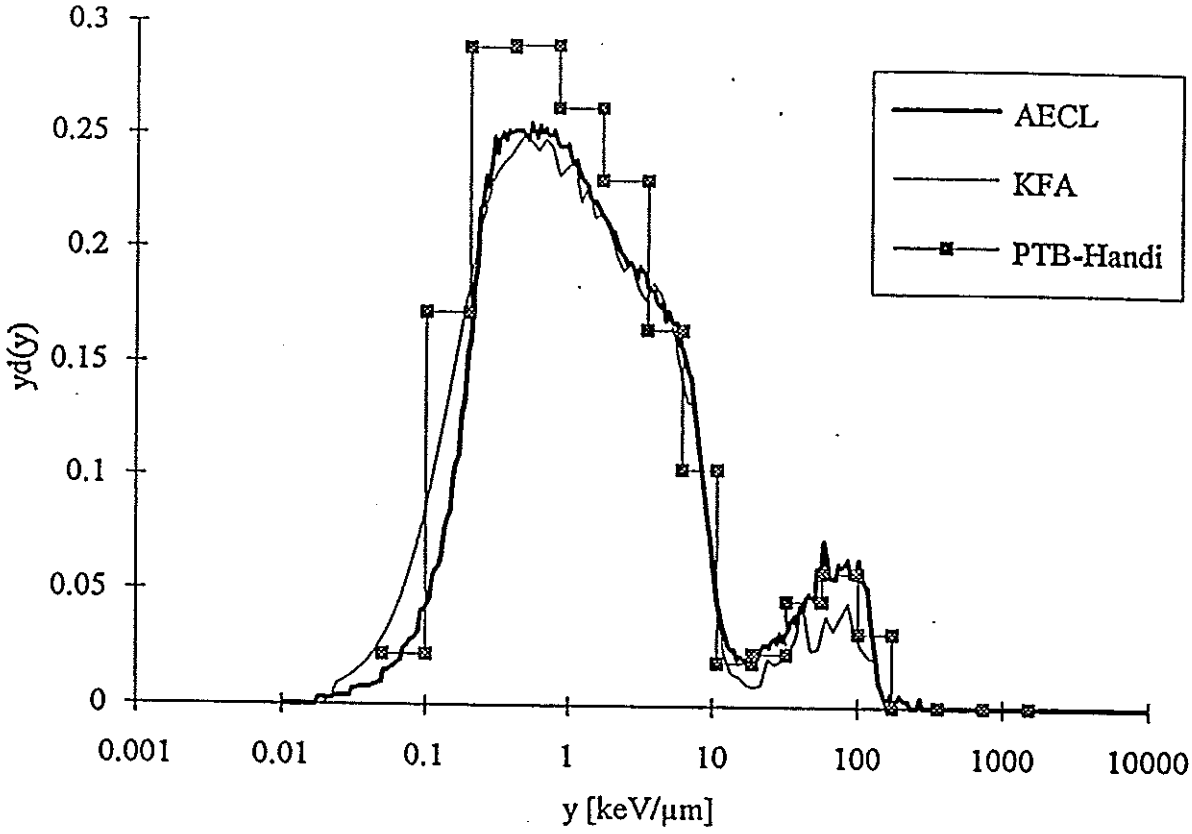

Figure 4.9a

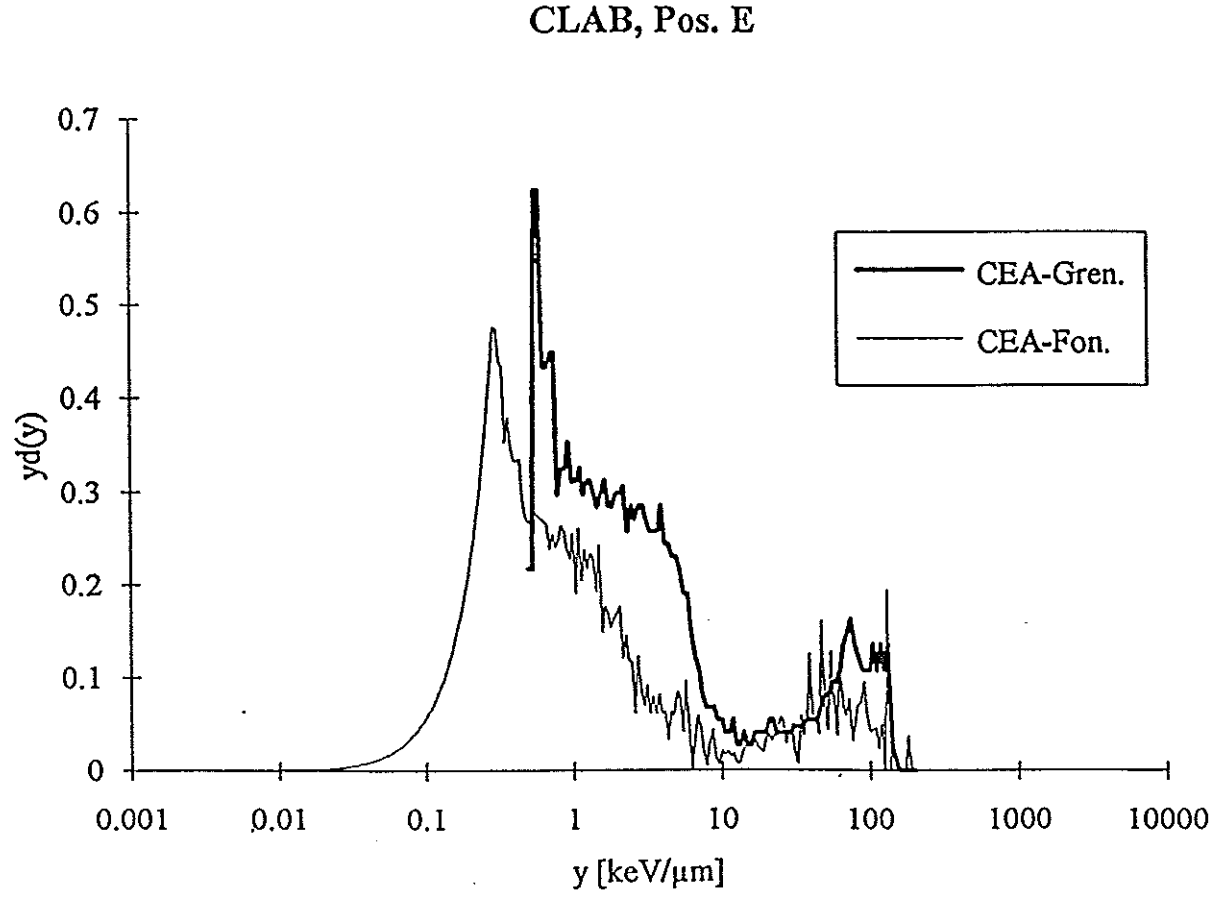

Figure 4.9b

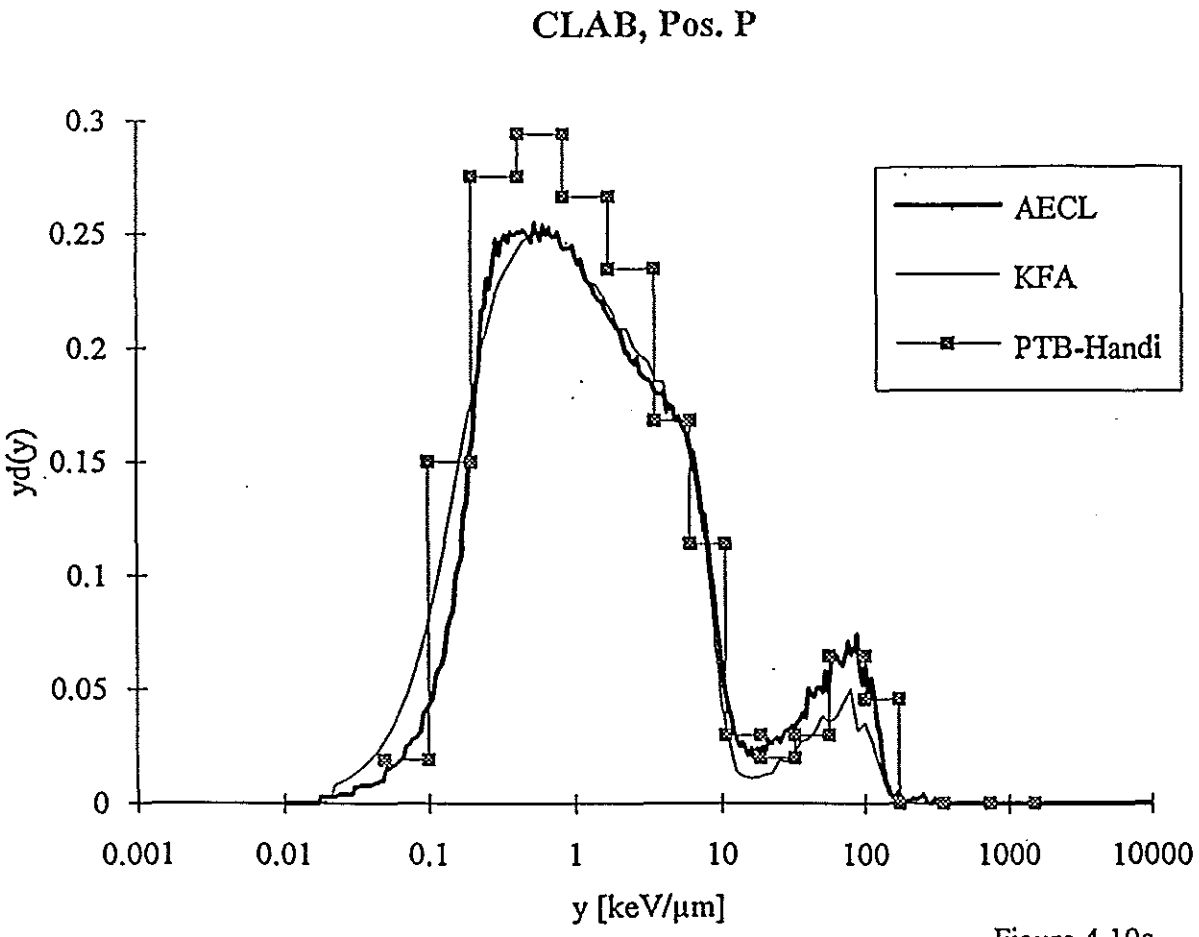

Figure 4.10a

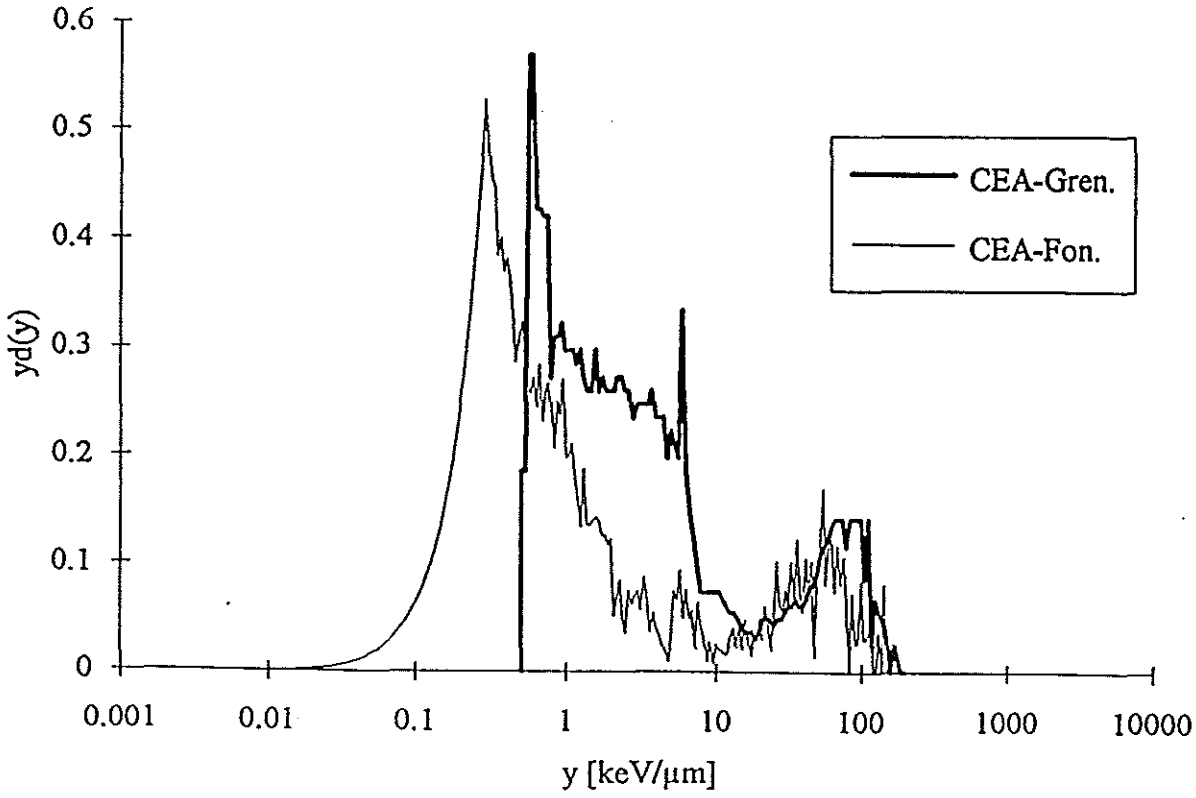

Figure 4.10b

5. MEASUREMENTS WITH PERSONAL DOSEMETERS

P. Drake
Vattenfall AB, Ringhals, S-430 22 Väröbacka, Sweden
D.T. Bartlett
National Radiological Protection Board, (NRPB), Chilton, U.K.

Three different phantoms were used for the irradiations of dosemeters at Ringhals and CLAB.

1. A 30 cm diameter polyethylene sphere from PTB was used for a few of the irradiations of dosemeters on phantom. This phantom is similar to a 12" Bonner sphere. One dosemeter was placed in the centre of the sphere, four dosemeters were placed at 90° intervals on the equator of the sphere, one dosemeter was placed on top of the sphere and one dosemeter was placed under the sphere. The sphere was mainly used for irradiation of PTB dosemeters. These irradiations provided information concerning H'(10) and/or $H_p(10)$ at different angles.
2. A 15 cm x 30 cm x 30 cm PMMA slab phantom from Ringhals was used for irradiations of several dosemeter types on phantom. This type of phantom is recommended by ICRU in publication 47 for calibration of dosemeters in photon fields. [1]. The Ringhals PMMA phantom is described by Drake. [2].
3. A new phantom was constructed for this project. The phantom was made from a mixture of paraffin (70 %) and boron acid (30 %, less than 10 % boron of the total phantom weight). The phantom consists of two halves each 7.5 cm x 15 cm x 19 cm with rounded outer edges and corners. On each face of the combined phantom there are 2 shallow excavations just deep enough to hold the inner parts of a Rados TLD. During the irradiations the dosemeters were covered by 2 mm of plastic. The composition of the phantom, with paraffin to thermalize neutrons and boron to capture neutrons, was chosen to decrease the transmission and back scatter of neutrons through or from the phantom as compared with a PMMA phantom. The phantom has been tested together with a pure paraffin phantom and the PMMA phantom described above for reflectance and transmission of neutrons in the neutron field from a collimated ^{252}Cf source. The test was performed with lithium-borate TLD-pellets as the sensitive element. The test showed that only 4% of the incident neutrons were transmitted through 7.5 cm of boron-paraffin while 15 cm thickness was needed to achieve the same reduction for the paraffin and PMMA phantoms. The test also showed that the reflectance from the boron-paraffin phantom was negligible.

The dosemeters were placed on the different phantoms on top of a 30 cm diameter and 5 mm thick steel plate. The phantoms were secured with a textile fibre stripe to the steel plate before the measurements started at positions inside containment. The steel plate was fixed to a steel stand. The stand was adjusted such that the centre of the phantom was placed 106 cm above the floor. During measurements inside the containment the stand was fastened to a steel line which was secured to steel railings. Special care was taken to ensure the correct height of the phantom and that the centre of the front face of the phantom was placed vertically above the identification mark on the floor for each position before the measurement started.

The measurements with each phantom-dosemeter combination were performed for time periods which allowed reasonable statistical errors.

The measurements at CLAB could be performed without missile protection and the dose equivalent rates were lower than at Ringhals. At CLAB only two PTB and one ENEA

dosemeter types were used. The PTB sphere phantom with dosemeters was placed on a steel stand with an alumimium top plate.

The available time periods were not long enough to allow low statistical errors with each phantom-dosemeter combination.

References

[1] *Measurement of Dose Equivalents from External Photon and Electron Radiations. International Commission on Radiation Units and Measurements.* 1992. ICRU Report 47. ICRU, Bethesda, Maryland, USA.

[2] P Drake, *Conversion Factors for the Calibration of Personal Dosemeters in 4- 7 MeV Photon Fields.* (Internal report). Published in short form 1993 in Radiation Protection Dosimetry 46 (1993), 23 - 29.

5.1 Measurements with PTB Personal Dosemeters

M. Luszik-Bhadra and M. Matzke
Physikalisch-Technische Bundesanstalt (PTB), Bundesallee 100,
D-38116 Braunschweig

5.1.1 Types of dosemeter and dosemeter characteristics

The etched track dosemeter used has been developed at PTB. With this dosemeter it is possible to get rough spectrometric dose information in 3 neutron energy intervals [1]. Within this intercomparison the strong angular dependence of the dosemeter response when fixed on a phantom was also utilised to determine the direction of the incident neutrons. For this purpose 6 track dosemeters were positioned on a 30 cm diameter PE sphere at 0° (towards the direction reactor/fuel container), +90°, -90° (right and left side as seen from the reactor/fuel container), 180° and also at the top and at the bottom of the sphere. In case of the irradiations at Ringhals the bottom dosemeter could not be fixed.

The TLD-albedo dosemeter used for this intercomparison has been developed by Piesch et al. [2] and is used for routine personnel monitoring in Germany. At the Ringhals reactor 6 TLD-albedo dosemeters (Alnor capsules with 0.9 mm thick Harshaw TLD 600 and TLD 700 chips) were fixed in the same way on the PE sphere as the track dosemeters. In order to save time at CLAB 4 TLD-albedo dosemeters were irradiated simultaneously with the track dosemeters and positioned at ±45° and ±135°.

The fluence response characteristics (normal incidence) of 2 components of the neutron dosemeter are shown in Table 5.1.1 [1]. The directional dependence of this dosemeter is shown in Table 5.1.2 ([3] and irradiations with thermal neutrons (bismuth filtered reactor beam) at the PTB). These sets of data have been supplemented using data for a new design of dosemeter and combined to give the 76 fluence response of the dosemeter for rotational (ROT) (planar isotropy) and isotropic (ISO) fields. Table 5.1.3 gives adjustment factors to be applied to the fluence response characteristics in order to obtain the rotational (ROT) and isotropic (ISO) fluence response characteristic.

5.1.2 Measurements and results

Personal dosemeters (etched track and TLD albedo dosemeters) were irradiated at the Ringhals reactor (positions A and F) and at a fuel transport container at CLAB (positions D and P). The dosemeters were irradiated and mounted on a 300 mm diameter PE sphere.

The track dosemeter reading and corresponding dose equivalent rates for the track dosemeter are given in Table 5.1.4. The dosemeters were calibrated in such a way that they indicate approximately H'(10) (Wagner et al. [4]) and normalised to unity for ^{252}Cf. The readings of the dosemeter are given in 2 energy intervals: E_n <70 keV and E_n >70 keV.

The TLD-albedo dosemeter has been designed to conservatively indicate H'(10) in the front half space [4]. Its calibration factor must either be determined in the radiation field of interest or can be taken from generalised calibration curves [5, 6] for various application areas. For the measurements described here the calibration curve for the application area N1 (heavy shielding) was applied for both the Ringhals and the CLAB irradiations. The dosemeter also gives estimates of the photon directional dose equivalent. The dosemeter H'(10) response for photons is normalised to unity for ^{137}Cs. The results are shown in Table 5.1.5.

References

[1] M. Luszik-Bhadra, W.G. Alberts, E. Dietz, S. Guldbakke and H. Kluge, *A Simple Personal Dosemeter for Thermal, Intermediate and Fast Neutrons Based on CR-39 Etched Track Detectors.* Radiat. Prot. Dosim. **44** (1992) 313 - 316.

[2] E. Piesch and B. Burgkhardt, *Albedo Dosimetry System for Routine Personnel Monitoring.* Radiat. Prot. Dosim. **23** (1988) 117 - 120.

[3] data from EURADOS.CENDOS 1992 Joint Irradiations, PTB Report (to be published)

[4] S.R. Wagner, B. Grosswendt, J.R. Harvey, A.J. Mill, H.J. Selbach and B.R.L. Siebert, *Unified Conversion Functions for the New ICRU Operational Radiation Protection Quantities.* Radiat. Prot. Dosim. **12** (1985) 231 - 235.

[5] (B. Burgkhardt and E. Piesch, *Field Calibration Technique for Albedo Neutron Dosemeters.* Radiat. Prot. Dosim. **23** (1988) 121 - 126.

[6] E. Piesch, private communication (1992)

Table 5.1.1: Fluence response of the dosemeter with and without air converter

E_n (eV)	$R_A(10^{-6})$ (E_n <70 keV)	R_A (10^{-6}) (E_n >70 keV)
Thermal	4.44	0
2 E3	3.36	0
2.5 E3	3.30	0
3 E3	3.19	0
4 E3	3.15	0
5 E3	2.96	0
6 E3	2.94	0
8 E3	2.85	0
1 E4	2.78	0
1.2 E4	2.81	0
1.5 E4	2.87	0
2.0 E4	2.94	0
2.5 E4	2.99	0
3 E4	3.11	0
4 E4	3.08	0
5 E4	2.87	0.37
6 E4	2.80	1.11
8 E4	0	4.18
1 E5	0	10.5
1.2 E5	0	20.2
1.5 E5	0	42.8
2.0 E5	0	68.6
2.5 E5	0	83.7
3 E5	0	91.9
4 E5	0	97.2
5 E5	0	104.8
6 E5	0	108.9
8 E5	0	122.2
1 E6	0	134.6
1.2 E6	0	144.9
1.5 E6	0	159.8
2.0 E6	0	173.8
2.5 E6	0	177.0
3 E6	0	170.4
4 E6	0	143.5
5 E6	0	132.8
6 E6	0	125.7
8 E6	0	120.1
1 E7	0	121.7
1.2 E7	0	127.3
1.5 E7	0	142.1

(The fluence responses of the dosemeter with air and without air have been subtracted to get the response of E_n < 70 keV, within the uncertainties of the measured values and the subtraction procedure the values for $E_n \geq 8$ E 4 eV were set to zero).

Table 5.1.2: Angle response of the dosemeter with air converter (measured on a PMMA slab phantom for fast neutrons and on a 30 cm dia PE sphere for thermal)

	θ (°)	R(θ)/R(0°)
Thermal	0	1.0
	30	0.78
	60	0.59
	90	0.79
	120	0.03
	150	0.04
	180	0.01
0.144 E6	0	1.0
	30	0.69
	60	0.19
0.565 E6	0	1.0
	30	0.67
	60	0.32
	85	0.14
1.2 E6	0	1.0
	30	0.73
	60	0.42
	85	0.17
Cf-252	0	1.0
	30	0.77
	60	0.39
	85	0.19
5.3 E6	0	1.0
	30	0.86
	60	0.38
	85	0.24
15.1 E6	0	1.0
	30	0.95
	60	0.54
	85	0.42

Table 5.1.3: Adjustment factors to obtain rotational (ROT) and isotropic (ISO) fluence response characteristics

	ROT	ISO
Thermal	0.46	0.46
0.1	0.40	0.40
1	0.40	0.37
1 E1	0.40	0.35
1 E2	0.40	0.33
1 E3	0.40	0.33
2 E3	0.40	0.33
1 E4	0.35	0.25
1 E5	0.32	0.18
1.44 E5	0.31	0.20
5.65 E5	0.32	0.23
1.2 E6	0.34	0.27
2 E6	0.35	0.28
5 E6	0.38	0.31
1.5 E7	0.51	0.47
2 E7	0.58	0.56

Table 5.1.4: Track dosemeter measurement results

Position	Irrad. time (h)	Dosemeter readings (tracks/cm^2)		Directional dose equiv. rate (µSv/h)	
		En<70 keV	En>70 keV	En<70 keV[1]	En>70 keV[2]
A, 0°	1.42	119 ± 30	148 ± 17	229 ± 58	298 ± 34
A, 180°	1.42	97 ± 26	25 ± 12	187 ± 50	50 ± 24
A, +90°	1.42	83 ± 26	45 ± 13	160 ± 50	90 ± 26
A, -90°	1.42	112 ± 27	37 ± 13	216 ± 52	74 ± 26
A, top	1.42	103 ± 29	113 ± 15	199 ± 56	227 ± 30
F, 0°	1.03	0	149 ± 17	0	410 ± 47
F, 180°	1.03	37 ± 24	2 ± 11	98 ± 63	6 ± 30
F, +90°	1.03	23 ± 24	36 ± 13	61 ± 63	99 ± 36
F, -90°	1.03	3 ± 24	40 ± 13	8 ± 63	110 ± 36
F, top	1.03	47 ± 24	16 ± 12	124 ± 63	44 ± 33
D, 0°	15.92	22 ± 28	102 ± 16	4 ± 5	18 ± 3
D, 180°	15.92	44 ± 23	0	8 ± 4	0
D, +90°	15.92	17 ± 24	22 ± 12	3 ± 4	4 ± 2
D, -90°	15.92	25 ± 25	34 ± 13	4 ± 4	6 ± 2
D, top	15.92	0	39 ± 13	0	7 ± 2
D, bottom	15.92	0	34 ± 12	0	6 ± 2
P, 0°	13.78	96 ± 29	88 ± 15	19 ± 6	18 ± 3
P, 180°	13.78	0	3 ± 11	0	1 ± 2
P, +90°	13.78	0	9 ± 11	0	6 ± 2
P,-90°	13.78	15 ± 23	10 ± 12	3 ± 5	2 ± 2
P, top	13.78	7 ± 23	6 ± 11	1 ± 5	1 ± 2
P, bottom	13.78	13 ± 23	0	3 ± 5	0

1 Calibrated with normal incident thermal neutrons, calibration factor $1/R_{Th} = 1/(366\ cm^{-2}\ mSv^{-1})$

2 Calibrated with normal incident neutrons of a ^{252}Cf source, calibration factor $1/R_{Cf}=1/(351\ cm^{-2}\ mSv_{-1})$

Table 5.1.5: Albedo dosemeter measurement results

Position	Irrad. time (h)	Dosemeter readings (mSv)			Directional dose equiv. rate (μSv/h)	
		M(i)	M(a)	Mph	neutrons[1]	photons[2]
A, 0°	1.62	6.83 ± 0.20	16.72 ± 0.51	0.55 ± 0.02	852±25	343 ± 13
A, 180°	1.62	5.12 ± 0.16	13.23 ± 0.45	0.42 ± 0.02	639±20	262 ± 13
A, +90°	1.62	4.38 ± 0.15	12.67 ± 0.45	0.46 ± 0.02	547±19	287 ± 13
A, -90°	1.62	4.58 ± 0.15	14.34 ± 0.47	0.49 ± 0.02	572±19	306 ± 13
A, top	1.62	5.95 ± 0.17	14.61 ± 0.47	0.51 ± 0.02	743±21	318 ± 13
F, 0°	1.08	2.92 ± 0.14	7.17 ± 0.39	0.27 ± 0.01	541±26	250 ± 9
F, 180°	1.08	1.06 ± 0.12	3.33 ± 0.36	0.14 ± 0.01	196±22	130 ± 9
F, +90°	1.08	1.89 ± 0.13	4.74 ± 0.37	0.23 ± 0.01	350±24	213 ± 9
F, -90°	1.08	1.15 ± 0.13	3.16 ± 0.36	0.17 ± 0.01	213±24	157 ± 9
F, top	1.08	1.55 ± 0.13	4.56 ± 0.37	0.20 ± 0.01	287±24	185 ± 9
D, +45°	15.92	1.72 ± 0.13	2.58 ± 0.36	0.41 ± 0.01	35±3	26 ± 1
D, -45°	15.92	1.81 ± 0.13	2.84 ± 0.36	0.42 ± 0.01	36±3	26 ± 1
D, +135°	15.92	0.37 ± 0.12	0.54 ± 0.35	0.17 ± 0.01	7±2	11 ± 1
D, -135°	15.92	0.55 ± 0.12	0.78 ± 0.35	0.21 ± 0.01	11±2	13 ± 1
P, +45°	13.78	1.16 ± 0.13	1.16 ± 0.35	0.25 ± 0.01	34±4	18 ± 1
P, -45°	13.78	1.28 ± 0.13	1.68 ± 0.35	0.30 ± 0.01	37±4	22 ± 1
P, +135°	13.78	0.13 ± 0.12	0.18 ± 0.35	0.07 ± 0.01	4±3	5 ± 1
P, -135°	13.78	0.42 ± 0.12	0.52 ± 0.35	0.14 ± 0.01	12±3	10 ± 1

1 Calibrated as proposed by Piesch using a generalised calibration curve for the application area N1 (heavy shielding)

2 Calibrated with a ^{137}Cs source

5.2 Measurements with NRPB Personal Dosemeters

D.T. Bartlett, R.J. Tanner and J.D. Steele
National Radiological Protection Board, (NPL), Chilton, U.K.

5.2.1 Types of dosemeter and dosemeter characteristics

The NRPB PADC neutron personal dosemeter was used to measure the neutron fields. The dosemeter is sensitive to thermal, epithermal and fast neutrons [1]. The fluence response data as a function of energy for normal incidence, as a function of angle, and for rotational (ROT) and isotropic (ISO) fields are shown in Table 5.2.1 and 5.2.2. These data were obtained for dosemeter mounted on a 300 x 300 x 150 mm PMMA slab phantom [2].

The photon dosemeter used was the NRPB/Siemens electronic personal dosemeter. The radiation detectors in this dosemeter are silicon photodiodes. The $H_p(10)$ response characteristic normalised to ^{137}Cs lies within the range ±20% for photon energies between 20 keV and 1.25 MeV and angles of incidence up to 60° (see Figure 5.2.1). The relative response at 6 to 7 MeV is 1.30 [3].

5.2.2 Measurements and results

Track dosemeters were irradiated at Ringhals reactor locations 'L', 'A', 'C' and 'F' and EPDs at 'A' and 'F'. The dosemeters were affixed to the sides of a 300 x 300 x 150 mm PMMA slab phantom. Track dosemeters were attached to all of the phantom sides in order to obtain data on the directional characteristics of the radiation field. EPDs were only fixed to the 'front' surface. The results of neutron and photon dosemeters are shown in Table 5.2.3. The neutron dose values are normalised to $H_p(10)$ ^{252}Cf normal incidence and the photon values to $H_p(10)$ ^{137}Cs normal incidence.

5.2.3 References

[1] D.T. Bartlett, J.D. Steele and D.R. Stubberfield, *Development of a Single Element Neutron Personal Dosemeter for Thermal, Epithermal and Fast Neutrons.* Nucl. Tracks. 12 (1986) 645 - 648.

[2] R.J. Tanner, D.T. Bartlett and D.J. Turner, *Performance of the NRPB PADC Neutron Personal Dosemeter in the 1992 EURADOS/CENDOS Joint Irradiations.* To be published as a PTB/GSF report).

[3] Further details are given in NRPB Technical Memorandum *EPD Response as a Function of Photon Energy and Angle of Incidence $H_p(10)$ and $H_p(0.07)$.* W.J. Iles, D.R. McClure and P. Watson (1993) and *EPD Response as a Function of Photon Energy and Angle of Incidence $H_p(10)$ and $H_p(0.07)$, 4.44 MeV and 6 to 7 MeV.* W.J. Iles and D.R. McClure (1993)).

Table 5.2.1: Neutron dosemeter fluence response characteristics

E_n (eV)	R_Φ (10^{-6})			
	0°	30°	60°	85°
Thermal	2.35	2.04	1.18	0.20
1 E-1	2	-	-	-
1 E1	0.60	-	-	-
1 E3	0.20	-	-	-
1 E4	0.20	-	-	-
1.44 E5	8.98	6.62	1.05	0.05
5.65 E5	60.7	39.6	12.8	4.2
1.2 E6	51.8	43.2	18.8	6.4
2 E6 (^{252}Cf)	43.8	36.2	19.4	8.4
5.3 E6	29.2	21.7	16.4	9.9
1.51 E7	41.0	39.6	26.4	21.5
4.4 E7	33.1	-	-	-
6.6 E7	25.0	-	-	-

Table 5.2.2: Neutron dosemeter fluence response characteristics rotational and isotropic fields

E_n (eV)	R_Φ (10^{-6})	
	ROT	ISO
Thermal	0.75	0.60
1 E-1	0.64	0.50
1 E1	0.19	0.15
1 E3	0.064	0.05
1 E4	0.064	0.05
1.44 E5	2.09	1.20
5.65 E5	14.7	9.28
1.2 E6	15.0	11.3
5.3 E6	9.65	8.21
1.51 E7	16.1	15.6
4.4 E7	16.6	14.0
6.6 E7	12.5	12.0

Table 5.2.3: Summary results table

Location	Irradiation	Date/Time	Dosemeter Position	Neutron Dose/ Dose Rate		Photon Dose/ Dose Rate	
				(μSv)	(μSv h^{-1})	(μSv)	(μSv h^{-1})
L (Reactor 4)	16/17 Nov	2010 to 0819	Front	700	58(8)*	690	57
			Back	65	5.3(0.4)	370	30
			Right	200	17(3)		
			Left	360	30(3)		
			Top	490	40(5)		
			Bottom	220	18(3)		
A (Reactor 4)	18 Nov	1215 to 1403	Front	700	390(14)	605	340
			Back	230	130(7)	490	270
			Right	280	160(21)		
			Left	350	200(6)		
			Top	560	310(18)		
			Bottom	Dosemeters dislodged during irradiation			
C (Reactor 4)	18 Nov	1417 to 1812	Front	1400	360(28)		
			Back	190	47(10)		
			Right	390	84†(18)		
			Left	320	82(12)		
			Top	490	120(23)		
			Bottom	380	97(11)		
F (Reactor 2)	19 Nov	0840 to 0941	Front	480	370†(30)		
			Back	63	62(26)		
			Right	65	64(5)		
			Left	150	140(40)		
			Top	120	120(21)		
			Bottom	220	210(51)		

*S.E.M
†non-uniform detector omitted from calculation

5.3 Measurements with Ringhals Personal Dosemeters

P. Drake
Vattenfall AB, Ringhals, S-430 22 Väröbacka, Sweden

5.3.1. Types of dosemeters and dosemeter characteristics

1. TLD

The dosemeters used at Ringhals are TLDs from Rados, Turku, Finland. The TL-dosemeter utilizes $^{7}LiF/Li_2B_4O_7$ combinations. The dosemeters are used with a plastic cover of 500 mg/cm^2 (called "TLD, LiF/LiB" below). [1]. The dosemeters can also be used with a boron plastic cover of equivalent thickness (called "TLD, Albedo" below). The boron plastic cover is of the type described by Piesch [2].

The response of the dosemeters to neutrons is normalized to the readings of a Studsvik 2202D remcounter in different locations in Ringhals 2, 3 and 4, this implies that the dosemeter readings are close to measurements of H*(10). It also implies that the position for an irradiation must be known in order to calculate personnel dose equivalents. In this project an overresponse factor of 10 per mSv for neutron irradiation as compared to photon irradiation was used for the lithium-borate pellets att the three positions A, F, and L at Ringhals and a factor 14 at position G respectively. This overresponse factor corresponds to previously measured overresponses in general areas inside the containments and to positions in shielded areas inside the Ringhals 2 containment respectively.

The dosemeter $H_p(10)$ response to photons is normalized to unity for ^{137}Cs. The energy and angular responses to photons were measured by Drake and Lund respectively. [1],[3]. The statistical uncertainty of repeated measurements is 4% at deselevels of about 2 mSv.

2. Bubble detector

Neutrometer, Bubble detector, from Apfel, USA. [4]. The dosemeter was used according to the manual. The response of the Neutrometers were characterized by the manufacturer and checked in the Oak Ridge National Laboratories Personnel Dosimetry Intercomparison Study 1992. [5],[6]. The Neutrometers are calibrated with an Am-Be source.

3. Electronic dosemeter

Rados electronic dosemeter RAD 80/100 with GM-detector from Rados, Finland. [7]. The dosemeter $H_p(10)$ response is normalized to unity for ^{137}Cs. The energy and angular responses were measured by Anttila and Thomson respectively [7],[8]. The response in high energy photon fields of GM-detectors of the same type as those in the RAD 80/100 dosemeters were checked by Allard. [9].

5.3.2. Measurements and results

The reported values are mainly averages from several different dosemeters on phantom.

1. TLD

		Neutrons		Photons
		TLD (LiB)	TLD (Albedo)	TLD (LiF)
Position	Phantom side			
A	front	1.34	1.37	0.42
	rear	0.89	0.94	0.28
	lateral	1.09		0.36
	top	1.36		0.34
	bottom	0.53		0.29
F	front	0.64	0.70	0.35
	rear	0.44	0.46	0.20
	lateral	0.47		0.18
	top	0.47		0.19
	bottom	0.22		0.13
G	front	0.16		0.06
	rear	0.14		0.08
	lateral	0.12		0.06
	top	0.18		0.08
	bottom	0.05		0.05
L	front	0.14	0.16	0.07
	rear	0.03	0.04	0.04
	lateral	0.08		0.04
	top	0.11		0.05
	bottom	0.05		0.04
D at Ringhals	front	0.03		0.03
	rear	0.02		0.02
	lateral	0.03		0.03
	top	0.02		0.03
	bottom	0.03		0.03
E at Ringhals	front	0.04	0.03	0.04
	rear	0.02	0.02	0.02
	lateral	0.02		0.03
	top	0.02		0.03

$H_p(10)/t$ measured dose equivalent rates in mSv/h with dosemeters positioned on the front face of a PMMA phantom (in positions G and D on a boron paraffin phantom).

2. Bubble detector

In position L the Neutrometer showed 0.23 mSv/h on the front face of the PMMA phantom. This is the only measurement with Neutrometer (bubble detector) on a phantom.

3. Electronic dosemeter

The Rados electronic GM-detector based dosemeters were only tested with two + two dosemeters in position A. The average of the readings with dosemeters on the PMMA slab phantom were 0.56 mSv/h on the front face and 0.46 mSv/h on the rear face. During this irradiation the PMMA slab phantom was complemented by the two halves of the boron paraffin phantom on the frontal and rear sides of the PMMA phantom respectively. The use of a larger total volume of the phantom decreased the readings of TL-dosemeters with a factor 1.35 as compared to using only the PMMA phantom. A correction with a factor 1.35 is included in the readings reported above.

References

[1] P. Drake, *Conversion Factors for the Calibration of Personal Dosimeters in 4- 7 MeV Photon Fields.* Internal report, Vattenfall, Ringhals Nuclear Power Plant, Väröbacka, Sweden. 1993, published in short form in Radiation Protection Dosimetry. Vol **46** (1993) 23 - 29.

[2] E. Piesch et al., *Properties of Personnel Neutron Dosimeters on the Basis of Intercomparison Results.* Radiation Protection Dosimetry **44** (1992) 267 - 271.

[3] E. Lund et al., *Lund 90 Experimental Determination of the Angular Dependence Factor for the Dose Equivalent for Photons in Calibration Phantoms of PMMA.* Accepted for publication in Radiation Protection Dosimetry.

[4] *Neutrometer User Instruction.* Apfel Enterprises Inc., New Haven, USA. 1992.

[5] R.E. Apfel, *New Passive Superheated Drop (Bubble) Dosemeters.* Radiation Protection Dosimetry **44** (1992) 343 - 346.

[6] *Article Concerning Neutrometer Results in Oak Ridge Intercomparison Study.* Apfel Enterprises Inc., New Haven, USA. 1992. News from Apfel Enterprises. Vol. 1.

[7] K. Anttilla, T. Hapalehto and H. Kalli, *Accuracy of RAD-80 Dosimeters under BWR Turbine Hall Conditions.* Lappeenranta University of Technology, Lappenranta, Finland. 1985. ISBN 951-763-310-6.

[8] I.M.G. Thompson, *The Adoption of the new ICRU Dose Equivalent Operational Quantities within the Central Electricity Generating Board of the United Kingdom.* Radiation Protection Dosimetry **28** (1989) 149 - 155.

[9] D.J. Allard, A.M. Nazarali and G.E. Chabot, Arthur D. Little, *The N-16 Gamma Radiation Response of Geiger-Müller Tubes.* Presented at the 8.th IRPA Congress in Montreal, Canada, 1992.

5.4 Measurements with AECL Personal Dosemeters

A.R. Arneja and A.J. Waker
AECL Research, Chalk River, Canada

5.4.1 Types of dosemeter and dosemeter characteristics

The type of dosemeter used was PADC (CR39) track etch dosemeter to measure fast and thermal neutrons. American Acrylics PADC of dimensions 20 x 20 mm is encapsulated in 0.13 mm polyethylene film which provides the proton radiator. Details of the dosemeter response characteristics are given in [1] but note the etch procedure has been changed to 1 hour chemical etch followed by 7 hours electrochemical etch at 20 kV cm^{-1} (rms), both etches in 6N KOH at 60°C. The thermal neutron response is provided by a small disc of lithium borate in contact with the higher background (rear) side of the PADC detector. The dosemeter shows little response to fast neutrons of energy less than 100 keV, but approximately constant $H_p(10)$ response between 100 keV and 5.3 MeV.

5.4.2 Measurements and results

Measurements were made at positions 'L', 'A' and 'F' at the Ringhals reactor. At positions 'A' and 'F' measurements were made using both a 300 x 300 x 150 mm PMMA slab phantom and a 300 mm diameter sphere of tissue equivalent material (RS1) at position 'L' only the slab was used.

The results are given in Table 5.4 below expressed as $H_p(10)$ rate ($\mu Sv\ h^{-1}$), based on calibration with ^{252}Cf at normal incidence.

Table 5.4: CL personal dosemeter results

Location		$H_p(10)$ rate ($\mu Sv\ h^{-1}$)	
		Slab phantom	Sphere phantom
Ringhals	L	110	-
	A	780	740
	F	420	380

[1] R.P. Bradley and F.N. Ryan, *Results for the 1990 EURADOS-CENDOS Irradiation Programme on Track Etch Detectors.* (PTB Report PTB-N-10 (1991) 2.6 to 2.8.).

5.5 Measurements with ENEA Personal Dosemeters

F. d'Errico, DCMN Pisa, and O. Civolani, ENEA, Bologna, Italy

5.5.1 Types of dosemeter and dosemeter characteristics

Three types of dosemeter were supplied by ENEA Bologna. A TLD γ dosemeter, a TLD thermal neutron dosemeter and a PADC (CR39) fast neutron dosemeter.

The TLD γ-dosemeter is composed of bare and filtered BeO detectors. A ^{60}Co source is used for calibration. A pair of algorithms is used to estimate photon energy. Air kerma is determined with a third algorithm that includes an energy dependent term. $H_p(10)$ and $H_p(0.07)$ can then be calculated from air kerma using energy dependent conversion factors. Relative to ^{60}Co, there is an over-response in terms of $H_p(10)$ of a factor of 2 at 100 keV decreasing to 1.5 at 30 keV. (For more details of the dosemeter response characteristics see, for example Ref. [1]).

The PADC (CR39) neutron dosemeter comprises a 25 x 30 mm piece of American Acrylics PADC with a 2 mm thick PMMA support encapsulated in a 0.2 mm thick plastic bag. The dosemeter responds to fast neutrons only. The normal incidence $H_p(10)$ response is about 25% higher at 144 kev relative to ^{252}Cf. (Further details of the dosemeter response characteristics may be found in Ref. [2]).

The PADC is complemented by a pair of ^{6}Li/^{7}Li Fluoride TLD chips cadmium shielded on the rear side. These measure the direct thermal neutron component of dose.

5.5.2 Measurements and results

Measurements were made at positions L and A at the Ringhals reactor and at CLAB positions P and D for all types of dosemeter. Dosemeters were mounted on the front face of a 300 x 300 x 150 mm PMMA slab phantom.

The results of the neutron and gamma dosemeters are given in the Table 5.3 below, expressed as μSv h^{-1} (H'(10) (considered equivalent to $H_p(10)$) normalised for their Cf and Co responses respectively. At CLAB, the response of the TLD's to thermal neutrons and to gammas were below the detection thresholds.

[1] L. Lembo, *Evaluation Procedures with the ENEA Personnel Dosimeter.* 179-182 in Intercomparison for Individual Monitoring, Research Co-ordination Meeting, IAEA, Vienna, 24-28the April 1989. PTB Report, PTB-DOS-20 (1991).

[2] Lembo and M. Beozzo, EURADOS/CENDOS 1990 Joint Irradiations, ENEA Bologna Results, pp .44 to 2.48 in Investigation of Individual Neutron Monitors on the Basis of Etched-Track Detectors: The 1990 EURADOS-CENDOS Exercise'. EURADOS-CENDOS Report 1992-02. PTB Report PTB-N-10 (1992).

Table 5.5: ENEA-Bologna personal dosemeter results

Location		H'(10) rate (μSv h^{-1})		
		PADC	TLD thermal neutron	TLD γ
Ringhals	L	175	130	55
	A	470	110	280
CLAB	P	40	-	-
	D	60	-	-

5.6 Summary of dosemeter measurements

An overwiev of the readings of the different dosemeters on phantoms in position **A** to **P** is presented in table 5.6.1 for neutrons and in table 5.6.2 for photons.

	Dosimeter readings in microsievert per hour						
	PTB Track	PTB Albedo	NRPB	AECL	LiB	Albedo	ENEA
Position/			PADC	CR-39	Ringhals	Ringhals	CR-39+TLD
Direction					Calibrated with remcounter		
A AP	527 (92)	852 (25)	390 (14)	760	1340 (54)	1370 (55)	580
A PA	237 (74)	639(20)	130 (7)		890 (35)	940 (38)	
A Lat	270 (77)	560 (19)	180 (14)		1090 (44)		
A top	426 (86)	743 (21)	310 (18)		1360 (54)		
A bottom					530 (21)		
F AP	410 (47)	541 (26)	370 (30)	400	640 (26)	700 (28)	
F PA	104 (93)	196 (22)	62 (26)	150	440 (18)	460 (18)	
F Lat	139 (99)	281 (24)	102 (23)		470 (19)		
F top	168 (96)	287 (24)	120 (21)		470 (19)		
F bottom			210 (51)		220 (9)		
G AP					160 (6)		
G PA					140 (6)		
G Lat					120 (5)		
G top					180 (7)		
G bottom					50 (2)		
L AP			58 (8)	110	140 (6)	160 (6)	205
L PA			5 (0.4)		30 (1)	40 (2)	
L Lat			24 (3)		80 (3)		
L top			40 (5)		110 (4)		
L bottom			18 (3)		50 (2)		
D AP	22 (9)	40 (3)	*				60
D PA	8 (4)	7 (2)					
D Lat	9 (6)						
D top	7 (2)						
D bottom	6 (2)						
P AP	37 (9)	40 (4)					40
P PA	1 (2)	6 (3)					
P Lat	6 (5)						
P top	2 (7)	* calculated from measurements					
P bottom	3 (5)	at 45 and 135 degrees					
Values in paranthesis are the statistical uncertainty as reported by the participants							

Table 5.6.1. Reported values of Hp(10) or H′(10) on different sides of phantoms. Part 1 neutrons. (Direction AP referes to the front side of the phantom)

	Dosimeter readings in microsievert per hour					
	PTB Albedo	Siemens-	LiF	Albedo(LiF)	ENEA	Rad 80
Position		NRPB EPD	Ringhals	Ringhals	TLD	Rados
Direction						
A AP	343	340	420	390	280	560
A PA	262	270	280	330		460
A Lat	297		360			
A top	318		340			
A bottom			290			
F AP	250		350	300		
F PA	130		200	250		
F Lat	185		180			
F top	185		190			
F bottom			130			
G AP			60			
G PA			80			
G Lat			60			
G top			80			
G bottom			50			
L AP		57	70	70	55	
L PA		30	40	40		
L Lat			40			
L top			50			
L bottom			40			
D AP	30	*				
D PA	10					
P AP	25					
P PA	5					
	* calculated from measurements					
	at 45 and 135 degrees					
Statistical						
uncertainty %	4 - 6		4	4		
as reported by the participants						

Table 5.6.2. Reported values of Hp(10) or H′(10) on different sides of phantoms. Part 2 photons. (Direction AP referes to the front side of the phantom)

6. MEASUREMENTS WITH PHOTON AND NEUTRON SURVEY METERS

compiled by L. Lindborg, SSI, Stockholm, Sweden

This chapter contains results observed with a specially designed superheated-drop (bubble) detector (6.1) developed at DCMN-Pisa as well as. results observed with conventional instruments such as GM-counters and remcounters are reported (6.2).

6.1 The DCMN-Pisa Neutron Area Monitor Based on Superheated Drop (Bubble) Detectors

F. d'Errico
Dipartimento di Costruzioni Meccaniche e Nucleari, Università degli Studi di Pisa, and Istituto Nazionale di Fisica Nucleare, Sezione di Pisa, I-56100 Pisa

6.1.1. Introduction

In the past decade, superheated drop (bubble) detectors [1] have gained widespread acceptance in the radiation protection dosimetry of neutrons. Various devices based on this technology have been developed: active monitors detecting drop vaporisations acoustically, as well as passive pen-size dosemeters relying on the optical or volumetric reading of the bubbles.

Common to all these is their manufacturers' attempt to eliminate the temperature dependence of the sensitivity, which is regarded as their major shortcoming. A different approach was developed in a joint effort by DCMN-Pisa and PTB Braunschweig: an area monitor was devised which relies on the temperature dependence as a method for the optimisation of the operation of the dosemeters [2,3]. A prototype based on this approach was first employed "in the field" during the EURADOS WG7/SSI measurements at Ringhals and CLAB.

6.1.2 Materials and Methods

The area monitor employs detector-vials containing 4 cm^3 of an emulsion of superheated halocarbon-12 droplets. Bubbles are counted acoustically through the detection of their explosive vaporisation events by means of piezo-electric transducers kept in contact with the vials. The original development consists in the active systems which stabilises the detectors to the temperature corresponding to their flattest ambient dose equivalent response. This it a time proportioning controller operating etched-foil heaters wrapped aroung the vials along with a Pt resistance temperature sensor [2].

The ambient dose equivalent response of this device as a function of detector's temperature and neutron energy was investigated in detail at the PTB with monoenergetic neutron beams in the thermal to 15 MeV energy range. The monitor prototype employed in Sweden was set to work at 30 °C. Later tests have shown that the optimal operating temperature for the SDDs is 32 °C.

Figure 6.1 reports the energy dependence of the ambient dose equivalent response at 30 °C. The response is quite flat: most data points for thermal and fast neutrons all between 3 and 7.5 bubbles per μSv, and a reference value of 5 was adopted. It may be observed that the response almost meets the ICRP recommendations on accuracy of measurements stating that differences from the true dose value shall be acceptable up to a factor of 1.5

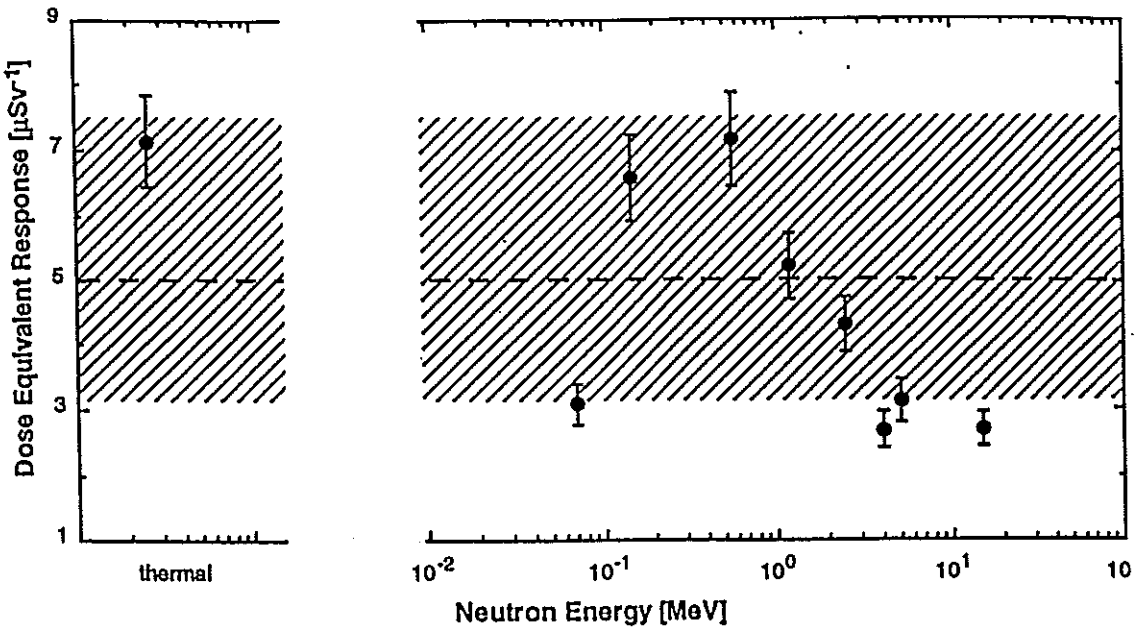

Figure 6.1: Ambient dose equivalent response of the DCMN-Pisa neutron area monitor operating at 30 °C, conversion factors from Wagner et al. [4]. The dashed line indicates the reference value of 5 bubbles per μSv. the shaded area indicates the region falling within a factor 1.5 of that value.

6.1.3 Results

The DCMN-Pisa monitor was employed at Ringhals, in measuring position "L", and at CLAB, in positions "P", "D", and "E".

In order to reach adequate counting statistics, the ideal procedure consists in the acquisition of several hundred counts (bubbles) at 100-count steps (to verify internal consistency). Due to time constains and to the low rate, respectively, at Ringhals and CLAB, measurement were limited to 200 - 300 bubbles in each position.

The experimental standard deviation was in the order of 7% in all cases. This is to be added quadratically to the uncertainties on the fluence response measurements (~7%) and to those deriving from the energy dependence of the dose equivalent response (assessed to be in the order of 10 - 12%, thanks to compensating effects with broad neutron spectra). As a result, the overall uncertainty on the final results is estimated be lower than 15%.

The ambient dose equivalent rates based on a flat ratio of 5 bubbles to 1 μSv, i.e. with no correction for the various neutron spectral distributions are reported in Table 1 of sect. 6.1.

Table 1: Ambient dose equivalent rates measured with the DCMN-Pisa neutron area monitor.

POSITION	$\dot{H}^*(10)$ [$\mu Sv\ h^{-1}$]
Ringhals-L	220
CLAB-P	40
CLAB-D	38
CLAB-E	38

6.1.4. References

[1] Apfel, R.E., *The Superheated Drop Detector.* Nucl. Instrum. Meth. **162** (1978) 603 - 608.

[2] d'Errico, F., Alberts, W.G., Apfel, R.E., Curzio, G., and Guldbakke, S., *Applicability of Superheated Drop (Bubble) Detectors to Reactor Dosimetry.* Reactor Dosimery ASTM STP 1228, American Society for Testing and Materials, Philadelphia (1994).

[3] d'Errico, F. and Alberts, W.G., *Superheated Drop (Bubble) Detectors and Their Compliance with ICRP 60.* Radiat. Prot. Dosim. **54** (1994) 357 - 360.

[4] Wagner, S.R., Großwendt, B., Harvey, J.R., Mill, A.J., Selbach, H.-J. and Siebert, B.R.L., *Unified Conversion Functions for the New ICRU Operational Radiataion Protection Quantities.* Radiat. Prot. Dosim. **38** (1991) 271 - 277.

6.2 Measurements with Conventional Survey Meters

The survey meters that took part in the exercise were instruments belonging to the two radiation protection organisations at Ringhals and CLAB and instruments brought along by the participants. The gamma measuring instruments were GM counters and the neutron dosemeters were commercially available remcounters and a Dineutron (Nardeux) instrument. the Swedish photon survey meters had been calibrated for ambient dose equivalent in a ^{137}Cs beam. The neutron survey meters had been calibrated in various ways as stated in Table 6.2.

The results reported are those stated by the participants.

The close agreement between GSF and PTB confirms the stable radiation condition during the exercise. The PTB instrument reads in average 7% larger values at the two reactors.

The results observed with GM-counters are presented in Table 6.3. The measurements by SSI and IAR were made as part of the investigation, while the measurements by Ringhals were made by different persons involved in the radiation protection service during the campaign. Again the agreement is rather good especially in the lock and at CLAB. At F and G there is a difference of about 18% between SSI and IAR, which may be caused by the different energy response of the two counters, Fig. 6.2. The IAR detector is less sensitive to photon energies in the interval 60 keV to at least 225 keV. For energies above 1.2 MeV the responses is less well known.

Table 6.2: Ambient dose equivalent rate due to neutrons at the different locations. H* has been measured and quality factors from ICRP21 have been used.

Laboratory	Ringh. 4, Lock mSv/h	Ringh. 4, A mSv/h	Ringh. 2, F mSv/h	Ringh. 2, G mSv/h	CLAB D µSv/h	CLAB E µSv/h	CLAB P µSv/h	Calibration beam
CLAB remcounter (Studsvik)					40	30	50	^{241}AmBe
Dineutron (Nardeux)					60	40	100	^{252}Cf
Ringhals remcounter (Studsvik)	0.23	1.50	1.00	0.10				as above
Dineutron (Nardeux)	0.17	1.50	0.69	0.20				
NPL Remcounter (Harwell)		2.68[b]						as calibrated by the manufacturer
IAR remcounter Anderson & Braun	0.216		0.789	0.122	41	33	41	D_2O moderated ^{252}Cf
GSF remcounter (Anderson & Braun)	0.305	2.158	1.088	0.233	53	44	51	^{241}AmBe
PTB remcounter (Leake)	0.332		1.146	0.248	52.3	44.2	52.2	D_2O moderated ^{252}Cf
DCMN-Pisa SDD monitor	0.220				38	38	40	monoenergetic neutrons

[b] Results from measurements in March 1993.

Table 6.3: Ambient dose equivalent rate determined with GM-based instruments

Laboratory	Ringh. 4, Lock mSv/h	Ringh. 4, A mSv/h	Ringh. 2, F mSv/h	Ringh. 2, G mSv/h	CLAB D µSv/h	CLAB E µSv/h	CLAB P µSv/h	Calibration field
SSI GM B (ZP 1201)	0.071	0.49	0.31	0.115	33	22	23	^{60}Co
GM A (ZP 1201)	0.074[b]	0.52[b]			33	22		
GM B	0.075[b]	0.53[b]						
Ringhals GM (Automess, ADI-1,ADI-3)	0.07	0.38	0.20	0.10				^{137}Cs
IAR GM (Alrad, ZP1320 PTFE)	0.073		0.262	0.097	34	26	26	^{60}Co

[b] Results from March 1993

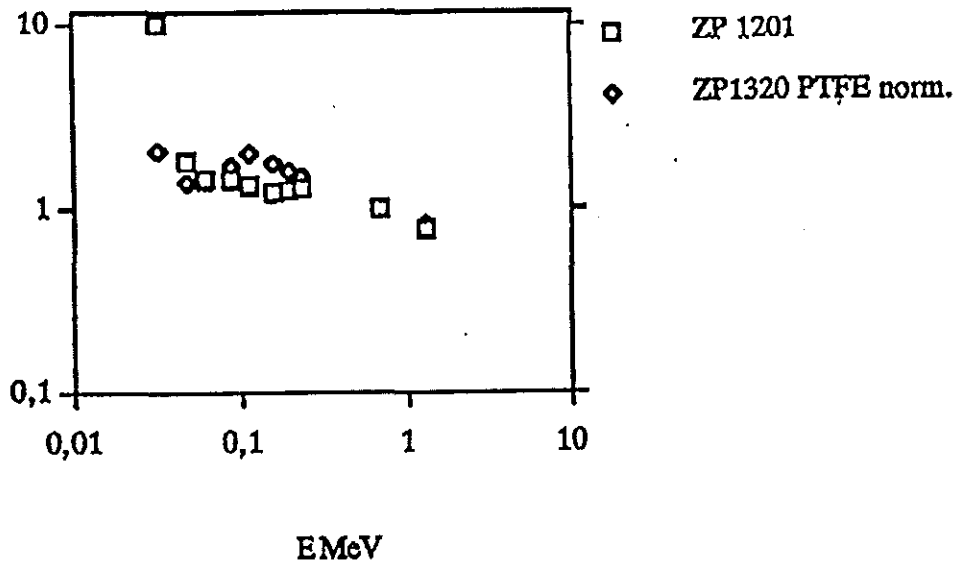

Figure 6.2: Photon energy calibration factors at different hard filtered x-ray beams (ISO) and ^{137}Cs and ^{60}Co gamma beams. The two GM tubes are ZP 1201 and ZP 1320 PTFE, which were used by SSI respectively IAR. The factors for ZP 1320 PTFE have been divided by 1.96 to become normalized to one at 662 keV. The calibration factor is the ratio between ambient dose equivalent and meter reading.

7. SUMMARY AND CONCLUSION

H. Klein
PTB, D-38116 Braunschweig, Germany

In close cooperation with EURADOS Working Groups #7 and #10, the Swedish Radiation Protection Institute (SSI) and the Radiation Protection Service at the nuclear power plants in Ringhals and at the Central interim storage facility in Oskarsham, a comprehensive comparison exercise has been carried out at workplaces in nuclear facilities. The main objective was to compare the different methods used to determine neutron dose quantities at workplaces employing various kinds of spectrometers, tissue equivalent proportional counters (TEPC), survey and personal dosemeters. The photon component of the mixed fields was also investigated.

The reports of the participants as submitted to the evaluators are compiled in this documentation. The papers therefore comprise a detailed documentation of the instruments employed, the response functions used in the unfolding procedures, the original count rates or pulse height spectra measured, and the corrections taken into account, e.g. for deadtime losses. As requested by the evaluators, spectral distributions, integral and group data were reported for fluence and/or dose equivalent rates. The evaluation showed that some data had to be revised, and these are indicated in the text or added as an appendix.

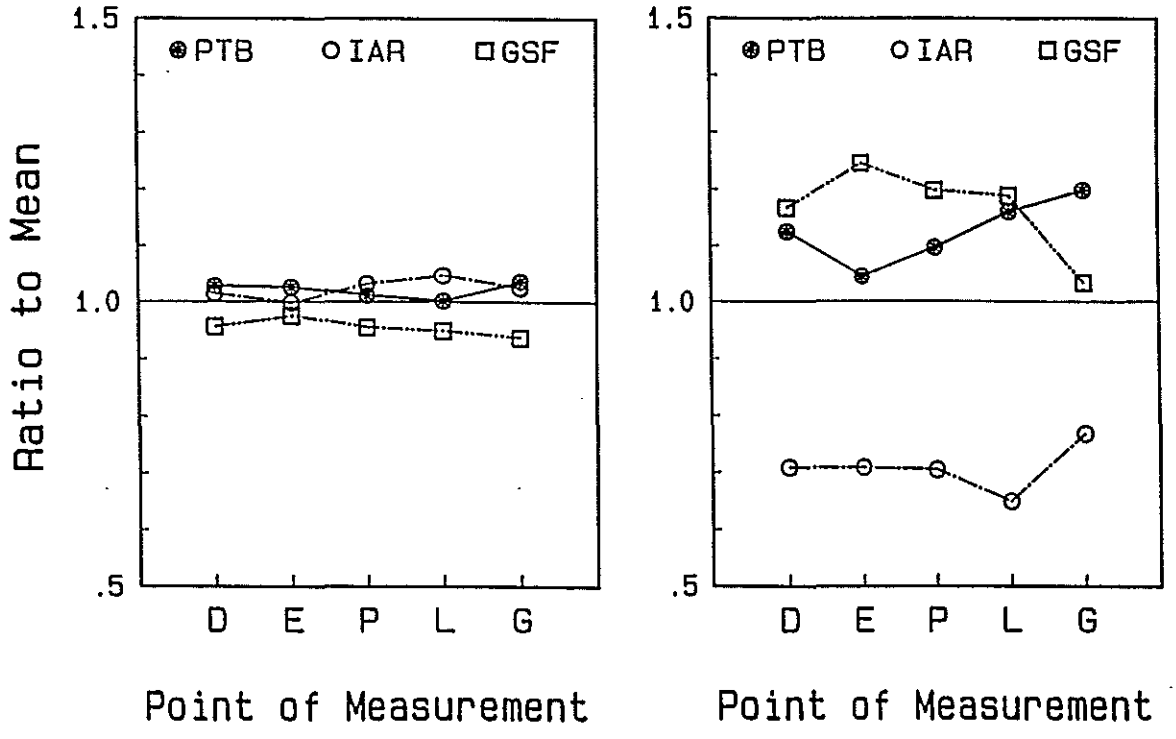

Figure 7.1: Ratio of the integral neutron fluence (left) or ambient dose equivalent (right) obtained from three sets of Bonners sphere measurements at various positions in the containment building of the PWR (L,G) and in the vicinity of a transport cask (D,E,P) to the unweighted mean value of the three results.

The general idea was to specify the radiation fields by means of spectrometric methods in order to establish dosimetric reference values for comparison with the readings of the various dosemeters employed. However, a comparison of the integral data obtained from the measurements with Bonner Sphere Spectrometers (BSS) (for details see section 3) already showed significant discrepancies (Fig. 7.1). Taking into account measurements at those positions where three BSS's were employed, we find excellent agreement of the analysed integral neutron fluence rates of better than 10% (Fig. 7.1a), but corresponding integral dose equivalent (DE) rates (Fig. 7.1b) show a systematic deviation of about 45% of one data set from the other two, which are in reasonable agreement (± 10%). It was suspected that these discrepancies were caused by differences of the spectral distributions, particularly at the upper end of the spectrum (Fig. 7.2). Fortunately, at some positions measurements were performed with proton recoil spectrometers, providing additional information in the neutron energy region above 50 keV.

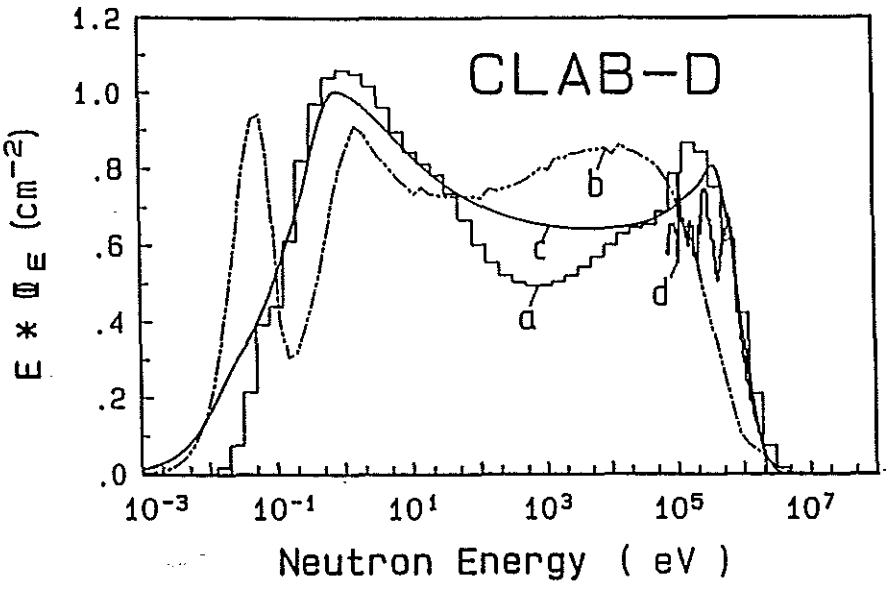

Figure 7.2: Spectral neutron fluence rate measured at position D with the Bonner sphere spectrometers of GSF (a), IAR (b) and PTB (c), and a set of proton recoil spectrometers of ZfK-KAI (d) (original data see section 3).

Measurements with TEPC's also produced discrepant results (for details see sect. 4). The scatter of the absorbed dose rates (± 15%, see Fig. 4.1 of sect. 4) is to be expected, particularly if the extreme environmental conditions in the containment building are taken into account. The much larger and partially systematic deviations of some neutron DE rates (± 50%, see Fig. 4.3 of sect. 4), however, indicate that the DE response of these instruments is not appropriate for the soft neutron spectra encountered in practice. A detailed analysis was necessary to understand the differences observed. The known DE response of the detectors and the evaluated spectral neutron fluence should be used to check the consistency of the expected and the measured TEPC readings. In any case, similar neutron spectra should be provided in the laboratory for calibration purposes.

Similarly, the large scatter of the DE readings of commercially available survey meters (see section 6) may be explained on the basis of their response functions and the evaluated spectral fluence.

Finally, various personal dosemeters were irradiated on phantoms indicating $H_{p,slab}(10)$ or H'(10) DE (see sect. 5). These data cannot be directly compared with the H*(10) values obtained from the spectrometric measurements unless the angular distribution of the radiation is known. As the spectrometers are designed and realized to have an isotropic response, as with the survey meters only ambient DE quantities can be determined. The angular dependent (spectral) neutron fluence could therefore only be obtained from the readings of 6 personal dosemeter mounted at different positions on the phantom. Taking into account the known angular and energy-dependent response of the dosemeters, the evaluated spectral fluence and the rough spectrometric properties of some of the dosemeters, an evaluation of these data should then relate the personal to the ambient DE data.

All the evaluations required were recently carried out and the results will be documented in detail in part II of this SSI report [1]. A summary has been presented at a workshop in Chalk River and will be published in its proceedings [2].

References

[1] Bartlett, D., Drake, P., Klein, H., Lindborg, L., Schmitz, T., Tichy, M., *Determination. of Neutron and Photon Dose Equivalent at Work Places in Nuclear Facilities of Sweden -An SSI-EURADOS Comparison Exercise*
Part II: Evaluation of the Results
SSI-report 95-16, ISSN 0282-4434, Stockholm, 1995 (to be published).

[2] Lindborg, L., Bartlett, D., Drake, P., Klein, H., Schmitz, T., Tichy, M., *Determination. of Neutron and Photon Dose Equivalent at Work Places in Nuclear Facilities of Sweden -A Joint SSI-EURADOS Comparison Exercise*
accepted for publication in Radiat. Prot. Dosim., 1995

SSI-rapporter

95-01. Publikationer
SSI-Informationsenheten. *Gratis*

95-02. Statens strålskyddsinstituts skyddskriterier för omhändertagande av använt kärnbränsle
Enheten för avfalls- och omgivningstillsyn *25 kr*

95-03. The use of Algae in monitoring discharges of radionuclides
- Experiences from the 1992 and 1993 monitoring programmes at the Swedish nuclear power plants
Pauli Snoeijs, Puck Simenstad *60 kr*

95-04. Kvalitetssäkring av egenkontrollen vid svenska kärnkraftverk och Studsvik AB Vattenburna utsläpp 1992.
Kemienheten *40 kr*

95-05. Miljökonsekvensbeskrivningar inför slutförvaring av använt kärnbränsle m.m.
Boverket, Riksantikvarieämbetet, Statens kärnkraftinspektion, Statens naturvårdsverk, Statens strålskyddsinstitut *60 kr*

95-06. Jämförelser mellan omgivningsmätningar och modellberäkningar av radioaktiva ämnen i fisk vid de svenska kärnkraftverken och Studsvik
Olle Karlberg *40 kr*

95-07. Kontrollmätning av låg- och medelaktivt avfall avsett att slutförvaras i SFR-1; 1994 års mätningar
Magnus Westerlind, Olof Karlberg, Gunilla Lindbom, Ingemar Lund *40 kr*

95-08. A BIOSPHERE MODEL for use in the SKI Project SITE-94
Runo A G Barrdahl *50 kr*

95-09. Kalibrerings- och normalieverksamheten vid riksmätplatsen under 1994
Ulf Nilsson, Jan-Erik Grindborg, Olle Gullberg och Göran Samuelson *40 kr*

95-10 Underlagsmaterial till SSIs granskning av SKBs komplettering av forskningsprogrammet för 1992
M Jensen, J Nolin, G Sundkvist *60 kr*

95-11. The SSI TOOLBOX Source Term Model SOSIM
- Screening for important radionuclides and parameter sensitivity analysis
R.Avila Moreno, R. Barrdahl, C. Hägg *50 kr*

95-12. Förslag till kursplan
Tillståndsbunden utbildning i strålskydd och utrustningens handhavande för personal i röntgenverksamheter
Medicinsk fysik och teknik, Enheten för röntgen och radioaktiva ämnen *50 kr*

95-13. Kärnkraftindustrins
- aktivitetsutsläpp
- yrkesexponeringar 1994
Huvudenheten för kärnenergi *50 kr*

95-14. Orienterande undersökning av effekten av vattenbehandlingsutrustning på radonhalten från borrade brunnar
Connie Boox, Geosigma AB *25 kr*

95-15. Determination of the Neutron and Photon Dose Equivalent at Work Places in Nuclear Facilities of Sweden
An SSI - EURADOS comparison exercise.
Part 1: Measurements and Data Analysis
H. Klein and L. Lindborg *100 kr*